Ligand binding and receptor network formation in the Tumor Necrosis Factor superfamily

A DISSERTATION
SUBMITTED TO THE FACULTY OF THE GRADUATE SCHOOL
OF THE UNIVERSITY OF MINNESOTA
BY

Christopher Carlin Valley

IN PARTIAL FULFILLMENT OF THE REQUIREMENTS
FOR THE DEGREE OF
DOCTOR OF PHILOSOPHY

Dr. Jonathan N. Sachs, Adviser

July 2012

Acknowledgements

My time at the University of Minnesota has been at times exciting, at times frustrating, and at times requiring utmost patience. But collectively, I view these experiences as overwhelmingly rewarding. It has been a gift to attend this institution, where I have experienced tremendous personal and intellectual growth. My experiences here have been shaped by a number of incredible people.

First and foremost I would like to thank my adviser, Jonathan Sachs. He took a risk in bringing me into the group, and he took an even bigger risk in allowing me to develop an experimental lab, setting up the trajectory of the research group for years to come. I appreciate his patience and understanding throughout this process. My graduate experience has been remarkable, and none of it would have been possible without his support. I owe much of my intellectual development to his mentoring, and for this I will forever be appreciative.

I would like to thanks to the Sachs lab members. Each of them, with a different perspective, contributed in some form to this thesis. First, I would like to thank Jason Perlmutter and William Drasler, colleagues whom I am happy to also call friends. I have greatly appreciated their support and friendship both on and off campus. I would also like to thank Anthony Braun for his help in computation and programming. A special thanks to Andrew Lewis, who rescued me from intellectual isolation when he joined the lab. His many experimental talents were greatly needed, as was his sense of humor. I'm happy to have worked with him. Thanks also to Deepti Mudaliar for her contributions to the development of the lab and for continuing where I left off on many projects. Last and certainly not least I would like to thank Steve Peery, the only student brave enough to work for me. He developed many of the resources and techniques still used in the lab, and his talents in the lab speak volumes.

I am especially grateful to my collaborators here and at various institutions. In particular, I would like to thank Ameeta Kelekar both for training me as well as allowing me to work in her laboratory at a time when I didn't have a lab to call my own. I am thankful for our meaningful interactions and owe much of my knowledge in apoptosis and cancer biology to her. I would also like to thank Jonathan Brody for his advice and help with manuscripts. Additionally, I would like to thank my committee members, David Thomas, Thomas Griffith, and Dave Odde, for providing valuable discussions and advice over the last several years and for helping to guide me along my way toward completing my degree.

Thanks are also in order to a number of people with whom I have worked or have helped me along the way. I would like to thank several members of the Thomas lab, specifically Suzanne Haydon and Ji Li, for sharing their knowledge and experiences in FRET, and also Christine Karim for her technical expertise in peptide synthesis. Also many thanks to Alessandro Cembran and Jiali Gao for running quantum calculations and for helping to write, edit, and revise our manuscript, which added a substantial layer to an interesting project.

I would like to thank my many friends at the University of Minnesota for helping me through this challenging experience and for providing an enormity of support. Also thanks also to my students over multiple semesters for helping me discover the fun in teaching.

Although my thesis work began six years ago, my experience as a scientist began in 2002 when I joined a lab as an undergraduate. I have to thank those who led me down this career path, for seeing something in me that I never saw in myself, and for teaching me that higher education is much more than coursework. A special thanks to Elaine Alarid, for giving me this opportunity as an undergraduate and for encouraging me to pursue a graduate education. Also, I would like to thank those who trained me during those years, including Amy Fowler and Natasha Solodin. Thanks are also in order for Stephanie Ellison-Zelski, for providing much inspiration and humor.

I would like to thank my family, especially my parents and brothers. Finally, I would like to thank Jane for her endless support and constant understanding. Her ability to motivate me during frustrating times and to calm me down during stressful times kept me on track during my graduate career. Her patience is unwavering and her kindness is relentless. Thank you, Jane, for your love and support. I couldn't have done any of this without you …and I promise to be home for dinner.

To Jane

For your love, support, and patience

Abstract

Tumor necrosis factor (TNF)-related apoptosis-inducing ligand (TRAIL), a cytokine with anti-tumor potential, binds to transmembrane TRAIL receptors and initiates apoptosis. Although much has been characterized regarding intracellular signaling of TRAIL receptors, early events outside the cell and within the plasma membrane remain poorly understood. The central focus of this thesis is to establish biophysical interactions involved in ligand binding and subsequent receptor structural changes resulting in receptor activation.

First, we demonstrate that TRAIL receptor 2 (death receptor 5, or DR5) forms receptor dimers in a ligand-dependent manner, and these receptor dimers exist within high molecular weight networks. We find that receptor dimerization relies upon covalent and non-covalent interactions between membrane-proximal residues, and that the transmembrane structure of two functional isoforms of DR5 are indistinguishable. This is the first evidence using endogenous, full-length receptor to demonstrate that DR5 networks are highly organized.

Further, we show that DR5, upon stimulation by ligand, migrates into cholesterol rich membrane regions, and ligand-induced dimerization and network formation rely on cholesterol within the plasma membrane. Depletion of membrane cholesterol prevents structural changes associated with ligand binding as well as function. Therefore, lipid biophysical properties play an active role in determining receptor structure and function.

Lastly, we identify and characterize a key, specific interaction between Methionine and aromatic residues that is critical for high affinity ligand-receptor binding and function in the TNF superfamily. Using structural bioinformatics, we demonstrate that this

interaction—which occurs at approximately 5Å separation—is present in approximately one-third of known protein structures. Quantum calculations of model compounds and biological molecules demonstrate that this interaction provides additional stabilization over hydrophobic interactions and at distances out to 7Å, suggesting that this interaction may have evolved in proteins where a high degree of stabilization is required at longer distances. This motif may be utilized in the rational design of therapeutics targeting a range of proteins, including TNF members.

In summary, our results characterize novel biophysical interactions between ligand-receptor, receptor-receptor, and receptor-membrane that together orchestrate a series of events that ultimately lead to cell death.

Table of Contents

List of Tables

List of Figures

Chapter 1

Chapter 2

Chapter 3

Chapter 4

Chapter 5

Chapter 6

Appendix A

Preface

The cellular membrane and its membrane proteins are critical for cell function. They provide a cell the ability to communicate with and respond to its surroundings, including the local environment as well as neighboring cells. The signals received by a cell include extracellular conditions (such as matrix stiffness), protein ligands (such as cytokines), non-protein molecules (such as hormones or neurotransmitters), and even ions. Regardless of its type, the signal must be propagated across the membrane in order for a cell to properly respond, and this process inevitably involves membrane proteins.

Membrane proteins constitute approximately 26% of protein-coded genes in the human genome [1] but represent approximately 60% of drug targets [2], and therefore localization within the membrane is a key factor in determining whether a particular protein represents a "druggable target".

The structure of a membrane protein is critical in understanding its function as the two are fundamentally linked, and the response to extracellular signals often involves structural changes, which further complicates this relationship between structure and function. Therefore, in response to an input, such as an extracellular ligand signal, the resulting function of a protein can be classified in terms of three interrelated characteristics: protein structure, protein dynamics, and protein environment [3].

The contents of this thesis begin to explore the paradigmatic relationship between the structure, dynamics, and environment of a family of membrane proteins, and how these relate to protein function in living cells. The fundamental, underlying questions may be applied to any number of complex signal transduction pathways through the membrane: How are signaling events outside the cell propagated across the membrane? And what role does the membrane, including the transmembrane region of the protein, play in this signal transduction process from outside to inside the cell?

Here, we characterize new biophysical interactions within a subset of proteins belonging to the tumor necrosis factor (TNF) superfamily. These interactions include ligand-receptor interactions, receptor-receptor interactions, and receptor-membrane interactions, which collectively orchestrate early signaling events within the membrane and ultimately result in controlled cell death. The proteins we explore here are clinically relevant and are currently under investigation in clinical trials for the targeted treatment of cancer. Therefore, understanding the molecular level structure, protein dynamics, and the relationship between the protein and its membrane environment will serve to aid in the design of novel therapeutics targeting this family of proteins.

Chapters in this thesis represent original work; published, in review, or in preparation for submission. For published articles, permissions to republish the full text and figures were obtained individually for each article.

Chapter 2 – Original manuscript in preparation for submission as an invited review article at *J Membr Biol.* **Valley CC** and Sachs JN. TNF ligand-induced clusters within the membrane.

Chapter 3 – Published manuscript reproduced with permission from: **Valley CC**, Lewis AK, Mudaliar DJ, Perlmutter JD, Braun AR, Karim CB, Thomas DD, Brody JR, Sachs JN. Tumor necrosis factor-related apoptosis-inducing ligand (TRAIL) induces Death Receptor 5 networks that are highly organized. *J Biol Chem.* 2012 Apr 10. Copyright The American Society for Biochemistry and Molecular Biology, Inc. 2012.

Chapter 4 – Original manuscript in preparation for submission. **Valley CC**, and Sachs JN. Membrane cholesterol is required for Death Receptor 5 network formation and signaling.

Chapter 5 – Manuscript is in currently in revisions at *J Biol Chem.* Reproduced with permission from: **Valley CC**, Cembran A, Perlmutter JD, Lewis AK, Labello NP, Gao J,

and Sachs JN. The Methionine-aromatic motif plays a unique role in stabilizing protein structure.

Chapter A1 – Published manuscript reproduced with permission from **Valley CC**, Perlmutter JD, Braun AR, Sachs JN. NaCl interactions with phosphatidylcholine bilayers do not alter membrane structure but induce long-range ordering of ions and water. *J Membr Biol.* 2011 Nov;244(1):35-42. Copyright Springer Science, LLC 2011.

Ideas generated during the experimentation and writing of several other manuscripts have played a role in the creation of this thesis. These manuscripts are listed below and are cited accordingly throughout the text:

Lewis AK, **Valley CC**, and Sachs JN. TNFR1 signaling is associated with backbone conformational changes of receptor dimers consistent with over-activation in the R92Q TRAPS mutant. Biochemistry. 2012 Jul 16 (Manuscript in press).

Pineda DM, Rittenhouse DW, **Valley CC**, Cozzitorto JA, Burkhard R, Leiby B, Winter JM, Weber MC, Londin ER, Rigoutsos I, Yeo CJ, Gorospe M, Witkiewicz AK, Sachs JN, and Brody JR. HuR's post-transcriptional regulation of death receptor 5 in pancreatic cancer cells. *Cancer Biology & Therapy.* 2012 Aug 1;13(10) (Manuscript in press).

Chapter 1. Introduction to membrane-bound death receptors in targeted cancer therapy

The homeostatic balance between cell proliferation and cell death in multicellular organisms controls overall cell number in populations of dividing and regenerating cells. Precise control of this homeostatic balance is critical for normal growth and development and is further highlighted in the regeneration of short-lived cells, such as blood cells, in mature organisms. Moreover, aberrant control of either proliferation or death can result in improper cell accumulation or excessive cell loss (Figure 1-1, from [4]) marked by pathologies such as cancer (i.e. uncontrolled growth of tumor cells) or neurodegenerative diseases such as Alzheimer's disease (i.e. spontaneous death of nerve cells) [4]. The checks and balances governing cell proliferation have been well characterized, and pathways resulting in cell death are equally complex and important for maintaining a viable population of functional, differentiated cells.

Recent discoveries characterizing the mechanisms underlying initiation and propagation of programmed cell death, or apoptosis, are continuing to shape the landscape of therapeutics targeting a range of diseases from arthritis to cancer. Specifically, initiating apoptosis exclusively in cancer cells, often via membrane-bound death receptors, while sparing normal cells continues to be the gold standard in cancer therapy [5–7] and is thus a focus of many cancer therapeutics currently in clinical trials [8–13] (see also clinicaltrials.gov). Therefore, understanding events in the initiation of apoptosis through these death receptors is critical in the rational design of novel therapeutics targeting cancer. This chapter serves as an introduction into the signaling

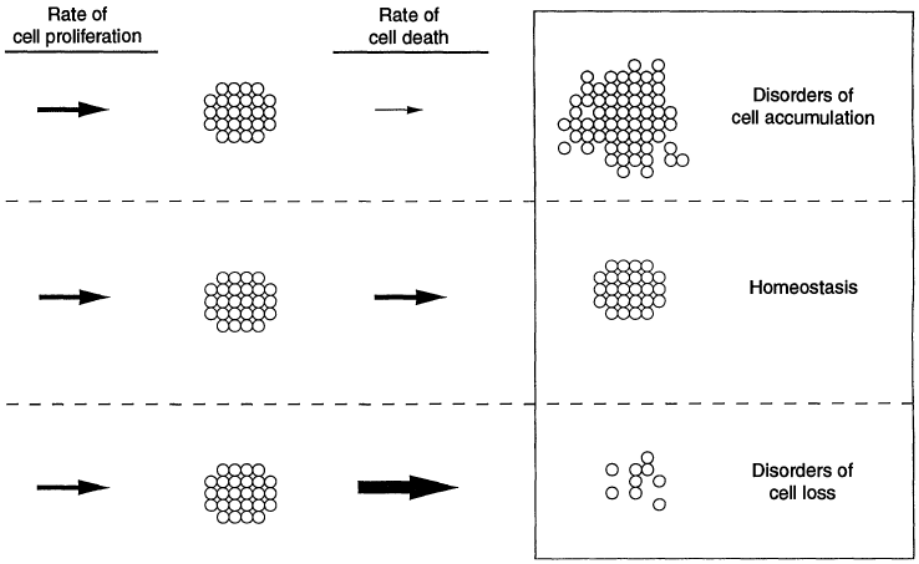

Figure 1-1. Homeostasis of cell populations in multicellular organisms involves proper regulation of the rates of cell proliferation and cell death. Aberrant control of either proliferation or death can lead to disorders of cell accumulation or cell loss (taken from C.B. Thompson, Science 1995 [4]**).**

pathways of programmed cell death through transmembrane (TM) death receptors, known as the extrinsic pathway of apoptosis. The goal of this introductory chapter is to familiarize the reader with the widely-accepted body of knowledge pertaining to tumor necrosis factor (TNF) receptor and death receptor signaling, including receptor structure and signaling events, both of which are critically important, as the overall scope of this thesis focuses on the relationship between the structure and function of these death receptors during early events of signal transduction within the membrane.

1.1. Apoptosis and the TNF superfamily

Apoptosis, a form of programmed cell death or cellular suicide, is triggered by one of two distinct, but not mutually exclusive, pathways known as the intrinsic (mitochondrial) and extrinsic apoptotic pathways (Figure 1-2, for review, see [14]). These

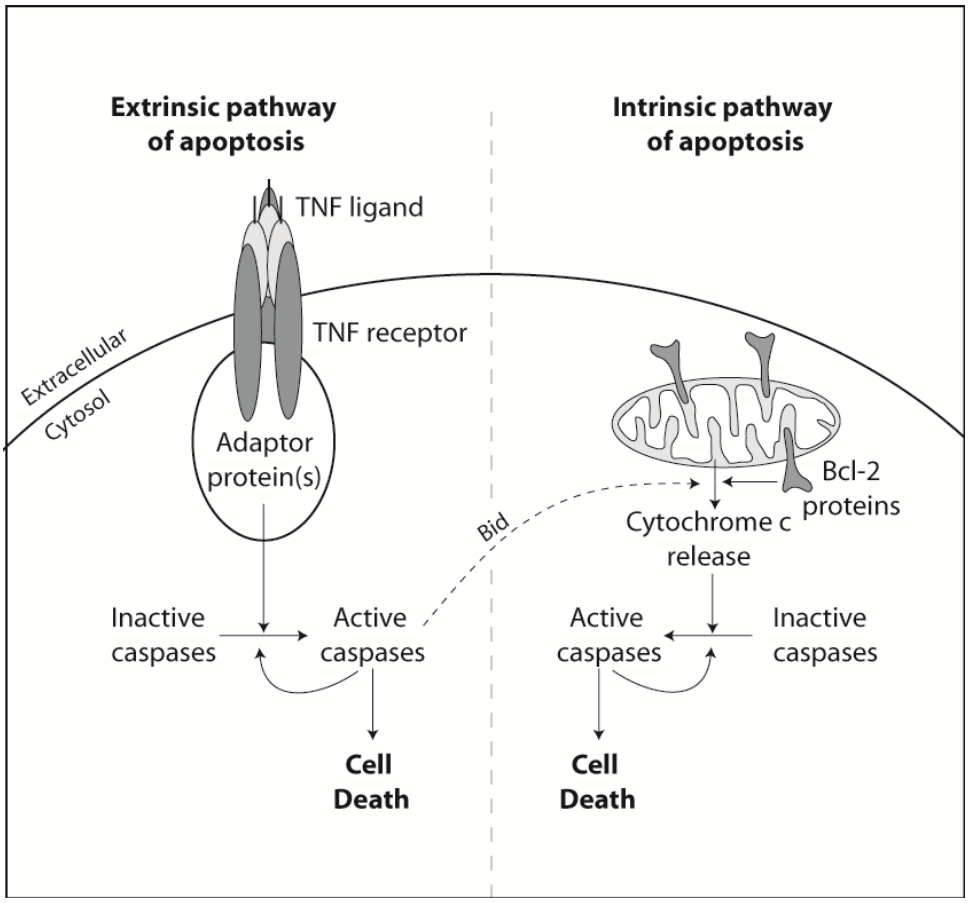

Figure 1-2. Apoptosis via the extrinsic pathway (left) and intrinsic pathway (right). The extrinsic pathway involves transmembrane tumor necrosis factor (TNF) receptors responding to extracellular TNF ligands, which initiates the intracellular pathways resulting in cell death. The intrinsic pathway involves Bcl-2 family of proteins regulating the release of cytochrome c from the intermitochrodrial space into the cytosol and subsequent cell death. These pathways are linked by Bid, a protein that, when cleaved by extrinsic activation, can activate the intrinsic pathway in a cell type-dependent manner. Activation of caspases is discussed below.

regulatory pathways yield several levels of control of cell death and allow a cell to initiate the suicide pathway from within the cell, for example in response to genetic damage (via the intrinsic pathway), and also allow for the ability to respond to death stimuli from neighboring cells or extracellular cytokines (via the extrinsic pathway), for example in the immunosurveillance.

The intrinsic pathway of apoptosis is regulated by a number of heterodimeric protein-protein interactions by proteins belonging to the Bcl-2 superfamily. The Bcl-2 family of proteins includes both pro-apoptotic and pro-survival members, which together work to positively and negatively regulate cell death [15,16]. Apoptosis via the intrinsic pathway ultimately results from the permeabilization of the mitochondria, and the release of cytochrome c from the mitochondrial inter-membrane space [17,18] (Figure 1-2, right). Cytochrome c within the cytosol triggers activation of the caspase cascade (caspases discussed further below) ultimately resulting in apoptotic cell death [19].

The extrinsic pathway of apoptosis (Figure 1-2, left), largely the focus of this thesis, is initiated in target cells via an external stimulus in the form of a ligand belonging to the TNF superfamily, a family of cytokines expressed either as soluble ligands present in the surrounding environment or as membrane-bound ligands anchored on a neighboring cell. The first two TNF ligands were discovered as anti-tumoral cytokines having 50% sequence identity and binding to the same membrane receptor. These ligands, which came to be known as TNF-α and TNF-β, were subsequently purified [20–23]. Based on their protein sequences, cDNA for TNF-α and TNF-β were cloned [24] and, using those cDNA sequences, a number of homologous TNF ligands were discovered. It is now known, 25 years after their initial discovery, that TNF ligands, of which there are approximately 20, initiate a range of physiological responses including inflammation (via the NFκB pathway), proliferation (via the MAPK pathway), and apoptotic cell death.

TNF ligands exert their effects by binding to cognate receptors expressed on target cells (Figure 1-3, taken from [25]). These type I TM receptors belong to the TNF receptor (TNFR) superfamily, and bind their respective TNF ligand (or ligands—some have multiple cognate ligands, and most ligands have multiple target receptors) with both high affinity and high specificity. The TNFR superfamily contains approximately 30 members (Figure 1-3) that are expressed in a range of cell types and tissues (see Appendix B, p. 181, for a list of ligands and receptors and their expression profiles) [26]. Although TNF receptors in general activate a range of intracellular pathways, every

receptor activates pro-inflammatory pathways primarily through NFκB. However, certain receptors preferentially activate alternative pathways, such as apoptosis.

TNF receptors can generally be classified into two categories based on the presence or absence of an intracellular death domain [27], a sequence of ~80 amino acids within the cytoplasmic domain (Figure 1-3, receptor death domains indicated by intracellular red boxes). The receptors that contain an intracellular death domain are capable of recruiting intracellular adaptor proteins that initiate apoptotic cell death, a number of which are currently being explored as "druggable" targets.

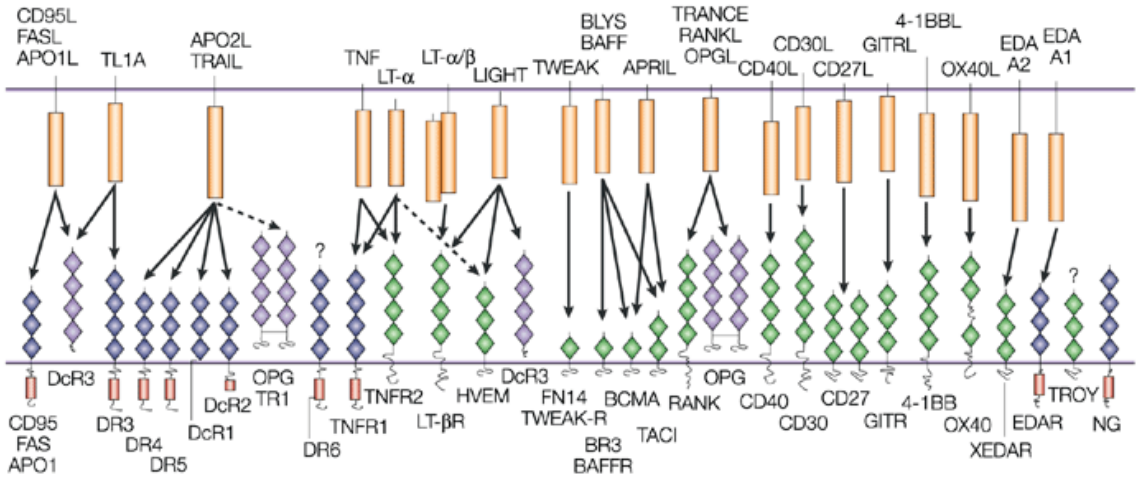

Figure 1-3. The TNF superfamily of ligands (top, orange rectangles) and receptors (bottom) illustrating ligand-receptor pairs (arrows). Within the receptors, the diamonds represent cysteine rich domains and red boxes represent receptor cytoplasmic death domains. (Taken from A. Ashkenazi. Nature Reviews Cancer 2004 [25]**).**

1.2. TRAIL and TRAIL receptors

Within the TNF superfamily exists a group of ligands and receptors whose primary function is the initiation of apoptosis [28]. These ligands, namely TNF-related apoptosis-inducing ligand (TRAIL, also called Apo2L) [29] and FasL (also called CD95L) [30], bind to transmembrane TNF receptors, TRAIL receptors and Fas (CD95), respectively, and initiate apoptosis. TRAIL has been shown to exhibit specific anti-tumor

activity, killing a range of tumor cells in culture and in animal models while sparing normal cells [31–38], in contrast to FasL and FasL-like agonists, which exhibit systemic cytotoxicity [39,40]. Therefore, TRAIL and TRAIL-like agonists are of particular interest in the treatment of cancer.

TRAIL, a 281 amino acid member of the TNF superfamily of ligands [29], is expressed as a type II membrane protein and can be cleaved at the cell surface to form a soluble TRAIL molecule. TRAIL, like all TNF ligands, functions by binding specifically to TRAIL receptors on the surface of target cells. There are four primary receptors for TRAIL: TRAIL-R1, -R2, -R3, and -R4 [41–46]. All TRAIL receptors contain an extracellular ligand-binding domain and a single-pass α-helical TM domain. TRAIL-R1 and -R2 (death receptor 4 or DR4, and death receptor 5 or DR5, respectively) contain an intracellular death domain and are thus capable of initiating apoptosis [47]. TRAIL-R3 and -R4 (known as decoy receptors 1 and 2, or DcR1 and DcR2, respectively) either lack or have a truncated intracellular death domain and are unable to initiate apoptosis upon ligand stimulation (Figure 1-4). Death and decoy receptors together regulate sensitivity to TRAIL by promoting and inhibiting TRAIL-induced apoptosis, respectively [48,49]. That cancer cells, compared to normal cells, display increased sensitivity to TRAIL has led to the reasonable speculation that the relative expression level of death and decoy receptors determines overall sensitivity to TRAIL and agonists [33,50]. However, receptor expression is widely varied across cell lines [51] with no obvious correlation between TRAIL-sensitive and TRAIL-resistant cells. TRAIL sensitivity is further complicated by receptor post-translational modifications [52] as well as intracellular regulatory proteins [51,53]. To date, it is not entirely clear why tumor cells display increased sensitivity to TRAIL, nor is it understood why certain tumor cells are TRAIL resistant.

Expression of DR5 is tightly regulated, both at the transcriptional and translational level. DR5 is expressed in a p53-dependent and p53-independent manner [54]. In response to DNA damage, DR5 is upregulated in response to p53 activation [7,54–56]. TRAIL works synergistically with other death-inducing agents via the p53-dependent expression of DR5 that sensitizes cancer cells, but not normal cells, to TRAIL

[57]. Therefore it is plausible that activation of p53 via existing chemotherapeutics may sensitize TRAIL-resistant cells to DR5-targeted therapies. As such, a tremendous amount of work has gone into investigating the combined effects of DR5 ligands (including TRAIL and antibody agonists) in combination with existing therapies that upregulate DR5 at the cell surface and sensitize cancer cells to DR5-induced apoptosis (for a non-exhaustive list of examples, see [58–65] or for review, see [66–70]). However, to date, little work has been carried out to study the molecular mechanism of TRAIL- and agonist-induced apoptosis through DR5.

1.3. TRAIL – death receptor signaling

TRAIL induces apoptosis by binding death receptors at the cell surface thus initiating signal transduction across the membrane. Within the cell, ligand-induced signaling events are relatively well-defined. After receptor engagement by ligand outside the cell, the intracellular death domain recruits intracellular adaptor proteins to form the death-inducing signaling complex (DISC) [71]. The DISC is comprised of activated receptor death domains, the Fas-associated death domain (FADD), and procaspase-8 (Figure 1-4) [47,72,73], through complex interactions involving death domains and death effector domains within these proteins [74–78]. Procaspase-8, upon binding FADD, is activated to caspase-8 thus initiating the cell death process within the cell.

Caspases are the intracellular executioners of apoptotic cell death [79,80]. Generally, caspases, or cysteine-aspartate specific proteases, are synthesized and constitutively expressed as inactive zymogens known as procaspases. Their activation involves proteolytic cleavage from a full length procaspase zymogen, releasing the N-terminal death effector domain (DED) and also resulting in two caspase fragments ranging in size, on the order of 10 and 20 kD. The heterodimeric interaction between these cleaved subunits forms the catalytic domain [81,82].

Apoptotic caspases are divided into two groups, initiator and effector caspases. Initiator caspases, such as caspase-8 and -10 (within the extrinsic pathway) or caspase-9

(within the intrinsic pathway) are the first caspases activated in response to a death signal. Activated initiator caspases cleave and activate effector caspases, such as caspase-3, and active effector caspases are directly responsible for the digestion of proteins critical for cell function [80]. The amplifying pathway of initiator/effector caspase activation is known as the caspase cascade.

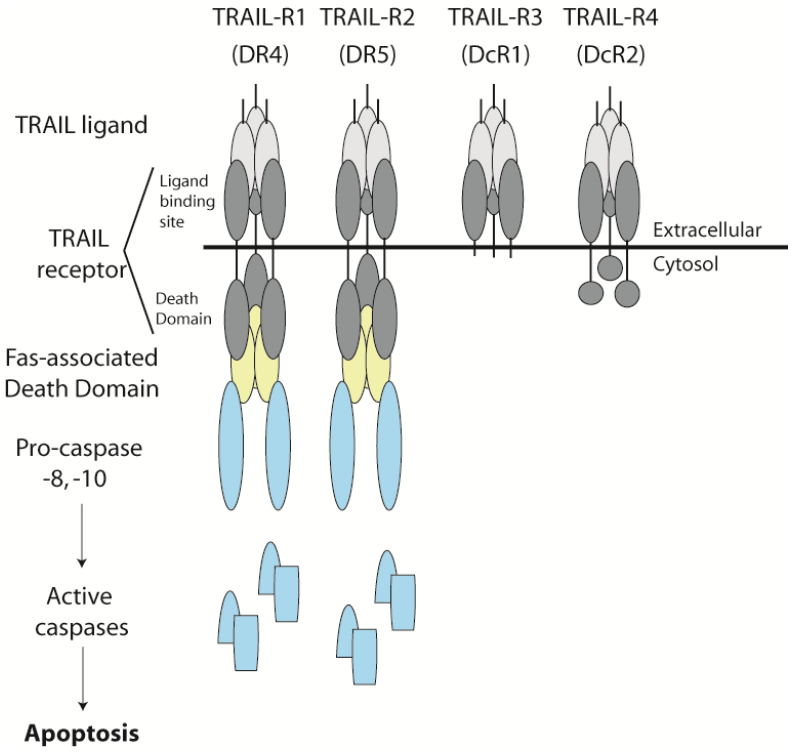

Figure 1-4. A summary of TRAIL receptor signaling. All TRAIL receptors have an extracellular ligand binding domain. TRAIL-R1 and -R2 (death receptor 4 and 5, respectively) have intracellular death domains capable of recruiting downstream factors, such as FADD and caspase-8. TRAIL-R3 and -R4 (decoy receptors 1 and 2) either lack an intracellular death domain or have a truncated, inactive death domain and are incapable of intracellular signaling.

TRAIL activation of DR5 initiates the caspase cascade primarily through activation of caspase-8 [83], although in the absence of caspase-8, activation of the homologous caspase-10 also occurs via DISC formation. According to the "Induced

Proximity" model [84–86], clustering of procaspase-8 upon recruitment to the DISC results in activation by autoproteolytic cleavage [87]. Therefore the structure arrangement of death receptors in the membrane, and the ligand-induced structural rearrangement, is an important factor in recruitment and activation of downstream signaling molecules.

1.4. TNF ligand-receptor complexes: Structure and Function

The function of TNF ligand-receptor complexes is intrinsically linked to the structure of these proteins. Numerous crystal structures have been solved of TNF superfamily members, which include soluble trimerized ligands [88–93], monomeric receptors [94,95], pre-assembled receptors [96,97], and ligand-receptor complexes [94,98–104]. Collectively, these structural studies show that ligand and receptor members within the TNF family have a general structural homology. The ligands consist primarily of β-sheet secondary structure, and sequence alignment predicts that the majority of TNF ligands share in this structural homology. Receptor extracellular domains are generally lacking in secondary structure but are held together by a series of cysteine rich domains (CRDs), with numerous disulfide bonds within these CRDs giving TNF receptor members a high degree of structural homology despite having low primary sequence homology.

TRAIL has the same basic fold and secondary structure as other TNF family ligands [92], having a β-sheet jelly roll fold that is predominant within the interior of the ligand. Each TRAIL monomer is made up of two β-sheets, with each sheet comprised of four β-strands. Soluble TRAIL exists primarily as a homotrimer, with one of the β-sheets buried upon ligand trimerization. Additionally, the structure reveals the presence of a metal binding site near the bottom of the ligand trimer made up of three cysteine residues (Cys230 in each TRAIL monomer within the symmetric trimer) bounded through a zinc ion. This metal binding motif is critical for TRAIL stability and cytotoxicity [92,105–107], and removal of the zinc ion by chelating agents reduces TRAIL cytotoxicity 90-fold [92].

DR5 is the only TRAIL receptor for which a crystal structure exists. Based on these structural studies [99–101], the DR5 extracellular domain is comprised of three CRDs that maintain the structure of the extracellular domain. DR5 interacts with the TRAIL primarily through two elongated loops that come in close proximity with regions of the ligand. These loops, called the 50s loop (residues 51-65) and 90s loop (residues 91-104) [99], make up the bulk of the interface between the wedge shaped ligand and the receptors, found at the interface formed between ligand protomers within the trimerized ligand (Figure 1-5, A and B, a specific motif in the 90s loop is characterized in Chapter 5). In the ligand-bound state, the three receptor protomers are entirely independent, separated by the length of the ligand (Figure 1-5, A). Based on the position of the last resolved residue proximal adjacent to the putative transmembrane domain, the structure suggests a receptor TM separation of 50 angstroms between monomers [99], and thus the TM domain has been presumed to play no role in ligand-induced signal transduction across the membrane.

The homologous lymphotoxin-α-TNFR1 complex, solved in 1993 [98], shows a similar ligand fold and a comparable receptor symmetry, forming an axisymmetric complex of three tightly interacting ligand protomers and three non-interacting receptor protomers, each found at the groove formed by two adjacent ligand units (Figure 1-5, C). The TRAIL-DR5 and LTα-TNFR1 complexes share a high degree of structural homology (Figure 1-5, compare A and C, B and D). Based on the overall structural homology, the relevant signaling complex has been considered to be ligand-induced trimerization of receptors within the membrane.

The notion of ligand-induced trimerization of monomeric receptors within the membrane was first put into question in 2000, when a domain within the extracellular region of the receptor was found to drive the ligand-independent assembly of Fas [108], TNFR1, and TNFR2 [109]. This domain, named the pre-ligand assembly domain (PLAD), is found within the membrane distal region of the receptor (within CRD1), and drives the ligand-independent assembly of receptors within the membrane. Moreover, the

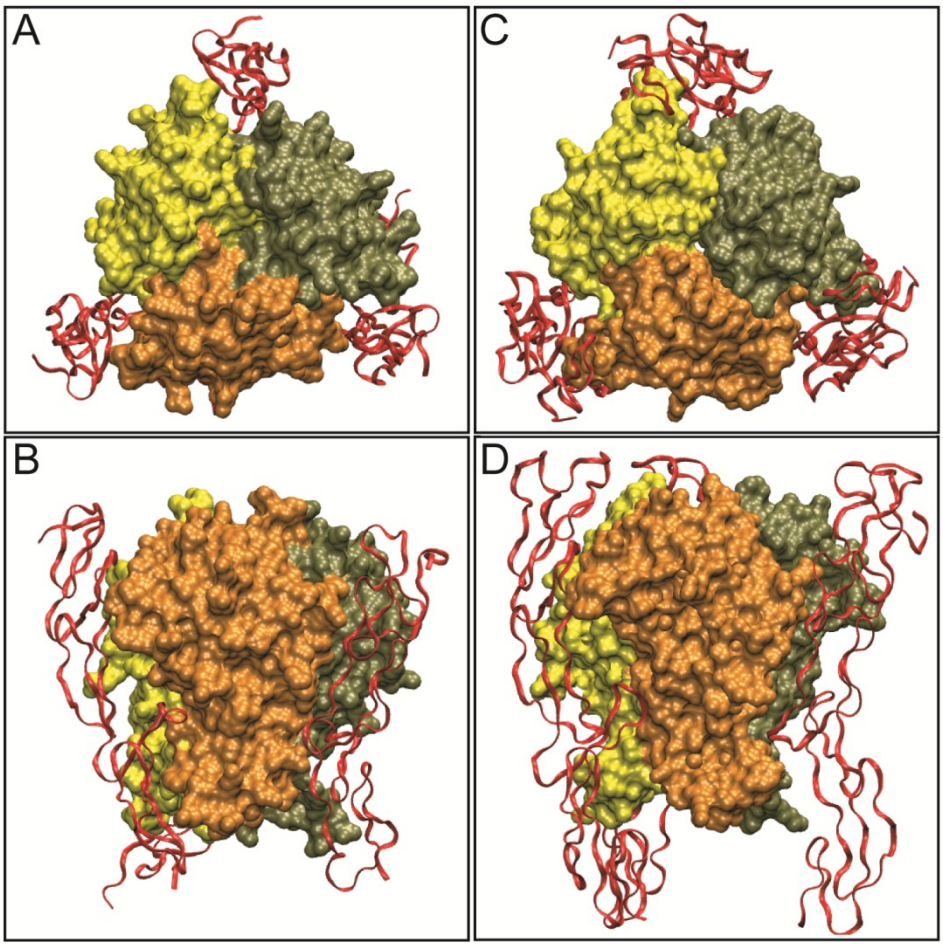

Figure 1-5. (A-B) The TRAIL-DR5 complex (PDB ID 1d0g, from Hymowitz et al. [99]**) shows a tightly interacting trimeric TRAIL (shown as surface representation in yellow gray and orange) recruiting three non-interacting receptor protomers (shown as ribbons in red). Shown is the top view (A) and the side view (B). The predicted transmembrane domain follows the last resolved receptor residue at the bottom. (C-D) The structurally homologous LTα-TNFR1 complex (PDB ID 1tnr, from Banner et al.** [98]**) again shows the trimeric LTα (surface representation, yellow, gray and orange), and three non-interacting receptor protomers (red ribbons). Shown is the top view (A) and side view (B).**

location of the PLAD is in agreement with the region of TNFR1 that forms extensive receptor-receptor contacts in a ligand-independent crystal structure [97]. The PLAD has also been shown to promote hetero-oligomeric interactions between death and decoy receptors for TRAIL, and thus ligand-independent assembly is thought to play an important role in the regulation of TRAIL-induced death [110]. In all cases, deletion of

the PLAD prevents not only ligand-independent receptor interactions but also reduces ligand binding and abolishes ligand-dependent activity. Thus it was presumed, based on large deletions, that ligand-independent receptor assembly is required for ligand binding and function. That is, the ligand-induced receptor structure is somehow intrinsically linked to the ligand-independent receptor structure, and therefore ligand binding may induce a structural reorganization of pre-assembled receptors within the membrane rather than simply coordinating a trimeric receptor assemblage of monomeric units.

Our understanding of the interactions within the soluble domains—both intracellular and extracellular—is substantial in comparison to the role of the TM domain, which is yet unknown and largely unstudied. Evidence of this exists in a number of TRAIL-DR5 signaling schematics within the literature whereby DR5 signaling involves extensive interactions within the extracellular and intracellular domains, and no role of the TM domain (our own version of this schematic is shown in Figure 1-4, compare interactions in the extracellular, TM, and intracellular domains). Moreover, recent evidence has shown that ligand-dependent activity involves the formation of large receptor aggregates within the membrane, on the order of 300-500nm in diameter (which, given the size of the crystal structure, would include hundreds of trimeric units), for both Fas and DR5 [111,112]. Therefore, the notion that the trimerized complex is the relevant signaling structure is giving way to large, organized networks of ligands and receptors. That crystallography of numerous complexes is in disagreement with observations of the protein within the plasma membrane highlights the structural importance of domains not found within the crystal structure, and that the relationship between the structure and function is highly dependent on the interactions involving multiple domains.

The next chapter will review the TRAIL-DR5 (and other TNF ligand-receptor pairs) signaling pathways in the context of these recent discoveries, namely that the structure-function relationship involves the formation of large networks within the plasma membrane, and that the membrane itself—including TM and membrane-proximal residues of the receptor—play a critical role in signaling.

Chapter 2. TNF receptor clustering and network formation in the membrane

The tumor necrosis factor (TNF) superfamily is comprised of approximately 20 cytokine ligands that regulate a range of physiological responses including inflammation and cell death. TNF ligands exert their effects by binding to transmembrane TNF receptors (TNFRs), of which there are approximately 30 with each binding to one or two specific ligands [25,113] (Figure 1-3, p. 8, and see Appendix B, p. 181). Upon ligand binding, TNFRs undergo an unknown structural or stoichiometric change and subsequently trigger signaling across the plasma membrane into the cell. Although there has been much speculation about ligand-induced, receptor-mediated signal transduction, the molecular mechanism by which extracellular events propagate signal transduction across the membrane is poorly understood. Given their involvement in a number of physiological and pathological processes, it is critical to understand these aspects of TNF signaling, as these membrane receptors provide a number of potential targets in the treatment of various pathologies from rheumatoid arthritis to cancer.

In Chapter 1, the role of individual domains within TNFRs was described in detail. However, our understanding of individual components of these receptors is sophisticated in comparison to the concerted function of the entire protein. Further, the relationship between the structure and function of TNF receptors is complicated by recent evidence that they function as macromolecular receptor aggregates within the complexity of the plasma membrane [111,112,114]. Although an increasing amount of evidence points to the formation of large TNF ligand-receptor networks in the membrane, TNF signaling is rarely discussed in the context of network formation. Moreover, the membrane is known to play a role in TNF receptor signaling, often through lateral

heterogeneity in the form of so-called lipid rafts [115,116], however it is unknown how the membrane regulates signaling at a basic level. The paradigmatic relationship between TNF receptor structure, dynamics, and environment dictate receptor function in response to an external stimulus, in this case a TNF ligand.

The goal of this chapter is to explore the relationship between structure, dynamics and environment of TNF receptor members in the context of ligand-induced network formation. These structural, dynamic, and environmental changes involve explicit biophysical interactions within extracellular, intracellular, and TM domains and involve ligands, receptors, and downstream proteins. These signal transduction pathways are also driven in part through the interaction between proteins (both ligand and receptor) and the membrane. We therefore review the active regulation of signaling by the plasma membrane and the role of the membrane in driving network formation and TNF signaling. Future chapters will focus on elucidating the mechanism and structure of network formation within the membrane (Chapter 3) as well as the active role of these lipid microdomains in the driving the interactions that stabilize these networks (Chapter 4).

2.1. Stoichiometric structural disagreement as evidence for TNFR1 networks

The primary structure of TNF receptors is both well-characterized and generally conserved among all TNFRs [117]. Our collective knowledge of the secondary and tertiary structure of these receptors is largely based on crystallography of several structurally homologous complexes [93,97–101]. The relationship between the structure and function of tumor necrosis factor (TNF) receptors was originally based on several homologous crystal structures that suggested function was a consequence of a ligand-induced stoichiometric receptor change. In 1993, Banner et al. solved the first crystal structure of the prototypical TNF receptor, TNFR1, in complex with one of its two common ligands, lymphotoxin-α (LTα, also called TNFβ) (Figure 2-1 A, side view) [98]. Within this complex, the trimeric LTα recruits three non-interacting receptor protomers,

with each receptor protomer forming extensive contacts with two of the three symmetric ligand protomers (Figure 2-1 B, top view, and C, schematic). Therefore, the generally accepted mechanism for TNFR1 activation was a stoichiometric recruitment of three receptor monomers which caused intracellular domain aggregation and subsequent activation. This mechanism for ligand-induced trimerization was also in agreement with ultracentrifugation studies of soluble extracellular domains of TNF ligand-receptor showing TNFR exists as a monomer in solution, and that the ligand-bound complex favors a stoichiometry of three receptor units for each trimeric ligand [118].

In 1995, Naismith et al. produced two dimeric structures of TNFR1 in the absence of ligand thus providing, in their interpretation, the first indirect structural evidence for network formation [97]. These two structures, denoted parallel and anti-parallel conformations, represent two potential stable conformations of receptor dimerization in the absence of ligand, where the parallel conformation is generally the accepted ligand-independent structure of TNFR1. The anti-parallel conformation is considered the less relevant of the two structures for several reasons. First, for interactions reported in the anti-parallel structure to exist, both receptor protomers would lie flat on the membrane, inconsistent with the upright conformation of the trimeric structure. Also, residues involved in dimeric interactions between receptor protomers in the anti-parallel conformation overlap those involved in interactions between ligand and receptor, and therefore the anti-parallel structure precludes TNF binding. That the general acceptance of the parallel model over the anti-parallel model is in part a result of the physical location of the two receptors with respect to the membrane highlights the importance of physical restrictions provided by the membrane in dictating receptor oligomerization.

The parallel receptor structure, however, places both receptor protomers upright in the membrane (Figure 2-1 D, side view, and E, top view). Moreover, the extensive non-covalent interactions between membrane distal regions in CRD1 (which later became known as the PLAD [109]) of each receptor protomer are distinct from TNF ligand binding regions reported in the trimeric structure. Therefore, it is conceivable that ligand-independent dimeric receptor interactions (schematized in Figure 2-1 F) persist after

binding the trimeric ligand (schematized in Figure 2-1 C). The resulting model, proposed by Naismith et al., simultaneously combines the trimeric ligand-receptor interactions (Figure 2-1, B and C) and dimeric receptor-receptor interactions (Figure 2-1, E and F) thus producing the first instance of a ligand-induced hexagonal network (schematized in Figure 2-1G) [97]. However, all of the aforementioned studies neglect transmembrane and intracellular residues as well as the membrane itself which, as described later, provide important biophysical interactions that are involved in the structure of these ligand receptor networks, and are not captured by crystallography of the extracellular, soluble domain alone.

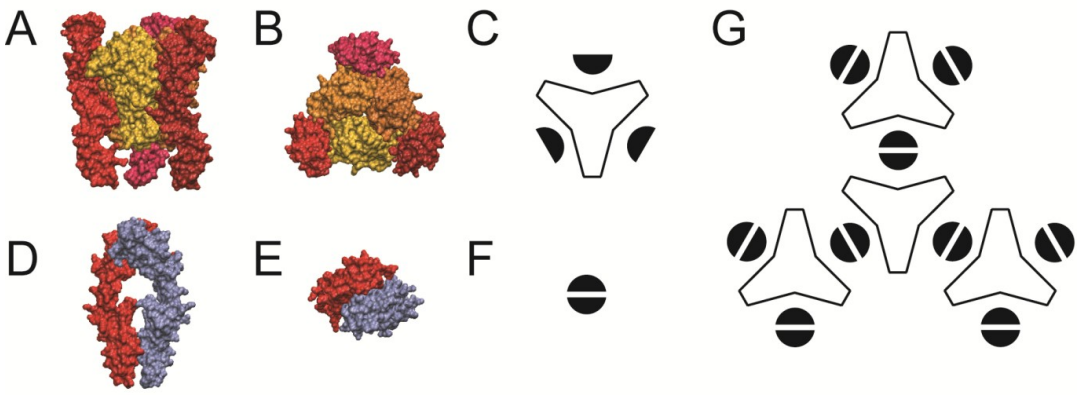

Figure 2-1. (A-C) Crystal structure of LTα-TNFR1 complex [98]**; shown is the (A) side view, where the membrane would be at the bottom, (B) top view, and (C) top view schematic. LTα is shown in yellow/orange and the TNFR1 receptor is shown in red. (D-F) Crystal structure of the ligand-independent TNFR1 dimer complex** [97]**; shown is the (A) side view, membrane would be at the bottom, (E) top view, and (F) schematic. Two identical receptor protomers are shown in red and blue. (G) Schematic of network formation based on ligand-receptor trimer structure (C) and receptor-receptor dimer structure (C), taken from Naismith et al.** [97]**.**

2.2. Death receptor structures: Extracellular trimerization and intracellular dimerization

Trimeric crystal structures of TRAIL alone [92] and in complex with DR5 were later solved in 1999-2000 [99–101], offering further evidence that the trimeric ligand recruits three non-interacting receptor protomers to form a trimeric ligand-receptor complex. Structurally homologous to the LTα-TNFR1 complex [98] (see Figure 1-5, page 14), activation of DR5, like TNFR1, was considered a stoichiometric event, whereby TRAIL co-recruitment of three receptor protomers, which resulted in death domain "clustering" and intracellular activation. However, the precise stoichiometry of these ligand-induced death domain "clusters," as they were often called, is not commonly specified, highlighting the uncertainty in the mechanism of signal transduction across the membrane. Further, since the crystal structures of the TRAIL-DR5 complexes (as well as that of LTα-TNFR1) are comprised only of the extracellular domains of both ligand and receptor, it is yet unclear whether activation is a result of a stoichiometric engagement of the ligand, or a ligand-induced structural change of pre-assembled receptors, since no ligand-independent crystal structure of DR5 exists. In either case, as with TNFR1, the role of the transmembrane domain has largely been unexplored, and therefore it is unknown precisely how ligand-induced extracellular events dictate intracellular activation.

Upon activation, the intracellular death domains of DR5 recruit the Fas-associated death domain (FADD) [47,74–76,119], and FADD then recruits the initiator caspase-8 or caspase-10 [83,120]. Coincidentally, around the same time as crystal structures were solved for trimeric TRAIL-DR5 complexes, several research groups solved the crystal structure of caspase-8 and simultaneously published their findings which, from the intracellular perspective, offered a different view of death receptor stoichiometric activation [121,122]. The active caspase-8 is comprised of a heterodimeric interaction between α and β proteolytic subunits, denoted p12 and p18 after their observed molecular masses. The symmetric homodimer is formed through extensive interactions between like β-strands in apposed p12 subunits, and each p12 subunit in turn forms close interactions

with the p18 subunit. The surrounding α-helices form the substrate binding sites, as shown by the active caspase-8 in complex with an inhibitor, ZEVD [121]. Therefore, while the extracellular domain is widely considered trimeric, the active caspase-8, comprised of two p12-p18 subunits (in a p18-p12-p12-p18 conformation) is dimeric in nature.

Further support for a model of caspase-8 dimerization came in two simultaneously published papers in 2003 showing that the active form of caspase-8 is indeed dimeric [123,124]. Through *in vitro* studies of purified caspase-8, Donepudi et al. [124] compare the oligomeric state and activity of wild type procaspase-8 with a mutant form unable to undergo autoproteolytic cleavage. Using size exclusion chromatography, the wild type, cleavable procaspase-8 elutes as a mixture of monomers and dimers (where monomer indicates the α/β unit, and dimer indicates two α/β units, as described above). Size exclusion chromatography of the uncleavable caspase-8 mutant eluted largely as monomeric with low enzymatic activity. Interestingly, the very small amount of dimeric caspase-8 was as enzymatically active as the wild type caspase-8 dimer, leading the authors to conclude that dimerization precedes proteolytic processing and is the driving force for caspase-8 activation. Similar results were observed using gel filtration chromatography to isolate fractions containing the monomeric and dimeric caspase-8, where the majority of enzymatic activity is present in the dimeric fraction [123]. A model for dimer-induced activation of caspase-8 is consistent with other caspases, notably caspase-1 [125] and caspase-9 [126,127], for which similar data exist.

In addition to supporting the dimeric model of death receptor activation, caspase-8 exists in a balance between monomeric and dimeric forms, with the dimeric state favored at high concentrations. This idea that local concentrations play a role in self-activation is in support of the so called “Induced Proximity” model, introduced in 1998 [84–86], suggesting that proximity-driven caspase-8 dimerization results in autoproteolytic cleavage and activation. For caspase-8, the Induced Proximity model was supported by evidence that chemically induced dimerization of an engineered, transiently overexpressed procaspase-8 results in self activation and subsequent cell death. Induced

Proximity models for TNF receptor associated proteins, such as RICK, RIP and IKK complexes, have also been proposed in a similar series of experiments, with transient overexpression and induced dimerization [128]. However, it is unclear whether induced proximity by engineered dimerization event relates to the physiological dimerization induced by initiation of the DISC through receptor structure within the membrane.

More recently, several crystallographic studies have solved separate components of the DISC, including the receptor death domain in complex with death domain of FADD. Scott et al. [129] solved the structure showing a tetrameric arrangement of four Fas receptor death domains in complex with four FADD death domains. However, this tetrameric structure represents two dimeric complexes, and therefore the authors conclude that Fas-FADD dimerization permits stabilization of the DISC complex, and activation of caspase-8 occurs via dimerization within large organized networks of extracellular trimers and intracellular dimers [129]. In a separate structural study by Wang et al. [130], the crystal structure of the Fas-FADD death domain is suggested to form via a clustering of numerous repeats. Specifically, the complex was found to be a large assemblage of between five and seven Fas death domains and five FADD subunits, and the predicted interface in this Fas-FADD cluster contains disease-related mutations. Therefore, there remains some ambiguity in the mechanism by which the Fas-FADD DISC is formed, and it is still unclear how trimeric ligand binding outside the cell induces proximity, either dimeric or multimeric, of intracellular domains. In either case, the formation of organized ligand-receptor networks could conceivably provide either Fas-FADD dimers, at the receptor-receptor boundary, or Fas-FADD multimers (between 5-7 units), as the vertices within a hexagonal network. Therefore, despite ambiguous structural and functional data, the network hypothesis does not preclude either result but warrants further investigation into network structure.

2.3. TNF receptor clustering inferred via detergent resistance

Fas ligand (FasL, CD95 ligand, APO-1L) and its cognate receptor Fas (CD95, APO-1), in their early discovery as an apoptosis-inducing ligand-receptor pair, ca. 1990 by Shigekazu Nagata [131], rapidly became the prototypical apoptosis-inducing pathway within the TNF receptor superfamily. The first evidence of Fas receptor aggregation was noted by the observation of high molecular weight (~220 kD), SDS- and β-mercaptoethanol (βME)-resistant clusters of Fas, observed by Western blot, induced by the addition of Fas ligand and anti-Fas antibody [71,132,133], although there remains discrepancy as to whether both induce such clusters [133]. Further, compared with the monomeric Fas receptor, these high molecular weight aggregates recruit intracellular signaling factors including FADD and caspase-8 as observed by immunoprecipitation of the DISC [134]. Therefore it was first proposed that ligand stimulation led to rapid aggregation of Fas in the membrane and subsequent DISC formation and activation of initiator caspases.

Clustering of Fas in response to ligand is associated with receptor redistribution into lipid rafts, characterized by their enrichment in sphingomyelin within the membrane and thus the generation of ceramide, and this increase in ceramide which drives formation of large lipid rafts [135]. It was later determined that cysteine palmitoylation of Fas provided a driving force for ligand-induced aggregation, and cysteine mutagenesis prevented both aggregation [134], and subsequent function [136]. Further, palmitoylation of Fas in response to ligand is associated with this redistribution into ceramide-rich microdomains [134,136]. Therefore, while resistance to detergent (SDS) and reducing agents (βME) may be used to characterize protein clustering, it is unclear whether detergent resistance is a result of extensive interactions between proteins (either receptors, ligands, or both), or is a result of ligand-induced changes in the biophysical properties of the membrane. Therefore, if both clustering and raft localization are studied using resistance to specific detergents, detergent resistance itself confounds the very result of raft localization and vice versa (discussed below).

2.4. Identifying clustering by fluorescence microscopy: SPOTS

Further evidence for the formation of large receptor clusters was discovered through fluorescence microscopy, published by a number of groups on several ligand/receptor pairs. The first notable result by Siegel et al. [111] characterized a change in the fluorescence pattern of immunostained Fas from a diffuse pattern in the plasma membrane in the absence of ligand to a punctate pattern representing a coordination of receptors in the membrane upon ligand stimulation. These macromolecular aggregates of Fas, on the order of 300-500 nm in size, were termed signaling protein oligomeric transduction structures, or SPOTS. SPOTS form rapidly in the membrane upon stimulation by ligand. Although Fas aggregation had been reported based on detergent resistance (as described above), the discovery of these clusters by fluorescence microscopy added additional complexities in that SPOTS formation depend highly on intracellular domains as well as downstream proteins; Fas DD mutation (disease related) or deletion both inhibit SPOTS formation as does the lack of FADD or caspase-8 [111]. Therefore, original crystallographic studies using only extracellular, soluble domains likely fail to capture important biophysical interactions within the TM and intracellular domains.

Similar experiments utilizing high-resolution fluorescence microscopy established a clustering paradigm for both TRAIL- and antibody agonist-mediated apoptosis through death receptor 5 [112,114,137]. The antibody, Apomab, binds DR5 specifically and induces receptor clustering and internalization, consistent with recruitment and activation of the DISC complex (including FADD and caspase-8) and ultimately apoptotic cell death, both in cultured cancer cells and in human pancreatic adenocarcinoma transplant xenograft models in nude mice. Also consistent with induced receptor clustering, cross-linking of Apomab ligand augments the activity in killing human tumor cells, but Apomab (regardless of cross-linking) has no effect on primary hepatocytes in culture. However, it is unknown whether cross-linking has any effect on the antitumor activity of Apomab *in vivo* in mouse xenograft models. Therefore the organization of the ligand plays a role in efficacy, conceivably through differences in induced receptor clustering,

and warrants further investigation (cross-linking and the organization of ligands discussed further below).

Receptor clustering at the cell surface is consistent with DISC recruitment and activity, therefore the formation of clusters may be useful in determining potential drug efficacy. Despite quantitative data regarding the level of SPOTS formation, the methodology for counting SPOTS involved a blind user counting clusters in over > 100 cells rather than a more robust algorithm [111]. Therefore, there is a need for a more universal method for quantification of the number and size of these clusters, and automation could provide more detailed analysis over a greater number of samples in, for example, tracking cluster formation during the course of receptor activation. We have developed an algorithm to quantify size and number of SPOTS based on high resolution fluorescence images and are currently exploring the time evolution of SPOTS formation as well as under different treatments to perturb the membrane of the target cell (see Chapter 4).

2.5. The structural organization of TNF ligand-receptor networks

The current methodology to investigate the formation of ligand-receptor clusters includes detergent-resistance, high resolution fluorescence microscopy, and cross-linking studies, however these methods do little to establish whether receptor clusters in the membrane resemble non-specific aggregation, or whether these clusters have a well-defined organization within the membrane. Despite the lack of evidence, there has been speculation regarding the organization of these clusters [97,138,139]. The most reliable of these is based on TNFR1 dimeric and trimeric crystal structures (Figure 2-1) [97], however careful examination reveals limitations not previously discussed, and network formation in the membrane via this model requires a structural transition (discussed below) [140].

Others have generated models of ligand-receptor networks, both for TNFR1 and DR5. For example, Ozsoy et al. also postulated that TNFR1 and TNFR2 undergo a

specific ligand-induced structural rotation and subsequent structural transition from ligand-independent dimers to form the ligand-receptor hexagonal mosaic network [138]. However there is little experimental evidence to suggest such detail in a molecular model. Alternatively, Francis Chan has generated a network stabilized through extensive contacts in both ligands and receptors via trimeric receptor interactions (rather than dimeric) within the membrane [139]. Further, the ligand-independent structure of this model, either dimeric or trimeric, undergoes an unknown conformational change where PLAD interactions are lost. The model also does not speculate as to what regions of the receptor (or ligand) drive clustering. Regardless of the model, it seems clear that the idea of stoichiometric-based activation, that ligand recruits three monomeric receptors, is losing credibility to a model where pre-assembled receptors undergo a (yet unknown) structural change causing extracellular network formation, intracellular DISC assembly, and activation.

We have provided the first evidence that ligand induced DR5 networks contain repeating units of receptor dimers, mediated via covalent and non-covalent interactions in both isoforms of DR5, described in depth in Chapter 3 [114]. These experiments—which utilize a cysteine residue unique to one DR5 isoform along with FRET—represent the first structural evidence that activation by ligand (both TRAIL and antibody agonists) induce a dimerization event of receptors—consistent with the active structure of intracellular domains and downstream proteins described above.

2.6. The structural organization of TNF ligands

Although the focus of this chapter—and this thesis—is the lateral organization of receptor networks within the membrane of target cells, it is critical to note that the organization of the ligand is equally important in determining functional outcome. TNF is a type II transmembrane protein and is therefore expressed as a single pass, membrane bound TNF from which metalloproteinase-mediated cleavage at the membrane results in the soluble TNF [141,142]. Moreover, the membrane-bound TNF (mTNF) and soluble

TNF (sTNF) have been shown to have distinct functions (for review, see [143]), with sTNF largely responsible for inflammatory response whereas mTNF is responsible for protecting against bacterial infections, chronic inflammation, and autoimmunity in mouse models [144].

Further, mTNF and sTNF have differential function in part due to their preferential binding to certain TNF receptors [145], though results are somewhat ambiguous. Studies have shown that mTNF signals primarily through TNFR2, and sTNF signaling through both TNFR1 and TNFR2 [146], however it has also been shown that immobilized TNF signals through both TNFR1 and TNFR2 and sTNF signals exclusively through TNFR1[147]. Similar results have been observed for TRAIL [145] and Fas [148,149], whereby membrane and soluble ligands trigger different responses and/or with different levels of activity. Moreover, the activity of soluble ligands (including TNF, Fas, and TRAIL) is linked to the use of cross-linkers, which can be used to cluster multimers of soluble ligands thereby partially recovering the function of the membrane-bound ligand. Fas has been shown to exhibit increased activity upon cross-linking, which produces two adjacent trimeric ligands [150]. Similarly, different TRAIL cross-linking requirements result in a differential ability to activate DR4 and DR5, with DR5 responding to cross-linked TRAIL and DR4 responding to cross-linked or non-cross-linked TRAIL [151]. The organization of TNF has been neatly explored using ligand-coated nanoparticles, resulting in differential activation of TNFR1 and TNFR2, depending on its conjugation to nanoparticles ranging in size from 0.1μm - 10μm [152]. These coated nanoparticles provide immobilized TNF in a manner similar to mTNF but more easily applied in controlled experimental systems and may allow for studying a range of ligand surface densities.

The organization of the ligand appears to be inherently linked to the structure of the receptor in the membrane. Specifically, studies comparing the extracellular, membrane-proximal “stalk” region of TNFR1 and TNFR2 have demonstrated clearly that the presence of an elongated stalk, as in TNFR2, precludes sensitivity to soluble ligand [147]. Moreover, this inhibitory effect of the stalk region is due to chemically specific

residues within this region, as mutation of the TNFR2 stalk to chemically inert residues regains sensitivity to sTNF. Therefore the organization of the ligand—via cross-linking or membrane expression—clearly has an effect on receptor activation, and the ligand organization is clearly linked to receptor structure, and this relationship should be explored in other receptors, both in culture and in animal models, in terms of ligand efficacy and anti-tumor cytotoxicity.

Perhaps one of the most intriguing lines of evidence highlighting the importance of receptor clustering is from Ranzinger et al. [153], demonstrating the importance of the spatial arrangement of TNF for receptor function. Using TNF-functionalized, nanostructured surfaces (rather than TNF-coupled nanoparticles), the authors demonstrate the dependence of receptor function on the separation between ligand units, whereby the level of ligand activity is inversely proportional to the average distance between these ligands on nanostructured surfaces. While the homogenously coated surface results in the highest degree of ligand function, an average spacing between ligands of 58 nm retained a significant functionality over ligands spaced at 290 nm. Although this is interesting from a clustering perspective, it is unclear whether and how immobilized ligands separated by 58 nm immobilized may elicit the angstrom scale network formation proposed by us and others. Alternatively, this discrepancy in length scale may represent two distinct and coincidental events associated with ligand binding: a ligand-induced structural change to an active receptor conformation, and co-clustering of active receptors to provide a high localized concentration able to overcome intracellular inhibition. Therefore, it is interesting to wonder whether organized angstrom-level network formation is indeed necessary for function, or alternatively whether a certain number of active, non-interacting receptors per unit area of cell membrane is sufficient to trigger intracellular signaling events.

The ultimate goal is to utilize DR5-targeted ligands to selectively eradicate tumors within animal models. An additional complicating factor in using antibody *in vivo* is the interaction between therapeutic antibodies and the IgG Fc receptor (FcγR), immunoglobulins expressed on immune effector cells, and which play a major role in the

activity of exogenous antibody ligands (for review, see [154]). Accordingly, the ability of FcγRs to engage exogenous DR5 agonistic antibodies has implications in the clinical value of DR5-targeted therapy, as recent evidence demonstrates that the antitumor activity of DR5 agonistic antibodies in mouse models "have an absolute requirement for coengagement" with a particular FcγR [155]. This discovery thus places greater emphasis on Fc engineering, and therefore ligand organization, that has been previously acknowledged.

2.7. Structural modeling of dynamic TNFR network formation – induced fit vs. conformational selection

TNFR1 is unique in that it is the only TNF receptor for which its structure is known in both ligand-independent and ligand-bound states, as discussed above. Even as such, the structural transition associated with signal initiation outside the cell is unclear. Perhaps more confusingly, comparison of the TNF receptor in its unbound and ligand-bound states yields a root mean squared deviation (RMSD) of 1.68 or 1.97 Å (depending on the dimeric protomer selected, with the two protomers having an RMSD of 1.03 Å) [97]. Although authors have previously acknowledged a slight qualitative elongation of TNFR1 upon ligand binding, quantification via RMSD calculation reveals no definitive structural transition associated with ligand binding.

It is conceivable that both dimeric and trimeric interactions exist in accordance with the hexagonal network model, as originally proposed by Naismith et al. [97] and shown in Figure 2-1A. Further, it has been noted that CRD1, and thus the PLAD, may play a role stabilizing large ligand-receptor networks [156]. However, if the dimeric assembly is the functional signaling unit with the TNFR1 network, it is unclear what role ligand binding plays, and whether there exists a structural rearrangement consistent with signaling. We and others were motivated to use structural alignment of existing crystal structures to create a molecular model of such TNF ligand-receptor networks [140,156].

Using the two available TNFR1 crystal structures (receptor dimeric, and ligand-receptor trimeric, see Figure 2-1), structural alignment of the receptor protomer within

the trimeric LTα-TNFR1 with each receptor protomer of the dimeric TNFR1-TNFR1 structure, one may generate a "dimer of trimers" model—the smallest unit within the hexagonal network [140]. In generating this model—based on global alignment of receptor protomers—a problem with the original network model dictated by stoichiometric receptor rearrangement become immediately apparent. In the dimer of trimers model, the principle axes of neighboring ligands are angled at approximately 35 degrees (where no angle between the two would result in both trimers being orthogonal to the membrane). Therefore, crystallization of extracellular domains in the absence of the membrane produces a network that cannot exist on a planar membrane, and a structural transition must exist (Figure 2-2A) in order for large networks to form (Figure 2-2B).

The traditional view of ligand-receptor activation is that ligand binding induces receptor structural changes, and these structural changes result in receptor activity (Figure 2-2C). This induced-fit model is shown in Figure 2-2D), where ligand-induced structural changes result in an active receptor structure.

An alternative explanation has recently been proposed [140]. Using normal mode analysis of these structure, a potential structural transition from the ligand-independent to ligand-bound state has been described and is consistent with flattening of the dimer of trimers model—and a potential transition to a receptor active state [140]. Moreover, the backbone mobility of the receptor in the bound and unbound states are identical, indicating that intrinsic motion of the ligand-independent receptor may lead to, in rare circumstances, the active state [140]. It follows that ligand binding, along with the physical constraints provided by the planar membrane, may stabilize this active state of both receptor protomers, leading to the propagation of ligand-receptor networks by conformational selection (Figure 2-2 E).

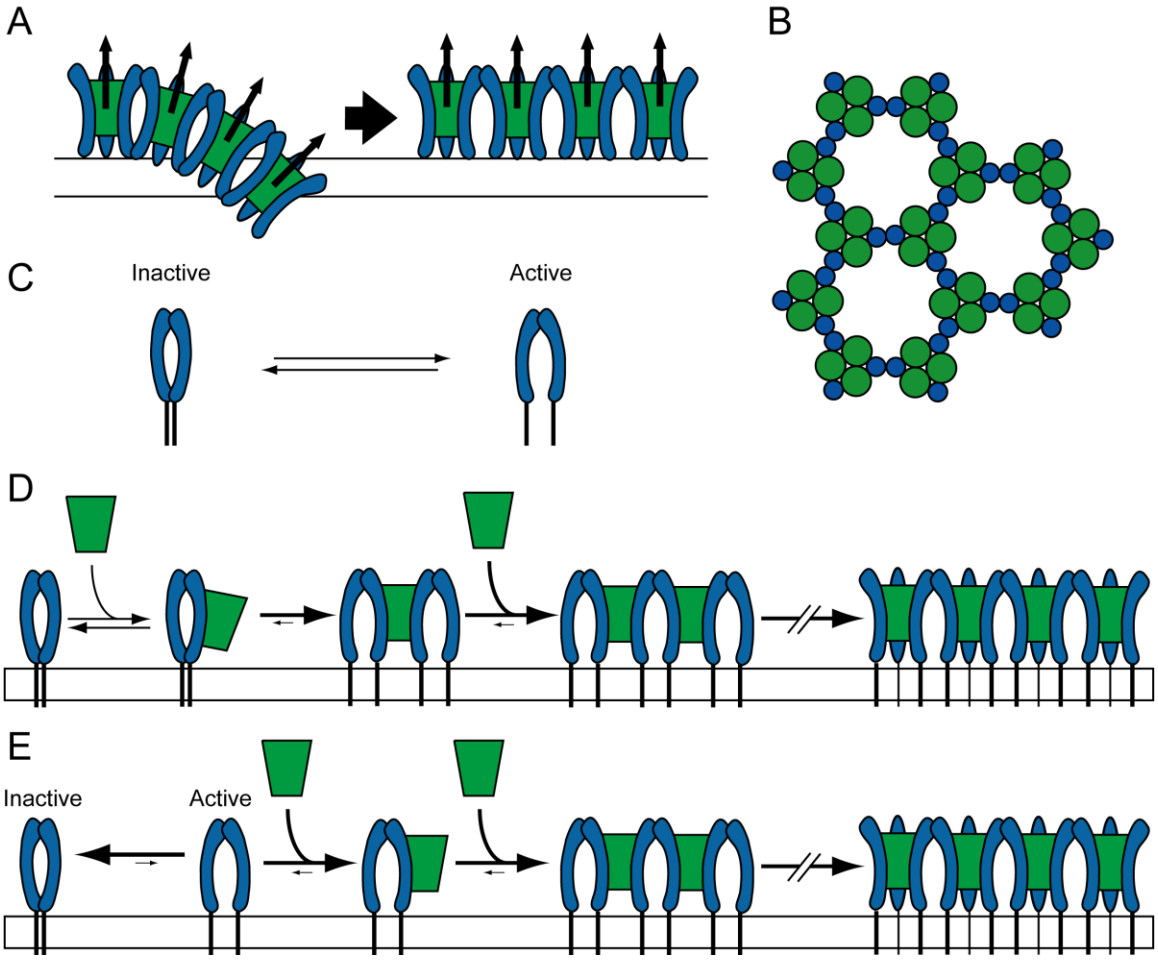

Figure 2-2. A structural model of the LTα-TNFR1 network can be constructed using the ligand-receptor trimer structure and receptor-receptor dimer structure (see Figure 2-1). Upon structural alignment, there exists a ~35˚ angle between the principle axis of adjacent ligand molecules, and therefore the network pitches into the plasma membrane (shown as parallel lines), suggesting a structural transition exists (A) in order to form hexagonal networks (B). This structural transition reportedly involves separation of TM helices (C) [140]**. (D) "Induced Fit" model demonstrates network formation by ligand-induced receptor structural changes resulting in receptor activation and network formation. (E) "Conformational selection" model suggests that motions intrinsic to the receptor dimer result in the active state, to which the ligand may bind. This "conformational selection" model may explain why receptor overexpression results in ligand-independent activity, and why a disease-related mutant, which exists as a dimer, has constitutive activity.**

This coarse model offers several intriguing possibilities. First, that activation of the receptor involves a conformational change of the dimeric species rather than any change in stoichiometry. Thus, ligand binding initiates activation by stabilizing the active dimer conformation rather than through induced trimerization. Second, this model predicts that function may be independent of organized network formation. If the dimer is the relevant species, and activity occurs through conformational changes to the dimer, it is conceivable that certain receptor mutations may result in constitutive activity. This is true in the case of R92Q, which is localized within the plasma membrane (unlike other disease-related TNFR1 mutants) and displays an increased level of ligand-independent activity [157]. Moreover, a significant structural difference of R92Q, compared to the wild type receptor, has been described in that there is a greater separation between TM domains, consistent with the normal mode predicted change upon ligand binding [140]. Thus ligand binding and network formation may serve two concomitant purposes: the stabilization of the active dimeric conformation and the concentration of active dimeric receptors to provide efficient intracellular signaling. This may help explain why, on nanostructured surfaces where ligands are separated by 58nm, a large length in comparison with modeled networks, is still able to initiate intracellular signaling.

Further, this model predicts that interactions in the PLAD are maintained upon ligand binding and involved in the formation of TNFR1 networks. Therefore the PLAD may have clinical significance as a targetable motif for the inhibition of TNFR1 signaling in the treatment of diseases such as arthritis. Interestingly, Deng et al. found that a soluble version of the PLAD (sPLAD) competes for receptor-receptor PLAD interactions, preventing ligand-independent receptor assembly and signaling *in vitro* and further acts as an inhibitor of arthritis in mouse models [158]. Although examination of ligand-independent and ligand-bound TNFR1 structures suggest no overlap exists between receptor-receptor PLAD interactions and ligand-receptor interactions [97,98], disruption of PLAD interactions, either by sPLAD or by mutagenesis/deletion, consistently disrupts the ability of receptor to bind ligand [109,110]. Therefore, the relationship between PLAD interactions and ligand binding may not be fully described by this network model.

2.8. Lipid rafts and the role of the membrane

TNF ligand-receptor signaling is further complicated by complex interactions between receptor proteins and the lipid bilayer. Specifically, the mobility of receptors between distinct regions of the plasma membrane has a role in ligand-induced receptor function. The plasma membrane—comprised of many types of lipids—is laterally heterogeneous, comprised of separated phases generally referred to as liquid ordered (L_o) and liquid disordered (L_d) domains that differ in their physical properties and biological functions [116,159,160]. Liquid ordered domains are characterized by their high cholesterol and sphingolipid content and have a higher degree of acyl chain ordering as well as a higher melting temperature [159]. These phase-separated, ordered domains within the fluid mosaic membrane, commonly referred to as lipid rafts, act as signaling platforms that facilitate signal transduction by recruiting signaling-competent proteins in a number of signaling pathways. Although these L_o domains—and proteins within these domains—are typically isolated and characterized by their resistance to specific detergents [161], termed detergent resistant membranes (DRMs), the relationship between biological membrane domains and DRMs is not fully established [162]. This is evident as proteins localization within DRMs depends on the detergent used for extraction [163], and further that isolation requires non-physiological temperatures [164]. Therefore, while many authors use the lipid rafts and DRMs interchangeably, it is critical to note the biophysical distinction between the physiological, phase-separated plasma membrane and the non-physiological tools often used to study these different phases [161,163,164].

TNFR1 localizes to lipid rafts in transiently transfected HeLa cells (determined based on DRM isolation), and deletion of the death domain prevents localization to DRMs shown by ultracentrifugation [165]. It is unknown whether TNFR1 raft localization correlates with network formation, however it is interesting to note that these results additionally show that overexpression leads to punctate fluorescence similar to

clustering, and that deletion of the death domain results in receptor distribution throughout the membrane [165]. This is similar to observations in death receptors that cluster formation can occur in transiently overexpressed cells even the absence of ligand [114], and that cluster formation requires the intracellular death domain [111,114].

At physiological receptor levels, it was shown that TNFR1 localization to DRMs increases within 10 minutes of treatment with TNFα, and that TNFR1 within these rafts are largely responsible for recruiting downstream factors resulting in NFκB activation [166]. However, TNFR1 signaling is complex in that it is known to induce both pro-survival (via NFκB activation) and pro-apoptotic (via caspase-8 activation) signals. This distinction between pro-survival and pro-apoptotic pathways was later found to occur via early signaling events in the membrane involving for formation of two different complexes based on their localization to detergent resistant and detergent soluble membrane (DSM) domains. Specifically, DRM/DSM localization resulted in one of two different intracellular protein complexes resulting either in NFκB activation or apoptotic cell death [167]. Moreover, these pathways are linked, whereby activation of the NFκB pathway results in the inhibition of caspase activation by FLIP [167–169]. Disruption of microdomains using MβCD prevents NFκB activation by preventing intracellular recruitment of RIP, and as a consequence the cells underwent apoptotic cell death, demonstrating that receptor localization to membrane microdomains plays an active role in not only signal propagation, but also in signal initiation, directing a cell toward NFκB activation or cell death. To date, no evidence exists to suggest that TNFR1 localization to L_o or L_d domains causes differential cluster formation and subsequent activation of pro-survival or pro-apoptotic pathways.

2.9. Concluding remarks

The activation of TNF receptors by their respective ligands involves the orchestration of large molecular assemblies within the membrane. Several lines of evidence suggest that the structural organization of TNF receptors within the membrane,

and transitions in the structural organization, have a profound impact on signal transduction. Here, we have simplified the ligand-induced formation of TNF receptor networks into three categorical molecular-level events: structure, dynamics and environment. Based on published data, it is likely that each plays a critical role in determining the functional outcome. Therefore, by recasting a complex system such as ligand-induced TNFR1 network formation this paradigm, one can begin to understand these individual attributes and their collective role in signal transduction.

In the next chapters, we will further explore this relationship by characterizing novel interactions between DR5 TM domains upon treatment with various ligand (Chapter 3). These TM interactions alter the receptor structure and are consistent with the formation of large receptor networks, offering the first evidence that there is a definitive structural organization within such networks. We further begin to characterize the role of the membrane in the formation of these networks (Chapter 4), where cholesterol-rich membrane regions are required for the dynamic structural events associated with network formation as well as function.

Chapter 3. TNF-related apoptosis-inducing ligand (TRAIL) induces Death Receptor 5 networks that are highly organized

3.1. Summary

Recent evidence suggests that TNF-related apoptosis-inducing ligand (TRAIL), a death-inducing cytokine with anti-tumor potential, initiates apoptosis by re-organizing TRAIL receptors into large clusters, although the structure of these clusters and the mechanism by which they assemble are unknown. Here, we demonstrate that TRAIL receptor 2 (DR5) forms receptor dimers in a ligand-dependent manner at endogenous receptor levels, and these receptor dimers exist within high molecular weight networks. Using mutational analysis, FRET, fluorescence microscopy, synthetic biochemistry, and molecular modeling, we find that receptor dimerization relies upon covalent and noncovalent interactions between membrane-proximal residues. Additionally, by using FRET, we show that the oligomeric structure of two functional isoforms of DR5 is indistinguishable. The resulting model of DR5 activation should revise the accepted architecture of the functioning units of DR5 and the structurally homologous TNF receptor superfamily members.

3.2. Introduction

Tumor necrosis factor (TNF)-related apoptosis-inducing ligand (TRAIL) is a member of the TNF superfamily of ligands [29] that triggers the extrinsic apoptotic pathway via death receptors 4 and 5 (DR4 or TRAIL-R1, and DR5 or TRAIL-R2, respectively) [42–44]. These type I membrane receptors serve as viable targets for cancer

therapeutics as pre-clinical models have demonstrated that recombinant TRAIL [32,170,171] and antibody agonists [9,10,172–175] targeting this pathway have potent anti-tumor activity without exhibiting systemic cytotoxicity [32,174]. Therefore, given the potential as a promising target in cancer, it is critical to characterize the precise mechanism by which death receptors initiate apoptosis in order to optimize existing TRAIL receptor-targeted therapeutic strategies [9,176–180]. However, despite the well-established sequence of signaling events downstream of receptor activation [25,181], how the initiating events in TRAIL-induced cell death (specifically events in the membrane) propagate a death signal remains unknown.

The crystal structure of the extracellular domain (ECD) of the TRAIL-DR5 complex [99–101] suggests that three receptor monomers tightly associate with the trimerized TRAIL [92] to form a symmetric ligand-receptor complex (Figure 3-1, A, PDB code 1d0g, shown is a top view of the complex). Additionally, based on the last resolved amino acid of the ECD, the trimeric receptor arrangement places the transmembrane (TM) domains of DR5 approximately 50 Å apart, and therefore interactions between the TM domains are presumed to have no role in TRAIL-DR5 signaling. The TRAIL-DR5 trimeric structure is consistent with the crystal structure of LTα-TNFR1 [98], a related TNF ligand-receptor pair, which is also a complex of three non-interacting receptor monomers and a tightly bound homo-trimeric ligand. Thus, based upon these crystal structures, it has reasonably been presumed that the relevant signaling event in the TNF-receptor superfamily is ligand-induced extracellular trimerization and subsequent trimerization of these receptors' intracellular regulatory domains (death-domains in the case of DR5). However, crystal structures and functional studies of downstream domains and proteins (including the death domain, FADD and caspase-8) suggest that the process may instead be dictated by receptor dimerization, not trimerization [121–124]. An additionally intriguing piece of evidence is a dimeric crystal structure of the ECD of TNFR1 in the absence of ligand [97](30), which is stabilized by the well-studied pre-ligand assembly domain (PLAD) [108–110] as well as by membrane proximal residues, for which no known role exists. In both the TNF receptors and DR5,

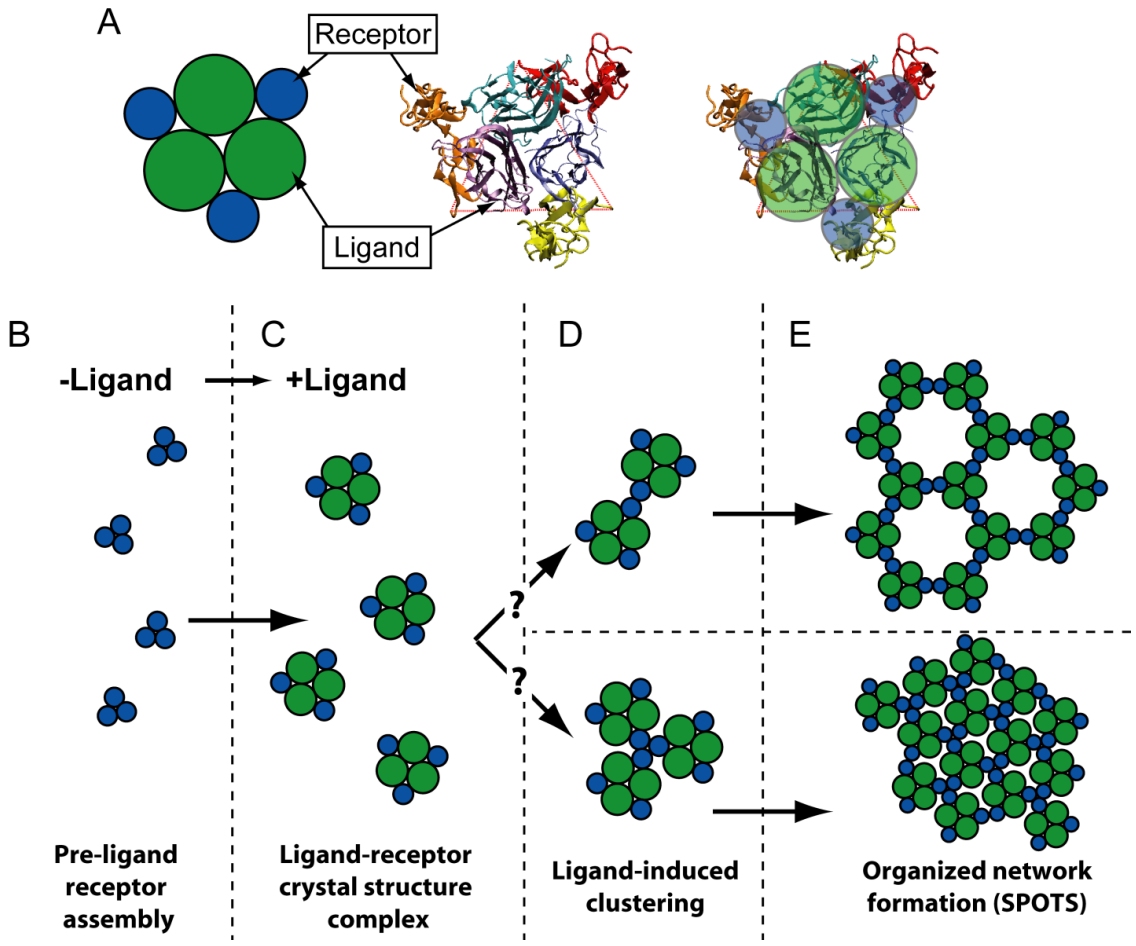

Figure 3-1. A current model for organized ligand receptor networks. A, TRAIL-DR5 crystal structure (center, Protein Data Bank code 1d0g, top view), a schematic representation (left), and an overlay (right). Dashed red line indicates the previously predicted transmembrane domain separation. B, in the absence of ligand, DR5 forms pre-ligand trimers via interactions within the pre-ligand assembly domain, although pre-ligand dimers have also been proposed. C, addition of TRAIL causes a structural re-organization from a pre-ligand state to the ligand-induced trimer state, as inferred by the trimeric ligand-bound crystal structure, as shown in A. D, ligand-induced structural changes allow for interactions of multiple ligand-receptor trimers resulting in early stage receptor clustering via dimerization or trimerization of ligand-receptor trimers, shown above and below, respectively. E, combination of trimeric ligand-receptor interactions (i.e. crystal structure trimer) and receptor-receptor interactions (either dimeric or trimeric) drives receptor clustering and the formation of large organized receptor networks.

the PLAD has been identified as crucial for ligand-binding, but there has been no definitive study to clarify the role of the dimeric TNFR1 complex in signaling. To date, no ligand-independent oligomeric structure of DR5 exists, nor is it known whether there is a relevant dimeric form of DR5.

Recently, our understanding of TNF receptors has been further complicated by a number of studies that show activation is associated with supramolecular receptor clustering within the membrane [111,132,153,182,183], with the most recent example being DR5 [112,184]. Visualized in fluorescence microscopy studies, these ligand-induced aggregates of receptors—previously referred to as signaling protein oligomeric transduction structures, or SPOTS—are on the order of 300-500nm in diameter. Despite considerable speculation about the physical character of SPOTS [138,139], the mechanism through which clusters form, and whether they have a specific structural organization are unknown, leaving open a significant and fundamental question: Are SPOTS simply co-localized aggregates formed via randomly organized, non-specific interactions between receptors? Or, more interestingly, are they highly-structured networks that possess stabilizing and targetable motifs? Owing to the difficulty of studying endogenous membrane receptors in their native states, no specific structural information has been available to begin to address this question.

Although no experimental data exists to support a molecular model of SPOTS, several hypothetical models of TNF ligand-receptor network structure have been put forth [138,139], two of which are schematized in Figure 3-1. In the absence of ligand, pre-formed receptor oligomers—shown as trimeric complexes (described below as our preferred model for DR5) but also suggested to be dimeric (e.g. in the case of TNFR1)—assemble in the plasma membrane via the membrane-distal residues of the PLAD (Figure 3-1, B). Based on available crystal structures [99–101], ligand binding first results in the formation of a symmetric trimer complex, which consists of three non-interacting receptor monomers held together by the trimeric TRAIL (Figure 3-1, C). Further clustering of these trimer complexes then proceeds by previously unproven interactions. In the case of TNFR1, clustering of trimer complexes has been hypothesized to proceed

via dimeric receptor interactions: one receptor monomer from each of the two adjacent, interacting trimeric complexes (Figure 3-1, D, top) [138]. Additional trimer complexes are similarly added thus leading to large network assemblies (Figure 3-1, E, top). This model potentially explains the occurrence of both trimeric ligand-receptor complexes (i.e. the crystal structure trimer complex) and the un-liganded dimeric receptor species [97]. The model also suggests that dimeric receptor interactions hold together a hexagonal mosaic of trimeric complexes and focuses on the receptor dimer (i.e. the dimeric receptor-receptor interaction embedded within the network of trimeric ligand-receptor complexes) as the intracellular, activating unit. An alternative model suggests that the network is held together by trimeric, not dimeric, receptor interactions (Figure 3-1, D and Figure 3-1, E, bottom) [139].

Here, we have evaluated whether TRAIL-induced rearrangement of DR5 involves the formation of a stable receptor dimer species, and whether that dimeric species exists within large, structured networks. In the process, we offer the first evidence that TM α-helices within TNF receptors form tightly associated bundles, and the first structural and functional interrogation of two distinct, alternatively-spliced DR5 isoforms.

3.3. Materials and Methods

3.3.1. Cell culture and reagents

Jurkat cells were cultured in RPMI-1640 media (HyClone). HEK293 cells were cultured in DMEM (HyClone). BJAB-derived cells [76,185] were cultured in RPMI-1640 with HEPES, sodium pyruvate, and L-glutamine (ATCC). All media were supplemented with 10% FBS, L-glutamine, penicillin and streptomycin. All cultures were maintained at sub-confluence at 37˚C and 5% CO2 in a water-jacketed incubator. Flag-sTRAIL (residues 114-281) was expressed in E. Coli and purified as previously described [186] using the pT7-Flag-1 inducible expression vector and anti-Flag resin (Sigma). DR5 antibody agonist (mAb631), DR5 surface staining antibody (mAb6311), and fluorescent secondary antibody (NL637) were purchased from R&D Systems. Antibodies for

Western blots, DR5 (#3696) and β-actin (#5125), were purchased from Cell Signaling Technologies. BJAB DR5-deficient and BJAB DR5-deficient + DR5-S cells were a kind gift from Andrew Thorburn [76,185].

3.3.2. Cloning and DNA constructs

Complementary DNA (cDNA) for full length DR5-S (residues 1-411) and DR5-L (residues 1-440) was cloned into pcDNA3.1(+) for transient expression in HEK293 cells. For transient expression in BJAB DR5-deficient cells, DR5-S (1-411) and DR5-L (1-440) were inserted into pIRES2-EGFP vector. For FRET analysis, extracellular and TM residues for DR5-S (1-211) and DR5-L (1-240) were inserted in-frame into pECFP-N1 and pEYFP-N1 vectors using EcoRI and BamHI sites. Both pECFP-N1 and pEYFP-N1 vectors contain the monomeric mutation A206K to the CFP or YFP preventing constitutive fluorphore clustering [187], and CFP/YFP show no affinity for each other (Figure 3-5, C, compare CFP+YFP co-transfection with CFP-YFP tandem construct). Mutation of DR5 constructs was carried out by two-step PCR mutagenesis. All constructs were verified by sequencing, and expression was verified by Western blot and cell surface staining. CFP and YFP constructs were additionally verified individually by fluorescence microscopy using both CFP and YFP filters. pECFP-N1 and pEYFP-N1 constructs were a gift from David D. Thomas and the CFP-YFP tandem constructs was a gift from Stanley G. Nathenson [188].

3.3.3. Fluorescence (Förster) Resonance Energy Transfer (FRET)

Briefly, sub-confluent HEK293 cells were transfected by calcium phosphate method of transfection with CFP- and/or YFP-tagged constructs shown in Figure 3-5, A with a two-fold excess of acceptor. Twenty-four to forty-eight hours post-transfection, cells were imaged using a Nikon Eclipse TE200 inverted microscope and a 40x objective lens. Fluorescent proteins were illuminated using an mercury lamb (XCite 120W Fluorescence Illumination System). Filters for excitation and emission of CFP (430/24nm

and 470/24nm, respectively) and YFP (500/20nm and 535/30nm, respectively) were controlled using an automated filter wheel (Ludl MAC6000). Steady state images were taken in 5-20 second intervals throughout the course of photobleaching, which took on average 5 minutes. Images were acquired using MetaMorph and analyzed using ImageJ software. Instrument-independent FRET efficiency was calculated using Equation 1, where F_{DA} is the donor fluorescence in the presence, and F_D is the donor fluorescence after acceptor photobleaching, as previously described [189]. Results for each experiment are based on ~50 cells taken from a single transfection over approximately 5 regions of interest, with each cell treated as an independent sample where cells having fluorescence primarily within the plasma membrane were studied. Reported averages and standard errors were calculated over the full sample of cells. All FRET experiments were repeated at least three times to confirm results.

Equation 1:

$$E = 1 - \frac{F_{DA}}{F_D}$$

In a separate experiment, multiple populations of cells were transfected at a CFP:YFP ratio ranging from1:0.5 to 1:4. FRET was measured using photobleaching as described and FRET efficiency was plotted as a function of YFP intensity. FRET efficiency vs. YFP intensity data were fit using a two-parameter saturable binding model, where the calculated FRET efficiency (FRET%) is a function of the measured local YFP intensity (YFP), described by Equation 2, and as previously described [187,189–191].

Equation 2:

$$FRET\% = \frac{FRET\%_{max} * YFP}{YFP + K_{d2}}$$

From this model-fit of the data were extracted two parameters: The maximum FRET efficiency ($E\%_{max}$) and the relative dissociation constant (K_{d2}), which yield information about the fluorophore separation (i.e. structure) and binding affinity,

respectively, for comparison of DR5 isoforms and mutants. Results shown are from three separate transfections at varying CFP:YFP ratio and the results were pooled, with each point representing data from a single cell. These experiments (i.e. multiple transfections at different CFP:YFP ratios) were repeated to verify reproducibility, though data from transfections done on separate days were not pooled.

3.3.4. Confocal microscopy

Imaging of ligand-receptor clusters in Jurkat cells was done as previously described [111,112]. Briefly, cells were washed with PBS and treated with a DR5-specific mouse antibody (R&D Systems, MAB631) agonist at 5 μg/ml for 1 hour. After washing, cells were treated with an anti-mouse secondary antibody labeled with either NorthernLights557 or NorthernLights637 (R&D Systems) used at 5 μg/ml for 30-60 minutes and washed. All incubations and washes were done in PBS + 1% FBS and at 4˚C to prevent receptor internalization. Labeled cells were transferred to pre-chilled poly-lysine coated 35 mm glass-bottom culture dishes (MatTek Corporation) for approximately 5-10 minutes at RT before imaging to allow cells to settle and clusters to form.

NorthernLights637 labeled clusters were imaged in an Olympus IX81 inverted microscope equipped with a FluoView FV1000 laser scanning confocal head (633nm laser excitation, 645-745 nm emission). Either 60x (1.42NA) or 100x (1.3NA) oil immersion objective lenses were used.

Z-stacks of NorthernLights557 labeled clusters were acquired using a Zeiss Cell Observer Z1 microscope equipped with a Yokogawa CSU-X1 confocal head using a 100x (1.40NA) oil immersion objective (561 nm laser excitation, 617/73 nm emission). The spinning disc confocal allowed image acquisition at multiple depths overcoming the sample photobleaching problem in the laser scanning confocal. Orthogonal sectioning and maximum intensity projections of Z-stacks were performed using the Zeiss Axiovision software.

3.3.5. Cross-linking and Western blot analysis

Jurkat or BJAB cells (DR5-deficient and re-expressing either DR5-S or DR5-L) were washed and treated with TRAIL or DR5-specific antibody agonist for 1 hour at 4˚C in PBS (pH 8.0) with rotation. Cells were subsequently cross-linked with 0.5-1mM BS3 (Pierce; a homo-bifunctional, amine-reactive, non-cleavable, membrane-impermeable cross-linker with an 11.4 Å spacer arm), for 30 minutes at room temperature. Cross-linked samples were quenched with 20mM Tris-HCl (pH 7.5) for 15 minutes at room temperature. Cells were pelleted by centrifugation and lysed in RIPA buffer (50mM Tris-HCl pH 7.5, 150mM NaCl, 0.5% Sodium deoxycholate, 0.1% SDS, 1% NP-40) supplemented with protease inhibitors and 10mM iodoacetamide for 1 hour at 4˚C. Total protein concentration of lysates was determined by BCA assay (Pierce) and equal amounts of total protein (typically ~100µg) were mixed with 2x Laemmli sample buffer with DTT and βME, boiled at 100˚C for 10 minutes, and loaded on 4-12% Bis-Tris SDS-PAGE gel (Invitrogen). For non-reducing conditions, lysates were mixed with 2x Laemmli sample buffer in the absence of DTT and βME, but samples were treated identically otherwise. Proteins were transferred to nitrocellulose membrane and probed using antibodies as described. To account for potential non-specific cross-linking in the presence of ligand, the same lysates were separated via SDS-PAGE and Coomassie stained (see Supplemental Results, Figure 3-8, p. 69).

3.3.6. Caspase activity and surface staining

BJAB DR5-deficient cells, $5x10^6$ cells in 400µl serum-free media, were transfected by electroporation (200V, 975uF) with the indicated plasmid and moved back into 10ml complete media. Several hours after electroporation, live cells were isolated by ficoll gradient. Twenty-four to Forty-eight hours after transfection, cells were treated with a DR5-specific antibody agonist (mAb631) at 1µg/ml for 4 hours at 37˚C. Caspase activity was measured using CaspGLOW Red Active Caspase 8 staining kit (BioVision),

gating on live, GFP-positive cells by flow cytometry (FACSCalibur). Additionally, DR5 surface expression was measured on unstimulated cells by antibody staining using a non-agonistic DR5 antibody and fluorescent secondary antibody. DR5 surface expression was determined by flow cytometry using an identical gating scheme for live, GFP-positive cells. Data was analyzed using FlowJo software (Tree Star, Inc.).

3.3.7. Prediction of helical transmembrane domains

The sequence-based prediction of helical transmembrane domains was based on a hidden Markov model via the TMHMM Server v 2.0, and protein sequences were obtained via the NCBI gene database.

3.3.8. Replica exchange molecular dynamics (REMD) simulations

Replica-Exchange Molecular Dynamics (REMD) simulations were run using the CHARMM software package [192] and force-field version parameter set 22 [193] with CMAP correction [194] and the MMTSB toolset [195]. All simulations were run using an implicit bilayer model, GBSW (Generalized Born with switching function) [196,197]. For the monomer simulations, the bilayer hydrophobic thickness was set to 25 Å, 30 Å, or 35 Å, with a switching length of 0.3 Å in each case. The starting configuration was a single ideal helix, placed in the center of the bilayer, aligned with the bilayer normal axis. For the dimer simulations, the bilayer hydrophobic thickness was set to 32 Å. REMD simulations were run using 16 replicas, over a temperature range of 300 – 600 K. A switch was attempted every 2 ps, with an observed switching frequency of ~25%. All analysis was performed on the lowest temperature replica (300 K). Simulations were run using a 2 fs time step for a duration of 10 ns for each state (i.e. a total of 160 ns when considering the number of replicates).

3.3.9. Synthesis, Purification and Analysis of DR5-TM

Solid-phase peptide synthesis of DR5-TM (Sequence: TPASPCSLSGIIIGVTVAAVVLIVAVFVSKSLLYKK) was carried out with a PE Biosystems Pioneer^{TM} using standard, double-coupling cycles of Fmoc/*t*Bu-chemistry with HATU/DIEA as coupling reagents, in the presence of NMP. The sequence was assembled on Fmoc-Lys-PEG-PS resin (initial load 0.18 mmol/g). The synthesis was optimized using pseudoproline dipeptides: Fmoc-Val-Ser ($\psi^{Me,Me}$-Pro)-OH, Fmoc-Val-Thr ($\psi^{Me,Me}$-Pro)-OH, and Fmoc-Leu-Ser ($\psi^{Me,Me}$-Pro)-OH (Novabiochem, San Diego, CA). Final cleavage from the resin and side chain deprotection was carried out by treatment with reagent K: TFA, phenol, thioanisole, 1,2-ethanedithiol, water (82.5%, 5%, 5%, 2.5%, 5%), for 4 h at 25°C. The cleavage mixture was filtered and the resin washed with a small amount of reagent K. Combined filtrates were concentrated under nitrogen and precipitated in 30 ml of diethyl ether at 0 °C. Precipitated peptide was collected by centrifugation, and washed with ice-cold diethyl ether. The crude peptide was dissolved in 50% TFA and purified by HPLC on a C-4 column (Vydac, 214TP1010) using a Gold Beckman Coulter system. Protein elution was achieved with a linear gradient from 0 to 63% B (95% Isopropanol/4.9% H2O/0.1% TFA) in 40 minutes at a flow rate of 2.0 ml/minute with detection at 220 nm. The HPLC fractions were collected and analyzed by MALDI-TOF MS. The pooled fractions found to be essentially pure were lyophilized to yield 22% based on starting resin.

3.3.10. Analysis of DR5-TM by MALDI-TOF

Mass spectral data was acquired with a Bruker Biflex III Matrix-Assisted Laser Desorption/Ionization Time-of-Flight (MALDI-TOF) system. The sample was co-crystallized with the matrix 3,5-dimethoxy-4-hydroxycinnamic acid (sinapinic acid) and the data was collected in the linear mode, positive polarity, with an accelerating potential of 19 kV. Each spectrum is the accumulation of 100 to 400 laser shots. Mass

spectroscopy for DR5-TM yielded an *m/z* value of 3647 $[M + H]^+$, which is in agreement with the predicted value of 3646 Da.

HATU: N-[(dimethyamino)-1H-1, 2, 3-triazolo[4, 5-b]pyridino-1-ylmethylene]-N-methylmethanaminium hexafluorophosphate N-oxide

DIEA: N,N-Diisopropylethylamine;

NMP: N-Methyl-2-pyrrolidone

3.4. Results

3.4.1. DR5 is expressed as two functional isoforms that differ in their transmembrane domains

DR5 is expressed as two isoforms that differ by the insertion of 87 base pairs resulting from alternative splicing and the inclusion of an intron [198]. Translation of DR5 with and without this insertion results in the expression of long and short isoforms of DR5 at the protein level, respectively, referred to here as DR5-L and DR5-S (Figure 3-2, A). DR5-L contains an additional 29 amino acids at the junction between the extracellular and predicted transmembrane (TM) domains, including a cysteine residue at position 209. The organization of DR5 networks via ligand-induced dimerization may allow for interaction of DR5 TM α-helices as receptor TM domains are no longer confined to the 50Å separation observed in the TRAIL-DR5 complex crystal structure. Therefore, we wondered if physical interactions between the TM domains of DR5 receptor monomers play a role in the stabilization of receptor network.

We first sought to confirm the function of DR5-L and DR5-S. Both isoforms are functionally active, as expression of either DR5-S or DR5-L in DR5-deficient cells results in activation of caspase-8, both in a ligand-independent manner, consistent with previous results [52], and in a ligand-induced manner (Figure 3-2, B). Surface staining and flow cytometry confirmed approximately equal expression of DR5-S and DR5-L on the cell surface relative to the DR5-deficient control cell line (Figure 3-2, C). Further, protein lysates from cells expressing exclusively DR5-S or DR5-L illustrate the size

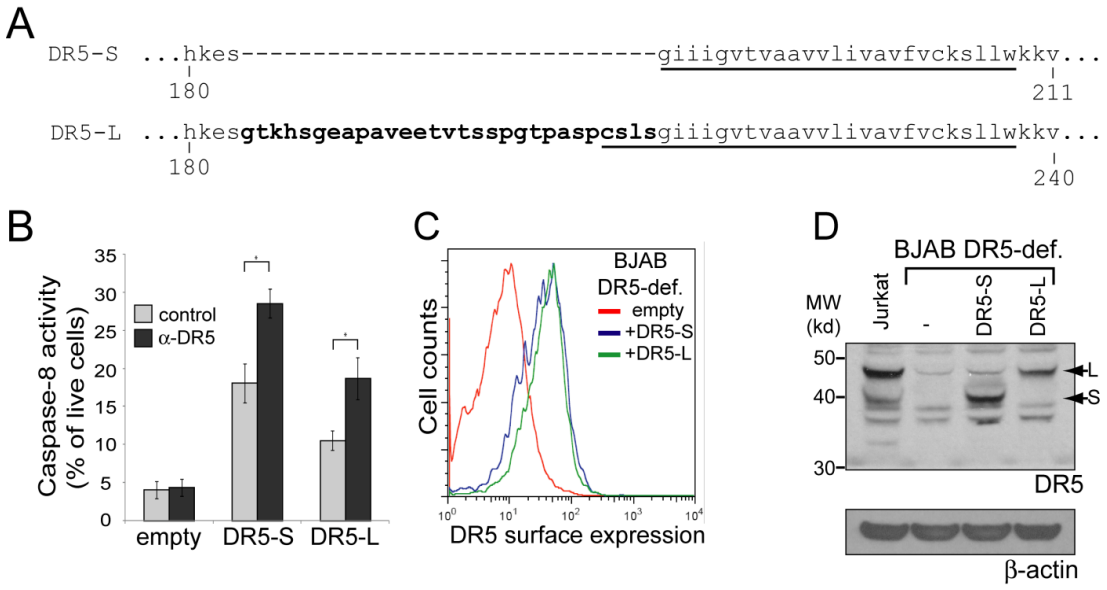

Figure 3-2. DR5 is expressed as two functional isoforms. A, transcription of two alternatively spliced isoforms results in the expression of DR5-S and DR5-L differing by 29 amino acids (bold) within the extracellular domain and predicted transmembrane domain (underlined). B, DR5-S or DR5-L (or empty vector control) were transiently transfected into BJAB DR5-deficient (DR5-def) cells and treated with a DR5-specific agonist antibody (α-DR5) as indicated. Flow cytometry analysis of caspase-8 activity shows a regain of function and ligand sensitivity with expression of DR5-S or -L. Results represent the level of caspase-8 activity (mean ± S.E.) for three independent experiments. C, surface expression in transiently expressing cells was quantified by surface staining and flow cytometry to show equal surface expression of DR5-S (blue) and DR5-L (green) and increased levels over vector transfected (red). D, whole-cell lysates from Jurkat cells, BJAB DR5-def cells, and DR5-def cells re-expressing DR5-S or DR5-L confirm the predicted size of DR5-S (40 kD) and DR5-L (43 kD).

difference by SDS-PAGE, running at approximately their predicted molecular weights of 40kD (DR5-S) and 43kD (DR5-L), respectively (Figure 3-2, D). Jurkat cells, which have been shown to express both isoforms at the mRNA level [198], also express both isoforms at the protein level (Figure 3-2, D). Importantly, we show here the first evidence that both isoforms of DR5 are both active and ligand-sensitive. Although DR5-S appears to activate caspase-8 to a greater extent than DR5-L (Figure 3-2, B, compare DR5-S and DR5-L), we do not suggest that DR5-S is necessarily more active as there are noticeable differences in expression level. Whether DR5-S and DR5-L differ in their oligomeric

structure, a primary focus of this study, has not been investigated to date. However, given the location of Cys209 of DR5-L—which, as we will describe below, is located within the contiguous TM α-helix—we wondered whether this cysteine residue could be used to identify potential interactions, covalent and non-covalent, within the DR5 TM domain.

3.4.2. Ligand-induced dimerization mediates DR5 network formation

It has been shown previously that ligands within the TNF superfamily (including TRAIL and a DR5 antibody agonist) induce receptor clustering within the plasma membrane [111,112,184]. Therefore we first used fluorescence microscopy to identify whether DR5 agonistic antibody binds and induces ligand-receptor clusters. Fluorescent-labeled agonist ligand binds DR5 on the surface of Jurkat cells—which endogenously express both DR5-S and DR5-L—and forms large clusters representing ligand-receptor complexes within the plasma membrane (Figure 3-3, A). Images were taken from a single confocal *xy* plane at approximately the midplane of the cell. Shown are the fluorescent, receptor-bound agonist ligand (Figure 3-3, A-i), transmitted light image (Figure 3-3, A-ii), and the overlay (Figure 3-3, A-iii) demonstrating that cluster formation occurs within the plasma membrane. Estimates of the cluster sizes based on these fluorescent images are on the order of 200-500nm in diameter, consistent with the estimated size of FasL-induced Fas clusters [111]. To determine if the ligand-receptor clusters are distributed throughout the plasma membrane of the entire cell, multiple confocal images (in the *xy*-plane) were acquired at varying depths (in *z*). Axial reconstruction at the cell mid-plane in each image clearly shows the distribution of fluorescent ligand-receptor clusters throughout the plasma membrane (Figure 3-3, B *xy*-, *yz*-, and *xy*-planes). Maximum intensity projection in the *xy*-plane illustrates the approximate size and distribution throughout the entire spherical cell (Figure 3-3, B, MIP). Collectively, confocal fluorescence microscopy results demonstrate that agonist binding to DR5 at the surface of the cell induces the formation of large clusters within the membrane, consistent with previous studies of DR5 and Fas, a related TNF receptor.

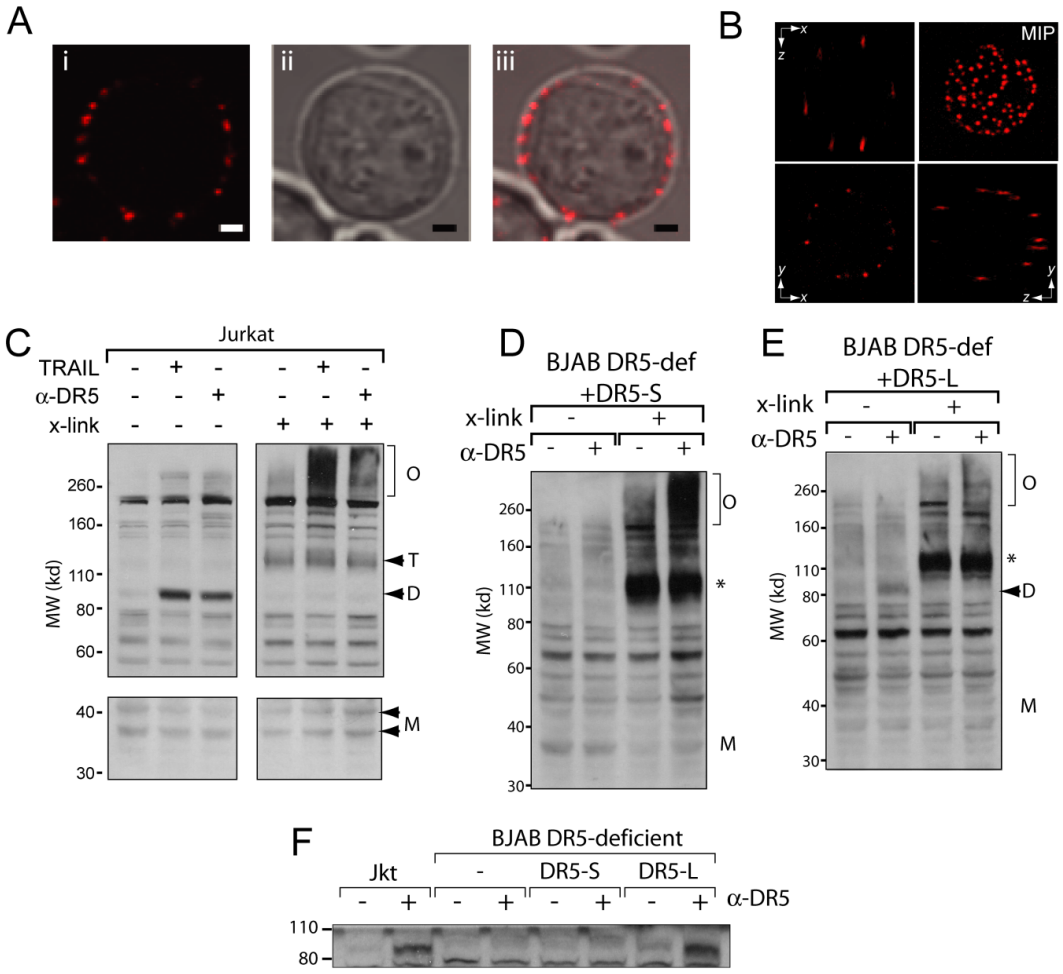

Figure 3-3. Ligand-induced DR5 dimers within high molecular weight networks. A, Jurkat cells were treated with an agonistic antibody specific to DR5 and stained with fluorescent secondary antibody. Confocal microscopy shows the formation of ligand-receptor clusters on the cell surface. Shown is the fluorescent-labeled agonist (panel i), transmitted light (panel ii), and an overlay (panel iii). Scale bar represents 2μm. B, confocal microscopy of agonist treated Jurkat shows ligand-receptor clustering in the xy-, yz-, or xz-focal plane at approximately the mid-line of the cell. Maximum intensity projection (MIP) in the xy-plane illustrates the size and distribution of these clusters. C, Jurkat cells were treated with TRAIL or DR5-specific agonist (α-DR5) and cross-linker (x-link) as indicated, and whole-cell lysates were run under nonreducing SDS-PAGE and probed for DR5. Highlighted are monomeric (M), dimeric (D), trimeric (T), and oligomeric (O) forms of DR5. D and E, similar experiment was run using BJAB DR5-deficient (DR5-def) cells +DR5-S or +DR5-L using α-DR5. Agonist causes the formation of a disulfide dimer in DR5-L cells but not in DR5-S cells, and dimer species exists within a high molecular weight complex. F, Jurkat, BJAB DR5-deficient, DR5-def. cells + DR5-S, and DR5-def.+DR5-L were treated with a DR5 agonist, and lysates were run under nonreducing conditions. Shown is the dimeric form of DR5, present upon treatment with ligand and only when DR5-L is expressed.

In order to begin to characterize the molecular architecture of ligand-induced DR5 clusters, and thus to illuminate new details regarding the various models of how DR5 oligomers stabilize networks (e.g. those in Figure 3-1, E), we used cross-linking of surface proteins with a membrane insoluble, amine-reactive cross-linker. This approach allowed us to capture the native oligomeric states of the receptor as they are in the cell membrane before they are lost on dissociating gels. Based on hypothetical network models (Figure 3-1, E) and the sequence of the DR5 TM domain, we hypothesized that TRAIL- or agonist-induced networks may be stabilized in part via close contacts between DR5 monomers, including interactions between TM domains. To date, it is unknown whether ligand-induced structural re-arrangement of DR5 results in stabilization of TM interactions, including disulfide bond formation via Cys209 unique to DR5-L. First, Jurkat cells were treated with TRAIL or DR5 antibody agonist as indicated and cell lysates were analyzed via non-reducing SDS-PAGE (Figure 3-3, C) [199,200]. The addition of the membrane impermeant cross-linker results in the formation of a ligand-independent receptor trimer, at the approximate molecular weight of three receptor monomer units (~120 kD, Figure 3-3, C, compare lanes 1 and 4). This result provides the first structural insight into pre-ligand receptor assembly and stoichiometry of DR5, which differs from the presumed pre-ligand dimeric state of TNFR1 [97] and motivates our choice in Figure 3-1, B. RNAi studies were used to confirm that this band is indeed DR5 (see Supplemental Results, Chapter 3.7, Figure 3-10, p. 71).

The addition of either TRAIL or antibody agonist causes the formation of high molecular weight DR5 clusters (200+ kD, Figure 3-3, C, lanes 5 and 6), reflecting the ligand-induced receptor clusters shown in Figure 3-3, A, and Figure 3-3, B. In the absence of cross-linker, the addition of TRAIL or agonist produces a distinct band at ~85kD, the expected molecular weight of two DR5 monomer units (Figure 3-3, C, compare lane 1 with lanes 2, 3), indicating the presence of a disulfide-linked receptor dimer species. That this is in fact a DR5 monomer-monomer interaction is further corroborated with mutational analysis and FRET experiments described below. That cross-linking of either TRAIL- or agonist-treated samples causes the disappearance of

this dimer band suggests that ligand-induced DR5 dimers are embedded within the high molecular weight clusters, and provides the first molecular details of the ligand-induced rearrangement of DR5 and higher-order structure of the TRAIL-DR5 network (Figure 3-1, E) and agonist-DR5 network. Analysis under reducing conditions abolishes the DR5 dimer in both the TRAIL and antibody agonist treated samples (see Supplemental Results, Figure 3-8 on p. 69 and Figure 3-9 on p. 70), indicating that ligand-dependent dimerization is driven through a cysteine disulfide bond, suggesting this may be DR5-L (further discussed below).

We note that the addition of ligand does not result in a molecular weight shift of the 120kD, pre-assembled receptor trimer (Figure 3-3, C, lane 4-6). Thus, we see no specific band at the predicted molecular weight of the ligand-receptor trimer complex (the crystal structure, which should be at ~180kD). Like the dimer, we interpret this to most likely mean that the ligand-bound trimeric structure (Figure 3-1, C) exists only transiently on its own before becoming embedded within the DR5 clusters. However, this accounting does not explain the persistence of the 120kD trimer band upon addition of TRAIL. It is possible that a steady-state level of pre-ligand assembled trimer is maintained in the membrane. Alternatively, this lack of shift in molecular weight may correspond to an inability to cross-link the TRAIL to the trimeric receptor. The distinction between these various possibilities remains unclear. Numerous attempts to identify TRAIL on these blots has proven unsuccessful, possibly due to a lack of sensitivity in detecting ligand bound to endogenous receptor or due to epitope masking (e.g. as a result of residing in a complex or due to cross-linker masking of the antibody epitope).

Because Jurkat cells express both isoforms of DR5, we tested whether the observed disulfide-bonded dimer is indeed DR5-L, likely given its additional cysteine residue. We generated two cell lines derived from a BJAB cell line previously selected for DR5 deficiency [76,185] expressing either the DR5-S or DR5-L isoform. The addition of a DR5-specific agonist induces clustering in both DR5-S and DR5-L lines (Figure 3-3, D, and Figure 3-3, E), though somewhat more so in the short isoform.

Importantly, however, the ligand-dependent formation of disulfide-linked receptor dimer occurs exclusively in cells expressing DR5-L (Figure 3-3, C-E, compare lane 2 in each Western). This result is recast in a separate non-cross-linked Western, focusing on the dimer molecular weight from four cell lines (Jurkat, BJAB DR5-deficient, BJAB-DR5-S and BJAB-DR5-L) (Figure 3-3, F). That disulfide-linked dimers of DR5-L do not occur in the absence of ligand despite ligand-independent trimerization suggests that 1) the free cysteine residue in un-liganded DR5-L is inaccessible, either by the receptor conformation or possibly by being buried in the membrane, and is thus unable to form disulfide linkages; and that 2) ligand-binding causes a conformation changes that exposes the free cysteine and thus promotes disulfide-bond formation. We note that, in both Jurkat and BJAB cell lines, there is an overall increase in DR5 intensity at all non-monomeric molecular weights upon addition of the cross-linker. Experiments with a reversible cross-linker suggest that cross-linking does not upregulate the receptor, therefore this difference in apparent total DR5 levels may more likely be due to epitope masking of certain populations of receptor and/or poor detection of monomeric DR5 under non-reducing SDS-PAGE.

3.4.3. DR5 dimers are stabilized via covalent and non-covalent interactions

Cells expressing DR5-S show no disulfide-linked dimer, however the similar presence of high molecular weight clusters indicates that DR5-S may also cluster via ligand-dependent dimerization, albeit exclusively through non-covalent interactions not detected by non-reducing SDS-PAGE. Moreover, in both DR5-S and DR5-L expressing cells, cross-linking of surface proteins results in the formation of a ligand-independent receptor trimer (Figure 3-3, C-E). Therefore, we tested whether DR5-S and DR5-L are able to form stable receptor oligomers, including both receptor dimers and trimers, through either covalent (i.e. disulfide) or non-covalent interactions in transiently transfected HEK293 cells. To assess disulfide-linked dimerization, HEK293 cells were transiently transfected with either DR5-S or DR5-L (Figure 3-4, A), as well as cysteine mutants (Figure 3-4, B), and lysates were isolated and run under reducing or non-

reducing conditions as indicated. Transient expression of DR5-L results in disulfide-linked dimerization while DR5-S is unable to form disulfide-linked dimers, and reducing of either DR5-S or DR5-L expressing cells produces entirely monomeric receptor (Figure 3-4, A). Mutational analysis of free cysteine residues within the TM domains of DR5-S (Cys203) and DR5-L (Cys209 and Cys232) demonstrates that disulfide dimers of DR5-L involve Cys209, the cysteine residue unique to DR5-L. Mutation of the TM Cys203/232 (a conserved TM cysteine residue in DR5-S and DR5-L, respectively, see Figure 3-2, A) has no affect on dimerization (Figure 3-4, B).

To evaluate non-covalent association of receptors, HEK293 cells were transiently transfected with DR5-S or DR5-L, and surface receptors were cross-linked as described and cell lysates analyzed via SDS-PAGE. Interestingly, while non-cross-linked receptors are entirely monomeric, cross-linking of surface receptors shows that oligomeric receptor structures are stable within the membrane at high levels of receptor expression in the absence of ligand (Figure 3-4, C). Non-covalent dimers of DR5-S are present, though the short isoform has a greater tendency to form high molecular weight aggregates in the absence of ligand. That DR5-S exists as dimeric species when concentrated at the cell surface, suggests that, like DR5-L, it may exist as a dimer within ligand-receptor networks (despite lacking the cysteine) (Figure 3-1, E). Under these overexpressed conditions, DR5-L primarily forms receptor dimers and trimers (Figure 3-4, C), with a notable reduction in higher order molecular weight clusters as compared to DR5-S, consistent with the difference in the BJAB cells (Figure 3-3, D and Figure 3-3, E). The presence of oligomeric receptor species in transiently expressing cells indicates that overexpression due to the unregulated CMV promoter, and thus receptor crowding in the membrane, enables DR5 to adopt an active, oligomerized conformation, consistent with the observation that overexpression results in ligand-independent DR5 activity [52]. We note the lower level of background, non-specific bands in transiently expressing HEK293 cells (compared to

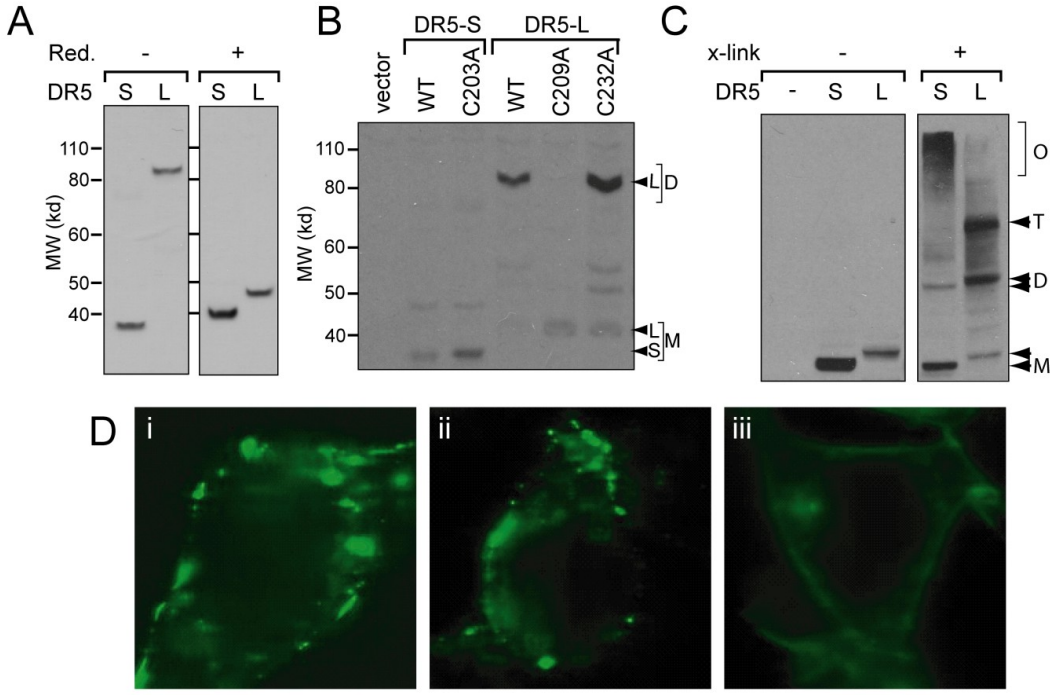

Figure 3-4. DR5 dimerization and network formation via covalent and non-covalent interactions. A, HEK293 cells were transiently transfected with DR5-S or DR5-L, and lysates were run on SDS-PAGE in the absence or presence of reducing agents (Red.). Transient overexpression of DR5-L, but not DR5-S, in HEK293 cells causes spontaneous disulfide dimer formation. B, cysteine mutagenesis within the transmembrane domain, including Cys-203 in DR5-S and Cys-209 and Cys-232 in DR5-L, demonstrates that disulfide dimerization of DR5-L occurs via Cys-209, a cysteine residue unique to the long isoform. Highlighted are the monomeric (M) and dimeric (D) forms of DR5. C, HEK293 cells transiently expressing DR5-S or -L (or vector control) were surface cross-linked (x-link) and run on SDS-PAGE gel. Surface cross-linking shows the similarities and differences in the organization of DR5-S and DR5-L. Consistent with stabilization of an active conformation, dimer formation occurs in both DR5-S and DR5-L under transient overexpression. DR5-S forms high molecular weight clusters, whereas DR5-L is primarily dimeric and trimeric. Highlighted are monomeric (M), dimeric (D), trimeric (T) and oligomeric (O) forms of DR5. D, full-length YFP-tagged DR5-S (panel i) shows a high degree of receptor clustering within the membrane, forming large receptor aggregates, consistent with cross-linking experiments. Full-length YFP-tagged DR5-L (panel ii) shows some degree of clustering in the membrane, but it has a more diffuse pattern than DR5-S. Consistent with previous studies, removal of the cytosolic domain results in homogeneous localization throughout the plasma membrane, as observed with DR5-S-YFP lacking a cytosolic domain (panel iii).

Jurkat and BJAB results in Figure 3-3), which is a result of receptor overexpression relative to other proteins.

To verify these Western blot results that, at overexpressed receptor levels, DR5 clusters occur in the absence of ligand, DR5-S and DR5-L were tagged with a C-terminal YFP fluorophore, and the resulting plasmid transfected into HEK293 cells for fluorescence imaging. The function of both DR5-S-YFP and DR5-L-YFP was confirmed by their ability to activate caspase-8, with DR5-agonist augmenting caspase-8 activity, similar to the untagged receptor when expressed in DR5-deficient BJAB cells (see Supplemental Results, Figure 3-11 on p. 73). Using confocal microscopy, we observe the formation of large clusters of DR5-S-YFP in the plasma membrane in the absence of ligand (Figure 3-4, D-i). Expression of DR5-L-YFP, though somewhat clustered, exhibits a more diffuse pattern of fluorescence in the plasma membrane (Figure 3-4, D-ii), suggesting a lesser degree of clustering consistent with cross-linking results. As a control, removal of the cytosolic domain results in a diffuse localization of both DR5-S (Figure 3-4, D-iii) and DR5-L (data not shown) in the plasma membrane, confirming a potential role of the death domain in cluster formation as previously described [111]. In addition to demonstrating that overexpression of DR5 results in ligand-independent oligomerization, confocal microscopy results demonstrate that surface cross-linking of DR5 is non-random, as DR5-S and DR5-L show different patterns of fluorescence, consistent with results in agonist-treated BJAB cells expressing DR5-S or DR5-L (Figure 3-3, B and C) and 293 cells (Figure 3-4, C).

3.4.4. DR5 transmembrane α-helices form dimeric bundles in both isoforms

Accordingly, to further measure receptor structure in the membrane of a living cell, we performed fluorescence resonance energy transfer (FRET), using CFP- and YFP-tagged DR5 and tumor necrosis factor receptor 1 (TNFR1) as a control (Figure 3-5, A). Placement of the fluorophore immediately downstream of the TM domain allows for analysis of TM separation. Similar constructs have been used to study receptor assembly

in DR5, Fas and TNF systems using FRET [201]. While truncation of the cytosolic domain precludes the formation of ligand-independent receptor clusters (Figure 3-4, D), this placement of the fluorophore immediately downstream of the TM domain still yields measurable energy transfers. This demonstrates that truncated receptors retain the ability to oligomerize via extracellular and transmembrane residues (the focus of this study), and further allows for detailed analysis of TM domain oligomerization and the relative role of TM residues including Cys209. The function of XFP-tagged DR5 constructs, both full length and truncated, was evaluated in BJAB DR5-deficient cells (see Supplemental Results, Figure 3-11 page 73).

FRET was measured by acceptor selective photobleaching [189–191], where an increase in donor fluorescence after selective photobleaching of the acceptor provides a quantitative measure of energy transfer efficiency between fluorophores (Figure 3-5, B). Transfection of DR5-CFP and -YFP constructs yields significant energy transfer over donor-only controls, with DR5-L, 0.402, having a significantly higher energy transfer than DR5-S, 0.327 ($p<0.05$) (Figure 3-5, C). Although co-transfection of DR5-S and DR5-L leads to measurable levels of hetero-oligomeric FRET, 0.164, the amount of energy transfer is significantly lower ($p<0.001$) than in the homo-oligomeric case. The hetero-oligomeric interaction of DR5-S or DR5-L with TNFR1 yields negligible energy transfer, 0.022 and 0.040, respectively (Figure 3-5, C), indicating that the DR5-S/DR5-L hetero-oligomeric interaction, though less favorable than the homo-oligomeric interaction, is still present and may represent a physiologically relevant structure in the plasma membrane.

Mutation of DR5-L Cys209 to alanine results in a significant decrease in the FRET efficiency of DR5-L to a level statistically indistinguishable from that observed for DR5-S (Figure 3-5, D). This result is consistent with the idea that receptor oligomerization of DR5-L, directed in part through Cys209 disulfide dimerization, results in a structure and/or association kinetics that differ with those of DR5-S. Although the FRET efficiency of DR5-L C209A is identical to that of DR5-S, this mutation did not increase the propensity for heterodimer formation with DR5-S, suggesting that the

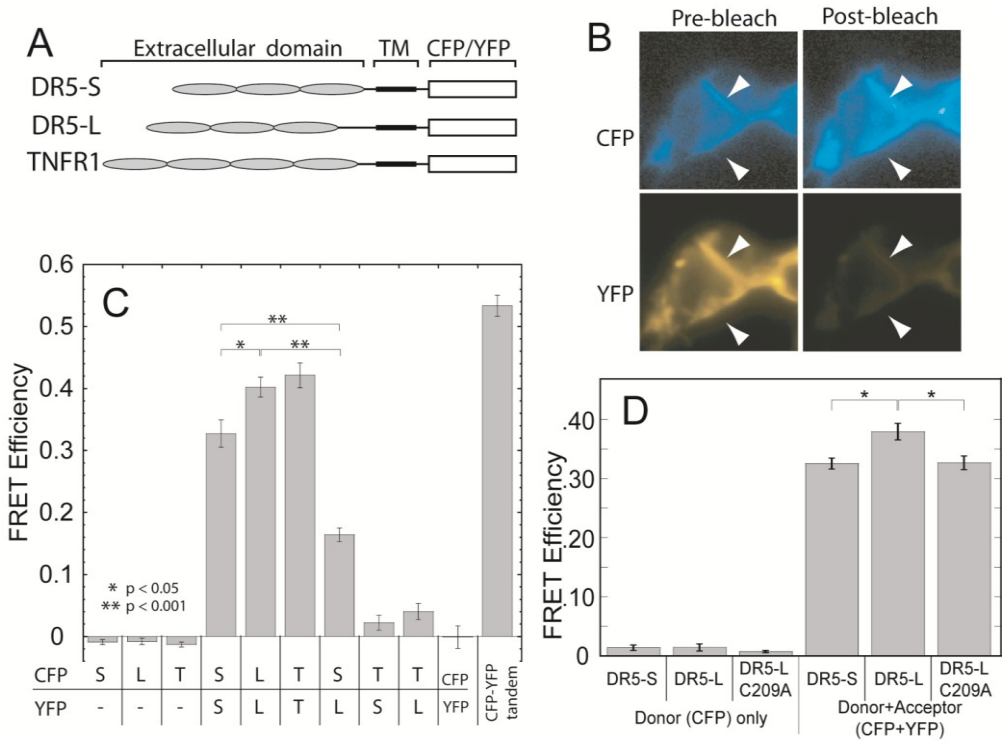

Figure 3-5. DR5-S and DR5-L differ in their FRET efficiency as dictated through Cys209. A, FRET constructs, DR5-S, DR5-L, and TNFR1, were truncated and labeled shortly after the predicted transmembrane domain. B, acceptor photobleaching FRET in TNFR1, used as a control, shows an increase in donor (CFP) fluorescence after selective photobleaching of the acceptor (YFP). C, co-transfection of donor and acceptor plasmids in HEK293 cells shows significant differences in energy transfer between DR5-S and DR5-L. Additionally, hetero-oligomer formation is less favorable than homo-oligomerization of either DR5-S or DR5-L. Neither DR5-S nor DR5-L is able to form hetero-oligomeric complexes with TNFR1. Note: * indicates statistically significant with p<0.05; ** indicates statistically significant with p< 0.001. D, mutation of DR5-L C209A causes a significant reduction in DR5-L FRET to a level indistinguishable from DR5-S.Note: * indicates statistically significant with p<0.05.

relatively low hetero-oligomerization affinity is not due to the high affinity of DR5-L self-association via disulfide bond. Rather, differences in hetero-oligomerization may be a result of isoform-dependent differences in the vertical position of the PLAD, protein localization within the membrane due to TM domain differences, or perhaps a difference in affinity due to TM orientation.

The observation of measurable steady-state FRET efficiencies clearly indicates that oligomeric receptor complexes exist in the cell membrane. FRET efficiency increases with either the fraction of receptors in oligomeric complexes or the proximity of donors and acceptors within the complex. Thus it was unknown whether the observed differences in FRET efficiency between DR5-S, DR5-L and DR5-L C209A are due to a change in the equilibrium of association or a change in the structure of the dimer (i.e. the separation of the fluorophores). To elucidate these two independent factors, FRET measurements were made in HEK293 cells at varying YFP concentration, and FRET efficiency was plotted as a function of YFP intensity (Figure 3-6, A-C). FRET efficiency (FRET) increases with increasing YFP intensity ([YFP]), and the data was fit to a hyperbolic saturable binding curve of the form $FRET = (FRET_{max} * [YFP]) / (K_{d2} + [YFP])$ as previously described [187,189,191]. From this fit two parameters were extracted: the maximum FRET efficiency ($FRET_{max}$, the theoretical limit of FRET efficiency at large [YFP]) and the relative dissociation constant, K_{d2} (the YFP concentration at which half-maximum FRET is observed), yielding information about fluorophore separation and relative binding affinity, respectively. DR5-S and DR5-L C209A show a similar increase in FRET efficiency with increasing acceptor concentration whereas DR5-L shows a sharp increase in energy transfer at low levels of YFP, thus favoring the complexed state. Despite differences in the equilibrium of oligomerization, the maximum FRET in each case is approximately equal, indicating that fluorophore separation in the receptor-complexed state is the same for DR5-S, DR5-L and DR5-L C209A (Figure 3-6, D). These results suggest that receptor assembly involves TM dimerization, forming similar oligomeric structures even in the absence of disulfide bond formation.

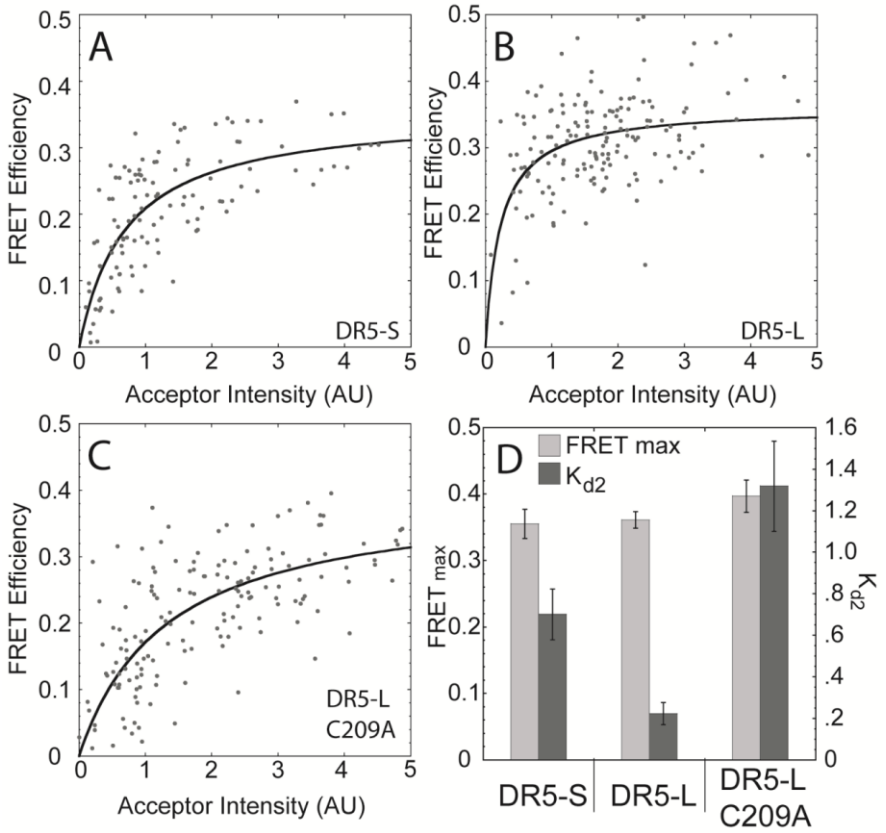

Figure 3-6. DR5-S and DR5-L differ in their self-associating affinity but not in their TM domain separation. A–C, transfection of donor and acceptor constructs at varying acceptor (YFP) levels shows increasing FRET at higher YFP concentration. Each data point represents calculated FRET efficiency at a measured YFP intensity for an individual cell. Curve fits (solid lines) are based on a two-parameter saturable binding curve. D, parameters from the curve fit, maximum FRET efficiency, and Kd2 suggest that the fluorophore separation of the DR5-S, DR5-L, and DR5-L C209A in the complexed state are indistinguishable (light bars), but the effect of the cysteine residue is to reduce the dissociation constant and thus favor oligomerization (dark bars).

In general, interactions between TM domain α-helices can provide a driving force for intermolecular assembly and are involved in the physiologic function and pathogenic dysfunction in a number of TM signaling molecules [202–205]. However, in the crystal structures of the ECD of the TRAIL-DR5 complex (which do not include any of the additional residues in the DR5L isoform), the last resolved residues place the three TM α-helices ~50Å apart. This has led to the conclusion that the TM helices of DR5 are independent and non-interacting, a presumption that is propagated in all molecular schematics of TNF receptors (for example, see Chapter 1, Figure 1-4, p. 11). Conversely, the pre-ligand dimeric structure of TNFR1 places the TM helices less than 20Å apart, suggesting that if this is the dimer structure that is embedded within a supramolecular network, that the TM helices may in fact form a stable dimeric bundle within the membrane. Therefore, we next tested whether synthetic DR5 TM peptides, in the absence of regulation by soluble domains, have the propensity for self-association. Synthetic DR5 TM peptides were reconstituted into DPC micelles in the absence and presence of reducing agents and were then cross-linked, or not, with glutaraldehyde. We observe the covalent dimerization of TM peptides via Cys209 disulfide bonding with samples prepared in the absence of reducing agents (Figure 3-7, A). The addition of reducing agents during sample preparation precludes dimer formation. Moreover, cross-linking of reduced samples shows the DR5 TM domain has only a low propensity to dimerize via non-covalent interactions, suggesting that non-covalent interactions within the TM domain alone may not be sufficient for receptor dimerization. Non-reduced, cross-linked samples show that the disulfide-linked dimer species may be able to recruit an additional monomer or dimer, indicating some level of higher order TM domain clustering through both covalent and non-covalent interactions, consistent with results in HEK293 cells expressing the full length protein (Figure 3-4, C). Time-resolved FRET analysis using labeled peptides also confirms that DR5 TM peptides exist as oligomers in detergent, both in the presence and absence of reducing agent.

We predicted the structure of the monomeric and disulfide-linked TM domain using replica exchange molecular dynamics (REMD) simulations [206]. As expected

from sequenced-based α-helical TM prediction tools (see Figure 3-2, A), several of the residues in the long isoform form a contiguous helix and insert in the membrane (Figure 3-7, B). Additionally, the structural prediction of the DR5 TM monomer suggests a potential role for the widely-conserved GG4 (GxxxG) helix dimerization motif [207–209], which has approximately the same circumferential location on the α-helix as Cys209. REMD simulation of the disulfide-linked DR5 TM dimer further shows a non-covalent GG4 interaction in the disulfide-linked state (Figure 3-7, C). In the symmetric

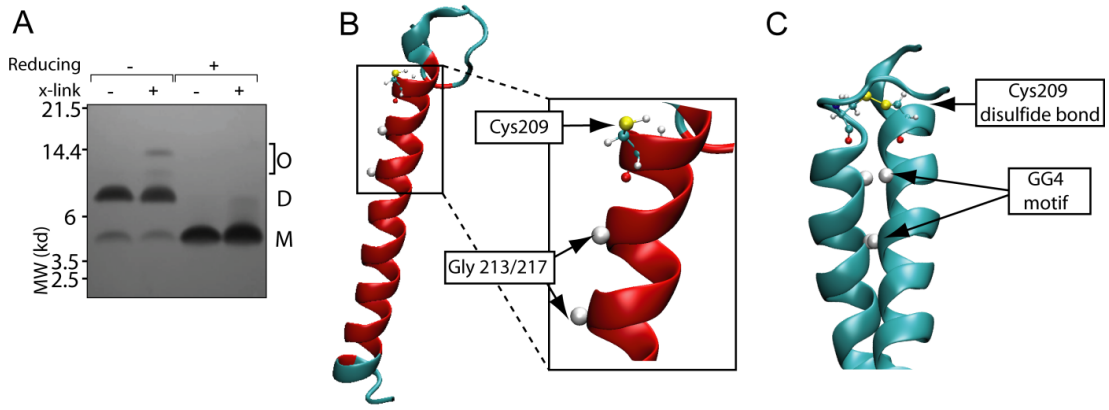

Figure 3-7. Transmembrane domain clustering of DR5. A, synthetic DR5-L TM peptide was reconstituted in DPC micelles in the absence and presence of reducing agents and glutaraldehyde cross-linker (x-link) as indicated, run on SDS-PAGE gel, and analyzed by silver stain. Results show that DR5-L TM domain may form higher order clusters, including TM trimers and tetramers under nonreducing, cross-linked conditions. Samples prepared in the presence of reducing agents do not recruit additional TM helices, suggesting a possible TM domain role in higher order receptor clustering. Highlighted are monomeric (M), dimeric (D), and oligomeric (O) forms of the TM peptide. B, replica exchange molecular dynamics simulation of the monomeric DR5-L TM domain embedded in a membrane shows contiguous α-helix formation of four amino acids unique to DR5-L, including Cys-209. Helical residues shown in red are located within bilayer. C, replica exchange molecular dynamics simulation of the membrane embedded, disulfide-linked DR5-L dimer predicts one possible α-helical TM structure that includes a GG4 (GxxxG) interaction at the dimer interface.

dimer, this dimerization motif lies on the same helical interface as the Cys residue forming a CxxxGxxxG sequence in the long isoform. It is unclear how often a cysteine residue occurs in proximity to a GG4 motif, though a brief bioinformatics search reveals that several membrane proteins contain the CxxxGxxxG motif within the TM domain, including LST1, a protein that spontaneously forms disulfide-linked homodimers [210], and death receptor 4, a related TRAIL receptor for which no known TM interactions exist (though we note that the motif is located in a different region of the predicted TM helix than in DR5). Collectively, these results show a strong role for TM α-helix dimers in the overall architecture of activated DR5.

3.5. Discussion

The current understanding of the structure-function relationship in the TRAIL-DR5 complex is based not on native, full length protein expressed at endogenous levels, but rather on crystals of fragmented soluble domains, the behavior of overexpressed receptors in model cell lines, and fluorescence imaging at the whole-cell level. These studies have provided highly useful information about the fundamental role of the PLAD, ligand-binding and death domains and suggested a role for supramolecular clustering. However, little has been done to elucidate the structural and molecular mechanisms in early events of DR5 signaling. It is therefore of great interest and difficulty to understand the nuanced role of not just the specific interactions between TRAIL and DR5, but also between DR5 monomers, and exactly how the sum of such interactions result in the orchestration of macromolecular aggregates visible by fluorescence microscopy [112].

Supramolecular clustering of receptors, including TNFR1, Fas and DR5 has emerged as a potentially powerful paradigm shift in the field of apoptotic signaling. The canonical view of a single trimeric ligand-receptor structure is giving way to a revised picture of highly organized networks of ligands and receptors driven through stable receptor-receptor interactions in multiple domains that vary in their stoichiometry to generate large aggregates of ligand-receptor trimeric structures [138,139]. The first network model was put forth by Francis Chan and suggests that ligand causes

aggregation of pre-assembled dimeric receptors via extensive receptor-receptor interactions in a tri-fold symmetry [139]. A second network model was put forth by Ozsoy et al. suggesting that trimeric TNF engages a pre-formed receptor dimer complex and cause a 120° rotational conformational change resulting in dimeric activation and formation of a network in the form of a hexagonal mosaic of ligand-receptor trimers [138]. While both models are intriguing, they lack the necessary diverse experimentation and evidence to support their foundation: a ligand-induced, dynamic reorganization of pre-ligand assembled dimers that enables specific receptor-receptor interactions that stabilize the network.

Our results from an endogenous system (Jurkat cells) and corroborated in model systems (BJAB and HEK293 cells) provide the first substantive support for these types of models, shown in Figure 3-1, E, in which TRAIL-induced networks display an organization via DR5 dimerization through membrane-proximal residues. In the case of DR5, our data suggests that pre-formed receptor *trimers*—different from the pre-assembled dimers observed in the case of TNFR1—are engaged by trimerized TRAIL [92] to form a TRAIL-DR5 trimer complex during which the receptors undergo a conformational change that exposes the dimeric interaction motifs. We have shown that this motif includes interactions between TM domain α-helices, (e.g. the Cys209 in the case of DR5-L, and possibly GxxxG in the case of both DR5-L and DR5-S), but we do not rule out the likely possibility that the interaction is further stabilized by interactions in the ECD and intracellular domains as well (for example those in or near the PLAD and death domain). This ligand-induced structural rearrangement promotes formation of receptor dimers that tether the trimeric ligand-receptor complex (Figure 3-1, D) thus driving the formation of organized receptor networks (Figure 3-1, E). Therefore, formation of the network serves two general purposes. First, network formation stabilizes the receptor dimer species which may in turn stabilize the dimerization of intracellular death domains as well as caspase-8—suggested by structural and functional data to be the active conformation. Also, network formation may provide a high, local concentration of active, dimeric intracellular death domains able to overcome inhibitory pathways.

In the context of the hypothetical network models (Figure 3-1, E), one interpretation of our data is that ligand-induced dimerization via TM residues (including both Cys209 disulfide bond formation and non-covalent association) occurs between neighboring trimeric structures of ligand and receptor. An alternative and equally valid interpretation of the data is that ligand induces a dimeric association (via Cys209 disulfide bond or non-covalent interactions) within a trimeric ligand-receptor structure—that is, TM association occurs between two receptor monomers within a crystal structure unit. This intra-trimeric TM association would likely tend to oppose network formation, as intra-trimeric association would leave only one free TM domain to associate with an adjacent trimeric unit. Thus, in the extreme case where every ligand-independent, pre-assembled trimer forms an intra-trimeric association upon ligand binding, one would expect a maximum of two trimeric ligand-receptor units per cluster. In the more realistic case, where intra-trimeric association occurs in a percentage of these complexes, network size would tend to be limited due to a lack of free TM helices. In the context of DR5-L, if irreversible, intra-trimeric Cys209 disulfide bond formation occurs in a fraction of all trimeric ligand-receptor complexes, we would expect less network formation and a potentially less functional isoform of DR5. Interestingly, all of our data is consistent with this interpretation, that DR5-L tends to form networks to a lesser extent than DR5-S (see Figure 3-3, D-E and Figure 3-4, C) and is less functional (see Figure 3-2, B). Therefore, we cannot rule out the possibility for intra-trimeric TM association, which may be irreversible in the case of DR5-L. Additionally, we cannot rule out the possibility that receptor networks may be stabilized via trimeric receptor bundles (Figure 3-1, E, compare top [138] and bottom [139] models), or potentially even by tetrameric receptor bundles via combinations of covalent (Cys209 disulfide) and non-covalent (GG4) interactions, as predicted by studies with the purified TM peptide (see Figure 3-7, A). Ongoing efforts include quantification of cluster size (see Chapter 4) and differences in cluster size between DR5-S and DR5-L isoforms.

A second important facet of this study, in particular for the ongoing efforts to target DR5 in the treatment of cancer, is the validation and further understanding of two

DR5 isoforms expressed on the protein level in human cancer cells. To date, no pattern of DR5-S or DR5-L expression in normal versus tumor cells is known, though it is intriguing to postulate that the presence of DR5-S and/or DR5-L isoforms in tumor cells may serve as a viable predictive biomarker for TRAIL-based targeted therapy and/or any agent that may rely on engaging this pathway. Although the expression of two DR5 isoforms (at the mRNA level) was first noticed relatively early after the discovery of DR5 [198,211], no studies have investigated the difference, structural or functional, between the two, and only a few publications have acknowledged the expression of the two isoforms at the protein-level [52,212,213]. The functional role of the 29 amino acid insertion in DR5-L is yet unknown, though the sequence is rich in structurally active residues, such as proline, as well as chemically active residues, such serine or threonine residues that may be modified by phosphorylation or glycosylation as previously shown [52]. It is possible that, with the addition of 29 amino acids, the cysteine residue evolved to hold the TM helices in an active conformation that is otherwise less favorable due to the increased flexibility from the additional residues upstream.

Whether there is functional significance to our finding that DR5-S and DR5-L preferentially form homo-oligomers over hetero-oligomers remains unknown. Mutation of C209A does not increase the ability of DR5-L to interact with DR5-S, suggesting that the reduced propensity for hetero-oligomerization is not solely due to disulfide bonds favoring heterodimerization of DR5-L. That DR5-S and DR5-L have a low propensity to form hetero-oligomers begs the question of whether one has a higher affinity for decoy receptors (which do not have free cysteines), thus influencing its activity. More generally speaking, studying the functional difference of the two isoforms in their native, endogenous states is remarkably difficult and reflects a ubiquitous challenge to biophysicists attempting to make headway in natural, cellular systems. Any measure of protein function (e.g. caspase activation or cell death) must be normalized to the total, active protein content in the plasma membrane. However, even in our stable BJAB lines expressing exclusively one of the two isoforms, we were unable to quantify relative receptor efficiency because of uncontrollable and non-quantifiable differences in total

protein expression. Even if one were able to quantify exact receptor densities in the plasma membrane and further determine how many of these proteins are active, it is unclear that the relationship between receptor density and function is strictly linear, further complicating a determination of an isoform-dependent efficiency per receptor. Quantifying these aspects of receptor activation may become possible through ongoing studies that employ higher-resolution microscopy and time-resolved FRET measurements or may require a more complicated combination of cell biology and biophysics as has been attempted for DR5, as well as in the study of a separate class of receptor networks [153,214,215].

3.6. Concluding Remarks

We have shown that early events in TRAIL-induced signaling via DR5 involves structural re-organization and receptor dimerization within large protein complexes, and that dimerization is mediated by membrane-proximal residues. This is the first evidence to suggest that ligand-induced receptor clusters are highly organized, and that they are likely regular arrays or regularly-structured networks. Moreover, given the structural and functional evidence that dimerization of intracellular domains as well as downstream signaling proteins is critical for their activation, the ligand-induced receptor dimerization event appears to be a crucial step in DR5 activation. Here, we took advantage of a free cysteine residue in DR5-L to identify a novel protein-protein interaction motif and show that the fluorophore separation in the DR5-L disulfide-linked structure is indistinguishable from that of DR5-S. Thus, at endogenous receptor levels, ligand-induced dimerization occurs via, at least in part, the TM domain, a domain in the TNF receptor superfamily that has remained largely unstudied. More broadly, given their structural homology—both monomeric and ligand-bound—many other TNF receptor superfamily members likely undergo a similar dimerization event that is critical for signal propagation through the membrane. Ongoing efforts to understand the functional relevance of TNF receptor networks should clarify whether they exist as a mechanism to

concentrate intracellular signals (in order to overcome biochemical thresholds), whether the network formation itself causes the key conformational change associated with signaling, or both.

3.7. Supplemental Results

3.7.1. TRAIL induces disulfide linked dimers of DR5 within high molecular weight networks, and cross-linking with BS3 does not cause non-specific aggregation of TRAIL and non-DR5 proteins

We have shown that both TRAIL and a DR5-specific antibody agonist induce network formation that involves dimerization of receptor monomer units. To conclusively determine whether the observed dimer is formed via disulfide bond, Jurkat cells were treated with and without TRAIL and cell surface cross-linker, and lysates were analyzed by SDS-PAGE and Western (Figure 3-8, A). In the absence of reducing agents the addition of TRAIL results in the formation of receptor dimers, and cross-linking causes the dimer band to disappear, presumably because it is embedded in high molecular weight clusters (> 260 kD), as described in the main text. Under reducing conditions, on the other hand, the dimer band is absent under all conditions, indicating that ligand-induced dimerization is mediated by disulfide bond formation. The clusters are still observed in cross-linked samples run under reducing conditions, indicating that disulfide bonds are not necessary the detection of networks via SDS-PAGE and Western blot. The addition of cross-linker potentially could result in non-specific cross-linking of TRAIL and DR5 to nearby, but unrelated membrane proteins. While we expect that any cross-linker promiscuity would likely be insensitive to the addition of TRAIL (Figure 3-3, C, compare lanes 4 and 5), we wanted to rule out the possibility that the addition of TRAIL is increasing the overall level of high molecular weight protein species in the presence of cross-linker. The same cell lysates used in Figure 3-8A were separated under reducing conditions and the gel Coomassie stained (Figure 3-8B). Staining of all proteins in the lysate shows no detectable change in the band pattern upon TRAIL addition,

indicating that the observed increase in DR5 at high molecular weights (Figure 3-3, C-E and Figure 3-8A) are not a result of random cross-linking upon the addition of TRAIL.

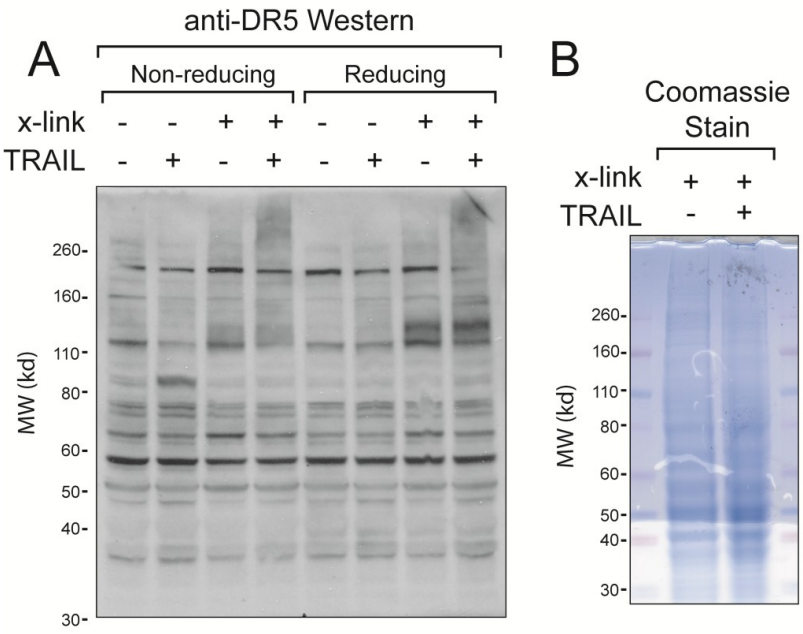

Figure 3-8. Jurkat cells were treated with TRAIL or control (PBS) and subsequently cross-linked as indicated with a cell surface cross-linker. (A) Whole cell lysates were run in the absence or presence of reducing agents, transferred to nitrocellulose, and analyzed for DR5 oligomerization. (B) Cross-linked, whole cell lysates were reduced, separated on a 4-12% SDS-PAGE gel, and Coomassie stained.

3.7.2. TRAIL causes disulfide linked dimers in the presence and absence of ligand enhancers

It has been suggested that agonist antibody cross-linking, or enhancement of ligand prior to treating cells increases its activity by clustering the ligand into multimers of the trimeric ligand complex. We tested whether Flag-TRAIL in the absence or presence of an enhancing anti-Flag antibody has any effect on DR5 dimerization. Flag-TRAIL was pre-incubated with an enhancing agent (anti-Flag antibody) at room temperature for 15 minutes. TRAIL was incubated with Jurkat cells as before. The addition of a ligand enhancer has no affect on the ability of TRAIL to produce DR5

dimers and high molecular weight clusters, suggesting that ligand-induced dimerization of DR5 is not dependent on antibody-mediated clustering of TRAIL (Figure 3-9). The addition of an antibody agonist also produces dimeric DR5, at an identical weight,

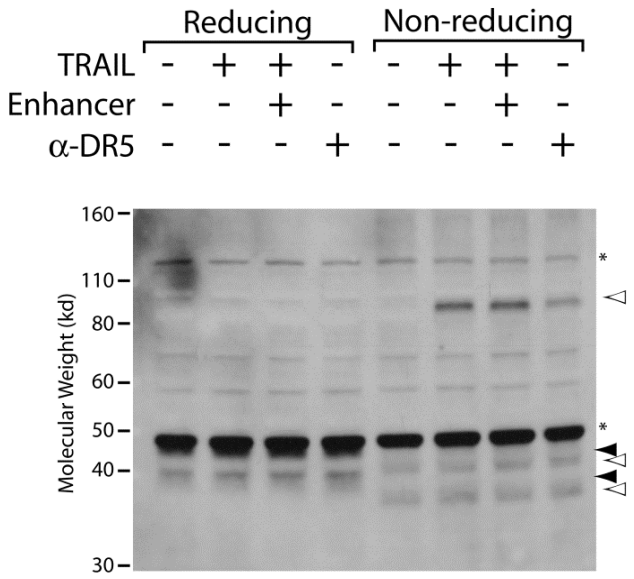

Figure 3-9. Jurkat cells were treated with Flag-TRAIL (with and without an anti-Flag enhancer, see Supplemental Methods, p. 75) or a DR5-specific antibody agonist (α-DR5) as indicated. Whole cell lysates were run under non-reducing or reducing (with βME and DTT) conditions, transferred to nitrocellulose, and analyzed for DR5 dimerization. Closed arrowheads indicate DR5 under reducing conditions and open arrowheads indicate DR5 under non-reducing conditions, including the dimer species at approximately 80kD. The asterisk indicates a strong unknown band associated with this particular antibody (ProSci anti-DR5 antibody).

suggesting that the addition of ligand—either TRAIL or antibody agonist—induces dimerization and correlates with receptor function.

3.7.3. Pre-ligand assembly of DR5 results in receptor trimers

Pre-ligand assembly is critical for ligand binding and function of DR5. In determining the molecular architecture of ligand-induced DR5-networks, we found that

cross-linking of surface proteins results in the formation of DR5 trimers at approximately 120kD (see Figure 3-3, C-E). To confirm that this band is indeed DR5, we knocked down DR5 in Jurkat cells by transfection of shRNA and selection (see Supplemental Methods, Section 3.8.4, p. 75). DR5 knockdown cells and the parental (wild type) Jurkat cells were cross-linked, or not (as described in the Experimental Procedures, Section 3.3.5), and lysates were separated via SDS-PAGE and analyzed by Western blot. Cells stably expressing shRNA targeting DR5 show a reduced band at ~120kD, confirming that cross-linking of Jurkat cells in the absence of ligand produces a distinct band corresponding to pre-ligand, trimeric DR5 (Figure 3-10).

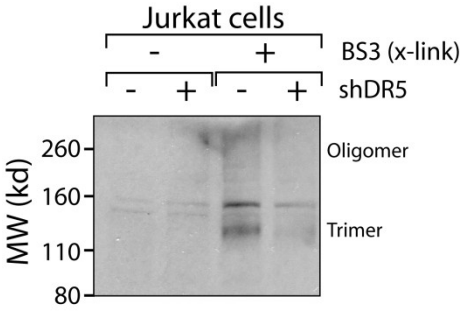

Figure 3-10. DR5 was knocked down in Jurkat cells via shRNA transfection and selections (see Supplemental Methods, p. 75). The DR5-knockdown cells (and parental Jurkat cells as a control) were cross-linked using BS3 surface cross-linker, and whole cell lysates were analyzed by Western blot using an antibody against DR5.

Further, we have noted that this trimer band is not diminished in the presence of TRAIL or agonist. Based on the model presented in Figure 3-1, it would seem likely that pre-assembled DR5 trimers, upon binding TRAIL (or agonist), would decrease the amount of trimeric DR5, perhaps shifting this band upwards by the molecular weight of the trimer. We have offered two interpretations for our observation that the 120kD trimeric DR5 band persists in the presence of TRAIL or agonist. First, it is conceivable that the chemistry and/or linker-length of the cross-linker is such that networks are more readily cross-linked than individual trimeric ligand-receptor (i.e. crystal structure) units. That is, perhaps the crystal structure unit is not chemically cross-linkable (at least not

with BS3). Alternatively, it is possible that ligand binding to pre-assembled trimers, resulting in the formation of high molecular weight networks, drives further pre-assembly of DR5, replenishing the pool of pre-assembled complexes.

3.7.4. Full-length, fluorophore-tagged DR5 is functional

Death receptors, as other proteins, are often tagged with GFP and variants to study localization, distribution and structure. Here, we use XFP-tagged DR5 to determine molecular-level structure and binding kinetics as well as cellular localization and distribution of both truncated and full length DR5. We evaluated the function of these receptors, including truncated (lacking the cytosolic domain) and full length, tagged and untagged as shown in Figure 3-11, top. Briefly, each construct was transiently transfected into BJAB DR5-deficient cells, and activity was assessed by a fluorescent caspase-8 marker in the absence and presence of a DR5-specific agonist ligand. Activity results are shown in Figure 3-11, bottom. Control transfections (empty pIRES2-EGFP or pEYFP-N1 vectors) show no difference in caspase-8 activity compared to untransfected cells, nor do these cells have any sensitivity to ligand. As a positive control, cells were transfected with DR5-S-IRES-GFP, resulting in co-expression of untagged DR5-S and GFP. DR5-S-IRES-GFP transfected cells have an increased basal level of caspase-8 activity, and the addition of ligand augments the level of caspase-8 activation, showing that receptor expression increases ligand sensitivity.

Transfection of truncated DR5-S-YFP (residues 1-211), where YFP is located just downstream of the predicted transmembrane domain, results in no caspase-8 activity. Further addition of agonist does not increase caspase-8 activity, confirming the role of the intracellular domain (including the functional death domain) in receptor function. Transfection of the full length DR5-S-YFP (residues 1-411), where YFP is covalently

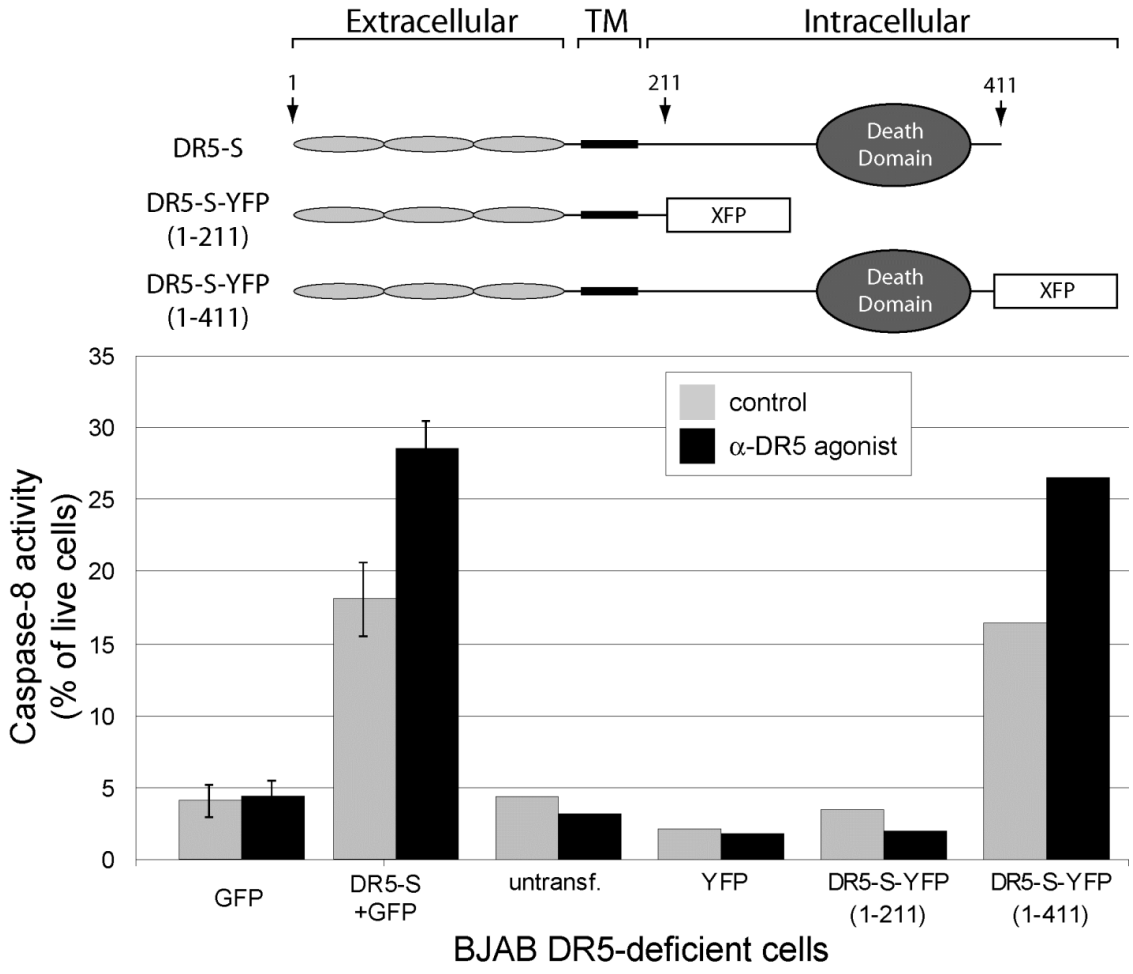

Figure 3-11. (Top) Untagged and tagged DR5 constructs are shown. The truncated DR5-S includes residues 1-211 and the full length includes residues 1-411. The full length, untagged DR5-S was cloned into an IRES-EGFP vector for co-expression of DR5-S and GFP. (Bottom) BJAB DR5-deficient cells were transfected with the indicated plasmid: GFP, DR5-S + GFP, YFP, DR5-S-YFP (1-211 truncated) and DR5-S-YFP (1-411 full length). Twenty-four to forty-eight hours post-transfection, cells were treated for 4 hours with either DR5-antibody agonist (black bars) or control (gray bars), and caspase-8 activity was measured by flow cytometry using a red fluorescent marker for active caspase-8. The results represent the percentage of live, GFP- or YFP-positive cells with active caspase-8, compared to an untreated control.

linked to the C-terminus of DR5-S, results in comparable levels of ligand-independent and ligand-induced caspase-8 activation. Collectively, these results show clearly that full length DR5-S is equally functional both in the untagged and XFP-tagged (C-terminus) form. Truncation of DR5-S lacking the cytosolic domain (and thus the death domain) results in no measurable activity, either in the absence or presence of ligand.

3.8. Supplemental Methods

3.8.1. Reagents and antibodies

*A*ntibodies against DR5 were purchased from Cell Signaling and ProSci. We note that the antibody obtained from ProSci shows a strong, unknown band at ~48kD, and since this band does not shift under reducing/non-reducing conditions (as is observed in transiently expressing cells), we conclude that this band is in fact not DR5. The caspase-8 activity kit was purchased from Biovision (CaspGLOW red Caspase-8 activity kit). Flag-TRAIL and an "enhancer" (typically an anti-Flag antibody) were purchased from Enzo Life Sciences.

3.8.2. Cloning

CFP and YFP, in the pECFP-N1 and pEYFP-N1 vectors (Clontech), respectively, were mutated to form the monomeric form of the fluorescent protein, the A206K mutation. DR5 was cloned into these vectors and sequence. Additionally, DR5 (full length) was cloned into the pIRES2-EGFP vector (Clontech) for co-expression of untagged DR5 with EGFP.

3.8.3. Transfection

Jurkat cells were transfected via electroporation at 200V and 975uF. Shortly after transfection, live cells were isolated by ficoll gradient centrifugation. Cells were analyzed as described approximately 48 hours after transfection.

3.8.4. DR5 knockdown

Jurkat cells were transfected with each of four different shRNA constructs targeting DR5. Cells were selected with puromycin (2μg/ml), and after selection live cells were isolated by ficoll gradient centrifugation. Live, puromycin-resistant cells were cultured for several weeks, and the resulting non-homogenous cell population was used to test whether the ~120kD band in the presence of cross-linker is indeed DR5.

3.8.5. TRAIL enhancing

TRAIL was enhanced using an "enhancing agent" purchased from Enzo Life Sciences to determine if antibody-mediated ligand cross-linking has any bearing on dimer formation. TRAIL was incubated with the enhancing agent for 15-20 minutes at room temperature, per the manufacturer's instructions, immediately prior to incubation with cells.

3.8.6. Caspase-8 activity

Cells were transfected by electroporation with the indicated plasmid, and shortly after electroporation live cells (i.e. cells that survived the electroporation process) were isolated by ficoll gradient centrifugation. Twenty-four to forty-eight hours after transfection, cells were treated with a DR5-specific antibody agonist and analyzed for active caspase-8. Briefly, live cells (based on FSC, SSC patterns) were analyzed for their expression of fluorescent protein (either GFP or YFP). Live, GFP/YFP + cells were analyzed for caspase-8 activity.

Chapter 4. Membrane cholesterol is required for Death Receptor 5 network formation and signaling

4.1. Summary

Death receptor 5 (DR5) is an apoptosis-inducing member of the tumor necrosis factor superfamily that, upon stimulation by extracellular ligands, activates intracellular pathways resulting in cell death. In Chapter 3, we demonstrated that DR5, upon stimulation by ligand, forms large clusters within the plasma membrane, and that cluster formation is mediated in part by interactions within the receptor transmembrane domain. However, it is unknown whether the membrane plays an active role in driving these transmembrane interactions or in the formation of large ligand-receptor networks. In this chapter, we demonstrate that stimulation by ligand results in the lateral migration of DR5 into cholesterol-rich membrane domains. We further show that extraction of membrane cholesterol inhibits ligand-induced structural changes and also the activation of intracellular signaling. These results highlight the importance of the plasma membrane in DR5 signaling and enhance our view of the relationship between the structure and function of DR5 to include heterogeneous complexities of the membrane.

4.2. Introduction

Death receptor 5 (DR5), a type I transmembrane receptor, is an apoptosis-inducing member of the tumor necrosis factor (TNF) receptor superfamily that functions upon activation by TNF-related apoptosis-inducing ligand (TRAIL) or other agonists [29,44,117,216,217]. The TRAIL-DR5 signaling pathway is of great therapeutic interest, as exogenous TRAIL prevents tumor growth and, in contrast to other apoptosis-inducing

ligands such as FasL, does not exhibit systemic cytotoxicity [32]. Moreover, DR5 is widely regarded as a potential target in the treatment of cancer [170,218–220] with a number of its ligands, including recombinant human TRAIL and antibody agonists, currently in clinical trials [8–13] (see also clinicaltrials.gov). Therefore, understanding the molecular level detail of relevant events involved in TRAIL- and agonist-DR5 signal propagation, including events within the membrane, may prove to be useful in the discovery of novel DR5-directed therapeutics as well as in understanding therapeutics currently in clinical trials.

TRAIL- and agonist-induced apoptosis through DR5 involves the formation of large receptor networks, estimated to be 300-500 nm, in the plasma membrane (see Chapter 3, Figure 3-3, p. 50 also [111,112,114]). Moreover, these networks are organized through ligand-induced dimerization of DR5 driven through covalent and non-covalent interactions in membrane-proximal residues upon ligand stimulation [114]. That ligand stabilizes a specific dimeric receptor structure is consistent with crystallographic and functional evidence that intracellular protein domains and downstream proteins form stable and functional dimeric complexes [85,121–124,129]. Given that ligand-induced dimeric interactions of DR5 occur in part via membrane-proximal residues, we wondered whether the membrane plays an active role in driving the dimeric interaction of TM residues as well as the formation of large, organized receptor networks.

Lateral heterogeneity in the plasma membrane [115,116] is involved in signaling of TNF and death inducing ligands through their respective membrane receptors (reviewed in Chapter 2, section 2.8). The prototypical TNF receptor, TNFR1, localizes to cholesterol-rich lipid microdomains, often referred to as lipid rafts, and recruits downstream signaling proteins [165,166]. The death receptor Fas has been shown to localize to rafts in a ligand-dependent manner [221], though others have observed ligand-independent raft localization [222]. There is evidence that DR5 migrates into cholesterol rich microdomains upon stimulation [223], and recruits intracellular factors within such domains [224–227], however it is unknown whether localization within cholesterol-rich

lipid microdomains is associated with ligand-induced changes in receptor structure, including DR5 dimerization and clustering.

Here, we have addressed the question of whether DR5 recruitment into cholesterol-rich lipid microdomains is consistent with the formation of large receptor networks as previously described (Chapter 3). We found that DR5 is recruited into cholesterol-rich, detergent resistant membrane fractions upon stimulation by antibody agonist. We further show that cholesterol is required for ligand-induced structural changes, including DR5 dimerization as well as the formation of DR5 networks. Further, extraction of membrane cholesterol diminishes DR5-mediated activation of caspase-8 upon stimulation by agonist. These results offer the first evidence that lateral heterogeneity within the plasma membrane plays a role in driving ligand-induced receptor structural changes (i.e. dimerization and network formation) and function of DR5, further developing our view of the structure-function relationship of DR5 to include complexities involving the membrane.

4.3. Materials and Methods

4.3.1. Cell culture and reagents

Jurkat cells were cultured in RPMI-1640 media (HyClone) supplemented with 10% FBS, L-glutamine, penicillin and streptomycin and maintained at sub-confluence at 37˚C and 5% CO2 in a water-jacketed incubator. DR5 antibody agonist (mAb631), and fluorescent secondary antibody (NL557) were purchased from R&D Systems. DR5 antibody for Western blots was purchased from Cell Signaling Technologies.

4.3.2. Isolation of detergent resistant membrane (DRM) fractions

Detergent resistant membrane (DRM) and detergent soluble membrane (DSM) fractions were isolated as previously described [163,164,223]. Briefly, Jurkat cells (10^8 cells) were treated with DR5 agonist or control, resuspended in 550 µl TNE buffer

(150mM NaCl, 2mM EDTA in 50mM Tris-HCl, pH 7.4) and homogenized 20 times using a 25 gauge needle. Homogenate (500 µl) was mixed with an equal volume of 2% Triton X-100 in TNE buffer supplemented with protease inhibitors (yielding a 1% Triton X-100 final concentration) and lysis proceeded for 30 minutes on ice. Samples were centrifuged at 10,000g for 5 minutes at 4˚C, and post-nuclear supernatants (1ml) were mixed with 2ml of 56% sucrose and transferred to a SW41 ultracentrifuge tube and overlaid with 5ml of 35% sucrose and 5ml of 5% sucrose. All sucrose solutions were prepared in TNE buffer [164]. Step gradients were centrifuged at 39,800 rpm (271,000g), 4˚C for 18 hours using a SW41Ti rotor centrifuge. Gradients were fractionated into 9 fractions of equal volume using a Gradient Station (BioComp Instruments). Protein content in each fraction was measured by BCA assay (Pierce) and compared to a BSA standard curve. Cholesterol content in each fraction was measured using Amplex Red cholesterol assay (Invitrogen Life Technologies). DR5 migration into DRM fractions was analyzed by TCA precipitation and Western blot analysis, using equal volumes of each fraction.

4.3.3. Caspase-8 activity

Caspase-8 activity was measured as previously described [114]. Jurkat cells were treated with a DR5-specific antibody agonist 1µg/ml for 4 hours at 37˚C. Caspase activity was measured using CaspGLOW Red Active Caspase 8 staining kit (BioVision) according to manufacturer instructions. Fluorescent labeled active caspase-8 was detected by flow cytometry (FACSCalibur) over 50,000 cells. Data was analyzed using FlowJo software (Tree Star, Inc.), where identical gating schemes were used to determine the percentage of caspase-8 active cells and thus fold activation.

4.3.4. Cholesterol extraction from the membrane

To extract membrane cholesterol, Jurkat cells were washed in PBS and resuspended in serum-free media (RPMI-1640). Cells were treated with methyl-beta-

cyclodextrin (MβCD, Sigma-Aldrich), prepared immediately before use and used at a final concentration of 5mM. Treatment with MβCD was done at 37˚C for 30 minutes, and cells were washed extensively with PBS after treatment and before stimulation with agonist.

4.3.5. Western blot

Jurkat cells were washed with PBS and treated with DR5-specific antibody agonist for 1 hour in PBS. Cells were pelleted by centrifugation and lysed in RIPA buffer (50mM Tris-HCl pH 7.5, 150mM NaCl, 0.5% Sodium deoxycholate, 0.1% SDS, 1% NP-40) supplemented with protease inhibitors and 10mM iodoacetamide for 1-2 hours at 4˚C. Total protein concentration of lysates was determined by BCA assay (Pierce) and equal amounts of total protein (~80μg) were mixed with 4x NuPAGE sample buffer (in the absence of reducing agents), boiled for 10 minutes, and loaded on 4-12% Bis-Tris SDS-PAGE gel (Invitrogen). Proteins were transferred to nitrocellulose membrane and probed using an antibody against DR5 (Cell Signaling) and anti-rabbit HRP-conjugated secondary antibody (GE Amersham) and detected using ECL Plus (GE Amersham).

4.3.6. Confocal microscopy

Imaging of ligand-receptor clusters in Jurkat cells was done as previously described [114]. Briefly, cells were washed with PBS and treated with a DR5-specific mouse antibody (R&D Systems, MAB631) agonist at 5 μg/ml for 1 hour. After washing, cells were treated with an anti-mouse secondary antibody conjugated with NorthernLights557 (R&D Systems) used at 5 μg/ml for 30 minutes and washed. All incubations and washes were done in PBS + 1% FBS and at 4˚C (or on ice) to prevent active receptor internalization. Labeled cells were transferred to pre-chilled poly-lysine coated 35 mm glass-bottom culture dishes (MatTek Corporation) for approximately 5 minutes at RT before imaging to allow cells to settle and clusters to form. Fluorescent labeled cells were imaged in an Olympus IX81 inverted microscope equipped with a

FluoView FV1000 laser scanning confocal head (543nm laser excitation, 555-655 nm emission) using a 100x (1.3NA) oil immersion objective lens. All confocal images were acquired with the same properties (zoom, laser intensity and resolution) and images were processed identically for direct qualitative and quantitative comparison.

4.3.7. Quantitative analysis of confocal images

Confocal fluorescent images were quantitatively analyzed to determine the approximate size and intensity of ligand-receptor networks in the membrane. Images were imported into and analyzed using MatLab, where the center of the cell was approximated, and the fluorescence intensity was calculated using axial integration for each value of theta. The result is a distribution of total fluorescence intensities at each angle between 0 and 360 degrees, representing the circumference of the cell, where the 0 degree mark is located at 3 o'clock. For clarification, several clusters are highlighted in the confocal images and in the quantitative analysis are shown as indicated by the arrowheads.

4.4. Results

4.4.1. DR5 migrates to cholesterol rich membrane fractions upon agonist stimulation

The importance of cholesterol rich regions in TNF receptor signaling has been noted, however the specific effect of DR5 agonistic antibodies is not well defined. We first sought to establish whether stimulation of Jurkat cells with a DR5 agonistic antibody causes redistribution of DR5 into cholesterol-rich regions of membrane. Jurkat cells were treated with agonistic antibody (α-DR5), cells were lysed, and detergent soluble and resistant membrane fractions (DSM and DRM, respectively) were isolated by sucrose gradient ultracentrifugation (Figure 4-1, A) using a step gradient and collecting fractions of equal volume. High fraction numbers represent high density, detergent soluble membrane regions and proteins whereas lower fraction numbers represent lower density

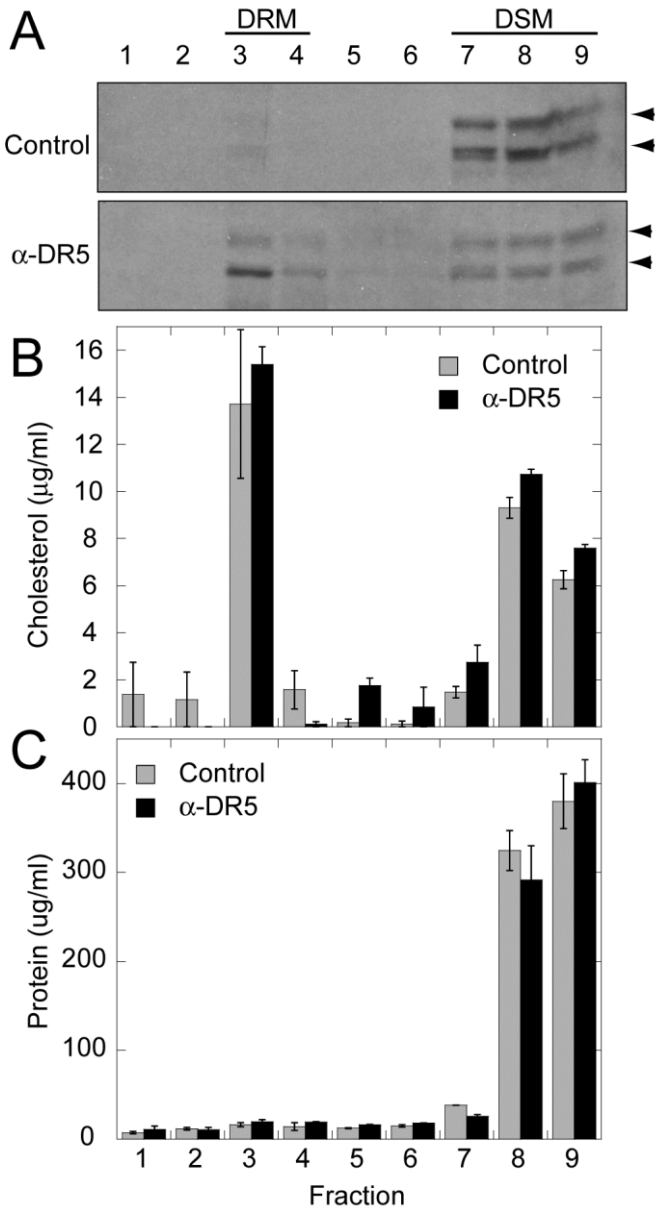

Figure 4-1. Agonist stimulation redistributes DR5 into cholesterol rich membrane regions. (A) Jurkat cells were treated with control (top) or DR5 agonist (α-DR5, bottom), and DRM fractions were isolated by Triton X-100 and sucrose gradient ultracentrifugation. Fractions 3-4 represent DRM, and fractions 7-9 represent DSM. Arrowheads indicate DR5-S and DR5-L isoforms. (B) Cholesterol content within each fraction shows a clear enrichment of cholesterol in fraction 3, the DRM fraction, with no dependence on agonist stimulation. (C) Protein content in each fraction shows no significant movement of total protein upon DR5 agonist stimulation.

regions. Analysis by Western blot using an antibody against DR5 (Figure 4-1, A) shows that, upon stimulation with agonist, DR5 clearly moves from a high density fraction (fractions 7-9, DSM) to a lower density fraction (fractions 3-4, DRM), consistent with migration into low density, cholesterol-rich membrane regions.

Cholesterol content of each fraction was measured to ensure that low-density DRM fractions are enriched in cholesterol relative to other fractions. Low density fraction 3 is significantly enriched in cholesterol, and there is no change in the cholesterol distribution upon stimulation (Figure 4-1B). We further measured the protein content of each fraction. While the majority of protein is found in high-density, DSM fractions, we observe no difference in the distribution of total protein upon the addition of agonistic antibody. Therefore we conclude that agonist-induced migration into cholesterol-rich fractions is specific to DR5. Collectively, these results demonstrate clearly that DR5 is mobile in the membrane and is redistributed into cholesterol rich membrane regions upon stimulation by antibody agonist.

4.4.2. Depletion of membrane cholesterol inhibits Caspase-8 activity via DR5 signaling

DR5 is redistributed into cholesterol-rich membrane regions upon agonist stimulation, therefore we wondered whether membrane cholesterol is required for agonist-induced function of DR5. Methyl-β-cyclodextrin (MβCD) is a cyclic oligosaccharide capable of removing cholesterol from cultured cells [228,229] and is often used to disrupt protein localization within detergent resistant membranes [163,164]. Jurkat cells were pretreated with MβCD (or control) to remove cholesterol from the membrane and then treated without and with DR5 agonistic antibody. Caspase-8 activity was determined using a fluorometric marker that irreversibly binds active caspase-8, and fluorescence of individual cells was measured by flow cytometry. Jurkat cells having cholesterol in the membrane (i.e. not treated with MβCD) efficiently activate caspase-8 upon the addition of DR5 agonist, as the distribution of fluorescence indicates a large number of cells with activated caspase-8 (Figure 4-2A, compare gray and black

distributions). Pre-treatment with MβCD results in a reduced ability of these cells to activate caspase-8, seen by a lack of shift to cells with activated caspase-8 (Figure 4-2B, compare gray and black distributions). Using an identical gating scheme on these populations we differentiated between the populations in the bimodal distributions in Figure 4-2, A and B as inactive and active caspase-8, and the activation of caspase-8 is shown in Figure 4-2. Jurkat cells with normal levels of cholesterol show a 9-fold activation of caspase-8 upon the addition of DR5 agonist. Jurkat cells with reduced cholesterol in the membrane, by pretreatment with MβCD, have only a 2.5-fold activation of caspase-8 (Figure 4-2C). That treatment with MβCD reduces activation of caspase-8 via activation of DR5 substantiates the necessity for membrane cholesterol in efficient signal transduction, consistent with the agonist-induced migration into cholesterol rich membrane regions (Figure 4-1).

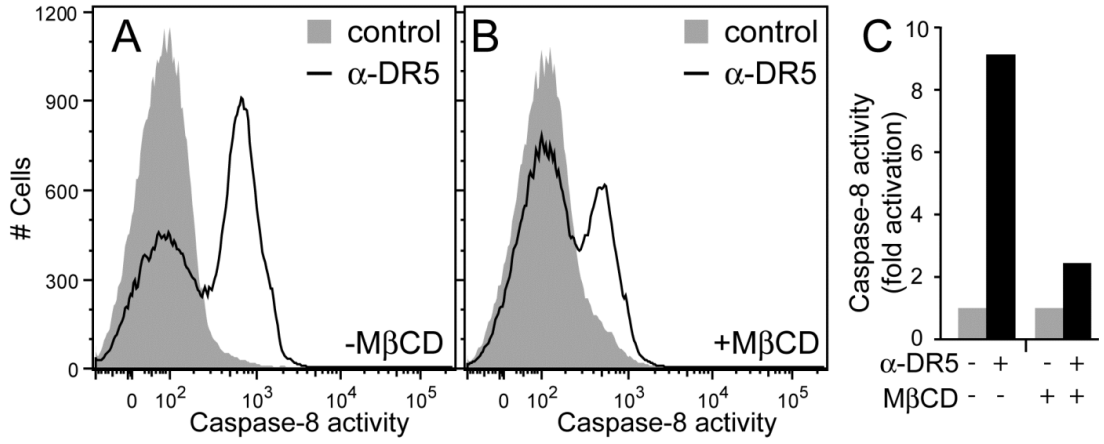

Figure 4-2. Membrane cholesterol is required for DR5-mediated activation of caspase-8. (A-B) Jurkat cells were pre-treated with control (A) or MβCD (B), washed, and treated with vehicle control (grey distribution) or DR5 agonist (α-DR5, black line). Caspase-8 activity was measured by flow cytometry. (C) Using similar gating scheme, fold activation of caspase-8 is shown. MβCD has a profound effect on caspase-8 activation in response to DR5 agonist stimulation.

4.4.3. Membrane cholesterol is required for dimerization of DR5 in response to ligand

Cholesterol-rich membrane microdomains, often referred to as lipid rafts, are known to drive the formation of large protein complexes [115,116]. However, it is unknown whether the formation of DR5 networks is dependent on the presence of cholesterol in the plasma membrane. We have shown previously that, upon the addition of antibody agonist, DR5 forms disulfide-linked dimers that exist within high molecular weight networks (Chapter 3, Figure 3-3, p. 50) [114]. Therefore, we wondered whether extraction of membrane cholesterol has any bearing on ligand-induced DR5 dimerization. Jurkat cells were pre-treated with MβCD (5mM) or vehicle control, and cells were subsequently washed and treated with DR5 antibody agonist and lysed. Equal amounts of

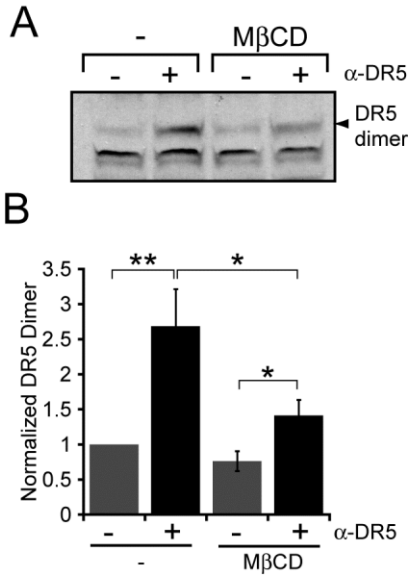

Figure 4-3. Membrane cholesterol is required for ligand-induced DR5 dimerization. (A) Jurkat cells were pre-treated with control or MβCD as indicated, and cells were washed and treated with with control or DR5 agonist (α-DR5). Whole lysates were analyzed by Western blot to observe DR5 dimerization (at approximately 85 kD). (B) Quantification of Western blots demonstrates that extraction of membrane cholesterol causes a reduction in ligand-induced DR5 dimerization. Note * indicates $p < 0.05$ and ** indicates $p < 0.01$.

total protein were run on non-reducing SDS-PAGE and DR5 dimerization was analyzed by Western blot (Figure 4-3). Control cells, having normal amounts of cholesterol in the membrane, show ligand-induced DR5 dimer formation as previously described [114], however cells pre-treated with MβCD have a diminished ability to form DR5 dimers (Figure 4-3A).

Quantification of these bands shows that, in normal cells, the addition of ligand causes a four-fold increase in dimeric population of DR5. After pre-treatment of Jurkat cells with MβCD, ligand causes only a 2.5-fold increase in DR5 dimerization. Therefore DR5 dimerization, which relies on cholesterol in the plasma membrane, is consistent with receptor activation, further suggesting that DR5 dimerization via TM residues is a key event in signal transduction across the membrane.

4.4.4. Membrane cholesterol is required for the efficient formation of ligand-receptor networks

DR5 agonistic antibody induces DR5 dimerization, and DR5 dimers exist within receptor clusters in the membrane (Chapter 3) [114]. Given that extraction of membrane cholesterol prevents DR5 dimerization in response to ligand, we further tested whether the same treatment prevents the formation of ligand-receptor networks. Ligand-receptor networks, or SPOTS, are commonly identified using confocal fluorescence microscopy [111,112,114]. Jurkat cells were pre-treated with MβCD (or control), to extract membrane cholesterol, and cells were subsequently treated with DR5 antibody agonist. Receptor-bound agonist was labeled with fluorescent secondary antibody and imaged using confocal microscopy to qualitatively determine the level of SPOTS formation within the membrane without and with treatment of MβCD (Figure 4-4)

Treatment with agonist results in the formation of large clusters in the membrane of control-treated cells (Figure 4-4, A), comparable to previous results [111,112,114]. Shown is the confocal midplane of the cell, however fluorescent SPOTS were found throughout the three dimensional plasma membrane based on observation of various confocal z-planes (see also Figure 3-3, B, p. 50). Figure 4-4, A shows the

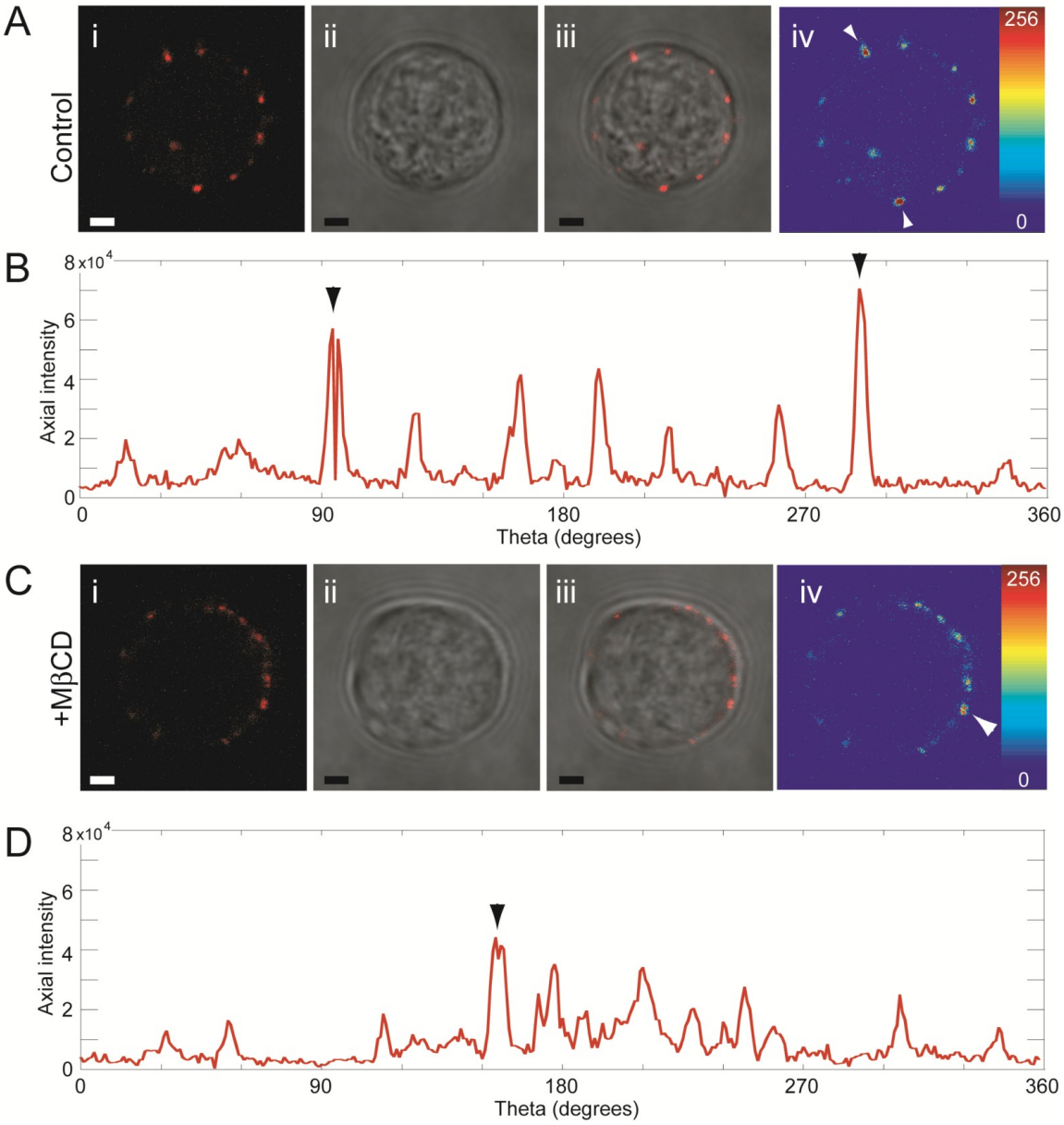

Figure 4-4. Membrane cholesterol is required for DR5 cluster formation in the plasma membrane. Jurkat cells were pre-treated with control or MβCD and subsequently treated with DR5 agonist and fluorescent secondary antibody. SPOTS were imaged using confocal microscopy (A, C), and SPOTS were radially quantified based on the distribution and intensity on a per-pixel basis. Treatment with MβCD causes a decrease in the number and intensity of DR5 clusters within the plasma membrane.

fluorescent-labeled ligand-receptor clusters (Figure 4-4, A-i), transmitted light (Figure 4-4, A-ii), and overlay (Figure 4-4, A-iii). Additionally, pixel brightness is shown to illustrate the intensity of SPOTS within the membrane (Figure 4-4, A-iv). Axial integration of fluorescence intensity illustrates the distribution and approximate size of the SPOTS in Jurkat cells with normal levels of cholesterol in the plasma membrane (Figure 4-4, B), where peaks indicate regions of high, localized fluorescence (for example, see Figure 4-4, Aiv and Figure 4-4, B, arrowheads).

Cells pre-treated with MβCD show a modest reduction in clustering of receptor-bound ligand as cells have a more uniform distribution of fluorescence in the membrane and less intense punctate pattern (Figure 4-4, C) compared to control cells. Figure 4-4, C shows the fluorescent-labeled ligand-receptor (Figure 4-4, C-i), transmitted light (Figure 4-4, C-ii), overlay (Figure 4-4, C-iii), and pixel intensity (Figure 4-4, C-iv). Radial quantification of fluorescence intensity in MβCD treated cells illustrates a difference in the distribution of fluorescence, where a lower level of cholesterol results in more diffuse fluorescence and fewer high-intensity clusters. Although ligand-receptor clusters still form to an extent (Figure 4-4, C-iv and Figure 4-4, D, see arrowhead), the reduction network formation is consistent with the moderate reduction in ligand-induced DR5 dimer formation after pre-treatment with MβCD (Figure 4-3). Thus, efficient formation of ligand-receptor clusters depends on the presence of cholesterol in the plasma membrane, however receptor network dimerization (Figure 4-3), receptor network formation (Figure 4-4), and receptor function (Figure 4-2) are not completely inhibited upon treatment with MβCD. That treatment with MβCD reduces the degree of network formation indicates that ligand induced signal transduction via the formation of ligand-induced receptor networks is dependent on the presence of cholesterol in the membrane.

4.5. Discussion

The plasma membrane is heterogeneously complex and plays an active role in signal transduction in a number of pathways, often through the segregation of

functionally related proteins into lipid raft microdomains that are rich in cholesterol [115,230]. Therefore efficient signal transduction is often dependent on physiological concentrations of cholesterol in the membrane, and depletion of membrane cholesterol results in changes in membrane protein assembly and signal transduction. Here, we have shown that apoptosis signaling initiated via DR5 involves migration to cholesterol-rich membrane regions, and structural changes induced by ligand as well as function rely upon cholesterol in the membrane.

In the absence of stimulation, DR5 resides within liquid disordered (L_d) regions of the plasma membrane, the so called "non-raft" regions low in cholesterol and characterized by their fluidity [160] and solubility in certain detergents [161]. Our results collectively demonstrate that DR5, upon stimulation by agonistic antibody, is translocated to cholesterol-rich membrane domains whereby the receptor undergoes structural changes causing dimerization and network formation. The formation of these ligand-receptor networks relies on membrane cholesterol and results in intracellular signaling events including activation of caspase-8. However, the precise sequence of events is yet unknown. It is interesting to wonder whether migration into rafts drives the formation of networks, and whether dimerization and network formation are a result of raft localization. Alternatively, network formation—propagated through ligand binding and subsequent structural changes—may in fact precede raft localization, whereby large signaling platforms may form around the network, thus stabilizing the network structure. A third possibility is that the formation of large DR5 networks is a result of clustering of smaller lipid raft domains to form larger, cholesterol-resistant lipid rafts that contain ligand-receptor networks [230].

The data presented here demonstrate clearly that cholesterol is required for ligand-induced structural changes and subsequent function of DR5. However, it is yet unclear precisely how cholesterol in the membrane dictates receptor structural changes. Lipid raft, or liquid-ordered (L_o) microdomains are often characterized by differences in their biophysical properties [159,160], and these biophysical differences may drive receptor interactions and network formation through several plausible mechanisms.

Acyl chains within cholesterol rich L_o domains are often more rigid than those within L_d domains [231]. Thus the formation of networks could rely on differences in lateral mobility within these L_o and L_d microdomains, promoting the stable interaction transmembrane residues of multiple receptors. It is interesting to note that treatment with MβCD decreases the diffusion coefficient of both raft and non-raft proteins [232], therefore dimerization and network formation may rely on a certain degree of lateral mobility within the membrane. Alternatively, cholesterol is known to have an influence on bilayer thickness [233], and changes in bilayer thickness—including those changes induced by cholesterol—dictate TM helix orientation in the bilayer [234]. Therefore, migration from L_o to L_d domains may cause TM helix reorientation, exposing dimerization motifs thus driving network formation. Although TM interactions exist within networks, cluster formation is also dependent on intracellular domains [111,114], therefore, it is yet unclear to what extent interactions between receptors and the membrane drive the formation of these clusters, and whether interactions between intracellular domains are dictated by events in the membrane, including TM interactions.

The most common method to study lateral migration into cholesterol-rich membrane microdomains is through the use of specific detergents to solubilize the membrane, where cholesterol-rich regions are often resistant to these detergents [161]. Although this method is widely used, there are several concerns—both general concerns as well as concerns specific to TNF receptors—associated with DRM isolation. Generally, the connection between the detergent resistance of certain membrane regions and their physiological significance is poorly established [162], and isolated DRM fractions, which require both non-physiological detergents as well as non-physiological temperatures, arguably do not reflect the physiological organization of the intact plasma membrane. Specific to TNF receptors, it is unclear whether resistance to detergents is necessarily indicative of lateral migration within the plasma membrane. It is conceivable that ligand-induced clusters of membrane receptors may themselves be resistant to certain detergents regardless of their localization within cholesterol-rich membrane regions. In fact, the first evidence of cluster formation in Fas, a related apoptosis-inducing membrane

receptor, was the formation of SDS-resistant populations of the receptor upon stimulation by ligand [134]. It is conceivable that DR5 networks may themselves be resistant to the same detergents used to isolate cholesterol-rich membrane regions (i.e. Triton X-100), and therefore results based exclusively on localization within DRM or DSM may be misleading. This calls for better methods to study raft/non-raft localization in living cells (i.e. in the absence of detergents), such as super resolution microscopy [235]. Such methods may be used to characterize not only localization within biological membrane microdomains, but also the temporal changes upon receptor activation—including the network size, recruitment of downstream proteins, and possibly complex internalization.

Collectively, our results demonstrate that initial events in agonist-induced DR5 signaling include migration to cholesterol-rich regions of the plasma membrane, dimerization, and network formation. Extraction of membrane cholesterol inhibits DR5 dimerization, network formation, and results in less activation of caspase-8, giving more evidence to suggest that ligand-induced dimerization of DR5 within large ligand-receptor networks is the relevant signaling event in DR5-mediated apoptosis. Further, given that DRMs plays a role in the function of a number of TNF receptors, it is interesting to wonder whether TM interactions and/or changes in TM helical orientation are involved in stabilizing networks of other TNF receptor members.

Chapter 5. The methionine aromatic motif plays a unique role in stabilizing protein structure and TNF ligand-receptor interactions

5.1. Summary

Of the twenty amino acids, the precise function of Methionine remains among the least well-understood. In order to establish a determining characteristic of Methionine that fundamentally differentiates it from purely hydrophobic residues, we have used *in vitro* cellular experiments, molecular simulations, quantum calculations and a bioinformatics screen of the Protein Data Bank. We show that approximately one-third of all known protein structures contain an energetically stabilizing Met-aromatic motif and, remarkably, that greater than 10,000 structures contain this motif more than ten times. Critically, we show that as compared to a purely hydrophobic interaction the Met-aromatic motif yields an additional stabilization of 1-1.5 kcal/mol. In order to highlight its importance and to dissect the energetic underpinnings of this motif, we have studied two clinically relevant TNF ligand-receptor complexes, namely TRAIL-DR5 and LTα-TNFR1. In both cases, we show that the motif is necessary for high-affinity ligand-binding as well as function. Additionally, we highlight previously overlooked instances of the motif in several disease-related Met-mutations. Our results strongly suggest that the Met-aromatic motif should be exploited in the rational design of therapeutics targeting a range of proteins.

5.2. Introduction

The biophysical and biochemical roles of Methionine (Met) remain among the least well-understood of the twenty amino acids. Mutations involving Met are associated with a number of pathological conditions, including Alzheimer's, Creutzfield-Jacob and von Willebrand's disease. Despite its role in such pathologies, the structural and thermodynamic consequences of Met mutations are not well-defined. Underlying this uncertainty, there remains an ambiguous biochemical classification of Met throughout the structural biology literature that reflects a poor understanding of its most basic biophysical interactions within structured proteins: at times Met can be classified as any one of a number of things, including non-polar, polar and weakly polar. Thus, in the context of protein folding and function, it remains fundamentally unclear how the sulfur atom differentiates Met from the other hydrophobic residues (e.g. Valine, Leucine and Isoleucine). In addition to the ambiguity of its role in stabilizing specific interactions within proteins and protein complexes, the quantum mechanical basis for its unique role has similarly remained elusive. Clarifying these ambiguities regarding Met is the focus of this study.

One potentially important finding regarding Met that has been largely overlooked is its propensity to interact with aromatic-containing residues including Tryptophan (Trp), Tyrosine (Tyr) and Phenylalanine (Phe). The higher-than-expected frequency of sulfur- and aromatic-containing residues in close proximity was first noted in a brief bioinformatics study of eight protein structures [236,237]. More extensive bioinformatics results extended these findings to include additional protein complexes as well as small molecules [238–240]. Efforts to understand the chemistry of the sulfur-aromatic interaction have relied upon studies of small model compounds; in particular, quantum and *in vacuo* classical mechanical calculations of the interaction between dimethyl sulfide (DMS) and benzene were consistent with the bioinformatics findings, as were results from an experimental study of DMS and methylnaphthalene, which observed a 1:1 interaction between sulfur- and aromatic-containing compounds [241]. Atomistic molecular dynamics (MD) simulations have previously shown the stability of a sulfur-

aromatic contact in a model α-helix [242,243]. Collectively, these studies suggest that the energy associated with a sulfur-aromatic interaction is on the order of 1-3 kcal/mol, the intermolecular distance is ~5.5Å (between the sulfur and the ring center), and that there is an orientational preference of 30°-60° (between the sulfur and the normal vector defined by the plane of the aromatic ring), depending on the nature of the aromatic group. Despite their apparent promiscuity, the functionality of sulfur-aromatic interactions has not been explored deeply within the context of full-length protein structures. Herein, we make use of *in vitro* experiments, molecular simulations, and quantum computation to describe sulfur-aromatic interactions within protein complexes that are central targets of molecular therapy.

We have studied two distinct tumor necrosis factor (TNF) ligand-receptor complexes, the TNF-related apoptosis-inducing ligand (TRAIL) in complex with death receptor 5 (DR5 or TRAIL receptor 2) [244] and lymphotoxin-α (LTα or TNFβ) ligand in complex with TNF receptor 1 (TNFR1) [245] (Figure 5-1), revealing potentially important Met sulfur-aromatic interactions. DR5 and TNFR1 are structurally homologous TNF receptors, having ~40% sequence similarity (and ~30% sequence identity) within their extracellular domains. Moreover, in their ligand-bound state, the structurally homologous complexes are formed via the high-affinity engagement of a trimeric ligand by three non-interacting receptor monomers forming a symmetric trimer unit. TRAIL binds DR5 (and other TRAIL receptors, death receptor 4 and decoy receptors 1 and 2) with nanomolar affinity [246], and this high-affinity, high-specificity binding has been attributed to a number of non-covalent interactions largely clustered within two receptor loops that bury deep within the ligand [244,247,248]. In DR5 these loops are known as the 50s loop (residues 51-65) and the 90s loop (residues 91-104), with interactions via the 90s loop accounting for 85% of the buried surface area of DR5 in the ligand-receptor complex [244] (Figure 5-1, TRAIL-DR5, see arrowheads). Comparison of the TRAIL-DR5 and LTα-TNFR1 complexes, shown in Figure 5-1, illustrates that a series of residues in TNFR1, the 100s loop—residues 105-110 (previously called the d-e loop)—has a well-defined conformation resembling the 90s loop of DR5 (Figure 5-1,

arrowheads). Upon careful examination of the interactions mediated by this binding loop in each structure, we noted that both complexes contain a motif consistent with the previously described interaction between sulfur-containing Met residue and aromatic-containing residues (Figure 5-1, see enlargement). In the TRAIL-DR5 complex, the distance between the DR5/Met99 sulfur atom and the TRAIL/Tyr237 aromatic ring is 5.4Å, and the separation between Met sulfur and Trp aromatic in the LTα-TNFR1 complex is 5.6Å. From an evolutionary standpoint, it is conceivable that such an interaction may have been conserved across protein complexes of the same superfamily, such as the TNF ligand-receptor superfamily. However, perhaps most intriguingly, in the LTα -TNFR1 structure, the pairing is reversed: the aromatic residue, Trp107, is found in the receptor whereas the sulfur-containing residue, Met120, is in the ligand, though the separation between sulfur and aromatic groups is comparable. Collectively, these observations suggest that the Met-aromatic interaction may not be an evolutionarily conserved motif in these TNF complexes, rather it is potentially a common motif that provides stabilization of protein structure as well as complex formation, such as high-affinity and high-specificity binding in the case of TNF ligand-receptor complexes.

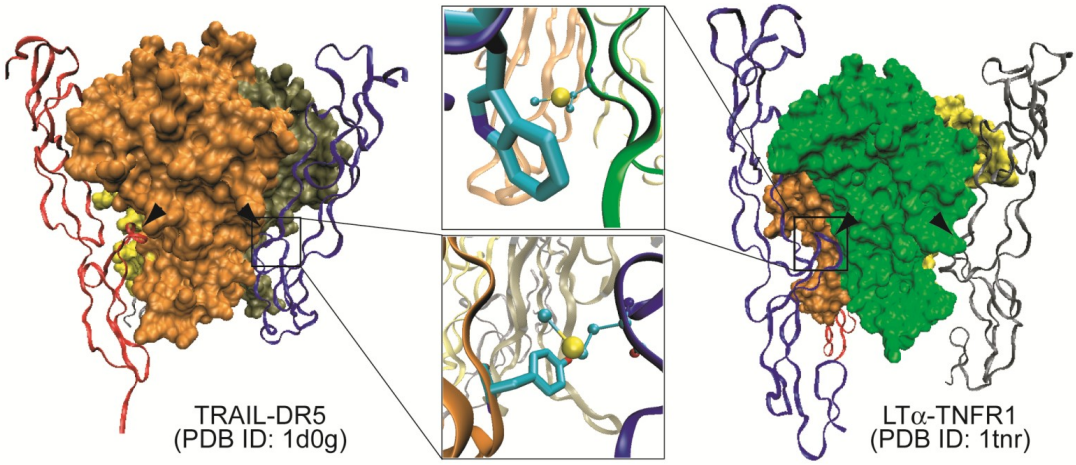

Figure 5-1. Crystal structures of the trimeric TRAIL-DR5 (left, PDB ID: 1d0g) and LTα-TNFR1 (right, PDB ID: 1tnr) complexes show a conserved binding loop in each receptor, the 90s loop in DR5 and the 100s loop in TNFR1, forming extensive contacts with the ligand (arrowheads). Within this binding region, both structures show a single methionine-aromatic interaction: DR5-Met99/TRAIL-Tyr237 (bottom box) and TNFR1-Trp107/LTα-Met120 (top box). Both interactions are at approximately 5Å separation.

Though there has been no specific discussion of the role of a sulfur-aromatic interaction in either complex, previous results suggest that these two residues are important for ligand binding in the TRAIL-DR5 complex [92,249]. Single amino acid mutation of DR5/Met99 almost completely abolishes ligand-receptor interaction, as was observed by co-immunoprecipitation (co-IP) studies [185]. Sequence alignment of DR5 with other TRAIL receptors show this Met residue to be conserved across all TRAIL receptors, further highlighting the potential importance of this motif (see Supporting Information). In a separate study, surface plasmon resonance measurements showed that mutation of Tyr237 increases TRAIL-DR5 dissociation five-fold [92]. However, despite their physical proximity and, in the case of TRAIL receptors, sequence identity, no relationship between these mutants—or these residues in general—has been proposed. Further, there is no empirical evidence to suggest that the sulfur- or aromatic-containing residues in LTα and TNFR1 (Met120 and Trp107, respectively) play any role in the ligand receptor interaction.

We demonstrate here that both Met and aromatic residues are necessary for high-affinity ligand-receptor binding and function in both the TRAIL-DR5 and LTα-TNFR1 complexes. We highlight the importance of this interaction using bioinformatics tools, molecular dynamics (MD) simulations, and quantum mechanical calculations. Our results demonstrate that, in comparison to a purely hydrophobic interaction with structural similarity, the sulfur-aromatic interaction at approximately 5Å separation is more stable and has an orientational preference, allowing for a stronger interaction at greater distances than is provided by the hydrophobic interaction via alkylic equivalent. Our quantum mechanical (QM) calculations indicate that dispersion effects are responsible for this behavior. In our model protein complexes, MD simulations produced a range of protein configurations consistent with those found within the Protein Data Bank (PDB). Collectively, the sulfur-aromatic interaction in TRAIL-DR5 and LTα-TNFR1 yields an interaction energy of approximately 1-1.5 kcal/mol greater than a hydrophobic interaction—and at a specific, longer distance—enough to disrupt the ligand-receptor interaction.

5.3. Materials and Methods

5.3.1. Cell culture and reagents

HEK293 cells were maintained in DMEM supplemented with 10% fetal bovine serum (HyClone), Pennicillin-Streptomycin, and L-glutamine. Jurkat cells were cultured in RPMI supplemented with 10% FBS, Penicillin-Streptomycin, L-glutamine and non-essential amino acids. Cells were maintained at subconfluence at 37°C and 5% CO2 in a water-jacketed incubator. Antibodies against DR5, TNFR1 and IκBα were purchased from Cell Signaling Technologies.

5.3.2. Cloning and ligand purification

Mutants of DR5, TNFR1, TRAIL and LTα were generated by the two-step PCR-based process of targeted mutagenesis with primers obtained from the University of Minnesota BioMedical Genomics Center. Wild type and mutant DR5 (Met mutants: M99A, M99V, M99I, and M99C) as well as wild type and mutant TNFR1 (W107A) were inserted into the pcDNA3.1(+) vector using EcoRI and XhoI restriction enzyme sites. All plasmids were verified by sequencing by the UMN Biomedical Genomics Center. We also note that the numbering of this residue varies within the literature; due to the presence of a ~52 amino acid N-terminal signaling sequence, Met99 is sometimes referred to as Met152 (within the described 90s loop), here we use the number of the mature protein as was used with the original TRAIL-DR5 structure [99].

Soluble TRAIL (residues 95-114) and LTα (residues 35-205), and mutants, were inserted in-frame with the Flag sequence (DYKDDDDK) in the pT7-Flag-1 expression vector. Ligands were produced and purified as previously described [250]. Briefly, N-terminal, Flag-tagged ligands were expressed in BL21(DE3) bacteria using IPTG and purified using Flag-affinity column (M2 anti-Flag agarose resin). Expression and purification was verified using Coomassie stain, concentrations were estimated using BCA assay, and activity of ligands was verified.

5.3.3. Co-immunoprecipitation and activity assays

HEK293 cells were transiently transfected with DR5 (WT or Met99 mutants) or TNFR1 (WT or W107A) using the calcium phosphate method. Twenty-four to forty-eight hours after transfection, Flag-TRAIL was added to cells at 500ng/ml for 30 minutes. Cells were washed three times in PBS to dilute excess, unbound ligand and subsequently lysed in NP-40 lysis buffer (50mM Tris, 75mM NaCl, 4mM EDTA, 1% NP-40) containing protease inhibitors on ice for 60 minutes. Lysate was recovered after centrifugation at 13,000g, 10 minutes at 4°C. Equal amounts of total protein (estimated by BCA assay) were subjected to immunoprecipitation using anti-Flag M2 agarose beads (Sigma) overnight at 4°C with gentle rotation. Beads were then washed with NP-40 buffer three times, resuspended in 2x Laemmli sample buffer with DTT and β-mercaptoethanol, boiled for 10 minutes and run on an SDS-PAGE gel (10%). Additionally, equal amounts of total protein from whole cell extract (WCE) were run on SDS-PAGE gel to verify equal expression of DR5 constructs. SDS-PAGE gels were transferred to nitrocellulose membrane and blotted for DR5.

TRAIL activity was measured by MTT assay. Cells were seeded at 2e5 cells per ml in a 96-well plate and treated with the indicated concentration of TRAIL for 24h. Cell viability was measured by incubation with MTT (0.5 mg/ml) during the last 3 hours of incubation. Percent cell viability was calculated relative to untreated wells. LTα activity was assessed by measured by IκBα degradation, a common marker for NFκB activation. Cells were plated at subconfluence and treated with the indicated concentration of LTα for 15 minutes and lysed. Equal amounts of total protein were loaded on SDS-PAGE and analyzed for IκBα expression—degradation of which indicates NFκB activity.

5.3.4. Bioinformatics

The Protein Data Bank (PDB, www.pdb.org) [251,252] was analyzed using Biopython toolset (www.biopython.org). A custom Python script utilizing the PDBParser was used to parse each PDB structural entity into its component parts (i.e. model, chain,

residue, atom) and access atomic coordinate data. The sulfur-aromatic distance is defined as the separation between the Met sulfur (SD atom) and the center of mass of the 6-membered aromatic ring. The angle is defined as the angle between the sulfur-aromatic vector and the normal vector of the aromatic ring. All interactions were calculated within a 20Å cutoff distance, but for clarity only those interactions within 10Å are shown. As a control, all interactions between aromatic groups and carbon (CH_2 and CH_3), nitrogen, oxygen and sulfur were calculated on a subset of the PDB representing a random collection of structures.

Analysis of the Biopython-generated data, including probability density, interactions by structure, and two dimensional histograms, was performed using Perl and Gnuplot. The sulfur-aromatic distance and angle were normalized by the shell volume, taking into account the radius and angle, respectively. Interactions were parsed according to aromatic type based on the residue (Phenylalanine, Tyrosine and Tryptophan). Interactions were also categorized as inter- or intra-chain interaction, with an inter-chain interaction corresponding to Met and aromatic residues within the different PDB chains, and intra-chain interaction corresponding to Met and aromatic residues within the same PDB chain.

5.3.5. Molecular dynamics simulations

Two systems were constructed using the CHARMM (v32) package. Crystal structures for TRAIL-DR5 (PDB ID: 1d0g) and LTα-TNFR1 (PDB ID: 1tnr) complexes were used as starting configurations. Missing TRAIL residues 132-143 were simulated briefly as in solution and inserted to form a continuous, soluble TRAIL (residues 119 to 281). Hydrogen atoms were added and all disulfide bonds present in the crystal structure were defined. To accommodate the zinc atom of the TRAIL complex—which interacts with the sulfur atom of cysteine 230 in each TRAIL chain as well as a chloride ion in a tetragonal geometry—a patch was created and implemented to define a rigid bond between the zinc ion and each of the three cysteine sulfur atoms as well as the chloride

ion. The geometry of these four atoms is maintained throughout the simulation. Structures were solvated in a waterbox of ~50,000 TIP3 water molecules including 284 resolved structural water molecules for TRAIL-DR5 and 138 for LTα-TNFR1. Sodium and chloride ions were added, and counter ions were added to neutralize the overall charge of the system. The complete, solvated TRAIL-DR5 and LTα-TNFR1 complexes—consisting of 138,163 and 136,995 atoms, respectively—were minimized and slowly heated to 300K with harmonic restraints on alpha carbon atoms. Systems were run completely unrestrained for 35-40ns using NAMD v2.6 in an isothermal, isobaraic (NPT) ensemble. A cutoff of 10Å was used for van der Waals interactions, and particle mesh Ewald (PME) summation was used for electrostatic interactions. The time step was 2 fs and all bonds involving hydrogens were fixed using the SHAKE/RATTLE algorithm with a tolerance (relative deviation) of 10^{-8}Å. Simulation trajectories were visualized using Visual Molecular Dynamics (VMD) program, and analysis was performed using CHARMM and Perl.

5.3.6. Quantum calculations

Three aromatic rings representative of the side-chains involved in the interactions with sulfur were selected: benzene, phenol, and indole. For each ring, the relaxed potential energy curves for the interaction with DMS and propane were computed for two conformations: one with the sulfur facing the ring ("down") and one with the sulfur pointing away from it ("up"). As an additional control, the "up" and "down" conformations were additionally run for dimethyl ether (DME) in complex with benzene. Structures were optimized with Gaussian 09 through a Z-matrix constraining the sulfur to be on the axis perpendicular to the center of the six-membered ring, and the two methyl groups to be symmetric with respect this axis. Geometry optimizations were performed at the M06-2X/6-311+G(d,p) [253,254] and MP2/6-311+G(d,p) levels, and for selected distances single point calculations were performed at the CCSD(T)/6-311+G(d,p)//MP2/6-31G(d) level. For similar systems, it has been shown [255] that non-

counterpoise-corrected triple-ζ M06-2X results are within 0.2 kcal/mol of the reference CCSD(T) extrapolated to the complete basis set limit. On the "up" minimum structure, we verified that expanding the basis set for M06-2X from 6-311+G(d,p) to aug-cc-pVTZ and aug-cc-pVQZ also results in less than 0.3 kcal/mol change.

To address how the DMS-aromatic interaction energy is affected by the wide distribution of distances and conformations observed in protein complexes, 128 structures were randomly sampled from the MD simulations for TRAIL-DR5 and LTα-TNFR1. The Cα-Cβ bond of the Met involved in the interaction was cut and saturated with hydrogen to yield DMS. Similarly, Y237 and W107 were truncated to p-cresol and 3-methyl-indole, respectively. In addition, for TRAIL-DR5 the effects of R191 were also investigated by truncating its side-chain to methyl guanidinium. For each structure, the DMS-aromatic interaction energy was computed at the HF, M06-2X, and MP2 levels using the aug-cc-pVDZ basis set (including basis set superposition error [256]) for all. Interaction energies were computed by subtracting the energy of the components at infinite separation (each fixed at the geometry in the complex) from the energy of the complex.

5.4. Results

5.4.1. The sulfur-aromatic interaction is a commonly occurring motif

Previous Previous statistical analyses of protein structures and small molecule compounds have suggested that an interaction exists between divalent sulfur and aromatic rings. These include informatics studies of the Brookhaven Protein Data Bank [236,237], a separate study of 36 protein structures [239], as well as a more recent analysis of the Cambridge Crystallographic Database of small molecule compounds [240]. Collectively, these results show a statistical enrichment of sulfur-containing residues in proximity to aromatic residues and with a specific geometrical conformation. However, there exists no recent analysis of the PDB, which now contains approximately 80,000 structures [251,252], nor is the prevalence of these interactions known. Here,

using Biopython [257] we analyzed a complete set of protein structures deposited in the PDB for close contacts between sulfur- and aromatic-containing residues to update the current bioinformatics dataset relating to sulfur-aromatic interactions. We define the sulfur-aromatic separation as the distance between the Met sulfur atom and the center of mass of the aromatic ring of tyrosine, tryptophan and phenylalanine.

In agreement with previous, smaller-scale bioinformatics results [239] we observe an enrichment of Met sulfur atoms within 7Å of any aromatic group, with a strong peak corresponding to a sulfur-aromatic separation of 5Å (Figure 5-2 A). As a control, we compared the Met sulfur-aromatic distribution with the distribution of distances of carbon (both methyl and methylene carbon atoms), nitrogen, oxygen and sulfur atoms to aromatic groups in a random subset of the PDB. While the control group shows a modest peak at approximately 5Å separation—likely a result of hydrophobic packing—the probability of finding any non-hydrogen atom (CH_2/CH_3, N, O and S) within 7Å of an aromatic ring is notably lower than that of finding a Met sulfur within the same distance (Figure 5-2 A, compare black and gray probability distributions). This radial probability density of interaction distances normalized by shell volume was used to define a distance cutoff for the interaction; we consider the sulfur-aromatic interaction to be any Met sulfur atom within 7Å of the aromatic ring center of mass, based on the first minimum in the distribution (Figure 5-2 A, arrowhead). Integration of the probability density distribution up to this cutoff reveals that Met sulfur atoms are almost twice as likely to be found within 7Å of an aromatic compared to the control group, which also includes methyl and methylene carbon, nitrogen and oxygen atoms within residue side chains. Analysis of high resolution crystal structures (the approximately 20,000 PDB structures having an X-ray resolution less than or equal to 1.8Å) yields an identical distribution, demonstrating that the observed enrichment is not a result of poor structural resolution, under which the placement of atoms depends on empirical force fields that may not accurately capture the interaction (see Supporting Information). Further examination of the individual control atoms, CH_2/CH_3, N, and O atoms within residue side chains shows no difference between high resolution structures and the complete PDB (see Supporting Information).

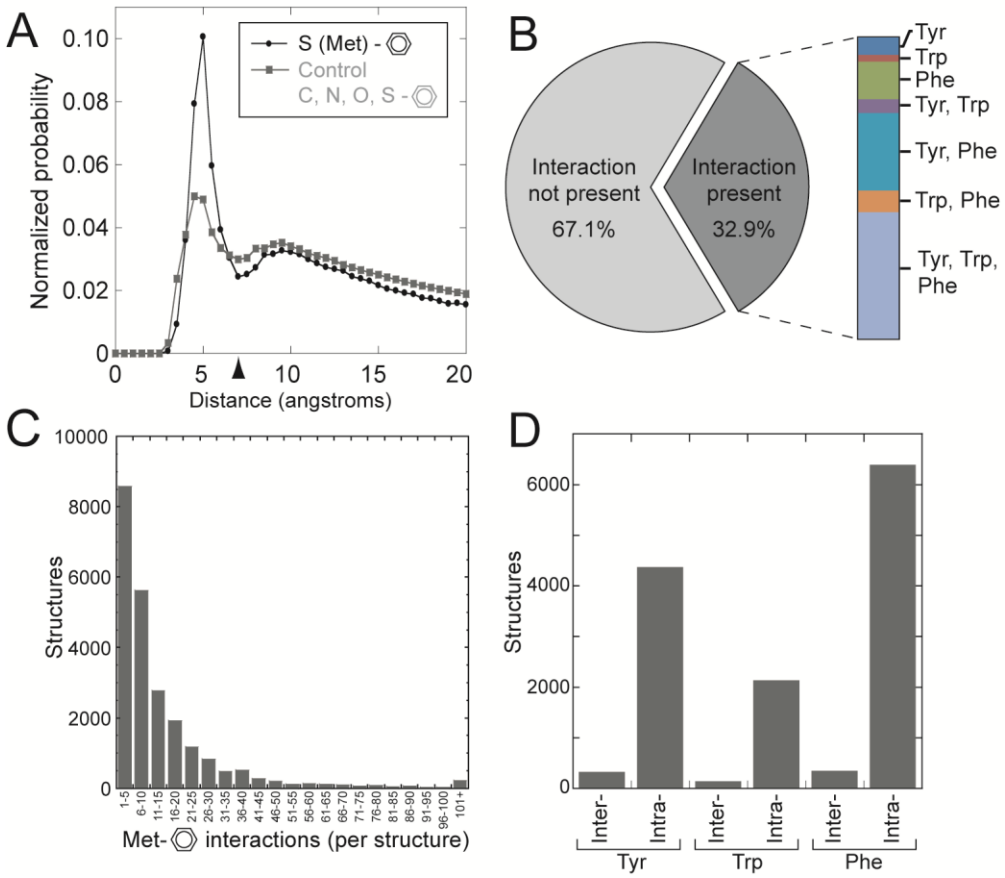

Figure 5-2. Structural bioinformatics analyses of the Protein Data Bank demonstrates the prevalence of the Met sulfur-aromatic motif. (A) Probability density of Met sulfur-aromatic interaction distances relative to the control shows an enrichment of methionine sulfurs within 7Å, indicated by the arrowhead. (B) Prevalence of Met-Aromatic interaction in all protein structures using a 7Å cutoff. (C) Number of Met-Aromatic interactions per structure. (D) Occurrence of inter- vs. intra-chain Met-Aromatic interactions.

Using the 7Å cutoff based on the radial distribution of distances (Figure 5-2 A, arrowhead), we next tested the prevalence of these sulfur-aromatic interactions within all known protein structures in the PDB. Previous studies have shown an enrichment of sulfur-atoms near aromatic residues [239,240], with 8% of methionines interacting with aromatic groups (using a modest 3.6Å cutoff) [258], and 22% of methionines interacting with pi-electron donors (a group of amino acids broader than just aromatics which includes cation-pi interactions in Arg, Lys, and His residues) [259]. However it is unknown how many proteins structures contain this motif, and, of those structures, how many interactions are present. Using a 7Å cutoff distance, we find that approximately 33% of all known protein structures contain at least one Met sulfur-aromatic motif (Figure 5-2 B, left). Phenylalanine is the most common aromatic group involved in this interaction, followed by tyrosine and tryptophan (Figure 5-2 B, right), which follows the relative frequency of each aromatic amino acid. Of all protein structures with sulfur-aromatic motifs, it is most common to have interactions with multiple aromatic types than single aromatic types, and protein structures that contain the motif with all three aromatic groups are surprisingly likely. This result suggests that the majority of protein structures in fact have multiple motifs, either with different or identical aromatic groups.

We next analyzed the PDB for the number of interactions per structure. Within the PDB, approximately 15,000 protein structures contain between one and ten interactions, and the majority of protein structures involving Met-aromatic interactions have more than 5 interaction motifs (Figure 5-2 C). Surprisingly, several protein structures contain more than 100, and one structure, a 24-oligomeric hemocyanin (PDB ID: 3ixw)—though large—has 388 interactions (Figure 5-2 C). Further, we analyzed the PDB to determine whether this interaction is more commonly found within a single protein chain (i.e. intra-chain interaction) for stabilization of secondary or tertiary structure or between different protein chains thus stabilizing a complex of proteins (i.e. inter-chain interaction stabilizing quaternary structure). The results, shown in Figure 5-2 D, highlight that the majority of the Met sulfur-aromatic interactions in the PDB occur between residues of a single protein chain (i.e. intra-chain interaction). However, this

could reflect that a majority of protein crystals, approximately 83%, represent single chain protein structures and may skew the interpretation. Regardless, a number of these interactions occur between sulfur aromatic groups of different protein chains, such as the interaction found in TRAIL-DR5 and LTα-TNFR1. Moreover, the remarkably high occurrence of these motifs leads us to believe that interaction between Met and aromatic residues plays a critical role in protein structure, primarily through stabilization of secondary and tertiary structure, as well as protein function, through stabilization of protein complexes.

5.4.2. Sulfur and aromatic groups are critical for binding and function

The structural comparison of the human TRAIL-DR5 and LTα -TNFR1 complexes reveals a similar interaction between Met and aromatic residues, tyrosine in TRAIL-DR5 and tryptophan in LTα -TNFR1 (Figure 5-1). We wondered whether interactions via the Met-aromatic pair are driven through hydrophobic interactions between Met methyl and methylene groups and the hydrophobic ring. Single amino acid point mutations were generated to the ligand and receptor to disrupt the sulfur-aromatic interaction and their activity assessed by immunoprecipitation and downstream signaling (Figure 5-3). DR5 Met99 was mutated to alanine, which reduced ligand binding to approximately 18% of wild type ligand-receptor interaction (Figure 5-3 A), as previously shown [185]. To investigate if larger hydrophobic groups could restore the original Met activity, we further mutated DR5 Met99 to valine and isoleucine, but the ability of these mutants to bind ligand did not increase with respect the alanine mutant as shown by immunoprecipitation (Figure 5-3 A, B). The observed relative binding capacity of valine and isoleucine is 29% and 18%, respectively, based on quantification of immunoprecipitation data. Mutation of Met99 to cysteine—with a sulfur-containing thiol group—did not regain function and completely disrupted the interaction between ligand and receptor (<5% binding), which is potentially a result of misfolded receptor due to disulfide bridge formation between Cys99 and the adjacent Cys100, which in turn

prevents the formation of a key structural disulfide bond between Cys100 and Cys86. Therefore, Met99 is a critical residue within the 90s loop of DR5 for its interaction with TRAIL, and stabilization of the ligand-receptor complex via this residue is not driven exclusively through hydrophobic interactions, as large hydrophobic residues do not regain the function of the sulfur-containing Met residue.

The Met residue is playing a considerable role in this motif via interactions that cannot be regained through hydrophobic residues, and consequently we hypothesize that the aromatic residue in the TRAIL is also critical for ligand binding and function. Therefore, we next sought to confirm that mutation of the aromatic tyrosine residue within TRAIL disrupts the function of the ligand. Soluble TRAIL (residues 114-281), and a single amino acid point mutant coding for TRAIL Y237A, were tagged with an N-terminal Flag sequence and purified from E. coli as previously described [250]. We assessed the ability of TRAIL (both wild type and the tyrosine mutant) to induce cell death in a dose-dependent manner by MTT assay to measure measuring cell viability. As expected, TRAIL induces cell death in Jurkat cells—expressing endogenous levels of DR5—with an ED50 of approximately 20ng/ml (Figure 5-3 C). Mutation of the tyrosine in the sulfur-aromatic binding motif decreases the activity of TRAIL several orders of magnitude, having an ED50 of approximately 10μg/ml (Figure 5-3 B, compare solid circles with open squares). This confirms the importance of Tyr237 in the TRAIL for its apoptosis-inducing activity.

Using similar methods, we tested the effect of mutations to the structurally homologous residues in the LTα -TNFR1 ligand-receptor complex, the function of which remains unknown. The aromatic residue (Trp107) of TNFR1 was mutated to alanine and transfected into HEK293 cells. The ability of wild type and mutant receptors to interact with LTα was again assessed by immunoprecipitation of the ligand-receptor complex. Mutation of Trp107 in TNFR1 results in a noticeable decrease in the interaction between ligand and receptor relative to the wild type receptor, despite approximately equal expression of receptor in both the wild type and mutant transfections (Figure 5-3 D), demonstrating the importance of this aromatic residue.

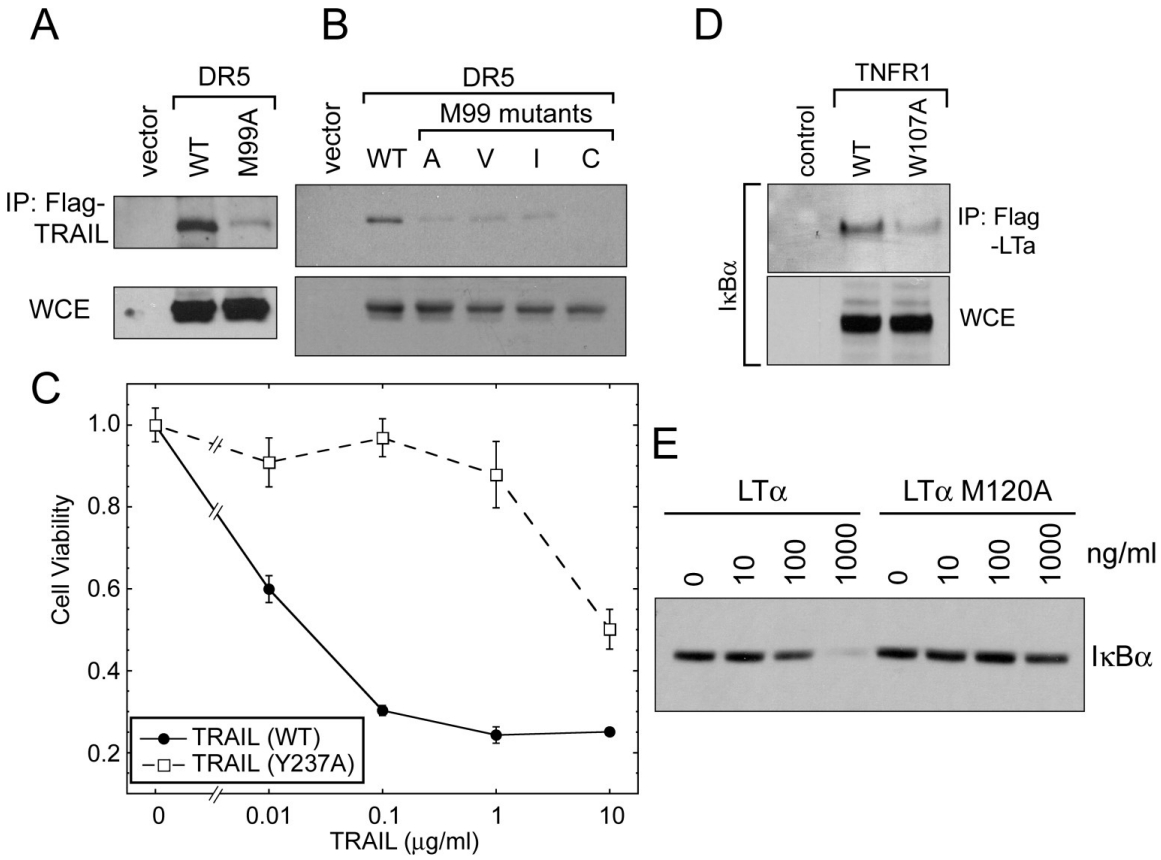

Figure 5-3. (A) Mutation of DR5 Met99 to alanine reduces ligand binding in transiently expressing HEK293 cells as measured by immunoprecipitation. (B) Mutation of DR5 Met99 to hydrophobic sidechains of increasing size (Ala, Val, Ile) does not recover the ligand-receptor interaction, measured by immunoprecipitation. The Met99 to Cys mutation completely prevents ligand binding, likely due to disulfide bond formation and misfolding (C) Jurkat cells were treated with TRAIL, WT and Y237A mutant, at various concentrations for 24 hours and cell viability was measured by MTT assay. Mutation of the aromatic-containing residue within the ligand reduces the activity of TRAIL. (D) Mutation of the aromatic-containing residue within the structurally homologous loop in TNFR1 disrupts interaction with its cognate ligand, LTα, measured by immunoprecipitation. Whole cell lysates show equal expression of wild type and mutant receptor. (E) Cells were treated with various concentrations of LTα, wild type and mutant. Mutation of the sulfur-containing methionine residue within LTα disrupts the function, shown by degradation of IκBα at various concentrations of ligand.

Further, we tested the function of LTα and mutants to the sulfur-containing Met120 residue by measuring IκBα degradation after the addition of various doses of ligand. Soluble LTα (both wild type and Met mutant) were purified, and Jurkat cells were treated with the indicated concentration of LTα for 20 minutes and subsequently lysed. Equal amounts of total protein lysate were analyzed by SDS-PAGE for IκBα expression, degradation of which is a common marker of NFκB activation (Figure 5-3 E). The addition of LTα results in noticeable degradation of IκBα; with approximately 50% of IκBα degraded at 100 ng/ml and nearly all of the IκBα is degraded at 1000 ng/ml. Addition of the mutated LTα, M120A, decreases the efficacy of the ligand both at low concentrations (causing no noticeable change in IκBα levels) and at high concentrations (with less than 40% degradation). These results demonstrate that Met120 in the LTα is critical for its functional activity. Thus both sulfur- and aromatic-containing residues play a critical role in stabilizing the high-affinity ligand-receptor interaction and greatly influence the ability of TNF to transducer its signal into the cell.

5.4.3. Quantum Mechanical calculations of sulfur- and aromatic containing model compounds

Bioinformatics and experimental results demonstrate a specific interaction involving the Met sulfur atom and aromatic rings, and this interaction is not found between other non-sulfur atoms and cannot be regained with larger hydrophobic residues (see Figure 5-2 and Figure 5-3). Therefore, we have used quantum mechanical electronic structure methods to investigate the origin of non-bonded interactions between sulfur-containing compounds and aromatic side chains and to differentiate these interactions from other, non-sulfur containing hydrophobic residues. In particular, Hartree-Fock (HF), MP2 and DFT (M06-2X) QM calculations were performed on model complexes between the sulfur-containing DMS and the side-chains of the aromatic amino-acids Phe, Tyr, and Trp: benzene (Figure 5-4 A), phenol (Figure 5-4 B), and indole (Figure 5-4 C), respectively. For comparison, QM calculations were also performed on the three aforementioned aromatics and propane, the sulfur-deficient, methylene carbon-analogue

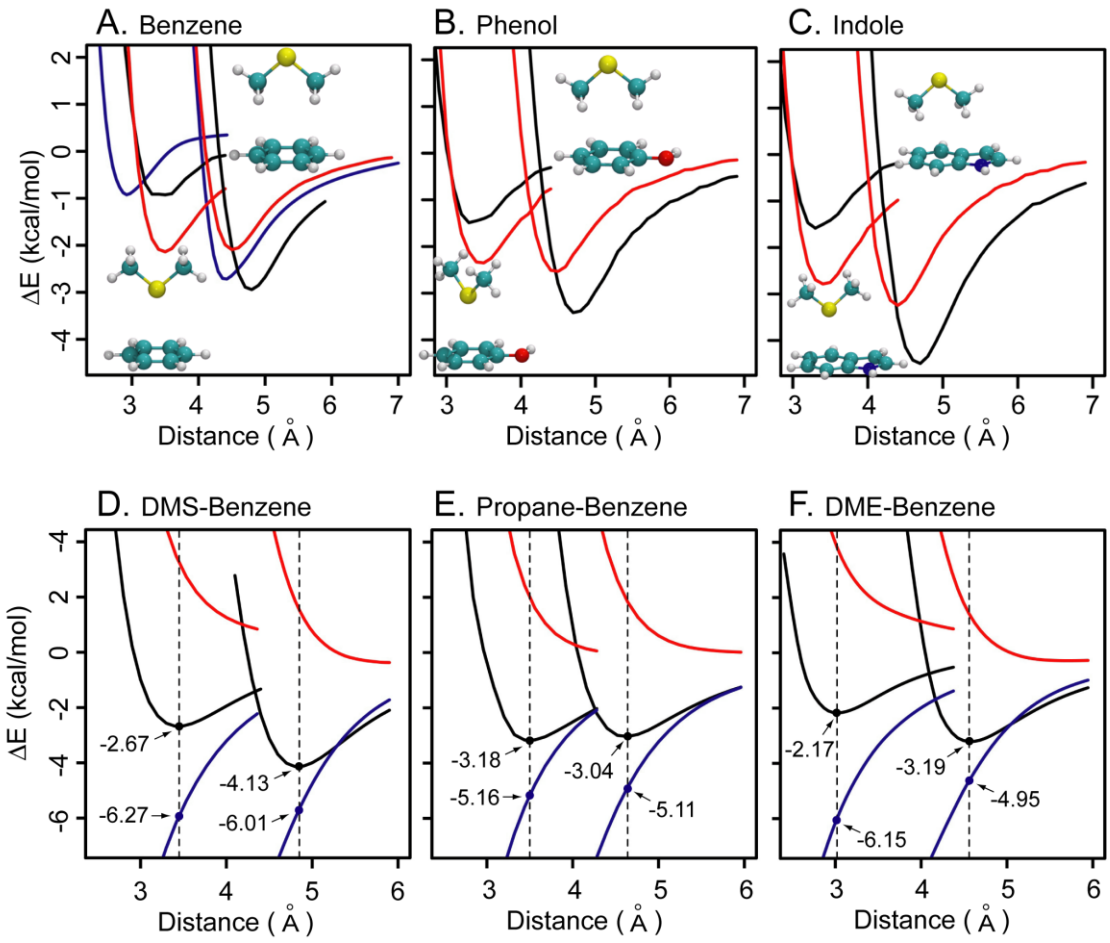

Figure 5-4. Sulfur-aromatic interaction provides additional stabilization over hydrophobic contacts due primarily to dispersion interactions. (A-C) Relaxed scans computed at the M06-2X/6-311+G(d,p) level for benzene (A), phenol (B), and indole (C) with DMS (black), propane (red), and DME (blue). The first and second minima correspond to the "down" and "up" conformations, respectively, shown by the illustration inset. The distance is taken to be the separation between the center of the aromatic ring and the sulfur atom (or equivalent for propane, DME). (D-F) The contribution of dispersion energy to overall binding for benzene complexes with DMS (D), propane (E), and DME (F). The dispersion contribution (blue) is computed as the difference between the MP2 (black) and HF (red) energies, both computed at the 6-311+G(d,p) level. Values at the MP2 minima (indicated by vertical dashed lines for the up and down configurations) are reported.

of DMS. Only for the benzene aromatic group, an additional set of calculations was performed for the oxygen-analogue dimethyl ether (DME). For each complex, the relaxed potential energy curve for the interaction was computed by varying the distance between the aromatic ring and DMS/propane/DME. Similar to previous studies [260,261], we investigated two conformations: DMS/propane/DME with the central atom (S, CH_2, or O) pointing upwards ("up" conformation) or downwards ("down" conformation) shown in Figure 5-4 A-C, top right and bottom left illustration insets, respectively.

In each conformation, the three complexes involving DMS (Figure 5-4 A-C, black line), propane (red line), and DME (blue line) display a well-defined minimum along the distance reaction coordinate, with a binding energy ranging between 1 and 5 kcal/mol. The "down" conformation minimum is characterized by a distance of about 3.4Å for both DMS and propane, while for DME the equilibrium distance is around 3.0Å. The "up" conformation minimum displays a larger separation for DMS (about 4.8Å) than for propane or DME (about 4.4Å). Particularly relevant to our study are the "down" and "up" conformation minima for propane, which are essentially isoenergetic (Figure 5-4 A-C, red lines), while the presence of sulfur in DMS strongly skews the energy landscape, favoring the "up" conformation by 2 to 3 kcal/mol over the "Down" conformation (Figure 5-4, A-C, black line, and Table 5-1). It is also important to recognize that the "up" conformation minimum for DMS is about 1 kcal/mol more stable than either "up" or "down" minima for propane. Therefore, the presence of sulfur makes the interaction about 1 kcal/mol more stable and adds a conformational preference towards longer distance. These results are further confirmed by *ab initio* calculations performed at the MP2 and CCSD(T) levels (see Table 5-1): while it seems that with respect to the reference CCSD(T), the complexes are slightly weakly bound using M06-2X and more strongly bound at the MP2 level; the relative energies of the minima are remarkably consistent across the different methods.

In order to characterize the origin of these minima, we plotted the contribution of the dispersion energy as a function of the reaction coordinate for DMS, propane, and DME in complex with benzene (Figure 5-4 D-F). We estimated the dispersion energy

(Figure 5-4 D-F, blue line) as the difference between the MP2 energies (Figure 5-4 D-F, black line) and HF energies (Figure 5-4 D-F, red line). It is interesting to note that HF has a fully repulsive potential, and thus the attraction basin that characterizes the MP2 profile originates entirely from dispersion interactions. The dispersion contributions are on the order of 5 to 6 kcal/mol and are stronger in both "down" and "up" minima for DMS (-6.27 and -6.01 kcal/mol, respectively) than for propane (-5.16 and -5.11 kcal/mol). The "down" minimum for DME, which takes place at a shorter distance (3.0Å), displays a dispersion contribution similar to DMS (-6.15 kcal/mol), but the contribution for the "up" minimum is -4.95 kcal/mol, similar to propane. This analysis suggests that most of the increased binding originating for DMS in the "up" minimum with respect to propane can be attributed to stronger dispersion interactions. This is qualitatively confirmed by electron density difference plots for the "up" conformation shown in Figure 5-5. In these plots we monitor the shift in electron density upon binding, which is an indicator of the combined effects of polarization and charge transfer. For the "up" conformation, the isocontours for all species appear to be similar, thus suggesting a similar contribution due to the polarization/charge transfer (Figure 5-5 A-C). A different picture is found in the "Down" conformation isocontours (Figure 5-5 D-F). Here, the presence of the lone pairs on the sulfur and oxygen atoms is clearly reflected by a loss of electron density in the region where the lone pair orbitals overlap with the π-system (Figure 5-5 D, F). Notice that the complex of DME, characterized by shorter bonding distance, shows the greatest electron density shift, followed by DMS. The isocontours for propane, on the contrary, are comparable in magnitude to those for the "up" conformation, thus suggesting a similar extent of electron rearrangement (Figure 5, compare B and E).

To summarize, the origin of the difference between DMS and propane is the result of the sum of *all* pairwise interactions, as pointed out by Nemethy et al.[262]. While for propane this sum is almost the same for either conformations, for DMS the presence of the lone-pairs on sulfur pointing towards the π-ring in the "down" conformation [263] makes this orientation less stable even if it is accompanied by a larger dispersion contribution than for propane. At the same time, the larger dispersion energy of DMS in

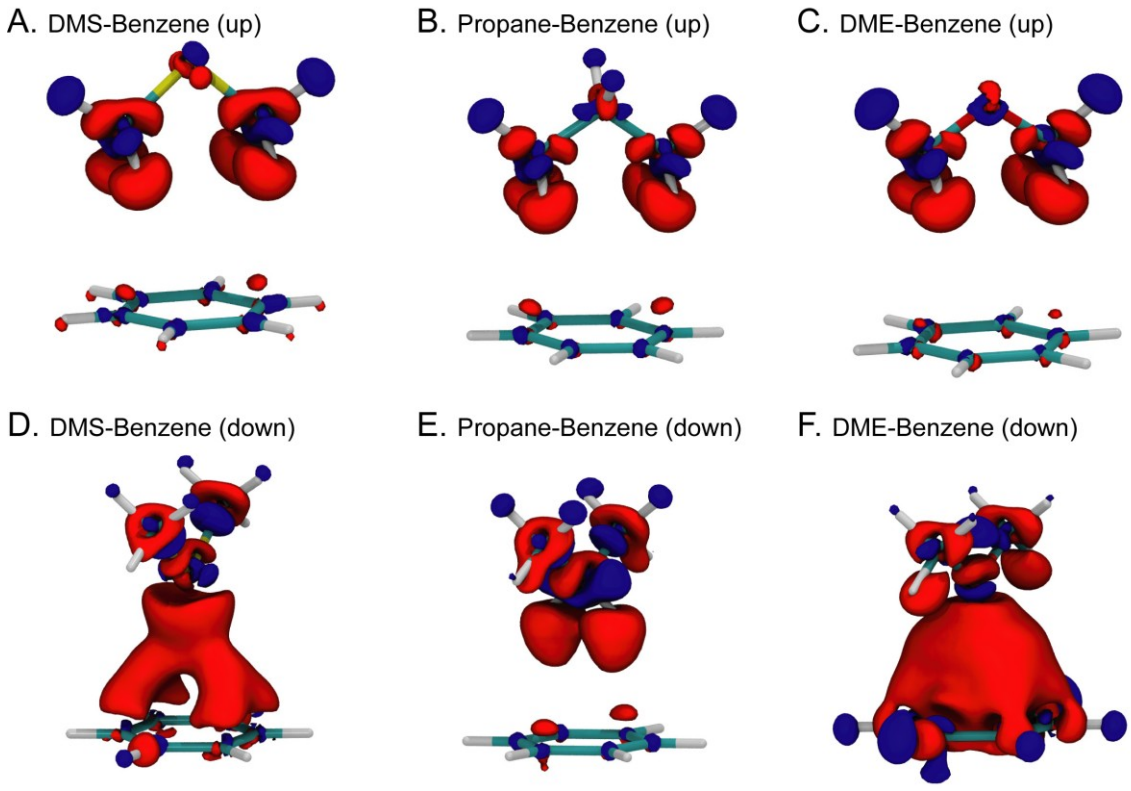

Figure 5-5. Electron density difference contours for each complex, DMS/Propane/DME – Benzene, in two different configurations, up and down. The electron density contours represent the difference between the electron density obtained at the complex geometry minimum and the species at infinite separation, each calculated at the M06-2X/6-311+G(d,p) level. The same isodensity value (0.0003) was used for all plots. Blue represents positive differences (i.e. gain of electron density in the complex state) and red represents negative differences (i.e. loss of electron density in the complex state).

comparison with propane can be attributed to the increased stability of the "up" conformation. That is, the dispersion energy of DMS in the "up" conformation, unlike the "down" conformation, is not outweighed by the lone-pair/π-ring electron repulsion. This explanation is further corroborated by the results for the DME complex: in the "up" conformation DME displays a behavior more similar to propane, both in the depth of the minimum and in the dispersion contribution (see Figure 5-4). This indicates that the origin of that minimum is best ascribed to dispersion contribution and not to effects due to the oxygen atom polarizing its neighboring atoms. On the other hand, in the "Down" conformation, the structure of DME complex behaves more similarly to that of DMS, although there is an even shallower minimum that can be possibly attributed to the "hardness" of its lone pairs when compared to the "softness" of the sulfur lone pairs.

5.4.4. Molecular dynamics simulations of the TRAIL-DR5 and LTα-TNFR1 complexes

Our results from QM calculations characterize the origin of the non-bonded sulfur-aromatic interaction as well as the specific energetic advantage and conformational specificity compared to purely hydrophobic contacts (Figure 5-4 and Figure 5-5). Moreover, our experimental evidence demonstrates clearly that sulfur- and aromatic-containing residues in TRAIL-DR5 and LTα-TNFR1 are critical for ligand binding and function (Figure 5-3), corroborating the increased probability of contacts between the sulfur-containing Met residue and aromatic residues throughout the Protein Data Bank (Figure 5-2). That a single interaction within a large, multi-protein complex has a profound ability to stabilize the structure led us to question the energy associated with the interaction between these side chains in biologically relevant structural configurations. Given the frequency with which such interactions occur in known protein complexes—including the number of complexes with more than 100 interactions—we aimed to characterize the biologically relevant interaction between Met sulfur and the aromatic-containing tyrosine and tryptophan side chains. To investigate a range of biologically relevant conformations we performed all-atom molecular dynamics simulations of the

TRAIL-DR5 and LTα-TNFR1 complexes. The geometrical configuration for the sulfur-aromatic interaction, including radial separation and angular orientation, is illustrated for TRAIL-DR5 and LTα-TNFR1 in Figure 5-6 A and B, respectively, and was calculated at each step over the equilibrated portion of a simulation trajectory. Additionally, shown in the TRAIL-DR5 complex is a nearby residue in the ligand, Arg191, shown previously to be important for binding [246] which forms an interesting Arg-Met-Tyr ligand-receptor motif that further stabilizes the complex via interactions with Met99 (discussed further below).

The radial and angular density distribution of the conformations sampled through MD for the Met-tyrosine interaction within the TRAIL-DR5 complex demonstrate the strong preference for an interaction at approximately 5Å and 45 degrees from the ring normal (Figure 5-6 C). The LTα-TNFR1 complex, where the Met residue of LTα is interacting with a tryptophan residue in TNFR1, shows a peak in density at approximately 5Å and 30 degrees from the ring normal (Figure 5-6 D). For comparison, the same density distributions calculated across the entire PDB for the Met-tyrosine and Met-tryptophan interactions are shown in Figure 5-6 E and F, respectively. The ensemble of Met-Tyr and Met-Trp structures sampled by each MD simulation (TRAIL-DR5 and LTα-TNFR1, respectively) each appear to be a subspace of the wider distribution obtained from the analysis of the PDB for each interaction. It is of interest to notice that while the radial peak around 5Å is unambiguously defined both in the MD and bioinformatics analyses, the angular dependence is less marked, especially in the PDB results. It is likely that the radial peak at 5Å is a more prominent characteristic of this interaction, while the angular dependence could be more dependent of the chemical surroundings of each specific motif. Collectively, these results highlight the radial dependence of the Met sulfur-aromatic interaction and, to a lesser extent, its angular dependence. Moreover, the MD trajectory is sampling a range of biological sulfur-aromatic interactions consistent with a range of different protein structures, and these structures can be used to more accurately estimate the interaction energy in an ensemble of relevant conformations.

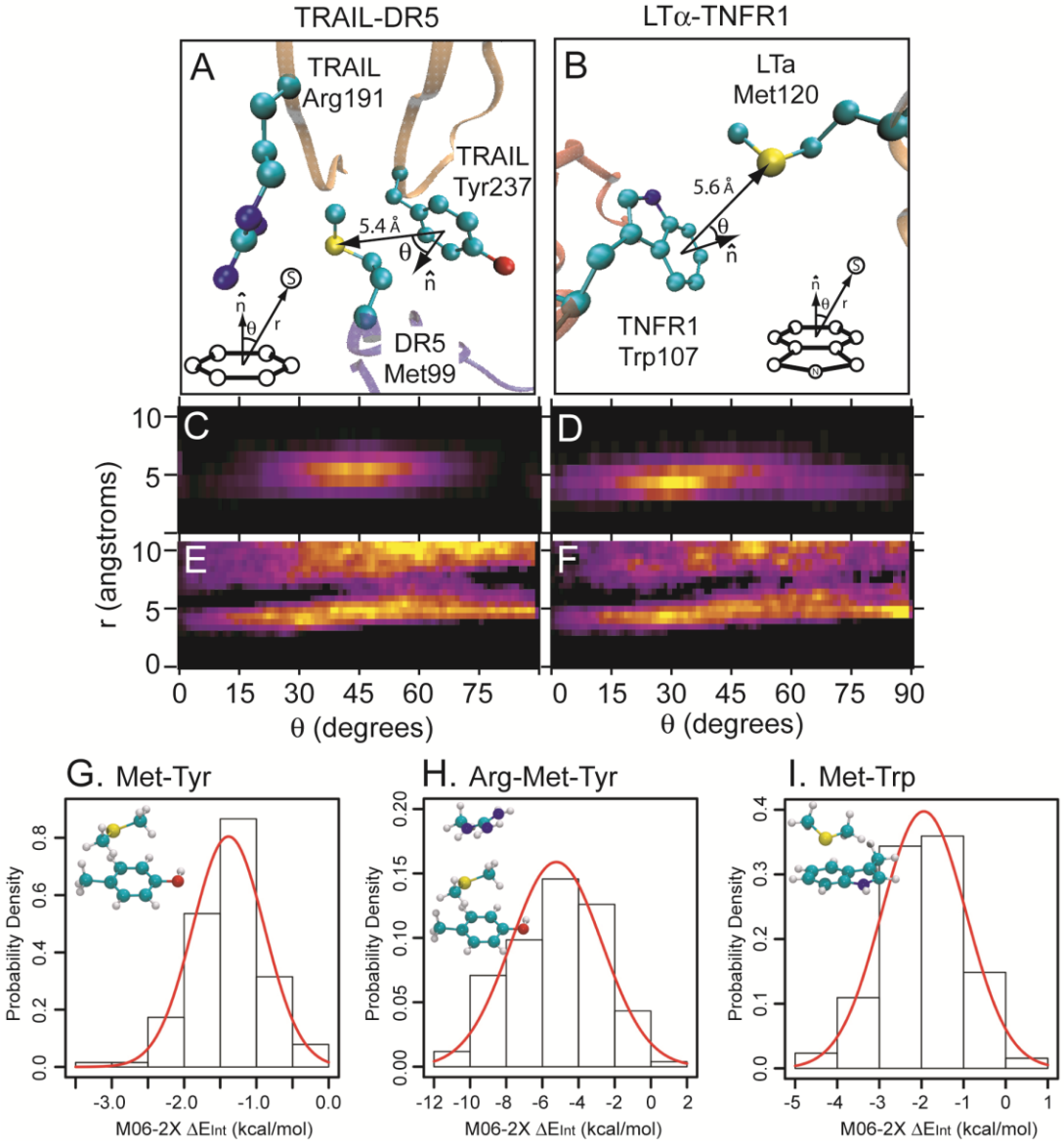

Figure 5-6. MD simulation of the TRAIL-DR5 and LTα-TNFR1 complexes. (A) The Met99/Tyr237 interaction in the TRAIL-DR5 complex. The nearby Arg191 is also shown. (B) The Met120/Trp107 interaction in the LTα-TNFR1 complex. (C-D) Radial and angular population distribution of the conformations sampled by MD of the TRAIL/DR5 (C) and of the LTα-TNFR1 (D) complexes, with warm colors representing a more frequent geometry. (E-F) Radial and angular population distribution analysis of the PDB: Met/Tyr (E), and Met/Trp (F) using the same color scheme. (G-I) Histograms of CP-corrected interaction energies for 128 structures taken from MD simulations corresponding to the Met-Tyr interaction in TRAIL-DR5 (G), the Arg-Met-Tyr interaction in TRAIL-DR5 (H), and the Met-Trp interaction in LTα-TNFR1 (I).

Thus, in order to probe the sulfur-aromatic interaction energy in a range of biological conformations, we randomly sampled 128 structures from the MD simulation trajectories. For each conformation, we computed the QM interaction energy and plotted the resulting histograms for TRAIL-DR5 complex (Figure 5-6 G) and LTα-TNFR1 complex (Figure 5-6 I). As expected, a wide distribution of interaction energies is sampled in both systems. The mean interaction energy can be bracketed between 1.4 and 1.9 kcal/mol (M06-2X and MP2 results, respectively) for Met-Tyr in TRAIL-DR5, and between 1.9 and 2.8 kcal/mol for Met-Trp in LTα-TNFR1.The calculated energies, in the 1-2 kcal/mol range, agree with experimentally determined results for this type of interaction [241,264]. The observation that in TRAIL-DR5 complex an arginine residue (Figure 5-6 A, see Arg191) is also in the proximity of side-chain of Met99 made us wonder if this could provide the means for an additional stabilization. Indeed, as shown in Figure 5-6 H, the presence of Arg191 strengthens the interaction, bringing the total interaction energy to 5.2 kcal/mol, which is in rough agreement with the importance of this arginine residue shown experimentally in which mutation to alanine results in a 3.9-fold increase in the dissociation constant as measured by surface plasmon resonance [246]. The arginine residue in the TRAIL-DR5 interaction thus provides a means to additional stabilization, which may have evolved as a result of the lower interaction energy between Met and tyrosine in this complex, whereas the tryptophan residue in the LTα-TNFR1 complex is sufficient alone for complex formation.

Table 5-1. Interaction energy at the energy-scan minimum computed at the M06-2X, (MP2), and {CCSD(T)} levels with the 6-311+G(d,p) basis set calculated for combinations of model compounds. Interaction energies were calculated for dimethyl sulfide (DMS) or propane (control) interacting with three different aromatic groups, benzene, phenol and indole, representative of the three aromatic amino acid side chains, in two different conformations (see Figure 5-5).

Structure, conformation, and method		Aromatic								
		Benzene			Phenol			Indole		
		M06-2X	MP2	CCSD(T)	M06-2X	MP2	CCSD(T)	M06-2X	MP2	CCSD(T)
DMS	Up	-2.94	-4.13	-3.62	-3.42	-4.89	-4.25	-4.50	-6.57	-
	Down	-0.93	-2.67	-2.16	-1.49	-3.36	-2.80	-1.58	-4.14	-
Propane	Up	-2.09	-3.04	-2.62	-2.53	-3.65	-3.15	-3.25	-4.82	-
	Down	-2.14	-3.18	-2.69	-2.35	-3.49	-3.03	-2.78	-4.50	-
DME	Up	-2.72	-3.19	-	-	-	-	-	-	-
	Down	-0.92	-2.17	-	-	-	-	-	-	-

5.5. Discussion

The biophysical and biochemical roles of nearly all the amino-acid residues have been well described. However, the precise role of the sulfur-containing Met residue remains poorly understood. Hydrophobic contacts via the Met residue, including methylene and methyl groups, are widely considered to be its major contribution to protein stability. If this is the case, what is the biological advantage of having a sulfur atom, rather than a methylene group, at the δ position? We present here the first case for a selective advantage, of approximately 1.5 kcal/mol, of the sulfur-aromatic interaction in conferring conformational specificity at distances up to ~5-6Å.

How does the energy associated with the sulfur-aromatic interaction motif compare to other stabilizing interactions found within protein complexes? The energy associated with a single sulfur-aromatic interaction is comparable to the interaction energy of a single salt bridge, a common interaction found in protein complexes with an interaction energy ranging from less than 1 kcal/mol to approximately 3.2 kcal/mol [265–268] and greater depending on the local environment [269,270]. However, the sulfur-

aromatic interaction also occurs at a larger distance (~5-6Å) than a salt bridge (typically < 4Å) and may be less sensitive to local environment changes, including pH of the solvent and the solvent itself. Additionally, while salt bridges have a significant energy penalty associated with side chain desolvation ,which may in fact exceed the energy of salt bridge formation[271], the non-polar nature of the Met and aromatic residues minimizes the desolvation energy penalty. The combination of these attributes in a sulfur-aromatic interaction yields a potentially more robust, and certainly unique, interaction than either purely hydrophobic contacts or salt bridges, and an interaction that occurs at longer distances.

Given the prevalence of the Met sulfur-aromatic interaction in known protein structures, it is conceivable that mutations of these residues may play a role in the protein structure of disease-related proteins. We found several examples of known disease-related Met mutations in which the structure of the protein of interest shows the Met in proximity to one or more aromatic residues. In von Willebrand disease, a single amino acid substitution (valine replacing the normal methionine residue) results in an overactive glycoprotein Ib alpha, associated with a bleeding disorder [272,273]. Upon examination of this structure we found the Met residue at the center of three aromatic residues (< 5Å separation), with a total of 5 aromatic residues within 7Å (see PDB ID: 1sq0), and mutation to valine was considered simply a non-specific loss of hydrophobic contact [274]. In a second example, mutation of Prion protein M129 is an allelic risk factor for the development of neurodegenerative diseases, such as Alzheimer's [275] as well as fatal familial insomnia and familial Creutzfield-Jacob [276]. This Met residue in the wild type Prion protein (PDB ID: 2kun) has three aromatic tyrosine residues within 10Å, the closest at 5.5Å separation [277]. Another example, a known mutation of the RET proto-oncogene, M918T, is associated with the development of thyroid carcinoma [278,279], and Met918 in the wild type structure (PDB ID: 2x2k) has 6 aromatic groups within 10Å, with the nearest at 5.4Å [280]. In addition to these examples, there are a number of disease-related Met mutations with no associated protein structure, including one structure where Met substitution results in thermal instability and improper protein

folding [281]. It is conceivable that other pathological Met mutations are a direct result of lost or gained interactions with aromatic residues, thereby changing protein stability, structure, and function.

Another interesting implication in the nature of the Met sulfur-aromatic interaction is the oxidation of certain amino acid side chains by reactive oxygen species, with Met being the most readily oxidized. Oxidized proteins accumulate during aging [282] and are associated with a number of age-associated pathologies including Parkinson's disease, Alzheimer's disease, cataracts, emphysema, and bronchitis [283–287]. The oxidation of methionine to methionine sulfoxide, MetO, occurs via the addition of an oxygen atom to the δ-sulfur atom in the methionine. Further, irreversible oxidation via the addition of a second oxygen atom results in methionine sulfone, $MetO_2$. Although the oxidation of Met residues is known to decrease protein conformational stability [288], it is unknown whether this loss of stability is associated with energetic changes in the Met sulfur-aromatic interactions. Moreover, in the case where sulfur- and aromatic-containing residues are important in complex formation—shown here in the TRAIL-DR5 and LTα-TNFR1—it is unknown how the oxidation of Met sulfur may influence binding, complex formation, and subsequent function. However, it is conceivable that the addition of an oxygen molecule (or molecules) to the δ-sulfur would disrupt both dispersion and electrostatic interactions present in the sulfur-aromatic motif, as described here, or at least reduce them in view of the subtle distance and angular requirements for this interactions to be effective.

Given the potential impact of the Met sulfur-aromatic motif in the stabilization of protein structures and complexes, and its role in disease, this motif presents a potentially enormous opportunity for rational drug design. Interestingly, certain TNF-targeted peptide antagonists may already be taking advantage of this motif. A peptide designed to mimic the Met-containing loop within TNFR1, known as WP9QY (amino acid sequence YCWSQYLCY, with the Trp107 analog underlined), has been found to bind both RANKL and LTα [289,290] and has been shown to reduce inflammation and bone resorption in mouse arthritis models [291,292]. The peptide is thought to antagonize the

ligand by binding the Met-containing surface of LTα, thus preventing the LTα-TNFR1 interaction. Although the role of the sulfur-aromatic interaction in this peptide-protein interaction has not been discussed, the sequence homology between the peptide antagonist and TNFR1—including the tryptophan residue in TNFR1 involved in the Met-aromatic motif—demonstrates that the sulfur-aromatic interaction may be exploited in the rational design of therapeutics.

To conclude, the methionine sulfur-aromatic interaction is a unique motif that is prevalent in protein structures, and that provides a specific role in stabilization of protein structures. The prevalence of the sulfur-aromatic interaction and its relevance in a number of pathologies, including known disease-associated mutations of Met as well as age-associated diseases related to Met oxidation, presents a unique opportunity to utilize this motif in the rational design of therapeutics.

5.6. Supporting Information

Methionine is conserved in all TRAIL receptors

TRAIL receptors bind TRAIL with both high specificity and high affinity, on the nanomolar level [92,293]. Based on the interaction between TRAIL and DR5, determined through crystallography by three separate groups [99–101], there are two primary binding loops, known as the 50s and 90s loops in DR5 (see main text). The interaction between sulfur-containing methionine residue (residue 99 in DR5) and the aromatic-containing tyrosine residue (residue 237 in TRAIL) exists in DR5. Although no empirical structures exist for other TRAIL receptors in complex with TRAIL, we wondered whether the Met residue—which is critical for ligand binding and function—is found in other TRAIL receptors.

Using basic local alignment sequencing tool (BLAST), we aligned the extracellular region of these receptors and found that Met99 within the 90s loop of DR5 is conserved across all TRAIL receptors (see Table 5-2, highlighted Met residue). Also shown is the sequence identity within the extracellular region of each protein. This

suggests that the conserved Met residue is critical for TRAIL binding to all TRAIL receptors, including both death and decoy receptors.

Table 5-2. A list of death and decoy receptors and the conservation of the Met residue within the 90s binding loop. Note: * indicates TRAIL-TRAIL receptor structure is available through the PDB, including PDB codes: 1d0g, 1dv4, and 1du3 [99–101].

HGNC Symbol	Receptor name	Structure available?	Sequence	Identity
TNFRSF10B	TRAIL-R2 (DR5)	Y*	...GTFREEDSPE**M**CRKC...	-
TNFRSF10A	TRAIL-R1 (DR4)	N	...GTFRNDNSAE**M**CRKC...	65%
TNFRSF10C	TRAIL-R3 (DcR1)	N	...GTFRNENSPE**M**CRKC...	52%
TNFRSF10D	TRAIL-R4 (DcR2)	N	...GSFQDKNSPE**M**CRTC...	55%

Sulfur-aromatic interaction does not depend on structural resolution

We have demonstrated that the Met sulfur-aromatic motif occurs with a higher-than-expected frequency within known protein structures in the Protein Data Bank (PDB), however, capturing this interaction relies on a certain level of protein structural resolution. The refinement of a protein structure involves mapping of individual atoms to an experimentally determined electron density map, and poor resolution in the initial crystallographic steps may be propagated resulting in inaccuracies within the finalized structure. To minimize these errors, sophisticated force fields are used to place the atoms of a protein structure, however if an interaction is not accurately represented within a force field, atomic placement may be biased by these inaccuracies. Therefore, we wondered whether the Met sulfur-aromatic interaction is represented in high-resolution crystal structures.

From the PDB, we extracted high-resolution protein structures having an X-ray resolution less than or equal to 1.8 Å. Structural bioinformatics was carried out on this subset of the PDB, which included 20,178 of the ~70,000 structures within the entire PDB, and the results are presented in Figure 5-7. In the complete PDB, a noticeable enrichment of Met sulfur atoms within 7Å of an aromatic ring is observed, with a clear

maximum at 5Å separation (Figure 5-7 A, see also, Figure 5-2. In comparison, the same interaction within high-resolution structures shows an identical distribution, with a clear enrichment at less than 7Å separation and a maximum probability at 5Å (Figure 5-7 B). In both cases, comparison to the control, which includes methyl/methylene carbon, nitrogen and sulfur, demonstrates that the sulfur-aromatic interaction is enriched relative to non-sulfur atoms (Figure 5-7, A and B, compare black and red lines). The distributions for individual groups is shown in Figure SI1, C and D, demonstrating no clear difference between the entire PDB and only high-resolution structures. Therefore, the Met sulfur-aromatic interaction does not depend on crystallographic resolution and refinement by certain force-fields.

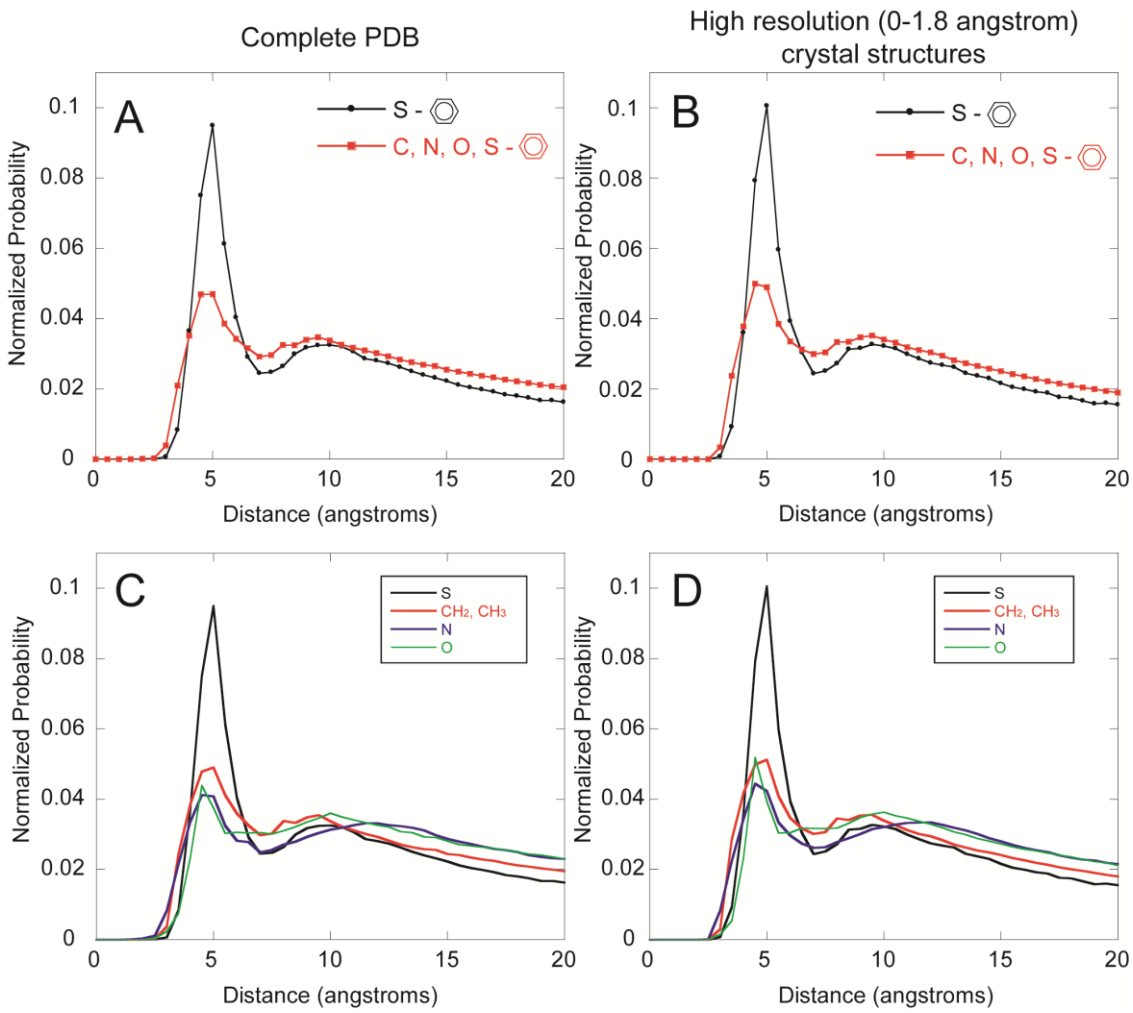

Figure 5-7. Met sulfur-aromatic interaction is found in high-resolution protein structures. A subset of the PDB, based on structural resolution (X-ray resolution ≤ 1.8 Å), was extracted and analyzed as before, including sulfur-aromatic and control-aromatic probabilities (A, black and red lines). For comparison, the bioinformatics result from the entire PDB is shown (B). The control, which includes methyl and methylene carbon atoms, nitrogen and also oxygen, was parsed into its individual atom types for further comparison between high resolution structures (C) and the entire PDB (D), which show no clear dependence on X-ray resolution.

Chapter 6. Concluding remarks and future work

The ligand-independent organization and ligand-induced re-organization of TNF receptors within the membrane plays a key role in signal transduction across the membrane. The notion of trimeric ligand-receptor interactions is giving way to coordinated signaling platforms comprised of networks organized by discrete biophysical interactions in the extracellular, transmembrane, and intracellular domains. Outside the cell, given the number of structurally homologous complexes, there is little doubt that trimeric ligand-receptor interactions are involved in signaling. However, in the absence of other regulatory domains (notably TM and intracellular domains, and also the membrane), it is unclear precisely how the ligand-induced trimerization drives either network formation. Nor is it fully understood how trimerization activates intracellular domains—via death domain oligomerization (either in dimers or multimers).

Here, we have described novel, ligand-dependent dimeric interactions between TM domains of receptor units within large networks (Chapter 3). We have also demonstrated that receptor dimers exist within high molecular weight network and is a precursor to activation of downstream signaling pathways, such as caspase-8 (dimerization and network formation occurring on the order of minutes and caspase-8 activation occurring on the order of hours). Further, that ligand-mediated receptor dimerization is consistent with the active structure of intracellular regulatory domains (DR5 death domain) as well as downstream factors (FADD and caspase-8) leads us to believe that TM-mediated dimerization is a key signaling event in signal propagation across the membrane. Collectively, our results establish a new paradigm in TRAIL-DR5 signaling, whereby ligand-induced structural changes cause TM-mediated dimerization and stabilization of large networks.

We have established a direct link between membrane cholesterol and ligand-induced structural events that are responsible for efficient TRAIL- and agonist-induced activation of caspase-8 through DR5 (Chapter 4). The ligand-induced re-distribution of DR5 into cholesterol-rich lipid microdomains serves to alter the structure of TM domains resulting in receptor dimerization and stabilization of networks. Therefore, the plasma membrane, through biophysical differences between phases, plays an active role in signaling by inducing receptor TM structural changes in response to ligand, and these structural changes result in dimerization and network formation.

Additionally, we have identified a motif in the TNF ligand-receptor interface that nearly abolishes ligand binding through a unique interaction between Methionine and aromatic-containing residues (Chapter 5). The Met sulfur-aromatic motif exists in multiple TNF ligand-receptor complexes, and is present in approximately one third of known protein structures. This motif, which lies in the ligand binding pocket of both TRAIL-DR5 and LTα-TNFR1, may be utilized in rational drug design, for example in small molecule inhibitors. Abolishing this ligand-binding motif may additionally be used in further studying network formation and function (described below).

In summary, our findings begin to describe a number of biophysical interactions that orchestrate extracellular ligand binding and subsequent network formation within the membrane, although much remains to be discovered regarding the dynamics of network formation and the precise structure of these networks. Therefore, a number of potential future experiments and ideas are presented below.

6.1 Quantification of SPOTS – formation and dynamics

We and others have shown that SPOTS form within minutes of the addition of ligand [111,112,114], however it is unknown whether the size and/or number of these clusters changes after their formation. Evaluation of SPOTS has primarily been qualitative, estimating size based on pixel dimensions and number using blind evaluators [111], but determining a distribution of sizes requires more precise methods for

quantification of size and number based on pixel intensity compared to background. Such methods are presented in Chapter 4, and can be further used for quantification of the size and number of SPOTS in the early stages after treatment with ligand. We are currently working to automate this process to calculate the size/number of SPOTS clusters, which could be easily applied for such an experiment.

Additionally, the structure of SPOTS could be used evaluated using super resolution techniques, such as PALM or STORM [294], where individual fluorophores are excited, and a point spread function is used to calculate fluorophore position within 2nm (compared to our methods, for which the resolution is based on the diffraction limit of ~200nm). Fluorescence lifetime imaging microscopy (FLIM) could also be used to study the angstrom-scale organization of these networks. FRET using wide field fluorescence microscopy and photobleaching, used here, provides an average energy transfer over a region of interest but yields no information regarding different populations—unbound, dimeric, trimeric, etc. By measuring fluorescence lifetimes in these networks, one could create a model-based fit to characterize energy transfer between dimeric populations, trimeric populations, etc., thus yielding significantly more information regarding the structure at the angstrom level, including fluorophore separation and mole fractions of each population.

6.2 Engineering ligands to disrupt network formation

As described in Chapter 2, the organization of the ligand is critical for the function of the receptor, and therefore careful engineering of ligands could be used to more accurately study network formation and function. For example, Ranzinger et al. used nanostructured surfaces to demonstrate the dependence of ligand density on function of TNFR1 [153]. This could be expanded to include DR5 signaling using immobilized TRAIL and antibody agonists at a range of ligand surface concentrations to correlate activity with ligand separation. Further, one could use this method to study the formation of SPOTS upon activation by different densities of immobilized ligands.

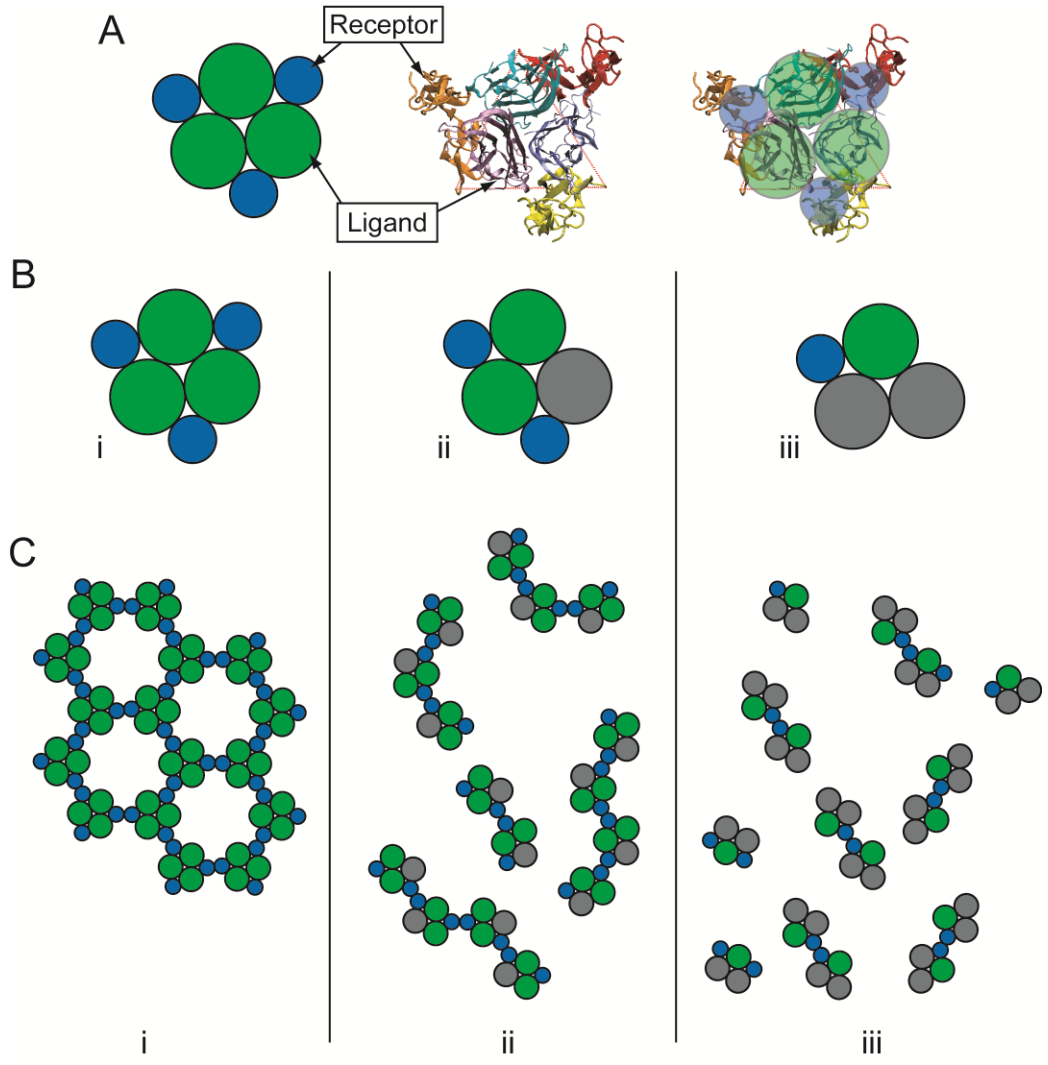

Figure 6-1. Engineered ligands to study network structure and formation. (A) Schematic representation of the TRAIL-DR5 complex, TRAIL is shown as green circles, DR5 is shown as blue circles. (B) Mutation of Tyr237 prevents ligand binding and function of TRAIL, and trimeric TRAIL can be generated as wild type (i), with one mutated Tyr237 (ii) and two mutated Tyr237 residues (iii). (C) The predicted network based on our structural model for wild type TRAIL, with network size and structure comparable to previous results (i), linear networks reduced in size with one Tyr237 mutation (ii), or near complete inhibition of network formation with mutation of two Tyr237 residues (iii). These results are predicted based on our working hypothesis of ligand-induced network structure in TRAIL-DR5.

Another method to study network formation and structure is to utilize the Tyr237 mutation shown to disrupt TRAIL-DR5 function (Chapter 5). This mutant could be used in combination with a single chain variant of TRAIL, whereby the three ligand chains forming the trimer are covalently linked as previously described [295,296]. Within a single chain TRAIL molecule, one could selectively mutate Tyr237 to the inactive alanine in one or two of the three ligand chains (Figure 6-1 B, gray circle represents an inactive ligand protomer within a covalently linked trimer). With all three ligand protomers capable of binding receptor, one would expect full network formation (Figure 6-1, C-i) as previously shown. Upon mutation of one ligand protomer, receptor networks would be restricted to linear arrangement of ligand-receptor molecules since the third ligand protomer would be inactive (Figure 6-1, C-ii). Mutation of two of the three ligand protomers would nearly completely disrupt networks, with a maximum repeat size of two (Figure 6-1, C-iii). Therefore combining the biophysical motifs characterized in Chapter 5 could be useful in studying the organization and stoichiometry of ligand-receptor networks described in Chapter 2 and studied in Chapter 3 and Chapter 4.

6.3 Molecular modeling of ligand-receptor networks

In addition to using experimental techniques to characterize the structure of TNF ligand-receptor networks, we can take advantage of available crystal structure data to construct molecular models of these receptors within the membrane. An all-atom representation of these networks would require computational resources beyond what is currently available, therefore these molecular models should be generated using coarse grained molecular dynamics (CGMD) simulations [297], where each coarse grained (CG) bead represents several heavy (i.e. non-hydrogen) atoms. A representative model is shown in Figure 6-2, A (top view) and B (side view). Simulations of these networks could be used to characterize novel interactions that drive network formation, and therefore the results could be tested experimentally using aforementioned techniques.

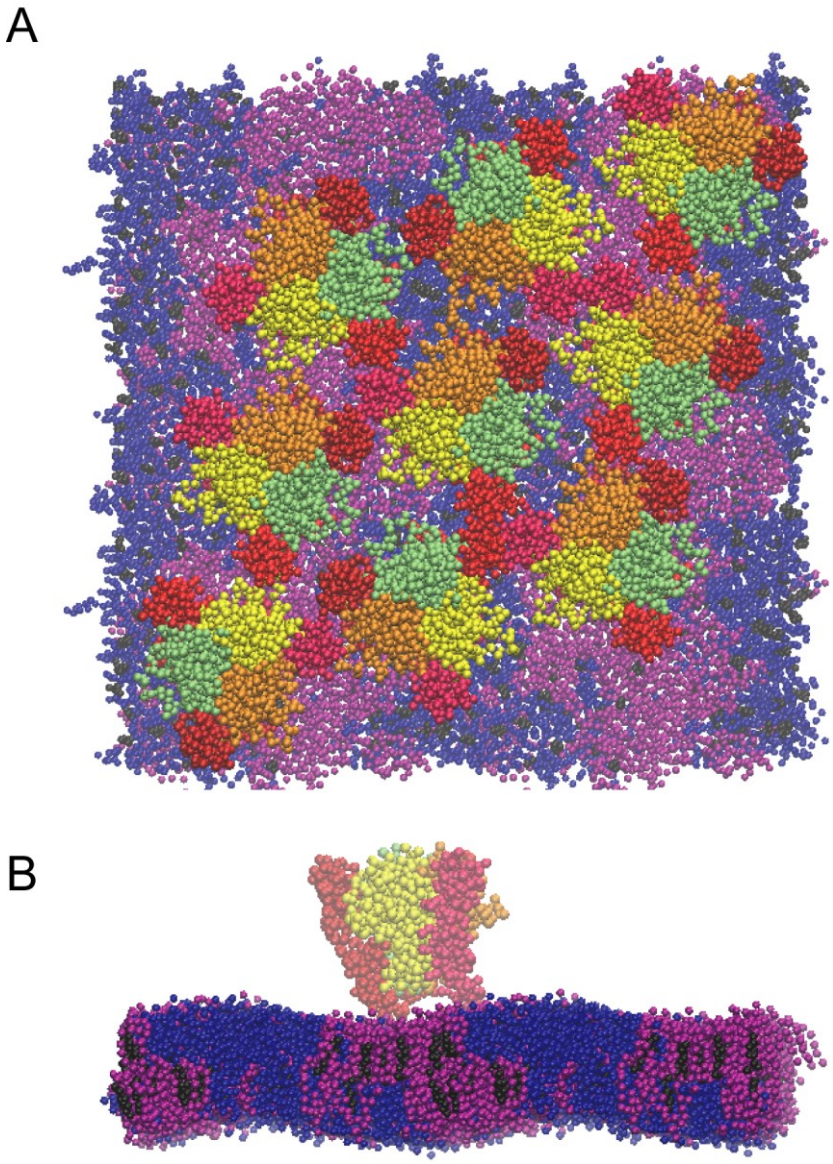

Figure 6-2. Molecular modeling of TRAIL-DR5 networks using coarse grained molecular dynamics (CGMD). (A) Top view of a molecular model of ligand-receptor networks. TRAIL is shown as yellow/orange/cyan beads and DR5 is shown as red beads. (B) Side view of TRAIL-DR5 complex within the lipid bilayer (water has been removed for clarity, and only a single ligand-receptor trimeric unit is shown for simplification). In both A and B, blue regions of the membrane are unsaturated lipids, purple regions are saturated lipids, and black is cholesterol, forming a phase separated bilayer used to study localization within raft/non-raft regions of the membrane.

Membrane complexities could be incorporated into these molecular models. For example, CGMD simulations have been used previously, by us and others, to characterize phase separated lipid bilayers containing mixtures of saturated and unsaturated lipids as well as cholesterol [298]. The organization and dynamics of receptor networks could be studied in these phase separated bilayers and compared to bilayers more accurately representing the liquid disordered membrane. Again, results obtained should be verified experimentally, and the combination of molecular level models and experimental verification can provide multiple levels of detail of these networks. This multi-scaled approach to studying network formation, using molecular models to design experiments and vice versa, can provide useful details not tractable through individual methods further elucidating the influence of protein structure, dynamics, and environment in dictating function.

References

1 Fagerberg L, Jonasson K, von Heijne G, Uhlén M & Berglund L (2010) Prediction of the human membrane proteome. *Proteomics* **10**, 1141-9.

2 Bakheet TM & Doig AJ (2009) Properties and identification of human protein drug targets. *Bioinformatics* **25**, 451-7.

3 Sachs JN & Engelman DM (2006) Introduction to the membrane protein reviews: the interplay of structure, dynamics, and environment in membrane protein function. *Annual Review of Biochemistry* **75**, 707-12.

4 Thompson CB (1995) Apoptosis in the pathogenesis and treatment of disease. *Science* **267**, 1456-62.

5 Almasan A & Ashkenazi A (2003) Apo2L/TRAIL: apoptosis signaling, biology, and potential for cancer therapy. *Cytokine & Growth Factor Reviews* **14**, 337-48.

6 Abdulghani J & El-Deiry WS (2010) TRAIL receptor signaling and therapeutics. *Expert Opinion on Therapeutic Targets* **14**, 1091-108.

7 El-Deiry WS (2001) Insights into cancer therapeutic design based on p53 and TRAIL receptor signaling. *Cell Death and Differentiation* **8**, 1066-75.

8 Yada A, Yazawa M, Ishida S, Yoshida H, Ichikawa K, Kurakata S & Fujiwara K (2008) A novel humanized anti-human death receptor 5 antibody CS-1008 induces apoptosis in tumor cells without toxicity in hepatocytes. *Annals of Oncology: Official Journal of the European Society for Medical Oncology/ESMO* **19**, 1060-7.

9 Ichikawa K, Liu W, Zhao L, Wang Z, Liu D, Ohtsuka T, Zhang H, Mountz JD, Koopman WJ, Kimberly RP & Zhou T (2001) Tumoricidal activity of a novel anti-human DR5 monoclonal antibody without hepatocyte cytotoxicity. *Nature Medicine* **7**, 954-60.

10 Rosevear HM, Lightfoot AJ & Griffith TS (2010) Conatumumab, a fully human mAb against death receptor 5 for the treatment of cancer. *Current opinion in investigational drugs* **11**, 688-98.

11 Georgakis GV, Li Y, Humphreys R, Andreeff M, O'Brien S, Younes M, Carbone A, Albert V & Younes A (2005) Activity of selective fully human agonistic antibodies to the TRAIL death receptors TRAIL-R1 and TRAIL-R2 in primary and cultured lymphoma cells: induction of apoptosis and enhancement of doxorubicin- and bortezomib-induced cell death. *British Journal of Haematology* **130**, 501-10.

12 Motoki K, Mori E, Matsumoto A, Thomas M, Tomura T, Humphreys R, Albert V, Muto M, Yoshida H, Aoki M, Tamada T, Kuroki R, Yoshida H, Ishida I, Ware CF & Kataoka S (2005) Enhanced apoptosis and tumor regression induced by a direct agonist antibody to tumor necrosis factor-related apoptosis-inducing ligand receptor 2. *Clinical Cancer Research : An Official Journal of the American Association for Cancer Research* **11**, 3126-35.

13 Zhang L, Zhang X, Barrisford GW & Olumi AF (2007) Lexatumumab (TRAIL-receptor 2 mAb) induces expression of DR5 and promotes apoptosis in primary and metastatic renal cell carcinoma in a mouse orthotopic model. *Cancer Letters* **251**, 146-57.

14 Fulda S & Debatin K-M (2006) Extrinsic versus intrinsic apoptosis pathways in anticancer chemotherapy. *Oncogene* **25**, 4798-811.

15 Chipuk JE, Moldoveanu T, Llambi F, Parsons MJ & Green DR (2010) The BCL-2 family reunion. *Molecular Cell* **37**, 299-310.

16 Cory S & Adams JM (2002) The Bcl2 family: regulators of the cellular life-or-death switch. *Nature Reviews. Cancer* **2**, 647-56.

17 Kluck RM, Bossy-Wetzel E, Green DR & Newmeyer DD (1997) The release of cytochrome c from mitochondria: a primary site for Bcl-2 regulation of apoptosis. *Science* **275**, 1132-6.

18 Green DR & Reed JC (1998) Mitochondria and apoptosis. *Science* **281**, 1309-12.

19 Zou H, Henzel W, Liu X, Lutschg A & Wang X (1997) Apaf-1, a Human Protein Homologous to C. elegans CED-4, Participates in Cytochrome c–Dependent Activation of Caspase-3. *Cell* **90**, 405-413.

20 Carswell EA, Old LJ, Kassel RL, Green S, Fiore N & Williamson B (1975) An endotoxin-induced serum factor that causes necrosis of tumors. *Proceedings of the National Academy of Sciences of the United States of America* **72**, 3666-70.

21 Green S, Dobrjansky A, Carswell EA, Kassel RL, Old LJ, Fiore N & Schwartz MK (1976) Partial purification of a serum factor that causes necrosis of tumors. *Proceedings of the National Academy of Sciences of the United States of America* **73**, 381-5.

22 Aggarwal BB, Moffat B & Harkins RN (1984) Human lymphotoxin. Production by a lymphoblastoid cell line, purification, and initial characterization. *The Journal of Biological Chemistry* **259**, 686-91.

23 Aggarwal BB, Kohr WJ, Hass PE, Moffat B, Spencer SA, Henzel WJ, Bringman TS, Nedwin GE, Goeddel DV & Harkins RN (1985) Human tumor necrosis factor. Production, purification, and characterization. *The Journal of Biological Chemistry* **260**, 2345-54.

24 Gray PW, Aggarwal BB, Benton CV, Bringman TS, Henzel WJ, Jarrett JA, Leung DW, Moffat B, Ng P & Svedersky LP Cloning and expression of cDNA for human lymphotoxin, a lymphokine with tumour necrosis activity. *Nature* **312**, 721-4.

25 Ashkenazi A (2002) Targeting death and decoy receptors of the tumour-necrosis factor superfamily. *Nature Reviews. Cancer* **2**, 420-30.

26 Aggarwal BB, Gupta SC & Kim JH (2012) Historical perspectives on tumor necrosis factor and its superfamily: 25 years later, a golden journey. *Blood* **119**, 651-65.

27 Screaton GR & Xu XN (2000) T cell life and death signalling via TNF-receptor family members. *Current Opinion in Immunology* **12**, 316-22.

28 Nagata S (1997) Apoptosis by Death Factor. *Cell* **88**, 355-365.

29 Wiley SR, Schooley K, Smolak PJ, Din WS, Huang CP, Nicholl JK, Sutherland GR, Smith TD, Rauch C, Smith CA & Goodwin RG (1995) Identification and characterization of a new member of the TNF family that induces apoptosis. *Immunity* **3**, 673-82.

30 Suda T, Takahashi T, Golstein P & Nagata S (1993) Molecular cloning and expression of the Fas ligand, a novel member of the tumor necrosis factor family. *Cell* **75**, 1169-78.

31 Takeda K, Yamaguchi N, Akiba H, Kojima Y, Hayakawa Y, Tanner JE, Sayers TJ, Seki N, Okumura K, Yagita H & Smyth MJ (2004) Induction of tumor-specific T cell immunity by anti-DR5 antibody therapy. *The Journal of Experimental Medicine* **199**, 437-48.

32 Walczak H, Miller RE, Ariail K, Gliniak B, Griffith TS, Kubin M, Chin W, Jones J, Woodward a, Le T, Smith C, Smolak P, Goodwin RG, Rauch CT, Schuh JC & Lynch DH (1999) Tumoricidal activity of tumor necrosis factor-related apoptosis-inducing ligand in vivo. *Nature Medicine* **5**, 157-63.

33 Gura T (1997) How TRAIL kills cancer cells, but not normal cells. *Science* **277**, 768.

34 Gliniak B & Le T (1999) Tumor necrosis factor-related apoptosis-inducing ligand's antitumor activity in vivo is enhanced by the chemotherapeutic agent CPT-11. *Cancer Research* **59**, 6153-8.

35 Sedger LM, Glaccum MB, Schuh JCL, Kanaly ST, Williamson E, Kayagaki N, Yun T, Smolak P, Le T, Goodwin R & Gliniak B (2002) Characterization of the in vivo function of TNF-alpha-related apoptosis-inducing ligand, TRAIL/Apo2L, using TRAIL/Apo2L gene-deficient mice. *European Journal of Immunology* **32**, 2246-54.

36 Ashkenazi A, Pai RC, Fong S, Leung S, Lawrence D a, Marsters S a, Blackie C, Chang L, McMurtrey a E, Hebert A, DeForge L, Koumenis IL, Lewis D, Harris L, Bussiere J, Koeppen H, Shahrokh Z & Schwall RH (1999) Safety and antitumor activity of recombinant soluble Apo2 ligand. *The Journal of Clinical Investigation* **104**, 155-62.

37 Lawrence D, Shahrokh Z, Marsters S, Achilles K, Shih D, Mounho B, Hillan K, Totpal K, DeForge L, Schow P, Hooley J, Sherwood S, Pai R, Leung S, Khan L, Gliniak B, Bussiere J, Smith C a, Strom SS, Kelley S, Fox J a, Thomas D & Ashkenazi A (2001) Differential hepatocyte toxicity of recombinant Apo2L/TRAIL versions. *Nature Medicine* **7**, 383-5.

38 Kelley SK, Harris LA, Xie D, Deforge L, Totpal K, Bussiere J & Fox JA (2001) Preclinical studies to predict the disposition of Apo2L/tumor necrosis factor-related apoptosis-inducing ligand in humans: characterization of in vivo efficacy, pharmacokinetics, and safety. *The Journal of Pharmacology and Experimental Therapeutics* **299**, 31-8.

39 Tanaka M, Suda T, Yatomi T, Nakamura N & Nagata S (1997) Lethal effect of recombinant human Fas ligand in mice pretreated with Propionibacterium acnes. *Journal of Immunology* **158**, 2303-9.

40 Ogasawara J, Watanabe-Fukunaga R, Adachi M, Matsuzawa A, Kasugai T, Kitamura Y, Itoh N, Suda T & Nagata S (1993) Lethal effect of the anti-Fas antibody in mice. *Nature* **364**, 806-9.

41 Degli-Esposti MA, Smolak PJ, Walczak H, Waugh J, Huang CP, DuBose RF, Goodwin RG & Smith CA (1997) Cloning and characterization of TRAIL-R3, a novel member of the emerging TRAIL receptor family. *The Journal of Experimental Medicine* **186**, 1165-70.

42 Walczak H, Degli-Esposti M a, Johnson RS, Smolak PJ, Waugh JY, Boiani N, Timour MS, Gerhart MJ, Schooley K a, Smith C a, Goodwin RG & Rauch CT (1997) TRAIL-R2: a novel apoptosis-mediating receptor for TRAIL. *The EMBO Journal* **16**, 5386-97.

43 Pan G, O'Rourke K, Chinnaiyan AM, Gentz R, Ebner R, Ni J & Dixit VM (1997) The Receptor for the Cytotoxic Ligand TRAIL. *Science* **276**, 111-113.

44 Pan G, Ni J, Wei YF, Yu G, Gentz R & Dixit VM (1997) An antagonist decoy receptor and a death domain-containing receptor for TRAIL. *Science* **277**, 815-8.

45 Marsters S a, Sheridan JP, Pitti RM, Huang a, Skubatch M, Baldwin D, Yuan J, Gurney a, Goddard a D, Godowski P & Ashkenazi A (1997) A novel receptor for Apo2L/TRAIL contains a truncated death domain. *Current Biology: CB* **7**, 1003-6.

46 MacFarlane M, Ahmad M, Srinivasula SM, Fernandes-Alnemri T, Cohen GM & Alnemri ES (1997) Identification and molecular cloning of two novel receptors for the cytotoxic ligand TRAIL. *The Journal of Biological Chemistry* **272**, 25417-20.

47 Schneider P, Thome M, Burns K, Bodmer JL, Hofmann K, Kataoka T, Holler N & Tschopp J (1997) TRAIL receptors 1 (DR4) and 2 (DR5) signal FADD-dependent apoptosis and activate NF-kappaB. *Immunity* **7**, 831-6.

48 Ashkenazi A & Dixit VM (1999) Apoptosis control by death and decoy receptors. *Current Opinion in Cell Biology* **11**, 255-60.

49 Sheridan JP (1997) Control of TRAIL-Induced Apoptosis by a Family of Signaling and Decoy Receptors. *Science* **277**, 818-821.

50 Zhang XD, Franco A, Myers K, Gray C, Nguyen T & Hersey P (1999) Relation of TNF-related apoptosis-inducing ligand (TRAIL) receptor and FLICE-inhibitory protein expression to TRAIL-induced apoptosis of melanoma. *Cancer Research* **59**, 2747-53.

51 Kim K, Fisher MJ, Xu SQ & El-Deiry WS (2000) Molecular determinants of response to TRAIL in killing of normal and cancer cells. *Clinical Cancer Research : An Official Journal of the American Association for Cancer Research* **6**, 335-46.

52 Wagner KW, Punnoose E a, Januario T, Lawrence D a, Pitti RM, Lancaster K, Lee D, von Goetz M, Yee SF, Totpal K, Huw L, Katta V, Cavet G, Hymowitz SG, Amler L & Ashkenazi A (2007) Death-receptor O-glycosylation controls tumor-cell sensitivity to the proapoptotic ligand Apo2L/TRAIL. *Nature Medicine* **13**, 1070-7.

53 Griffith TS, Chin WA, Jackson GC, Lynch DH & Kubin MZ (1998) Intracellular regulation of TRAIL-induced apoptosis in human melanoma cells. *Journal of Immunology* **161**, 2833-40.

54 Sheikh MS, Burns TF, Huang Y, Wu GS, Amundson S, Brooks KS, Fornace AJ & El-Deiry WS (1998) p53-dependent and -independent regulation of the death receptor KILLER/DR5 gene expression in response to genotoxic stress and tumor necrosis factor alpha. *Cancer Research* **58**, 1593-8.

55 Wu GS, Burns TF, McDonald ER, Jiang W, Meng R, Krantz ID, Kao G, Gan DD, Zhou JY, Muschel R, Hamilton SR, Spinner NB, Markowitz S, Wu GS & El-Deiry WS (1997) KILLER/DR5 is a DNA damage-inducible p53-regulated death receptor gene. *Nature Genetics* **17**, 141-3.

56 Burns TF, Bernhard EJ & El-Deiry WS (2001) Tissue specific expression of p53 target genes suggests a key role for KILLER/DR5 in p53-dependent apoptosis in vivo. *Oncogene* **20**, 4601-12.

57 Kim K, Takimoto R, Dicker DT, Chen Y, Gazitt Y & El-Deiry WS (2001) Enhanced TRAIL sensitivity by p53 overexpression in human cancer but not normal cell lines. *International Journal of Oncology* **18**, 241-7.

58 Wang G, Zhan Y, Wang H & Li W (2012) ABT-263 sensitizes TRAIL-resistant hepatocarcinoma cells by downregulating the Bcl-2 family of anti-apoptotic protein. *Cancer Chemotherapy and Pharmacology* **69**, 799-805.

59 Guo L, Fan L, Ren J, Pang Z, Ren Y, Li J, Wen Z, Qian Y, Zhang L, Ma H & Jiang X (2012) Combination of TRAIL and actinomycin D liposomes enhances antitumor effect in non-small cell lung cancer. *International Journal of Nanomedicine* **7**, 1449-60.

60 Meurette O, Fontaine A, Rebillard A, Le Moigne G, Lamy T, Lagadic-Gossmann D & Dimanche-Boitrel M-T (2006) Cytotoxicity of TRAIL/anticancer drug combinations in human normal cells. *Annals of the New York Academy of Sciences* **1090**, 209-16.

61 Soria J-C, Smit E, Khayat D, Besse B, Yang X, Hsu C-P, Reese D, Wiezorek J & Blackhall F (2010) Phase 1b study of dulanermin (recombinant human Apo2L/TRAIL) in combination with paclitaxel, carboplatin, and bevacizumab in patients with advanced non-squamous non-small-cell lung cancer. *Journal of Clinical Oncology: Official Journal of the American Society of Clinical Oncology* **28**, 1527-33.

62 Cuello M, Ettenberg SA, Nau MM & Lipkowitz S (2001) Synergistic induction of apoptosis by the combination of trail and chemotherapy in chemoresistant ovarian cancer cells. *Gynecologic Oncology* **81**, 380-90.

63 Munshi A, McDonnell TJ & Meyn RE (2002) Chemotherapeutic agents enhance TRAIL-induced apoptosis in prostate cancer cells. *Cancer Chemotherapy and Pharmacology* **50**, 46-52.

64 Naka T, Sugamura K, Hylander BL, Widmer MB, Rustum YM & Repasky EA (2002) Effects of tumor necrosis factor-related apoptosis-inducing ligand alone and in combination with chemotherapeutic agents on patients' colon tumors grown in SCID mice. *Cancer Research* **62**, 5800-6.

65 Wu X-X, Kakehi Y, Mizutani Y, Kamoto T, Kinoshita H, Isogawa Y, Terachi T & Ogawa O (2002) Doxorubicin enhances TRAIL-induced apoptosis in prostate cancer. *International Journal of Oncology* **20**, 949-54.

66 Hall MA & Cleveland JL (2007) Clearing the TRAIL for Cancer Therapy. *Cancer Cell* **12**, 4-6.

67 Oldenhuis CNAM, Stegehuis JH, Walenkamp AME, de Jong S & de Vries EGE (2008) Targeting TRAIL death receptors. *Current Opinion in Pharmacology* **8**, 433-9.

68 Wu GS (2009) TRAIL as a target in anti-cancer therapy. *Cancer Letters* **285**, 1-5.

69 Shanker A & Sayers T (2007) Sensitizing tumor cells to immune-mediated cytotoxicity. *Advances in Experimental Medicine and Biology* **601**, 163-71.

70 Zhao J, Lu Y & Shen H-M (2012) Targeting p53 as a therapeutic strategy in sensitizing TRAIL-induced apoptosis in cancer cells. *Cancer Letters* **314**, 8-23.

71 Kischkel FC, Hellbardt S, Behrmann I, Germer M, Pawlita M, Krammer PH & Peter ME (1995) Cytotoxicity-dependent APO-1 (Fas/CD95)-associated proteins form a death-inducing signaling complex (DISC) with the receptor. *The EMBO Journal* **14**, 5579-88.

72 Chaudhary PM, Eby M, Jasmin a, Bookwalter a, Murray J & Hood L (1997) Death receptor 5, a new member of the TNFR family, and DR4 induce FADD-dependent apoptosis and activate the NF-kappaB pathway. *Immunity* **7**, 821-30.

73 Sprick MR, Weigand M a, Rieser E, Rauch CT, Juo P, Blenis J, Krammer PH & Walczak H (2000) FADD/MORT1 and caspase-8 are recruited to TRAIL receptors 1 and 2 and are essential for apoptosis mediated by TRAIL receptor 2. *Immunity* **12**, 599-609.

74 Thomas LR, Henson A, Reed JC, Salsbury FR & Thorburn A (2004) Direct binding of Fas-associated death domain (FADD) to the tumor necrosis factor-related apoptosis-inducing ligand receptor DR5 is regulated by the death effector domain of FADD. *The Journal of Biological Chemistry* **279**, 32780-5.

75 Thomas LR, Stillman DJ & Thorburn A (2002) Regulation of Fas-associated death domain interactions by the death effector domain identified by a modified reverse two-hybrid screen. *The Journal of Biological Chemistry* **277**, 34343-8.

76 Thomas LR, Johnson RL, Reed JC & Thorburn A (2004) The C-terminal tails of tumor necrosis factor-related apoptosis-inducing ligand (TRAIL) and Fas receptors have opposing functions in Fas-associated death domain (FADD) recruitment and can regulate agonist-specific mechanisms of receptor activation. *The Journal of Biological Chemistry* **279**, 52479-86.

77 Thomas LR, Bender LM, Morgan MJ & Thorburn A (2006) Extensive regions of the FADD death domain are required for binding to the TRAIL receptor DR5. *Cell Death and Differentiation* **13**, 160-2.

78 Weber CH & Vincenz C (2001) A docking model of key components of the DISC complex: death domain superfamily interactions redefined. *FEBS Letters* **492**, 171-6.

79 Cohen GM (1997) Caspases: the executioners of apoptosis. *The Biochemical Journal* **326 (Pt 1**, 1-16.

80 Thornberry NA & Lazebnik Y (1998) Caspases: enemies within. *Science* **281**, 1312-6.

81 Han Z, Hendrickson EA, Bremner TA & Wyche JH (1997) A sequential two-step mechanism for the production of the mature p17:p12 form of caspase-3 in vitro. *The Journal of Biological Chemistry* **272**, 13432-6.

82 Stennicke HR & Salvesen GS (1997) Biochemical characteristics of caspases-3, -6, -7, and -8. *The Journal of Biological Chemistry* **272**, 25719-23.

83 Kischkel FC, Lawrence DA, Chuntharapai A, Schow P, Kim KJ & Ashkenazi A (2000) Apo2L/TRAIL-dependent recruitment of endogenous FADD and caspase-8 to death receptors 4 and 5. *Immunity* **12**, 611-20.

84 Shi Y (2004) Caspase activation: revisiting the induced proximity model. *Cell* **117**, 855-8.

85 Muzio M, Stockwell BR, Stennicke HR, Salvesen GS & Dixit VM (1998) An induced proximity model for caspase-8 activation. *The Journal of Biological Chemistry* **273**, 2926-30.

86 Salvesen GS & Dixit VM (1999) Caspase activation: the induced-proximity model. *Proceedings of the National Academy of Sciences of the United States of America* **96**, 10964-7.

87 Salvesen GS & Dixit VM (1997) Caspases: intracellular signaling by proteolysis. *Cell* **91**, 443-6.

88 Ito S, Wakabayashi K, Ubukata O, Hayashi S, Okada F & Hata T (2002) Crystal structure of the extracellular domain of mouse RANK ligand at 2.2-A resolution. *The Journal of Biological Chemistry* **277**, 6631-6.

89 Lam J, Nelson CA, Ross FP, Teitelbaum SL & Fremont DH (2001) Crystal structure of the TRANCE/RANKL cytokine reveals determinants of receptor-ligand specificity. *The Journal of Clinical Investigation* **108**, 971-9.

90 Eck MJ & Sprang SR (1989) The structure of tumor necrosis factor-alpha at 2.6 A resolution. Implications for receptor binding. *The Journal of Biological Chemistry* **264**, 17595-605.

91 Baeyens KJ, De Bondt HL, Raeymaekers A, Fiers W & De Ranter CJ (1999) The structure of mouse tumour-necrosis factor at 1.4 A resolution: towards modulation of its selectivity and trimerization. *Acta Crystallographica. Section D, Biological crystallography* **55**, 772-8.

92 Hymowitz SG, O'Connell MP, Ultsch MH, Hurst A, Totpal K, Ashkenazi A, de Vos AM & Kelley RF (2000) A Unique Zinc-Binding Site Revealed by a High-Resolution X-ray Structure of Homotrimeric Apo2L/TRAIL. *Biochemistry* **39**, 633-640.

93 Cha SS, Kim MS, Choi YH, Sung BJ, Shin NK, Shin HC, Sung YC & Oh BH (1999) 2.8 A resolution crystal structure of human TRAIL, a cytokine with selective antitumor activity. *Immunity* **11**, 253-61.

94 Zhan C, Patskovsky Y, Yan Q, Li Z, Ramagopal U, Cheng H, Brenowitz M, Hui X, Nathenson SG & Almo SC (2011) Decoy strategies: the structure of TL1A:DcR3 complex. *Structure* **19**, 162-71.

95 Kuester M, Kemmerzehl S, Dahms SO, Roeser D & Than ME (2011) The crystal structure of death receptor 6 (DR6): a potential receptor of the amyloid precursor protein (APP). *Journal of Molecular Biology* **409**, 189-201.

96 Liu C, Walter TS, Huang P, Zhang S, Zhu X, Wu Y, Wedderburn LR, Tang P, Owens RJ, Stuart DI, Ren J & Gao B (2010) Structural and functional insights of RANKL-RANK interaction and signaling. *Journal of Immunology* **184**, 6910-9.

97 Naismith JH, Devine TQ, Brandhuber BJ & Sprang SR (1995) Crystallographic evidence for dimerization of unliganded tumor necrosis factor receptor. *The Journal of Biological Chemistry* **270**, 13303-7.

98 Banner DW, D'Arcy A, Janes W, Gentz R, Schoenfeld H-J, Broger C, Loetscher H & Lesslauer W (1993) Crystal structure of the soluble human 55 kd TNF receptor-human TNFβ complex: Implications for TNF receptor activation. *Cell* **73**, 431-445.

99 Hymowitz SG, Christinger HW, Fuh G, Ultsch M, O'Connell M, Kelley RF, Ashkenazi A & de Vos a M (1999) Triggering cell death: the crystal structure of Apo2L/TRAIL in a complex with death receptor 5. *Molecular Cell* **4**, 563-71.

100 Cha SS, Sung BJ, Kim YA, Song YL, Kim HJ, Kim S, Lee MS & Oh BH (2000) Crystal Structure of TRAIL-DR5 Complex Identifies a Critical Role of the Unique Frame Insertion in Conferring Recognition Specificity. *The Journal of Biological Chemistry* **275**, 31171-31177.

101 Mongkolsapaya J, Grimes JM, Chen N, Xu XN, Stuart DI, Jones EY & Screaton GR (1999) Structure of the TRAIL-DR5 complex reveals mechanisms conferring specificity in apoptotic initiation. *Nature Structural Biology* **6**, 1048-53.

102 Mukai Y, Nakamura T, Yoshikawa M, Yoshioka Y, Tsunoda S-ichi, Nakagawa S, Yamagata Y & Tsutsumi Y (2010) Solution of the structure of the TNF-TNFR2 complex. *Science signaling* **3**, ra83.

103 Gong Y, Cao P, Yu H-jun & Jiang T (2008) Crystal structure of the neurotrophin-3 and p75NTR symmetrical complex. *Nature* **454**, 789-93.

104 Compaan DM & Hymowitz SG (2006) The crystal structure of the costimulatory OX40-OX40L complex. *Structure (London, England : 1993)* **14**, 1321-30.

105 Bodmer JL, Meier P, Tschopp J & Schneider P (2000) Cysteine 230 is essential for the structure and activity of the cytotoxic ligand TRAIL. *The Journal of biological chemistry* **275**, 20632-7.

106 Seol DW & Billiar TR (2000) Cysteine 230 modulates tumor necrosis factor-related apoptosis-inducing ligand activity. *Cancer Research* **60**, 3152-4.

107 Trabzuni D, Famulski KS & Ahmad M (2000) Functional analysis of tumour necrosis factor-alpha-related apoptosis-inducing ligand (TRAIL): cysteine-230 plays a critical role in the homotrimerization and biological activity of this novel tumoricidal cytokine. *The Biochemical Journal* **350 Pt 2**, 505-10.

108 Siegel RM (2000) Fas Preassociation Required for Apoptosis Signaling and Dominant Inhibition by Pathogenic Mutations. *Science* **288**, 2354-2357.

109 Chan FK-M (2000) A Domain in TNF Receptors That Mediates Ligand-Independent Receptor Assembly and Signaling. *Science* **288**, 2351-2354.

110 Clancy L, Mruk K, Archer K, Woelfel M, Mongkolsapaya J, Screaton GR, Lenardo MJ & Chan FK-M (2005) Preligand assembly domain-mediated ligand-independent association between TRAIL receptor 4 (TR4) and TR2 regulates TRAIL-induced apoptosis. *Proceedings of the National Academy of Sciences of the United States of America* **102**, 18099-104.

111 Siegel RM, Muppidi JR, Sarker M, Lobito A, Jen M, Martin D, Straus SE & Lenardo MJ (2004) SPOTS: signaling protein oligomeric transduction structures are early mediators of death receptor-induced apoptosis at the plasma membrane. *The Journal of cell biology* **167**, 735-44.

112 Adams C, Totpal K, Lawrence D, Marsters S, Pitti R, Yee S, Ross S, Deforge L, Koeppen H, Sagolla M, Compaan D, Lowman H, Hymowitz SG & Ashkenazi A (2008) Structural and functional analysis of the interaction between the agonistic monoclonal antibody Apomab and the proapoptotic receptor DR5. *Cell death and differentiation* **15**, 751-61.

113 Aggarwal BB (2003) Signalling Pathways of the TNF superfamily: A Double-Edged Sword. *Nature Reviews, Immunology* **3**, 745-756.

114 Valley CC, Lewis AK, Mudaliar DJ, Perlmutter JD, Braun AR, Karim CB, Thomas DD, Brody JR & Sachs JN (2012) Tumor necrosis factor-related apoptosis-inducing ligand (TRAIL) induces Death Receptor 5 networks that are highly organized. *The Journal of biological chemistry*.

115 Brown DA & London E (1998) Functions of lipid rafts in biological membranes. *Annual review of cell and developmental biology* **14**, 111-36.

116 Simons K & Ikonen E (1997) Functional rafts in cell membranes. *Nature* **387**, 569-72.

117 Bodmer J-L, Schneider P & Tschopp J (2002) The molecular architecture of the TNF superfamily. *Trends in biochemical sciences* **27**, 19-26.

118 Loetscher H, Gentzs R, Zulauf M, Lustigtl A, Tabuchill H, Schlaegers J, Brockhauss M, Gallati H & Manneberg M (1991) Recombinant 55-kDa Tumor Necrosis Factor (TNF) Receptor. , 18324-18329.

119 Kuang AA, Diehl GE, Zhang J & Winoto A (2000) FADD is required for DR4- and DR5-mediated apoptosis: lack of trail-induced apoptosis in FADD-deficient mouse embryonic fibroblasts. *The Journal of biological chemistry* **275**, 25065-8.

120 Kischkel FC, Lawrence DA, Tinel A, LeBlanc H, Virmani A, Schow P, Gazdar A, Blenis J, Arnott D & Ashkenazi A (2001) Death receptor recruitment of endogenous caspase-10 and apoptosis initiation in the absence of caspase-8. *The Journal of biological chemistry* **276**, 46639-46.

121 Blanchard H, Kodandapani L, Mittl PR, Marco SD, Krebs JF, Wu JC, Tomaselli KJ & Grütter MG (1999) The three-dimensional structure of caspase-8: an initiator enzyme in apoptosis. *Structure (London, England : 1993)* **7**, 1125-33.

122 Watt W, Koeplinger K a, Mildner a M, Heinrikson RL, Tomasselli a G & Watenpaugh KD (1999) The atomic-resolution structure of human caspase-8, a key activator of apoptosis. *Structure (London, England : 1993)* **7**, 1135-43.

123 Boatright KM, Renatus M, Scott FL, Sperandio S, Shin H, Pedersen IM, Ricci JE, Edris W a, Sutherlin DP, Green DR & Salvesen GS (2003) A unified model for apical caspase activation. *Molecular cell* **11**, 529-41.

124 Donepudi M, Mac Sweeney A, Briand C & Grütter MG (2003) Insights into the regulatory mechanism for caspase-8 activation. *Molecular cell* **11**, 543-9.

125 Talanian RV, Dang LC, Ferenz CR, Hackett MC, Mankovich JA, Welch JP, Wong WW & Brady KD (1996) Stability and oligomeric equilibria of refolded interleukin-1beta converting enzyme. *The Journal of biological chemistry* **271**, 21853-8.

126 Renatus M, Stennicke HR, Scott FL, Liddington RC & Salvesen GS (2001) Dimer formation drives the activation of the cell death protease caspase 9. *Proceedings of the National Academy of Sciences of the United States of America* **98**, 14250-5.

127 Pop C, Timmer J, Sperandio S & Salvesen GS (2006) The apoptosome activates caspase-9 by dimerization. *Molecular cell* **22**, 269-75.

128 Inohara N, Koseki T, Lin J, del Peso L, Lucas PC, Chen FF, Ogura Y & Núñez G (2000) An induced proximity model for NF-kappa B activation in the Nod1/RICK and RIP signaling pathways. *The Journal of biological chemistry* **275**, 27823-31.

129 Scott FL, Stec B, Pop C, Dobaczewska MK, Lee JJ, Monosov E, Robinson H, Salvesen GS, Schwarzenbacher R & Riedl SJ (2009) The Fas-FADD death domain complex structure unravels signalling by receptor clustering. *Nature* **457**, 1019-22.

130 Wang L, Yang JK, Kabaleeswaran V, Rice AJ, Cruz AC, Park AY, Yin Q, Damko E, Jang SB, Raunser S, Robinson CV, Siegel RM, Walz T & Wu H (2010) The Fas-FADD death domain complex structure reveals the basis of DISC assembly and disease mutations. *Nature structural & molecular biology* **17**, 1324-9.

131 Itoh N, Yonehara S, Ishii A, Yonehara M, Mizushima S, Sameshima M, Hase A, Seto Y & Nagata S (1991) The polypeptide encoded by the cDNA for human cell surface antigen Fas can mediate apoptosis. *Cell* **66**, 233-43.

132 Algeciras-schimnich A, Shen L, Barnhart BC, Murmann AE, Burkhardt JK & Peter ME (2002) Molecular Ordering of the Initial Signaling Events of CD95. *Society* **22**, 207-220.

133 Legembre P, Beneteau M, Daburon S, Moreau J-F & Taupin J-L (2003) Cutting edge: SDS-stable Fas microaggregates: an early event of Fas activation occurring with agonistic anti-Fas antibody but not with Fas ligand. *Journal of immunology (Baltimore, Md. : 1950)* **171**, 5659-62.

134 Feig C, Tchikov V, Schütze S & Peter ME (2007) Palmitoylation of CD95 facilitates formation of SDS-stable receptor aggregates that initiate apoptosis signaling. *The EMBO journal* **26**, 221-31.

135 Miyaji M, Jin Z-X, Yamaoka S, Amakawa R, Fukuhara S, Sato SB, Kobayashi T, Domae N, Mimori T, Bloom ET, Okazaki T & Umehara H (2005) Role of membrane sphingomyelin and ceramide in platform formation for Fas-mediated apoptosis. *The Journal of experimental medicine* **202**, 249-59.

136 Chakrabandhu K, Hérincs Z, Huault S, Dost B, Peng L, Conchonaud F, Marguet D, He H-T & Hueber A-O (2007) Palmitoylation is required for efficient Fas cell death signaling. *The EMBO journal* **26**, 209-20.

137 Austin CD, Lawrence D a, Peden A a, Varfolomeev EE, Totpal K, De Mazière AM, Klumperman J, Arnott D, Pham V, Scheller RH & Ashkenazi A (2006) Death-receptor activation halts clathrin-dependent endocytosis. *Proceedings of the National Academy of Sciences of the United States of America* **103**, 10283-8.

138 Ozsoy HZ, Sivasubramanian N, Wieder ED, Pedersen S & Mann DL (2008) Oxidative stress promotes ligand-independent and enhanced ligand-dependent tumor necrosis factor receptor signaling. *The Journal of biological chemistry* **283**, 23419-28.

139 Chan FK-M (2007) Three is better than one: pre-ligand receptor assembly in the regulation of TNF receptor signaling. *Cytokine* **37**, 101-7.

140 Lewis AK, Valley CC & Sachs JN (2012) TNFR1 signaling is associated with backbone conformational changes of receptor dimers consistent with over-activation in the R92Q TRAPS mutant. *Biochemistry*, 120716152713006.

141 Black RA, Rauch CT, Kozlosky CJ, Peschon JJ, Slack JL, Wolfson MF, Castner BJ, Stocking KL, Reddy P, Srinivasan S, Nelson N, Boiani N, Schooley KA, Gerhart M, Davis R, Fitzner JN, Johnson RS, Paxton RJ, March CJ & Cerretti DP (1997) A metalloproteinase disintegrin that releases tumour-necrosis factor-alpha from cells. *Nature* **385**, 729-33.

142 Wajant H, Pfizenmaier K & Scheurich P (2003) Tumor necrosis factor signaling. *Cell death and differentiation* **10**, 45-65.

143 Idriss HT & Naismith JH (2000) TNF alpha and the TNF receptor superfamily: structure-function relationship(s). *Microscopy research and technique* **50**, 184-95.

144 Alexopoulou L, Kranidioti K, Xanthoulea S, Denis M, Kotanidou A, Douni E, Blackshear PJ, Kontoyiannis DL & Kollias G (2006) Transmembrane TNF protects mutant mice against intracellular bacterial infections, chronic inflammation and autoimmunity. *European journal of immunology* **36**, 2768-80.

145 Wajant H, Moosmayer D, Wüest T, Bartke T, Gerlach E, Schönherr U, Peters N, Scheurich P & Pfizenmaier K (2001) Differential activation of TRAIL-R1 and -2 by soluble and membrane TRAIL allows selective surface antigen-directed activation of TRAIL-R2 by a soluble TRAIL derivative. *Oncogene* **20**, 4101-6.

146 Grell M, Douni E, Wajant H, Löhden M, Clauss M, Maxeiner B, Georgopoulos S, Lesslauer W, Kollias G, Pfizenmaier K & Scheurich P (1995) The transmembrane form of tumor necrosis factor is the prime activating ligand of the 80 kDa tumor necrosis factor receptor. *Cell* **83**, 793-802.

147 Richter C, Messerschmidt S, Holeiter G, Tepperink J, Osswald S, Zappe A, Branschädel M, Boschert V, Mann D a, Scheurich P & Krippner-Heidenreich A (2012) The Tumor Necrosis Factor Receptor Stalk Regions Define Responsiveness to Soluble versus Membrane-Bound Ligand. *Molecular and cellular biology* **32**, 2515-29.

148 Schneider P, Holler N, Bodmer JL, Hahne M, Frei K, Fontana A & Tschopp J (1998) Conversion of membrane-bound Fas(CD95) ligand to its soluble form is associated with downregulation of its proapoptotic activity and loss of liver toxicity. *The Journal of experimental medicine* **187**, 1205-13.

149 Suda T, Hashimoto H, Tanaka M, Ochi T & Nagata S (1997) Membrane Fas Ligand Kills Human Peripheral Blood T Lymphocytes, and Soluble Fas Ligand Blocks the Killing. *Journal of Experimental Medicine* **186**, 2045-2050.

150 Holler N, Tardivel A, Kovacsovics-Bankowski M, Hertig S, Gaide O, Martinon F, Tinel A, Deperthes D, Calderara S, Schulthess T, Engel J, Schneider P & Tschopp J (2003) Two adjacent trimeric Fas ligands are required for Fas signaling and formation of a death-inducing signaling complex. *Molecular and cellular biology* **23**, 1428-40.

151 Mühlenbeck F, Schneider P, Bodmer JL, Schwenzer R, Hauser a, Schubert G, Scheurich P, Moosmayer D, Tschopp J & Wajant H (2000) The tumor necrosis factor-related apoptosis-inducing ligand receptors TRAIL-R1 and TRAIL-R2 have distinct cross-linking requirements for initiation of apoptosis and are non-redundant in JNK activation. *The Journal of biological chemistry* **275**, 32208-13.

152 Bryde S, Grunwald I, Hammer A, Krippner-Heidenreich A, Schiestel T, Brunner H, Tovar GEM, Pfizenmaier K & Scheurich P (2005) Tumor necrosis factor (TNF)-functionalized nanostructured particles for the stimulation of membrane TNF-specific cell responses. *Bioconjugate chemistry* **16**, 1459-67.

153 Ranzinger J, Krippner-Heidenreich A, Haraszti T, Bock E, Tepperink J, Spatz JP & Scheurich P (2009) Nanoscale arrangement of apoptotic ligands reveals a demand for a minimal lateral distance for efficient death receptor activation. *Nano letters* **9**, 4240-5.

154 Nimmerjahn F & Ravetch JV (2011) FcγRs in health and disease. *Current topics in microbiology and immunology* **350**, 105-25.

155 Li F & Ravetch JV (2012) Apoptotic and antitumor activity of death receptor antibodies require inhibitory Fcγ receptor engagement. *Proceedings of the National Academy of Sciences of the United States of America*.

156 Branschädel M, Aird A, Zappe A, Tietz C, Krippner-Heidenreich A & Scheurich P (2010) Dual function of cysteine rich domain (CRD) 1 of TNF receptor type 1: conformational stabilization of CRD2 and control of receptor responsiveness. *Cellular signalling* **22**, 404-14.

157 Lobito AA, Kimberley FC, Muppidi JR, Komarow H, Jackson AJ, Hull KM, Kastner DL, Screaton GR & Siegel RM (2006) Abnormal disulfide-linked oligomerization results in ER retention and altered signaling by TNFR1 mutants in TNFR1-associated periodic fever syndrome (TRAPS). *Blood* **108**, 1320-7.

158 Deng G-M, Zheng L, Chan FK-M & Lenardo M (2005) Amelioration of inflammatory arthritis by targeting the pre-ligand assembly domain of tumor necrosis factor receptors. *Nature medicine* **11**, 1066-72.

159 Brown DA & London E (2000) Structure and function of sphingolipid- and cholesterol-rich membrane rafts. *The Journal of biological chemistry* **275**, 17221-4.

160 Brown DA & London E (1998) Structure and origin of ordered lipid domains in biological membranes. *The Journal of membrane biology* **164**, 103-14.

161 London E & Brown DA (2000) Insolubility of lipids in triton X-100: physical origin and relationship to sphingolipid/cholesterol membrane domains (rafts). *Biochimica et biophysica acta* **1508**, 182-95.

162 Brown DA (2006) Lipid rafts, detergent-resistant membranes, and raft targeting signals. *Physiology (Bethesda, Md.)* **21**, 430-9.

163 Schuck S, Honsho M, Ekroos K, Shevchenko A & Simons K (2003) Resistance of cell membranes to different detergents. *Proceedings of the National Academy of Sciences of the United States of America* **100**, 5795-800.

164 Lingwood D & Simons K (2007) Detergent resistance as a tool in membrane research. *Nature protocols* **2**, 2159-65.

165 Cottin V, Doan JES & Riches DWH (2002) Restricted localization of the TNF receptor CD120a to lipid rafts: a novel role for the death domain. *Journal of immunology (Baltimore, Md. : 1950)* **168**, 4095-102.

166 Legler DF, Micheau O, Doucey M-A, Tschopp J & Bron C (2003) Recruitment of TNF receptor 1 to lipid rafts is essential for TNFalpha-mediated NF-kappaB activation. *Immunity* **18**, 655-64.

167 Micheau O & Tschopp J (2003) Induction of TNF receptor I-mediated apoptosis via two sequential signaling complexes. *Cell* **114**, 181-90.

168 Irmler M, Thome M, Hahne M, Schneider P, Hofmann K, Steiner V, Bodmer JL, Schröter M, Burns K, Mattmann C, Rimoldi D, French LE & Tschopp J (1997) Inhibition of death receptor signals by cellular FLIP. *Nature* **388**, 190-5.

169 Varfolomeev EE & Ashkenazi A (2004) Tumor necrosis factor: an apoptosis JuNKie? *Cell* **116**, 491-7.

170 Ashkenazi A, Holland P & Eckhardt SG (2008) Ligand-based targeting of apoptosis in cancer: the potential of recombinant human apoptosis ligand 2/Tumor necrosis factor-related apoptosis-inducing ligand (rhApo2L/TRAIL). *Journal of clinical oncology : official journal of the American Society of Clinical Oncology* **26**, 3621-30.

171 Kelley SK & Ashkenazi A (2004) Targeting death receptors in cancer with Apo2L/TRAIL. *Current opinion in pharmacology* **4**, 333-9.

172 Camidge DR (2008) Apomab: an agonist monoclonal antibody directed against Death Receptor 5/TRAIL-Receptor 2 for use in the treatment of solid tumors. *Expert opinion on biological therapy* **8**, 1167-76.

173 Jin H, Yang R, Fong S, Totpal K, Lawrence D, Zheng Z, Ross J, Koeppen H, Schwall R & Ashkenazi A (2004) Apo2 ligand/tumor necrosis factor-related apoptosis-inducing ligand cooperates with chemotherapy to inhibit orthotopic lung tumor growth and improve survival. *Cancer research* **64**, 4900-5.

174 Li J, Knee DA, Wang Y, Zhang Q, Johnson JA, Cheng J, He H, Miller C, Li Z, Kowal C, Eckman J, Tang B, Yuan J, Chen L, Deveraux Q, Nasoff MS & Stover D (2008) LBY135, a novel anti-DR5 agonistic antibody induces tumor cell-specific cytotoxic activity in human colon tumor cell lines and xenografts. *Drug Development Research* **69**, 69-82.

175 Shanker A, Brooks AD, Tristan CA, Wine JW, Elliott PJ, Yagita H, Takeda K, Smyth MJ, Murphy WJ & Sayers TJ (2008) Treating metastatic solid tumors with bortezomib and a

tumor necrosis factor-related apoptosis-inducing ligand receptor agonist antibody. *Journal of the National Cancer Institute* **100**, 649-62.

176 Fesik SW (2005) Promoting apoptosis as a strategy for cancer drug discovery. *Nature reviews. Cancer* **5**, 876-85.

177 Guo Y, Chen C, Zheng Y, Zhang J, Tao X, Liu S, Zheng D & Liu Y (2005) A novel anti-human DR5 monoclonal antibody with tumoricidal activity induces caspase-dependent and caspase-independent cell death. *The Journal of biological chemistry* **280**, 41940-52.

178 Mahalingam D, Oldenhuis CNAM, Szegezdi E, Giles FJ, de Vries EGE, de Jong S & Nawrocki ST (2011) Targeting TRAIL towards the clinic. *Current drug targets* **12**, 2079-90.

179 Mahalingam D, Szegezdi E, Keane M, de Jong S & Samali A (2009) TRAIL receptor signalling and modulation: Are we on the right TRAIL? *Cancer treatment reviews* **35**, 280-8.

180 Pavet V, Beyrath J, Pardin C, Morizot A, Lechner M-C, Briand J-P, Wendland M, Maison W, Fournel S, Micheau O, Guichard G & Gronemeyer H (2010) Multivalent DR5 peptides activate the TRAIL death pathway and exert tumoricidal activity. *Cancer research* **70**, 1101-10.

181 Thorburn A (2007) Tumor necrosis factor-related apoptosis-inducing ligand (TRAIL) pathway signaling. *Journal of thoracic oncology : official publication of the International Association for the Study of Lung Cancer* **2**, 461-5.

182 Henkler F, Behrle E, Dennehy KM, Wicovsky A, Peters N, Warnke C, Pfizenmaier K & Wajant H (2005) The extracellular domains of FasL and Fas are sufficient for the formation of supramolecular FasL-Fas clusters of high stability. *The Journal of cell biology* **168**, 1087-98.

183 Wilson NS, Yang B, Yang A, Loeser S, Marsters S, Lawrence D, Li Y, Pitti R, Totpal K, Yee S, Ross S, Vernes J-M, Lu Y, Adams C, Offringa R, Kelley B, Hymowitz SG, Daniel D, Meng G & Ashkenazi A (2011) An Fcγ receptor-dependent mechanism drives antibody-mediated target-receptor signaling in cancer cells. *Cancer cell* **19**, 101-13.

184 Kohlhaas SL, Craxton A, Sun X-M, Pinkoski MJ & Cohen GM (2007) Receptor-mediated endocytosis is not required for tumor necrosis factor-related apoptosis-inducing ligand (TRAIL)-induced apoptosis. *The Journal of biological chemistry* **282**, 12831-41.

185 Bin L, Thorburn J, Thomas LR, Clark PE, Humphreys R & Thorburn A (2007) Tumor-derived mutations in the TRAIL receptor DR5 inhibit TRAIL signaling through the DR4 receptor by competing for ligand binding. *The Journal of biological chemistry* **282**, 28189-94.

186 Schneider P (2000) Production of recombinant TRAIL and TRAIL receptor: Fc chimeric proteins. *Methods in enzymology* **322**, 325-45.

187 Zacharias D a, Violin JD, Newton AC & Tsien RY (2002) Partitioning of lipid-modified monomeric GFPs into membrane microdomains of live cells. *Science (New York, N.Y.)* **296**, 913-6.

188 Bhatia S, Edidin M, Almo SC & Nathenson SG (2005) Different cell surface oligomeric states of B7-1 and B7-2: implications for signaling. *Proceedings of the National Academy of Sciences of the United States of America* **102**, 15569-74.

189 Autry JM, Rubin JE, Pietrini SD, Winters DL, Robia SL & Thomas DD (2011) Oligomeric interactions of sarcolipin and the Ca-ATPase. *The Journal of biological chemistry* **286**, 31697-706.

190 Hou Z, Kelly EM & Robia SL (2008) Phosphomimetic mutations increase phospholamban oligomerization and alter the structure of its regulatory complex. *The Journal of biological chemistry* **283**, 28996-9003.

191 Hou Z & Robia SL (2010) Relative affinity of calcium pump isoforms for phospholamban quantified by fluorescence resonance energy transfer. *Journal of molecular biology* **402**, 210-6.

192 Brooks BR, Bruccoleri RE, Olafson BD, States DJ, Swaminathan S & Karplus M (1983) CHARMM: A program for macromolecular energy, minimization, and dynamics calculations. *Journal of Computational Chemistry* **4**, 187-217.

193 MacKerell, AD, Bashford D, Dunbrack, RL, Evanseck JD, Field MJ, Fischer S, Gao J, Guo H, Ha S, Joseph-McCarthy D, Kuchnir L, Kuczera K, Lau FTK, Mattos C, Michnick S, Ngo T, Nguyen DT, Prodhom B, Reiher WE, Roux B, Schlenkrich M, Smith JC, Stote R, Straub J, Watanabe M, Wiórkiewicz-Kuczera J, Yin D & Karplus M (1998) All-Atom Empirical Potential for Molecular Modeling and Dynamics Studies of Proteins †. *The Journal of Physical Chemistry B* **102**, 3586-3616.

194 Mackerell AD, Feig M & Brooks CL (2004) Extending the treatment of backbone energetics in protein force fields: limitations of gas-phase quantum mechanics in reproducing protein conformational distributions in molecular dynamics simulations. *Journal of computational chemistry* **25**, 1400-15.

195 Feig M, Karanicolas J & Brooks CL (2004) MMTSB Tool Set: enhanced sampling and multiscale modeling methods for applications in structural biology. *Journal of molecular graphics & modelling* **22**, 377-95.

196 Im W, Lee MS & Brooks CL (2003) Generalized born model with a simple smoothing function. *Journal of computational chemistry* **24**, 1691-702.

197 Im W, Feig M & Brooks CL (2003) An implicit membrane generalized born theory for the study of structure, stability, and interactions of membrane proteins. *Biophysical journal* **85**, 2900-18.

198 Screaton GR, Mongkolsapaya J, Xu XN, Cowper a E, McMichael a J & Bell JI (1997) TRICK2, a new alternatively spliced receptor that transduces the cytotoxic signal from TRAIL. *Current biology : CB* **7**, 693-6.

199 Vilar M, Charalampopoulos I, Kenchappa RS, Simi A, Karaca E, Reversi A, Choi S, Bothwell M, Mingarro I, Friedman WJ, Schiavo G, Bastiaens PIH, Verveer PJ, Carter BD & Ibáñez CF (2009) Activation of the p75 neurotrophin receptor through conformational rearrangement of disulphide-linked receptor dimers. *Neuron* **62**, 72-83.

200 Vilar M, Charalampopoulos I, Kenchappa RS, Reversi A, Klos-Applequist JM, Karaca E, Simi A, Spuch C, Choi S, Friedman WJ, Ericson J, Schiavo G, Carter BD & Ibáñez CF (2009) Ligand-independent signaling by disulfide-crosslinked dimers of the p75 neurotrophin receptor. *Journal of cell science* **122**, 3351-7.

201 Chan FK, Siegel RM, Zacharias D, Swofford R, Holmes KL, Tsien RY & Lenardo MJ (2001) Fluorescence resonance energy transfer analysis of cell surface receptor interactions and signaling using spectral variants of the green fluorescent protein. *Cytometry* **44**, 361-8.

202 Li E & Hristova K (2006) Role of receptor tyrosine kinase transmembrane domains in cell signaling and human pathologies. *Biochemistry* **45**, 6241-51.

203 Li E, You M & Hristova K (2006) FGFR3 dimer stabilization due to a single amino acid pathogenic mutation. *Journal of molecular biology* **356**, 600-12.

204 Li R, Babu CR, Lear JD, Wand AJ, Bennett JS & DeGrado WF (2001) Oligomerization of the integrin alphaIIbbeta3: roles of the transmembrane and cytoplasmic domains. *Proceedings of the National Academy of Sciences of the United States of America* **98**, 12462-7.

205 Zhu H, Metcalf DG, Streu CN, Billings PC, Degrado WF & Bennett JS (2010) Specificity for homooligomer versus heterooligomer formation in integrin transmembrane helices. *Journal of molecular biology* **401**, 882-91.

206 Sugita Y & Okamoto Y (1999) Replica-exchange molecular dynamics method for protein folding. *Chemical Physics Letters* **314**, 141-151.

207 Senes A, Gerstein M & Engelman DM (2000) Statistical analysis of amino acid patterns in transmembrane helices: the GxxxG motif occurs frequently and in association with beta-branched residues at neighboring positions. *Journal of molecular biology* **296**, 921-36.

208 Senes A, Engel DE & DeGrado WF (2004) Folding of helical membrane proteins: the role of polar, GxxxG-like and proline motifs. *Current opinion in structural biology* **14**, 465-79.

209 Berger BW, Kulp DW, Span LM, DeGrado JL, Billings PC, Senes A, Bennett JS & DeGrado WF (2010) Consensus motif for integrin transmembrane helix association. *Proceedings of the National Academy of Sciences of the United States of America* **107**, 703-8.

210 Raghunathan A, Sivakamasundari R, Wolenski J, Poddar R & Weissman SM (2001) Functional analysis of B144/LST1: a gene in the tumor necrosis factor cluster that induces formation of long filopodia in eukaryotic cells. *Experimental cell research* **268**, 230-44.

211 Arai T, Akiyama Y, Okabe S, Saito K, Iwai T & Yuasa Y (1998) Genomic organization and mutation analyses of the DR5/TRAIL receptor 2 gene in colorectal carcinomas. *Cancer letters* **133**, 197-204.

212 Baritaki S, Huerta-Yepez S, Sakai T, Spandidos DA & Bonavida B (2007) Chemotherapeutic drugs sensitize cancer cells to TRAIL-mediated apoptosis: up-regulation of DR5 and inhibition of Yin Yang 1. *Molecular cancer therapeutics* **6**, 1387-99.

213 Yasuda T, Yoshida T, Goda AE, Horinaka M, Yano K, Shiraishi T, Wakada M, Mizutani Y, Miki T & Sakai T (2008) Anti-gout agent allopurinol exerts cytotoxicity to human hormone-refractory prostate cancer cells in combination with tumor necrosis factor-related apoptosis-inducing ligand. *Molecular cancer research : MCR* **6**, 1852-60.

214 Hartman NC & Groves JT (2011) Signaling clusters in the cell membrane. *Current opinion in cell biology* **23**, 370-6.

215 Manz BN, Jackson BL, Petit RS, Dustin ML & Groves J (2011) T-cell triggering thresholds are modulated by the number of antigen within individual T-cell receptor clusters. *Proceedings of the National Academy of Sciences of the United States of America* **108**, 9089-94.

216 Thorburn A (2004) Death receptor-induced cell killing. *Cellular Signalling* **16**, 139-44.

217 Schneider P & Tschopp J (2000) Apoptosis induced by death receptors. *Pharmaceutica acta Helvetiae* **74**, 281-6.

218 Rowinsky EK (2005) Targeted induction of apoptosis in cancer management: the emerging role of tumor necrosis factor-related apoptosis-inducing ligand receptor activating agents. *Journal of clinical oncology : official journal of the American Society of Clinical Oncology* **23**, 9394-407.

219 Gerspach J, Pfizenmaier K & Wajant H (2011) Therapeutic targeting of CD95 and the TRAIL death receptors. *Recent patents on anti-cancer drug discovery* **6**, 294-310.

220 Yang A, Wilson NS & Ashkenazi A (2010) Proapoptotic DR4 and DR5 signaling in cancer cells: toward clinical translation. *Current opinion in cell biology* **22**, 837-44.

221 Scheel-Toellner D, Wang K, Singh R, Majeed S, Raza K, Curnow SJ, Salmon M & Lord JM (2002) The death-inducing signalling complex is recruited to lipid rafts in Fas-induced apoptosis. *Biochemical and biophysical research communications* **297**, 876-9.

222 Muppidi JR & Siegel RM (2004) Ligand-independent redistribution of Fas (CD95) into lipid rafts mediates clonotypic T cell death. *Nature immunology* **5**, 182-9.

223 Song JH, Tse MCL, Bellail A, Phuphanich S, Khuri F, Kneteman NM & Hao C (2007) Lipid rafts and nonrafts mediate tumor necrosis factor related apoptosis-inducing ligand induced apoptotic and nonapoptotic signals in non small cell lung carcinoma cells. *Cancer research* **67**, 6946-55.

224 Min Y, Shi J, Zhang Y, Liu S, Liu Y & Zheng D (2009) Death receptor 5-recruited raft components contributes to the sensitivity of Jurkat leukemia cell lines to TRAIL-induced cell death. *IUBMB life* **61**, 261-7.

225 Gajate C & Mollinedo F (2007) Edelfosine and perifosine induce selective apoptosis in multiple myeloma by recruitment of death receptors and downstream signaling molecules into lipid rafts. *Blood* **109**, 711-9.

226 Delmas D, Rébé C, Micheau O, Athias A, Gambert P, Grazide S, Laurent G, Latruffe N & Solary E (2004) Redistribution of CD95, DR4 and DR5 in rafts accounts for the synergistic toxicity of resveratrol and death receptor ligands in colon carcinoma cells. *Oncogene* **23**, 8979-86.

227 Mérino D, Lalaoui N, Morizot A, Schneider P, Solary E & Micheau O (2006) Differential inhibition of TRAIL-mediated DR5-DISC formation by decoy receptors 1 and 2. *Molecular and Cellular Biology* **26**, 7046-55.

228 Klein U, Gimpl G & Fahrenholz F (1995) Alteration of the myometrial plasma membrane cholesterol content with beta-cyclodextrin modulates the binding affinity of the oxytocin receptor. *Biochemistry* **34**, 13784-93.

229 Kilsdonk EP, Yancey PG, Stoudt GW, Bangerter FW, Johnson WJ, Phillips MC & Rothblat GH (1995) Cellular cholesterol efflux mediated by cyclodextrins. *The Journal of biological chemistry* **270**, 17250-6.

230 Simons K & Toomre D (2000) Lipid rafts and signal transduction. *Nature reviews. Molecular cell biology* **1**, 31-9.

231 Schroeder R, London E & Brown D (1994) Interactions between saturated acyl chains confer detergent resistance on lipids and glycosylphosphatidylinositol (GPI)-anchored proteins: GPI-anchored proteins in liposomes and cells show similar behavior. *Proceedings of the National Academy of Sciences of the United States of America* **91**, 12130-4.

232 Kenworthy AK, Nichols BJ, Remmert CL, Hendrix GM, Kumar M, Zimmerberg J & Lippincott-Schwartz J (2004) Dynamics of putative raft-associated proteins at the cell surface. *The Journal of cell biology* **165**, 735-46.

233 Nezil FA & Bloom M (1992) Combined influence of cholesterol and synthetic amphiphillic peptides upon bilayer thickness in model membranes. *Biophysical journal* **61**, 1176-83.

234 Ren J, Lew S, Wang Z & London E (1997) Transmembrane orientation of hydrophobic alpha-helices is regulated both by the relationship of helix length to bilayer thickness and by the cholesterol concentration. *Biochemistry* **36**, 10213-20.

235 Sengupta P, Jovanovic-Talisman T, Skoko D, Renz M, Veatch SL & Lippincott-Schwartz J (2011) Probing protein heterogeneity in the plasma membrane using PALM and pair correlation analysis. *Nature methods* **8**, 969-75.

236 Morgan RS, Tatsch CE, Gushard RH, Mcadon JM & Warme PK (1978) CHAINS OF ALTERNATING SULFUR AND π-BONDED ATOMS IN EIGHT SMALL PROTEINS. *International Journal of Peptide and Protein Research* **11**, 209-217.

237 Morgan RS & McAdon JM (1980) PREDICTOR FOR SULFUR-AROMATIC INTERACTIONS IN GLOBULAR PROTEINS. *International Journal of Peptide and Protein Research* **15**, 177-180.

238 Rosenfield RE, Parthasarathy R & Dunitz JD (1977) Directional preferences of nonbonded atomic contacts with divalent sulfur. 1. Electrophiles and nucleophiles. *Journal of the American Chemical Society* **99**, 4860-4862.

239 Reid KSC, Lindley PF & Thornton JM (1985) Sulphur-aromatic interactions in proteins. *October* **190**, 209-13.

240 Zauhar RJ, Colbert CL, Morgan RS & Welsh WJ (2000) Evidence for a strong sulfur-aromatic interaction derived from crystallographic data. *Biopolymers* **53**, 233-48.

241 Bodner BL, Jackman LM & Morgan RS (1980) NMR study of 1: 1 complexes between divalent sulfur and aromatic compounds: A model for interactions in globular proteins. *Biochemical and Biophysical Research Communications* **94**, 807–813.

242 Viguera AR & Serrano L (1995) Side-chain interactions between sulfur-containing amino acids and phenylalanine in alpha-helices. *Biochemistry* **34**, 8771-9.

243 Cregut D & Serrano L (1999) Molecular dynamics as a tool to detect protein foldability. A mutant of domain B1 of protein G with non-native secondary structure propensities. *Protein science : a publication of the Protein Society* **8**, 271-82.

244 Hymowitz SG, Christinger HW, Fuh G, Ultsch M, O'Connell M, Kelley RF, Ashkenazi A & de Vos a M (1999) Triggering cell death: the crystal structure of Apo2L/TRAIL in a complex with death receptor 5. *Molecular cell* **4**, 563-71.

245 Banner DW, D'Arcy A, Janes W, Gentz R, Schoenfeld H-J, Broger C, Loetscher H & Lesslauer W (1993) Crystal structure of the soluble human 55 kd TNF receptor-human TNFβ complex: Implications for TNF receptor activation. *Cell* **73**, 431-445.

246 Hymowitz SG, O'Connell MP, Ultsch MH, Hurst A, Totpal K, Ashkenazi A, de Vos AM & Kelley RF (2000) A Unique Zinc-Binding Site Revealed by a High-Resolution X-ray Structure of Homotrimeric Apo2L/TRAIL. *Biochemistry* **39**, 633-640.

247 Cha SS, Kim MS, Choi YH, Sung BJ, Shin NK, Shin HC, Sung YC & Oh BH (1999) 2.8 A resolution crystal structure of human TRAIL, a cytokine with selective antitumor activity. *Immunity* **11**, 253-61.

248 Mongkolsapaya J, Grimes JM, Chen N, Xu XN, Stuart DI, Jones EY & Screaton GR (1999) Structure of the TRAIL-DR5 complex reveals mechanisms conferring specificity in apoptotic initiation. *Nature structural biology* **6**, 1048-53.

249 Bin L, Thorburn J, Thomas LR, Clark PE, Humphreys R & Thorburn A (2007) Tumor-derived mutations in the TRAIL receptor DR5 inhibit TRAIL signaling through the DR4 receptor by competing for ligand binding. *The Journal of biological chemistry* **282**, 28189-94.

250 Schneider P (2000) Production of recombinant TRAIL and TRAIL receptor: Fc chimeric proteins. *Methods in enzymology* **322**, 325-45.

251 Berman HM, Westbrook J, Feng Z, Gilliland G, Bhat TN, Weissig H, Shindyalov IN & Bourne PE (2000) The Protein Data Bank. *Nucleic acids research* **28**, 235-42.

252 Berman H, Henrick K & Nakamura H (2003) Announcing the worldwide Protein Data Bank. *Nature structural biology* **10**, 980.

253 Zhao Y, Schultz NE & Truhlar DG (2006) Design of Density Functionals by Combining the Method of Constraint Satisfaction with Parametrization for Thermochemistry, Thermochemical Kinetics, and Noncovalent Interactions. *Journal of Chemical Theory and Computation* **2**, 364-382.

254 Zhao Y & Truhlar DG (2006) A new local density functional for main-group thermochemistry, transition metal bonding, thermochemical kinetics, and noncovalent interactions. *The Journal of chemical physics* **125**, 194101.

255 Sherrill CD, Takatani T & Hohenstein EG (2009) An assessment of theoretical methods for nonbonded interactions: comparison to complete basis set limit coupled-cluster potential

energy curves for the benzene dimer, the methane dimer, benzene-methane, and benzene-H2S. *The journal of physical chemistry. A* **113**, 10146-59.

256 Boys SF & Bernardi F (1970) The calculation of small molecular interactions by the differences of separate total energies. Some procedures with reduced errors. *Molecular Physics* **19**, 553-566.

257 Cock PJA, Antao T, Chang JT, Chapman BA, Cox CJ, Dalke A, Friedberg I, Hamelryck T, Kauff F, Wilczynski B & de Hoon MJL (2009) Biopython: freely available Python tools for computational molecular biology and bioinformatics. *Bioinformatics (Oxford, England)* **25**, 1422-3.

258 Pal D & Chakrabarti P (2001) Non-hydrogen bond interactions involving the methionine sulfur atom. *Journal of biomolecular structure & dynamics* **19**, 115-28.

259 Imai YN, Inoue Y & Yamamoto Y (2007) Propensities of polar and aromatic amino acids in noncanonical interactions: nonbonded contacts analysis of protein-ligand complexes in crystal structures. *Journal of medicinal chemistry* **50**, 1189-96.

260 Ringer AL, Senenko A & Sherrill CD (2007) Models of S / pi interactions in protein structures : Comparison of the H2S – benzene complex with PDB data. , 2216-2223.

261 Cabaleiro-Lago EM, Carrazana-García JA & Rodríguez-Otero J (2009) Study of the interaction between water and hydrogen sulfide with polycyclic aromatic hydrocarbons. *The Journal of chemical physics* **130**, 234307.

262 Némethy G & Scheraga HA (1981) STRONG INTERACTION BETWEEN DISULFIDE DERIVATIVES AND AROMATIC GROUPS IN PEPTIDES AND PROTEINS. *Biochemical and Biophysical Research Communications* **98**, 482-487.

263 Duan G, Smith VH & Weaver DF (2001) Characterization of aromatic-thiol π-type hydrogen bonding and phenylalanine-cysteine side chain interactions through ab initio calculations and protein database analyses. *Molecular Physics* **99**, 1689-1699.

264 Morgan RS, Tatsch CE, Gushard RH, Mcadon JM & Warme PK (1978) Chains of Alternating Sulfur and π-Bonded Atoms in Eight Small Proteins. *International Journal of Peptide and Protein Research* **11**, 209-217.

265 Strop P & Mayo SL (2000) Contribution of surface salt bridges to protein stability. *Biochemistry* **39**, 1251-5.

266 Iqbalsyah TM & Doig AJ (2005) Anticooperativity in a Glu-Lys-Glu salt bridge triplet in an isolated alpha-helical peptide. *Biochemistry* **44**, 10449-56.

267 Tsai J & Levitt M (2002) Evidence of turn and salt bridge contributions to beta-hairpin stability: MD simulations of C-terminal fragment from the B1 domain of protein G. *Biophysical chemistry* **101-102**, 187-201.

268 Singh UC (1988) Probing the salt bridge in the dihydrofolate reductase-methotrexate complex by using the coordinate-coupled free-energy perturbation method. *Proceedings of the National Academy of Sciences of the United States of America* **85**, 4280-4.

269 Wimley WC, Gawrisch K, Creamer TP & White SH (1996) Direct measurement of salt-bridge solvation energies using a peptide model system: implications for protein stability. *Proceedings of the National Academy of Sciences of the United States of America* **93**, 2985-90.

270 Waldburger CD, Schildbach JF & Sauer RT (1995) Are buried salt bridges important for protein stability and conformational specificity? *Nature Structural Biology* **2**, 122-128.

271 Bosshard HR, Marti DN & Jelesarov I Protein stabilization by salt bridges: concepts, experimental approaches and clarification of some misunderstandings. *Journal of molecular recognition : JMR* **17**, 1-16.

272 Russell SD & Roth GJ (1993) Pseudo-von Willebrand disease: a mutation in the platelet glycoprotein Ib alpha gene associated with a hyperactive surface receptor. *Blood* **81**, 1787-91.

273 Moriki T, Murata M, Kitaguchi T, Anbo H, Handa M, Watanabe K, Takahashi H & Ikeda Y (1997) Expression and functional characterization of an abnormal platelet membrane glycoprotein Ib alpha (Met239 --> Val) reported in patients with platelet-type von Willebrand disease. *Blood* **90**, 698-705.

274 Dumas JJ, Kumar R, McDonagh T, Sullivan F, Stahl ML, Somers WS & Mosyak L (2004) Crystal structure of the wild-type von Willebrand factor A1-glycoprotein Ibalpha complex reveals conformation differences with a complex bearing von Willebrand disease mutations. *The Journal of biological chemistry* **279**, 23327-34.

275 Gacia M, Safranow K, Styczyńska M, Jakubowska K, Pepłońska B, Chodakowska-Zebrowska M, Przekop I, Słowik A, Golańska E, Hułas-Bigoszewska K, Chlubek D, Religa D, Zekanowski C & Barcikowska M (2006) Prion protein gene M129 allele is a risk factor for Alzheimer's disease. *Journal of neural transmission (Vienna, Austria : 1996)* **113**, 1747-51.

276 Goldfarb LG, Petersen RB, Tabaton M, Brown P, LeBlanc AC, Montagna P, Cortelli P, Julien J, Vital C & Pendelbury WW (1992) Fatal familial insomnia and familial Creutzfeldt-Jakob disease: disease phenotype determined by a DNA polymorphism. *Science (New York, N.Y.)* **258**, 806-8.

277 Ilc G, Giachin G, Jaremko M, Jaremko Ł, Benetti F, Plavec J, Zhukov I & Legname G (2010) NMR structure of the human prion protein with the pathological Q212P mutation reveals unique structural features. *PloS one* **5**, e11715.

278 Gimm O, Neuberg DS, Marsh DJ, Dahia PL, Hoang-Vu C, Raue F, Hinze R, Dralle H & Eng C (1999) Over-representation of a germline RET sequence variant in patients with sporadic medullary thyroid carcinoma and somatic RET codon 918 mutation. *Oncogene* **18**, 1369-73.

279 Eng C, Smith DP, Mulligan LM, Nagai MA, Healey CS, Ponder MA, Gardner E, Scheumann GF, Jackson CE & Tunnacliffe A (1994) Point mutation within the tyrosine kinase domain of the RET proto-oncogene in multiple endocrine neoplasia type 2B and related sporadic tumours. *Human molecular genetics* **3**, 237-41.

280 Mologni L, Rostagno R, Brussolo S, Knowles PP, Kjaer S, Murray-Rust J, Rosso E, Zambon A, Scapozza L, McDonald NQ, Lucchini V & Gambacorti-Passerini C (2010) Synthesis, structure-activity relationship and crystallographic studies of 3-substituted indolin-2-one RET inhibitors. *Bioorganic & medicinal chemistry* **18**, 1482-96.

281 Li T, Sandberg MA, Pawlyk BS, Rosner B, Hayes KC, Dryja TP & Berson EL (1998) Effect of vitamin A supplementation on rhodopsin mutants threonine-17 --> methionine and proline-347 --> serine in transgenic mice and in cell cultures. *Proceedings of the National Academy of Sciences of the United States of America* **95**, 11933-8.

282 Stadtman ER, Van Remmen H, Richardson A, Wehr NB & Levine RL (2005) Methionine oxidation and aging. *Biochimica et biophysica acta* **1703**, 135-40.

283 Glaser CB, Yamin G, Uversky VN & Fink AL (2005) Methionine oxidation, alpha-synuclein and Parkinson's disease. *Biochimica et biophysica acta* **1703**, 157-69.

284 Schöneich C (2005) Methionine oxidation by reactive oxygen species: reaction mechanisms and relevance to Alzheimer's disease. *Biochimica et biophysica acta* **1703**, 111-9.

285 Garner MH & Spector A (1980) Selective oxidation of cysteine and methionine in normal and senile cataractous lenses. *Proceedings of the National Academy of Sciences of the United States of America* **77**, 1274-7.

286 Vogt W (1995) Oxidation of methionyl residues in proteins: tools, targets, and reversal. *Free radical biology & medicine* **18**, 93-105.

287 Maier K, Leuschel L & Costabel U (1991) Increased levels of oxidized methionine residues in bronchoalveolar lavage fluid proteins from patients with idiopathic pulmonary fibrosis. *The American review of respiratory disease* **143**, 271-4.

288 Gao J, Yin DH, Yao Y, Sun H, Qin Z, Schöneich C, Williams TD & Squier TC (1998) Loss of conformational stability in calmodulin upon methionine oxidation. *Biophysical journal* **74**, 1115-34.

289 Ta HM, Nguyen GTT, Jin HM, Choi J, Park H, Kim N, Hwang H-Y & Kim KK (2010) Structure-based development of a receptor activator of nuclear factor-kappaB ligand (RANKL) inhibitor peptide and molecular basis for osteopetrosis. *Proceedings of the National Academy of Sciences of the United States of America* **107**, 20281-6.

290 Saito H, Kojima T, Takahashi M, Horne WC, Baron R, Amagasa T, Ohya K & Aoki K (2007) A tumor necrosis factor receptor loop peptide mimic inhibits bone destruction to the same extent as anti-tumor necrosis factor monoclonal antibody in murine collagen-induced arthritis. *Arthritis and rheumatism* **56**, 1164-74.

291 Aoki K, Saito H, Itzstein C, Ishiguro M, Shibata T, Blanque R, Mian AH, Takahashi M, Suzuki Y, Yoshimatsu M, Yamaguchi A, Deprez P, Mollat P, Murali R, Ohya K, Horne WC & Baron R (2006) A TNF receptor loop peptide mimic blocks RANK ligand-induced signaling, bone resorption, and bone loss. *The Journal of clinical investigation* **116**, 1525-34.

292 Suzuki Y, Aoki K, Saito H, Umeda M, Nitta H, Baron R & Ohya K (2006) A tumor necrosis factor-alpha antagonist inhibits inflammatory bone resorption induced by Porphyromonas gingivalis infection in mice. *Journal of periodontal research* **41**, 81-91.

293 Truneh A, Sharma S, Silverman C, Khandekar S, Reddy MP, Deen KC, McLaughlin MM, Srinivasula SM, Livi GP, Marshall LA, Alnemri ES, Williams WV & Doyle ML (2000) Temperature-sensitive differential affinity of TRAIL for its receptors. DR5 is the highest affinity receptor. *The Journal of biological chemistry* **275**, 23319-25.

294 Henriques R & Mhlanga MM (2009) PALM and STORM: what hides beyond the Rayleigh limit? *Biotechnology journal* **4**, 846-57.

295 Boschert V, Krippner-Heidenreich A, Branschädel M, Tepperink J, Aird A & Scheurich P (2010) Single chain TNF derivatives with individually mutated receptor binding sites reveal differential stoichiometry of ligand receptor complex formation for TNFR1 and TNFR2. *Cellular signalling* **22**, 1088-96.

296 Krippner-Heidenreich A, Grunwald I, Zimmermann G, Kühnle M, Gerspach J, Sterns T, Shnyder SD, Gill JH, Männel DN, Pfizenmaier K & Scheurich P (2008) Single-chain TNF, a TNF derivative with enhanced stability and antitumoral activity. *Journal of immunology (Baltimore, Md. : 1950)* **180**, 8176-83.

297 Marrink SJ, Risselada HJ, Yefimov S, Tieleman DP & de Vries AH (2007) The MARTINI force field: coarse grained model for biomolecular simulations. *The journal of physical chemistry. B* **111**, 7812-24.

298 Perlmutter JD & Sachs JN (2011) Interleaflet interaction and asymmetry in phase separated lipid bilayers: molecular dynamics simulations. *Journal of the American Chemical Society* **133**, 6563-77.

Appendix A. NaCl interactions with phosphatidylcholine bilayers do not alter membrane structure, but induce long-range ordering of ions and water

A.1. Summary

It is generally accepted that ions interact directly with lipids in biological membranes. Decades of biophysical studies on pure lipid bilayer systems have shown that only certain types of ions, most significantly large anions and multivalent cations, can fundamentally alter the structure and dynamics of lipid bilayers. It has long been accepted that at physiological concentrations NaCl ions do not alter the physical behavior or structure of bilayers composed solely of zwitterionic phosphatidylcholine (PC) lipids. Recent X-ray scattering experiments have reaffirmed this dogma, showing that below 1 M concentration, NaCl does not significantly alter bilayer structure. However, despite this history, there is an ongoing controversy within the molecular dynamics (MD) simulation community regarding NaCl/PC interactions. In particular, the CHARMM and GROMOS force fields show dramatically different behavior, including the effect on bilayer structure, surface potential, and the ability to form stable, coordinated ion-lipid complexes. Here, using long-timescale, constant-pressure simulations under the newest version of the CHARMM force field, we find that Na^+ and Cl^- associate with PC head groups in a POPC bilayer with approximately equal, though weak, affinity, and that the salt has a negligible effect on bilayer structure, consistent with earlier CHARMM results and more recent X-ray data. The results suggest that interpretation of simulations where lipids interact with charged groups of any sort, including charged proteins, must be carefully scrutinized.

A.2. Introduction

Biological membranes serve multiple functional roles in signal transduction, for example the organization and segregation of proteins (both soluble and membrane-bound) and the sequestration of ions to establish ionic gradients. It has long been accepted that some ions interact directly with certain lipids in membranes, and that these interactions have the capacity to influence a wide-array of physiological processes. Thus, much attention has been paid to understanding the full biophysical detail of how ions and lipids interact, how that interaction influences the behavior of water in a membrane's hydration shell, and how collectively these interactions perturb the underlying structure of the membrane. These efforts have been critical in determining the physical roles ions play in regulating membrane-protein structure and function.

Somewhat surprisingly, as the resolution of experimental and computational methods for studying atomic-scale interactions has increased, one of the most firmly entrenched assumptions regarding how NaCl interacts with membranes has been challenged. Historically, the defining experiments were carefully done electrophoretic mobility measurements that showed the surface (ζ) potential of PC vesicles was completely unaffected by NaCl, with the interpretation that NaCl was not binding to the headgroups (Bangham 1968, Eisenberg et al. 1979, Hanai et al. 1965, McDaniel et al. 1984, Winiski et al. 1986). Further, after decades of experimental structural measurements, any suggestion of NaCl-induced structural changes in PC bilayers has been, at best, extremely sparse. Recently, numerous molecular dynamics (MD) simulations have been utilized to study local and global effects of ion-lipid interactions (Bockmann et al. 2003, Khavrutskii et al. 2009, Lee et al. 2008, Pandit et al. 2003, Sachs and Woolf 2003, Sachs et al. 2004, Vacha et al. 2009) and to corroborate a wide-range of experimental results (Clarke and Lupfert 1999, Cunningham et al. 1988, Loosley-Millman et al. 1982, Macdonald and Seelig 1988, McDaniel et al. 1984, Pabst et al. 2007, Parsegian et al. 1979, Petrache et al. 2005, Petrache et al. 2006, Petrache et al. 2004, Roux M. and Bloom 1990, Rydall and Macdonald 1992, Szekely et al. 2011, Tatulian 1987, Winiski et al. 1986). However, disagreements have emerged in the data from

various simulations, most notably about whether NaCl binds tightly to PC headgroups and whether this binding induces significant structural changes in PC bilayers.

Originally, we ran short timescale CHARMM simulations of POPC lipids with NaCl, and our results suggested that, at physiological concentrations, while Na^+ does have affinity for PC headgroups, it is quite weak (Sachs et al. 2004). We also found that NaCl causes no detectable change in bilayer structure. Concurrently, several groups were using the GROMOS force-field to investigate similar questions. The GROMOS results, somewhat loosely supported at the time by fluorescence correlation spectroscopy (FCS) measurements that showed reduced lipid diffusion in the presence of NaCl, were quite alarming: Na^+ ions at physiological levels, it was claimed, have a high affinity for PC headgroups. In fact, Na^+ binding and complexation (with 3-4 lipids/ion) was so strong that it creates a positively charged layer in each monolayer's headgroup region and induces a strong, non-zero ζ-potential. Additionally, the results showed that NaCl thickens the PC bilayer by ~2 Å, thereby reducing the area per lipid (A_L) by ~4.9 $Å^2$ and significantly increasing the chain order. These GROMOS results have been quite widely propagated in the literature over the past several years. Not surprisingly, it has been shown that the interaction between Na^+ and/or Cl^- and PC headgroups, as well as the observed bilayer structural effects, are highly dependent on the ionic parameterization within the MD force-field (Cordomi et al. 2008).

In the meantime, a recent x-ray diffraction study has provided further, high-resolution experimental evidence that NaCl does not have a large effect on bilayer structure. The measurements were able to detect changes in bilayer structure, but found that significant changes occur only at NaCl concentrations greater than 1M (Pabst et al. 2007). At lower, physiological concentrations (~200mM NaCl), small but statistically irresolvable structural changes were observed, including a decrease in A_L (< $1Å^2$) as well as an increase in bilayer thickness (< 1Å). The reported order parameter remained unchanged at 200mM NaCl. It should be noted that these results do not preclude the possibility that NaCl at physiological concentrations can interact directly, or bind to lipid headgroups. The x-ray diffraction methods typically rely upon Fourier-reconstruction of

incomplete and truncated data—a model-dependent approach that may not reflect slight structural changes without an accurate model for reconstruction (Sachs et al. 2003).

Our aim here has been to update our older simulations using the newest CHARMM force-field (Klauda et al. 2010) at longer timescales in order to determine whether our earlier observations were an artifact of under-sampling and ensemble choice (constant as opposed to flexible surface area). We find that both Na^+ and Cl^- ions do interact transiently with the headgroups. But, consistent with our earlier simulations and the scattering data, there is negligible effect on bilayer structure. For comparison, we have also run GROMOS simulations which recapitulate the earlier claims of tight, essentially irreversible, ion binding and associated dramatic changes in bilayer structure.

A.3. Experimental Procedures

A.3.1. CHARMM Simulations

Systems were setup using the CHARMM molecular mechanics package (Brooks et al. 2009) with each system containing 128 POPC (1-palmitoyl-2-oleoyl-sn-glycero-3-phosphocholine, 16:0-18:1 PC) lipids fully hydrated (~42 TIP3P waters/lipid) in a solution without and with NaCl at a NaCl:H_2O ratio of 1:180. This setup is comparable to previous simulations (Bockmann and Grubmuller 2004, Bockmann et al. 2003), and were simulated for 300 nanoseconds using the NAMD molecular dynamics package (Phillips et al. 2005) (v 2.7b2) with the CHARMM36 force-field (Klauda et al. 2010) at T=300K with flexible unit cells (isothermal-isobaric, NPT, ensemble). Large systems contained 128 POPC lipids, ~125 TIP3P waters/lipid without and with NaCl again at a NaCl:H_2O ratio of 1:180 (90 each Na^+ and Cl^- ions), and were simulated for 300ns as before. The large system containing NaCl was simulated using the NBFIX parameters (Roux B. and Luo 2010), an ion-pairing parameter correction for accurate simulation at high electrolyte concentration. A separate system without NBFIX was also simulated for 300ns. All CHARMM results shown include the NBFIX parameters, though there was no noticeable difference in electron density profile or salt distribution (Figure A-11). That the NBFIX

parameters did not influence either electron density profile or salt distributions is likely a result of low average electrolyte concentrations (less than 0.5M NaCl) in our systems. The NBFIX parameter is critical for solutions with high electrolyte concentration (greater than 1M NaCl) where deviations in osmotic pressure between experiment and simulation are apparent (Roux B. and Luo 2010). However, NBFIX parameter was used to correct for potentially high local concentrations of NaCl within the system.

A.3.2. GROMOS Simulations

All simulations run under the "GROMOS" force field are defined as follows: Systems were run using GROMACS v4.5.3, with each system containing 128 Berger POPC lipids (Berger et al. 1997) fully hydrated using SPC water molecules (van Buuren et al. 1993) (~42 SPC water molecules per lipid). The starting bilayer configuration was taken from a pre-equilibrated 128 POPC lipid system provided by the Tieleman group (http://moose.bio.ucalgary.ca/). Ions were added to bulk water solution to match the CHARMM systems (NaCl:H_2O ratio of ~1:180). Systems were run at T=300K with flexible unit cells (isothermal-isobaric, NPT, ensemble). Simulations were carried out for 200ns and analysis was performed on equilibrated systems (100-200ns) using GROMACS and Perl.

A.3.3. Simulation Analysis

Analysis was performed on equilibrated trajectories (50-300ns) using CHARMM and Perl, utilizing an autocorrelation function as previously described (Lee et al. 2008) to determine the number of independent samples. Equilibration was determined by convergence of both A_L and the Na^+ distribution with respect to the bilayer normal. Electron density profiles were calculated by first re-centering the bilayer and applying periodic boundary conditions to water and NaCl. Electron density was calculated by normalizing to the bin volume determined by a *z*-bin size of 0.2 Å (*z*, the dimension of the bilayer normal) and the variable *x*- and *y*- box dimensions of the system at each step.

Results represent the time averaged electron density as a function of the distance from the center of the bilayer ($z = 0$). The 250ns CHARMM simulation trajectories and 100ns GROMOS simulation trajectories were output and analyzed at every 10,000 steps, or 20ps increments. Na^+ and Cl^- molar concentrations were calculated based on the number density of each ion and the calculated bin size.

Lipid order parameters, S_{CD}, were calculated for all atom CHARMM trajectories (using Perl) and for unified atom GROMOS system (using g_order). Results shown represent the average order parameter as a function of carbon number over the entire equilibrated trajectory. Na^+-lipid coordination numbers were calculated based on Na^+ distance to lipid carbonyl and phosphate oxygen atoms. Radial distribution functions between these groups were generated, and Na^+ ions closer than the minimum after the first peak in the RDF (cutoff at 3.22 Å) were considered as interacting with the headgroup.

The error for area per lipid and lipid order parameter were estimated using block sampling analysis as previously described (Grossfield and Zuckerman 2009). Briefly, error estimation of area per lipid and order parameter was calculated from converged trajectories considering a full range of block sizes. The block standard error (BSE) increases monotonically with larger block sizes and asymptotes at large block sizes; error was calculated based on the asymptotic value. The results for block sampling to estimate error for area per lipid and order parameter are shown in the Supporting Information. For area per lipid error estimation see Supporting Information, Section A.6, Figure A-9, p. 176, and for lipid order parameter error estimation see Supporting Information, Section A.6, Figure A-10, p. 177.

The water-dipole was calculated as previously described (Gurtovenko 2005, Sachs et al. 2004) where theta (θ) represents the angle between the water-dipole moment and the *z*-axis (normal to the bilayer). Results presented are the time-averaged $\langle\cos(\theta)\rangle$, as a function of *z*-distance from the bilayer center. Full isotropic rotation of water molecules corresponds to $\langle\cos(\theta)\rangle = 0$, and is observed in the absence of headgroup dipoles and salts.

A.4. Results

Figure A-1 illustrates the electron density profiles for the POPC systems containing ~42 H_2O/lipid and either 0 or 30 NaCl salts (30 of each ion). Using the CHARMM force-field, the addition of NaCl causes only a subtle change in the electron density profile (Figure A-1, A, compare black and gray lines), with a negligible effect on thickness (D_{HH}). Increased electron density in the water region is due to the added ions. Similar to our previous CHARMM simulations (Sachs et al. 2004), Na^+ ions are somewhat enriched near the headgroup region (~ 60% relative to their density at the limits of the water box) (Figure A-1, B, closed circles). Cl^- ions show slightly less, though still non-negligible enrichment outside the headgroup region (Figure A-1, B, open squares). Quite distinctly, the GROMOS simulations show that Na^+ ions have a significantly increased affinity for POPC lipids, having a 500% enrichment within the lipid headgroup region relative to the level at the simulated box's boundary (Figure A-1, D, closed circles). As expected, this causes a significant thickening of the bilayer (Figure A-1, C), consistent with previous GROMOS results (Bockmann et al. 2003, Lee et al. 2008, Pandit et al. 2003). Complete electron density profiles for these systems are available in Supporting Information, Figure A-4, p. 171 (CHARMM) and Figure A-5, p. 172 (GROMOS). In all cases, it is clear that these simulated boxes, the same approximate size as all previous salt/bilayer simulations, are not large enough to reach bulk NaCl levels ($[Cl^-] > [Na^+]$ at $z = 40$ Å), an issue that will be addressed further below.

The structural effects of NaCl using these two force-fields are summarized in Table 1. Notably, the effects on A_L, D_{HH} and lipid order are much greater under the GROMOS force-field than under CHARMM. Consistent with previous results, the GROMOS force-field shows a remarkable 5 $Å^2$ NaCl-induced decrease in A_L. This is compared to a 1.5 $Å^2$ decrease using CHARMM. Consistently, D_{HH} increases by 2.8 Å under GROMOS compared to a 0.5 Å under CHARMM. The observed structural changes due to NaCl using the GROMOS force-field cause a noticeable shift in the x-ray

scattering form factor (see Supporting Information, Figure A-7, p. 174), a result that is not supported by experimental evidence at comparable NaCl concentrations. Conversely, using the CHARMM force-field, the small structural changes observed upon salt addition are within the error of x-ray scattering measurements.

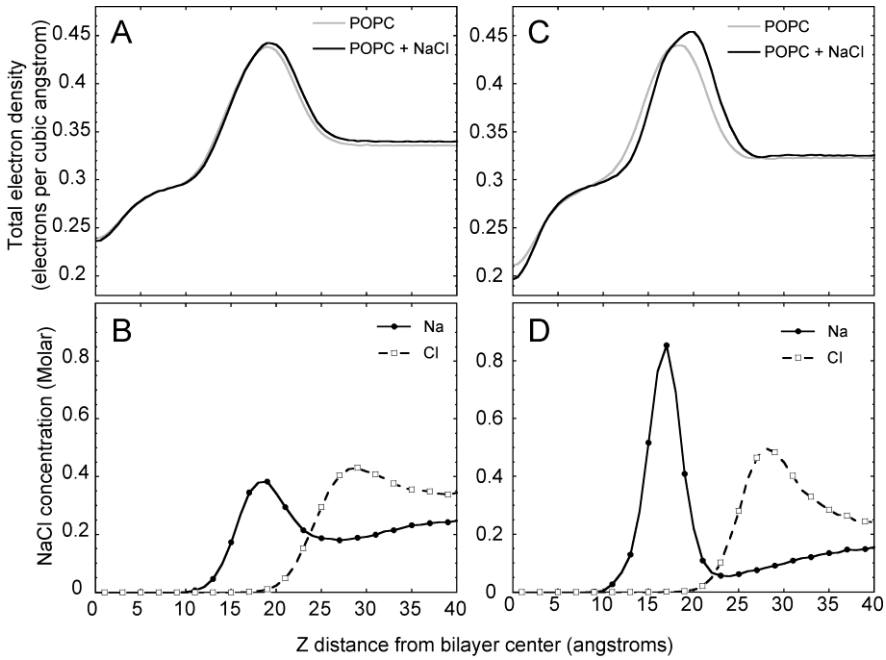

Figure A-1. NaCl affinity for POPC in CHARMM and GROMOS. Simulations demonstrate that Na+ and Cl- have an affinity for POPC bilayer, but the level of salt binding as well the effect on bilayer structure is highly dependent on force-field. (A) Long time scale simulations of POPC using the CHARMM force-field in the absence (gray line) and presence of NaCl (black line) show little structural effect of physiological levels of NaCl. (B) The distribution of Na+ (solid line) and Cl- (dashed line) show the affinity of ions for POPC, with an enrichment of Na+ ions in the headgroup region and an enrichment of Cl-outside the head headgroup region. (C) Identical POPC bilayer systems run using the GROMOS force-field show a marked difference in the bilayer thickness in the presence of NaCl (black line) compared to the pure POPC bilayer (gray line). (D) The ion distribution demonstrates under the GROMOS force-field a high enrichment of Na+ ions (solid line) deep in the headgroup region and a similar enrichment of Cl-ions (dashed line) outside the headgroup.

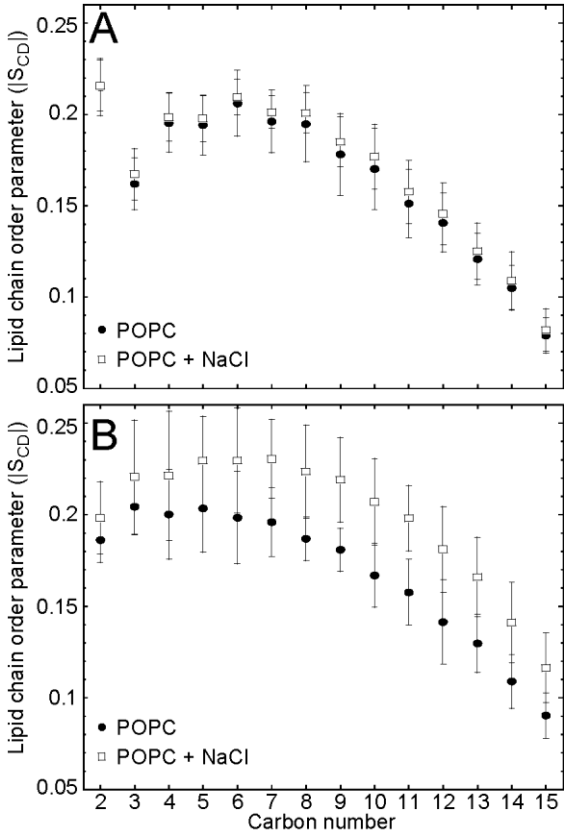

Figure A-2. NaCl and acyl chain ordering. The effect of NaCl on lipid ordering using CHARMM and GROMOS. (A) CHARMM force-field shows little induced ordering in either palmitoyl chains upon the addition of NaCl (open squares) compared to the pure system (filled circles). (B) Using the GROMOS force-field, the addition of NaCl (open squares) induces ordering of palmitoyl chains, consistent with the other structural changes shown in Table 1, but inconsistent with experimental data. Error was estimated using block sampling analysis (see Supporting Information, Figure A-10).

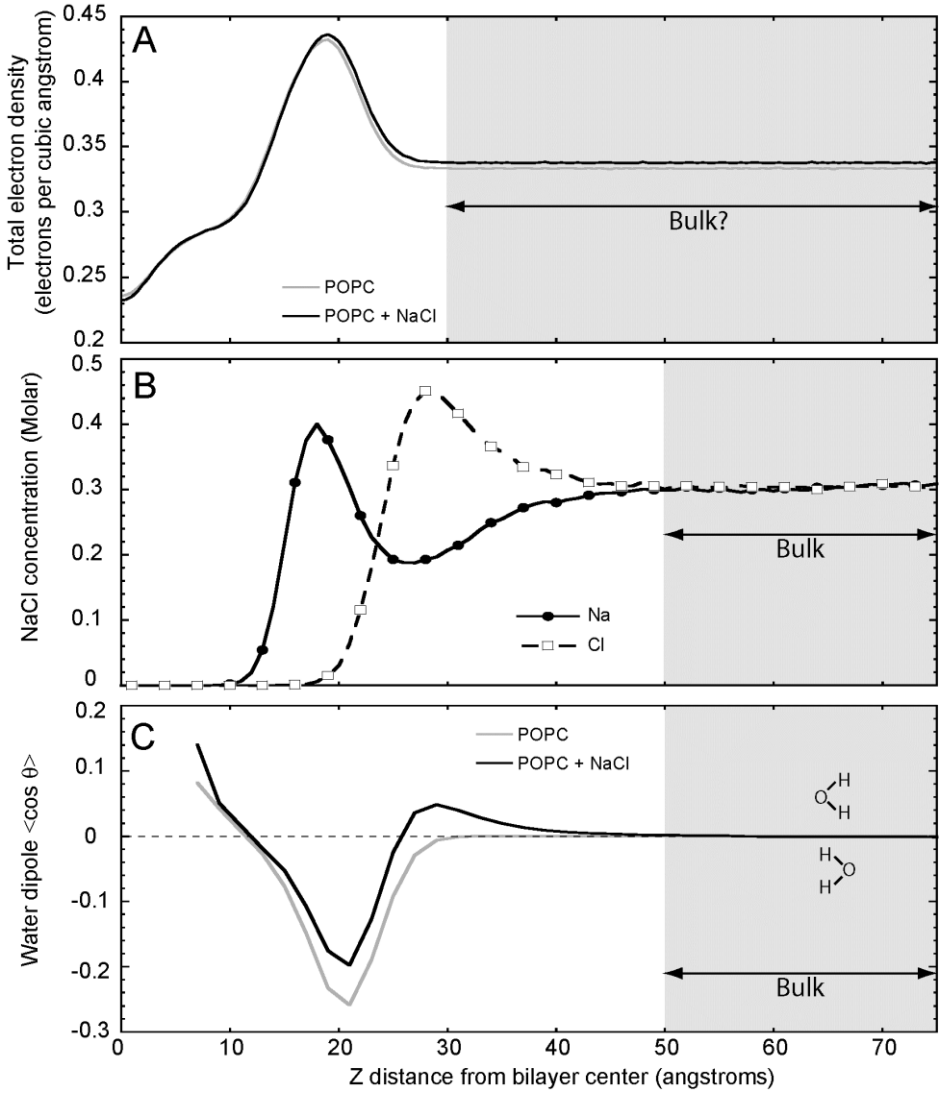

Figure A-3. NaCl induces long range ordering. Large, long time scale simulations of POPC lipids with additional water both pure lipid and with NaCl. (A) Electron density profiles of pure POPC (gray) or POPC + NaCl (black) demonstrate that the addition of more water and ions ion binding has little effect on bilayer structure. (B) The distribution of Na+ (solid line, closed circles) and Cl^- (dashed line, open squares) ions shows the layering effect of NaCl, and the overall ion concentration reaches bulk ~50-60 angstroms from the bilayer center. (C) The water dipole compared to the bilayer normal suggests the pure POPC bilayer effects water ordering out to ~30 angstroms from the bilayer center whereas POPC in the presence of NaCl causes further ordering of water molecules out to ~50 angstroms. In each figure, the perceived bulk of POPC in the presence of NaCl is shown in gray.

Table A-1. Structural effects of NaCl

System	POPC	NaCl	Simulation time (ns)	Area per lipid Å^2 (% change)		D_{HH} Å (% change)		$\|S_{CD}\|$ (Palm. C6)		Ion–lipid coordination nos.
CHARMM										
Pure	128	–	300	67.16	–	37.6	–	0.206	–	–
NaCl	128	+	300	65.67	(−2.22%)	38.1	(+1.33%)	0.209	(+1.46%)	1.75
GROMOS										
Pure	128	–	200	64.41	–	36.6	–	0.198	–	–
NaCl	128	+	200	59.39	(−14.63%)	39.4	(+7.65%)	0.229	(+15.64%)	3.1

Further, coordination numbers were calculated based on the localization of Na^+ ions near lipid carbonyl and phosphate oxygen atoms (with a cutoff based on the radial distribution function). The ion-lipid coordination number, the number of lipid carbonyl or phosphate groups surrounding a Na^+ ion in the headgroup region, as previously described (Lee et al. 2008), is markedly different using CHARMM, ~1.75, compared to GROMOS, ~3.1, consistent with the higher Na^+ enrichment in the headgroup region using GROMOS (detailed analysis of coordination number available in Supporting Information). Interestingly, using the CHARMM force-field, there is a strong correlation between lipid-ion coordination and residence time; Na^+ ions with longer residency time have a higher coordination number—Na^+ ions with a residency time greater than 5 nanoseconds are most often coordinated to 2 or 3 carbonyl or phosphate oxygen atoms (see Supporting Information, Figure A-7, p. 174). This suggests that the high degree of lipid-ion coordination observed using GROMOS is not precluded by using CHARMM, but occurs only rarely and correlates with ions becoming trapped by complexation with several headgroups.

As stated above, recent EPR measurements support long-standing knowledge that NaCl concentrations up to 300mM cause no detectable change in lipid ordering. We examined the effect of NaCl on order parameter, S_{CD}, and the force-field-dependent effect of NaCl on lipid chain order is dramatic. Under the CHARMM force-field, the addition of NaCl has little or no effect on chain ordering (Figure A-2, A), and the presence of NaCl with GROMOS causes a significant increase in lipid chain order (Figure A-2, B). The observed ordering effect induced by NaCl using GROMOS

coincides with bilayer thickening and a reduction in A_L. Using CHARMM, despite the small changes in A_L and bilayer thickness, there is no observable change in lipid tail ordering upon the addition of NaCl (for error estimation, see Supporting Information, Figure A-9, p. 176).

Because both Na^+ and Cl^- ions have a noticeable affinity for PC headgroups, we observed in Figure A-1 that the salt concentration in the fully hydrated bilayer (~42 H_2O/lipid) fails to reach a bulk concentration. This led us to question whether the addition of more water and ions would change the level of enrichment of either Na^+ or Cl^- in or near the PC headgroup region, and to establish how large a water box is necessary for these types of simulations. Large systems were constructed to contain the same number of lipids (128 equilibrated POPC lipids) but with three fold more water and ions (~125 H2O/lipid and 90 NaCl, thus keeping the NaCl:H_2O ratio at 1:180). These bilayers, with and without NaCl, were run for 300ns using the CHARMM force-field, and analysis was performed on equilibrated systems as before. Figure A-3 illustrates that the addition of more water and NaCl has a negligible effect on the bilayer thickness (Figure A-3, A) compared to the small system. The time-averaged distribution of ions (Figure A-3, B) shows that the addition of more NaCl does not increase the enrichment of Na^+ in the headgroup region. Further, we note that the addition of NaCl causes a marked increase in the distance at which the electrostatic effects of the bilayer can be observed by measuring the water dipole orientation (Figure A-3, C) as previously described (Gurtovenko 2005, Sachs et al. 2004). Notably, in the pure POPC system the water orientation reaches an isotropic distribution ($\langle \cos \theta \rangle = 0$, Figure A-3, C, dashed line) approximately 30 Å from the bilayer center, whereas the addition of ~300mM bulk NaCl to the system causes further ordering of water molecules out to ~50 Å, approximately consistent with the distance at which both Na^+ and Cl^- concentrations reach their bulk values (Figure A-3, C and D, shaded region represents bulk). Collectively, these results suggest that bilayer simulations in the presence of salt should contain significantly more water than has been previously considered full-hydration (~42 H_2O/lipid), a factor that is particularly important when using MD simulations with periodic boundary conditions to study ion

adsorption to a bilayer, and the resulting charge distribution and surface potential of a bilayer.

A.5. Discussion

Our MD simulations using the CHARMM force-field demonstrate that the addition of NaCl to a POPC bilayer yield structural results that are within the range of those observed in x-ray experiments. The Na^+ and Cl^- affinity for PC headgroups is clearly and highly dependent on the selection of parameter set, a somewhat unsettling, but not surprising result. Using CHARMM36, the affinity of Na^+ for PC headgroups is markedly lower than is observed using GROMOS, shown here and previously described (Pabst et al. 2007), and is only slightly higher than was observed using CHARMM27 with fixed A_L (Sachs et al. 2004). The effects on bilayer structure upon the addition of NaCl using CHARMM36 appear to more accurately reflect experimental observables; the slight decrease in lateral A_L and increase in bilayer thickness are within the range of the x-ray scattering uncertainty. In the CHARMM simulations where sufficient water is added (Figure A-3) we observe equivalent enrichment of Cl^- ions outside the headgroup region as Na^+ within the headgroup region, resulting in an electrical double layer and suggesting that the experimentally observed neutrality of PC vesicles in electrolyte solution may be a result of equal, but weak, cation and anion adsorption. That the total charge density integrates to zero by ~50Å from the bilayer center is thus, in a somewhat complicated way, consistent with electrophoretic mobility measurements. Reconciliation of the FCS data that suggested NaCl slows lipid diffusion remains a conundrum, though perhaps weak binding is sufficient to have this effect without the associated structural changes.

It is important for the simulation community that we demonstrated that lipid bilayers in the presence of NaCl exhibit long range ordering of both ions and water molecules—up to 60 Å from the bilayer center—as a result of the ion adsorption. Further simulations used to calculate charge-based distributions, such as potential gradients

across such bilayers, need to take into account the magnitude with which the lipid bilayer influences its surroundings, including the distribution of charged molecules and water. The significant differences in interaction between charged groups and lipids using CHARMM and GROMOS suggest that careful scrutiny of both parameters and system size are necessary depending on the system of interest, including not only various lipid-ion systems but potentially the simulation of membrane proteins with charged residues. If charged ions bind too tightly to lipid headgroups in MD simulations, in all likelihood, so do charged amino acids.

A.6. Supporting Information

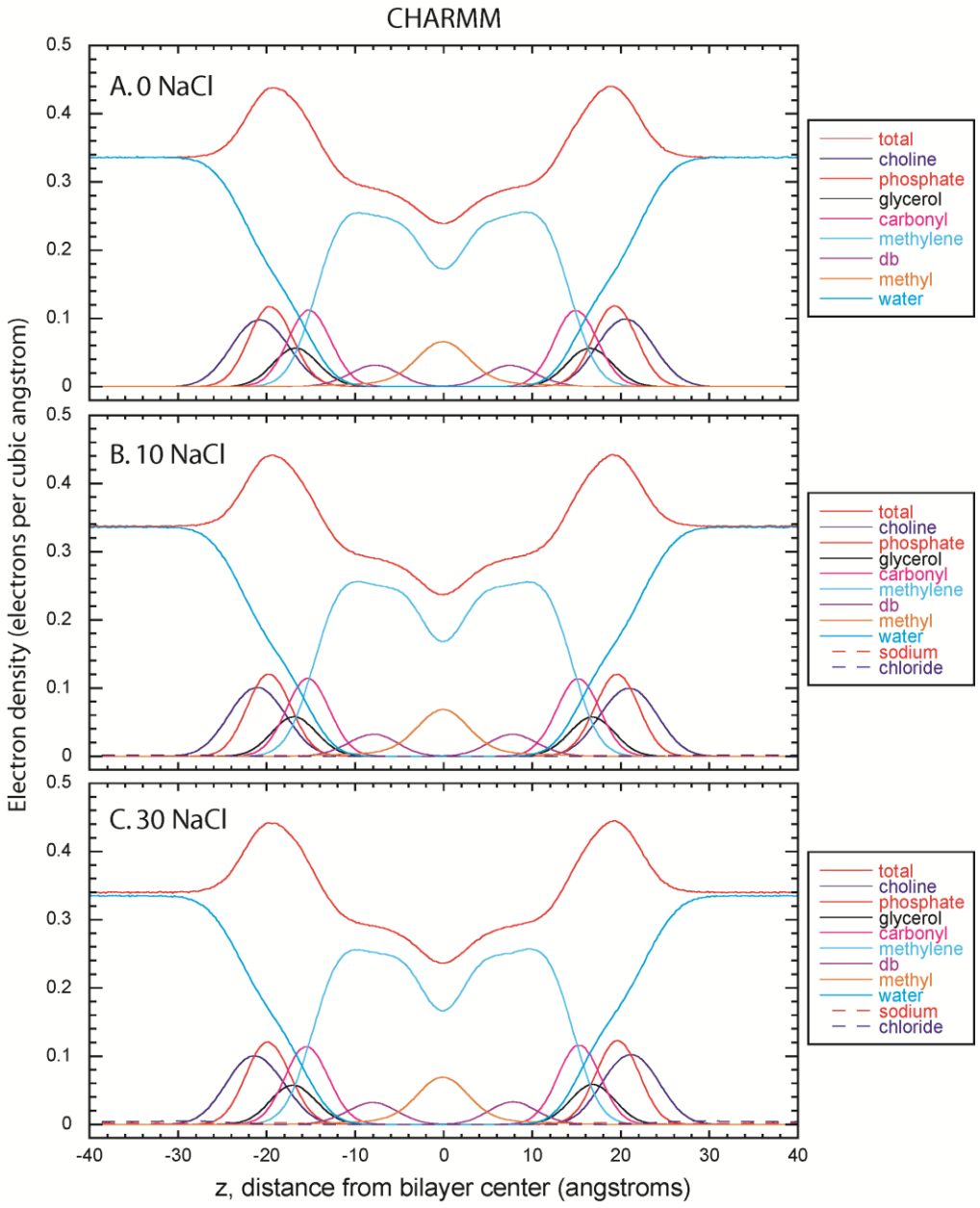

Figure A-4. CHARMM electron density profile.

Component electron density profile using the CHARMM force-field for pure POPC (A), POPC + 10 NaCl (B), and POPC + 30 NaCl, show no detectable change with the addition of NaCl using the CHARMM force-field.

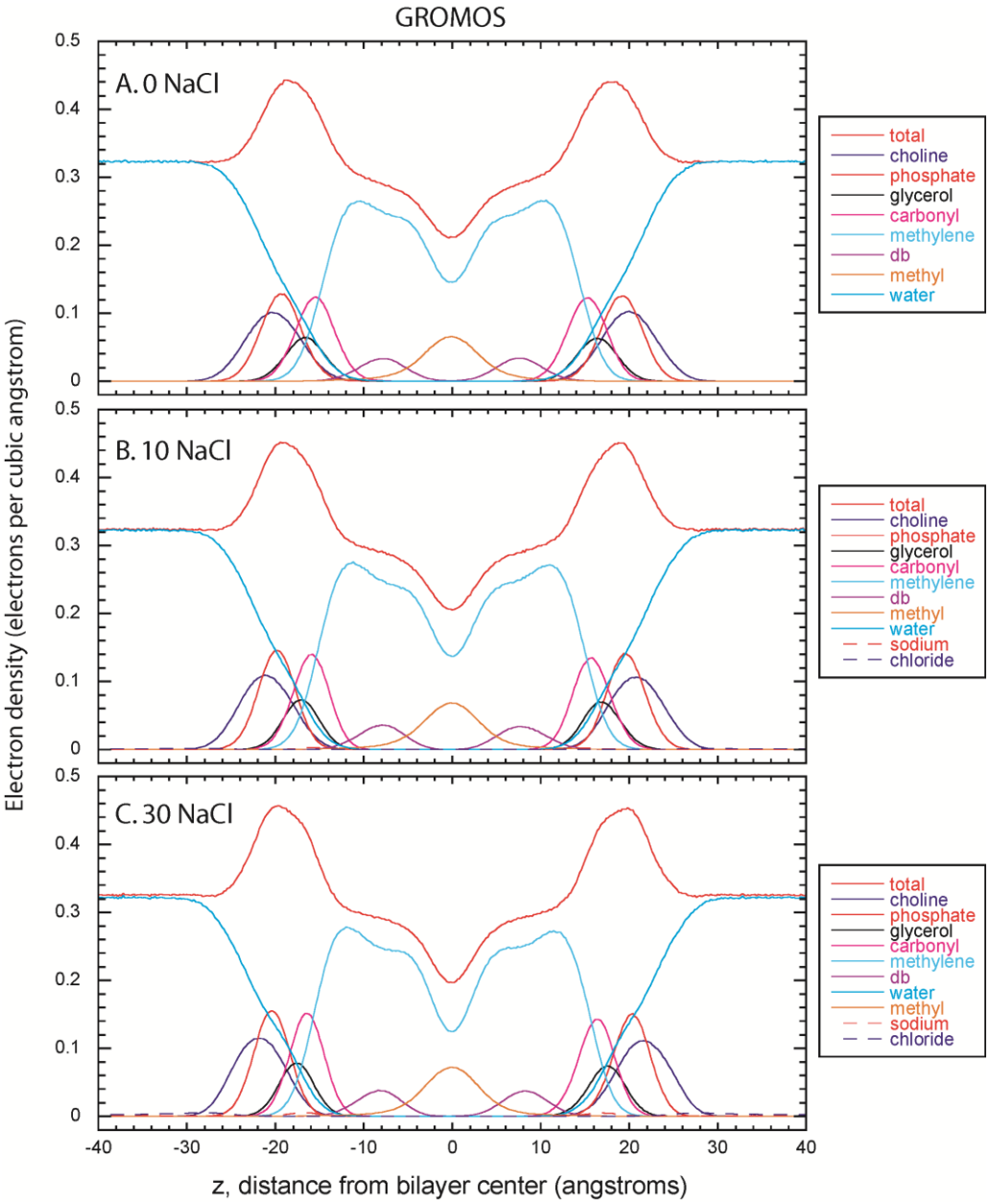

Figure A-5. GROMOS electron density profile.

Component electron density profile using GROMOS for pure POPC (A), POPC + 10 NaCl (B), and POPC + 30 NaCl, show a distinct thickening of the bilayer with the addition of NaCl.

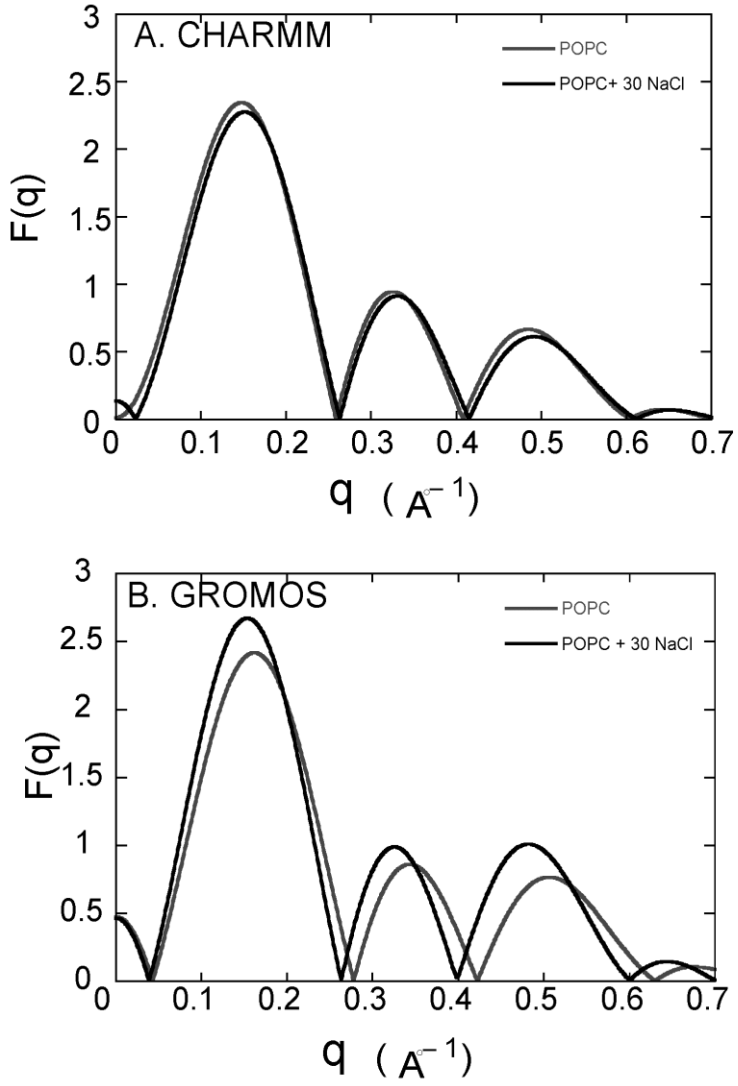

Figure A-6. CHARMM and GROMOS form factors.

The resulting form factors for CHARMM (A) and GROMOS(B) bilayers in the absence and presence of 30 NaCl molecules, shown in gray and black, respectively. (A) Addition of NaCl in the CHARMM force-field shows little change in the overall form factor. (B) Addition of NaCl in the GROMOS force-field shows a significant shift in the minima of the form factor, consistent with a thickening of the bilayer.

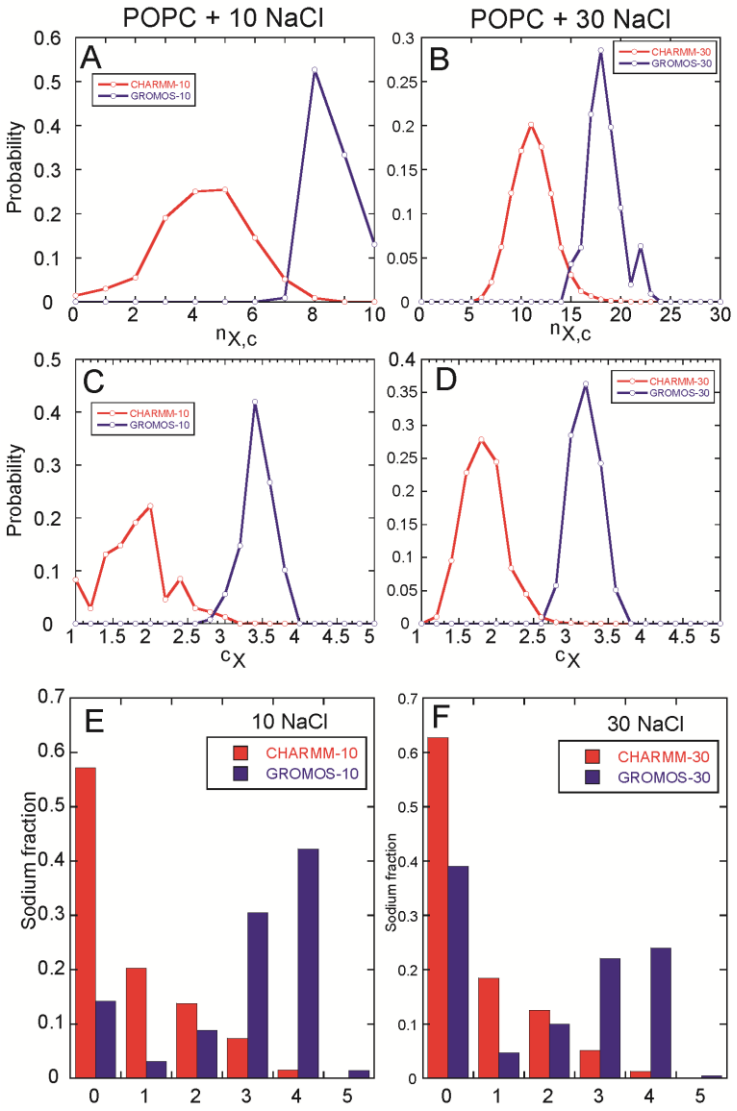

Figure A-7. Ion-lipid coordination. CHARMM (red) and GROMOS (blue) parameter sets differ in the affinity of sodium for lipids, shown as the distribution of bound sodium ions over the simulation (A-B) as well as the average sodium-ion coordination (C-D and E-F). Sodium-ion coordination number was calculated as previously described (Lee et al., 2008). Briefly, the lipid-ion coordination number, c_X, was calculated based on the number of lipid groups (carbonyl or phosphate) within the cutoff distance of a sodium ion, nc, and the number of sodium ions within a the cutoff distance of any lipid group (carbonyl or phosphate), $n_{X,c}$, using $c_X = n_C / n_{X,c}$.

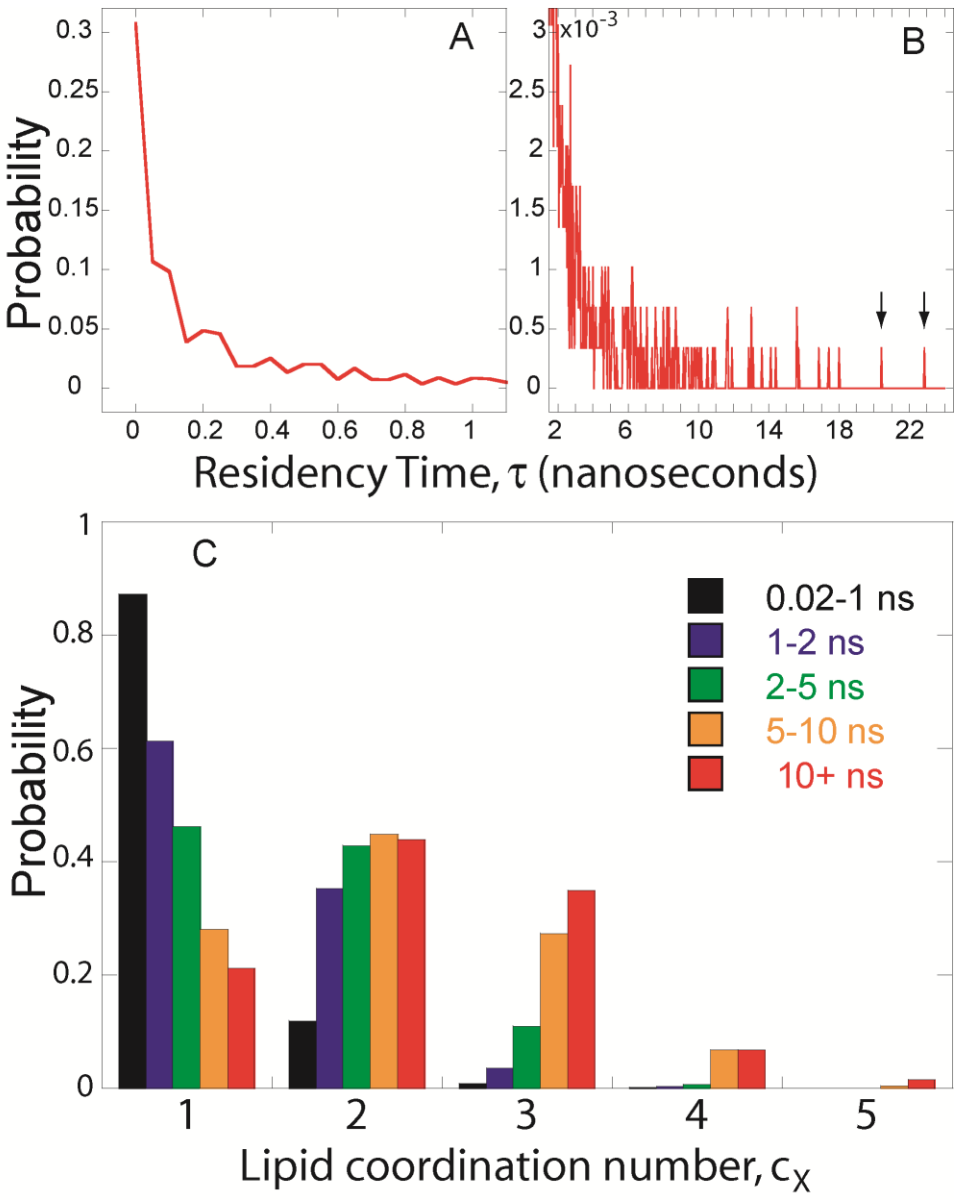

Figure A-8. Ion residency time. CHARMM coordination correlates with residence time. (A) Residence times show the majority of sodium ions leave the bilayer within 250ps. (B) Though infrequent, there are some ions bound for longer periods of time, some greater than 5ns, and even 20+ ns (arrows). (C) Plotting the coordination number as a function of residence time demonstrates that ions bound within the bilayer tend to coordinate with more lipid carbonyl or phosphate groups.

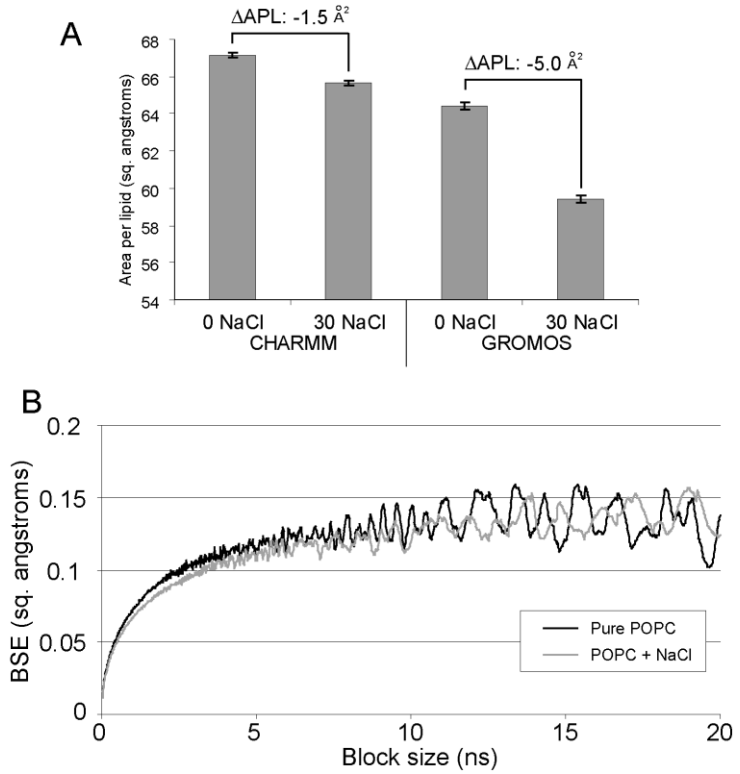

Figure A-9. Area per lipid. (A) Area per lipid (APL) for CHARMM and GROMOS force fields shown with error bars. The decrease in area per lipid for CHARMM, 1.5 Å2, represents a change of 2.2% compared to the pure system. The decrease in area per lipid for GROMOS, 5.0 Å2, represents a change of 7.8% compared to the pure system. (B) Estimation of the error associated with area per lipid in the CHARMM system was performed using the block sampling method (Grossfield and Zuckerman, 2009). The block standard error (BSE) increases monotonically with the block size and reaches an asymptotic value at approximately 10ns block size. Shown is the block standard error for the pure POPC system (black) and the system with NaCl (gray).

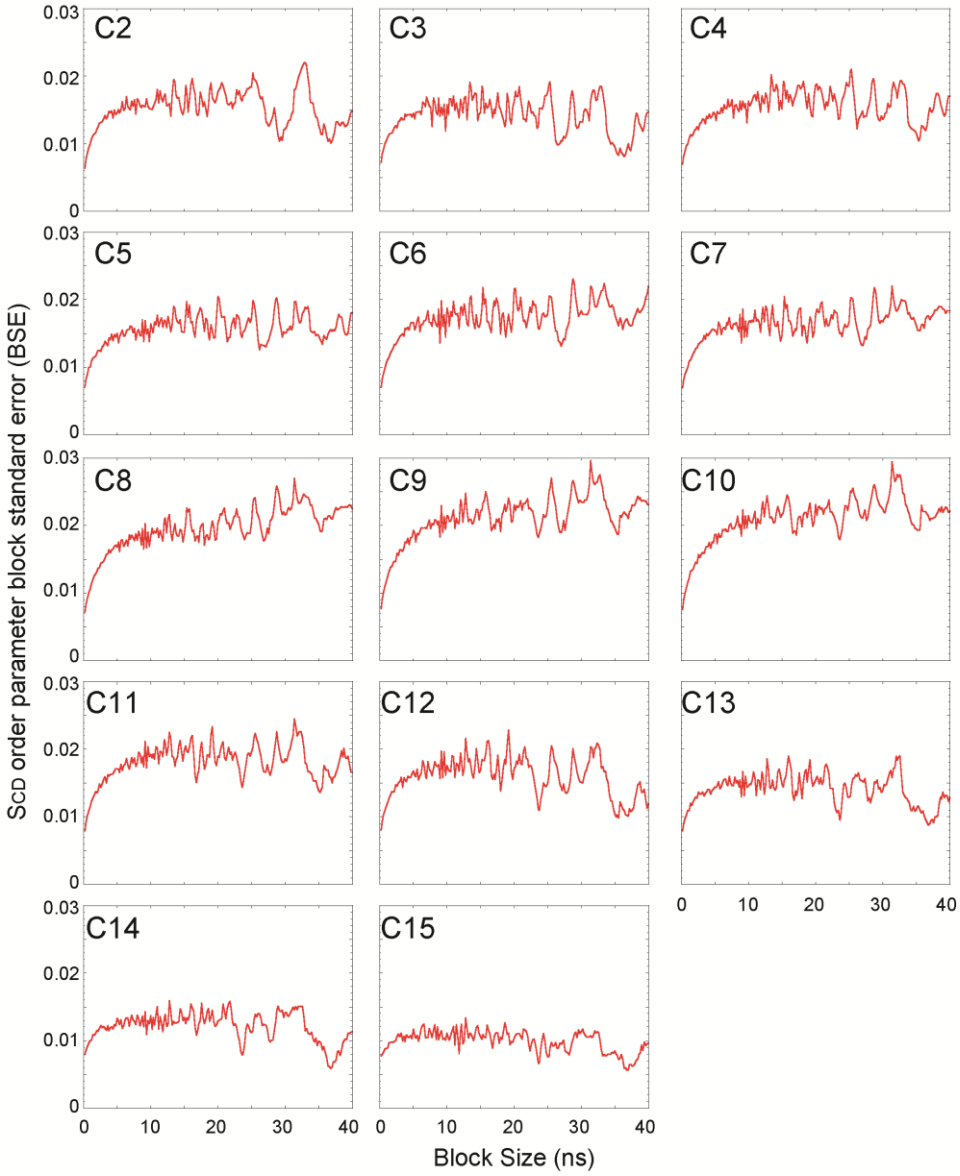

Figure A-10. Standard error estimation. Standard error was estimated for the order parameter data using block sampling as previously described (Grossfield and Zuckerman, 2009). Taking each carbon individually (C2-C15), the block standard error (BSE) was calculated for a range of block sizes. Error was estimated based on the asymptotic value of BSE at large block sizes (greater than 20ns). Shown is the BSE estimate for the CHARMM pure POPC system. Error for the CHARMM POPC + NaCl was calculated identically. Error for the GROMOS systems was calculated similarly using a range of block sizes between 20ns and 40ns.

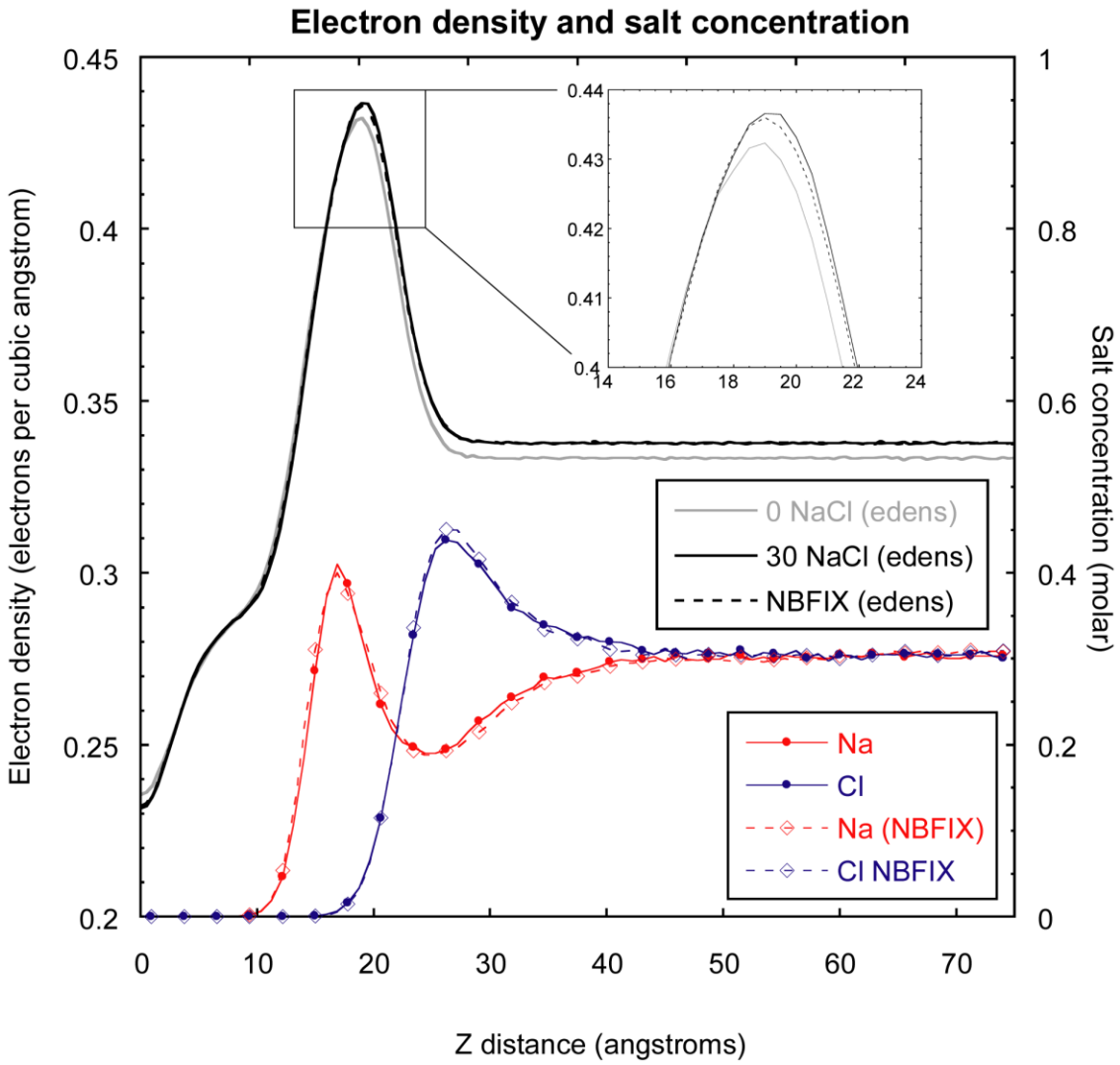

Figure A-11. The NBFIX patch. The large system containing NaCl was simulated using the NBFIX parameters, an ion-pairing parameter correction for accurate simulation at high electrolyte concentration. A separate system without NBFIX was also simulated for 300ns. Shown are the electron density profiles in the absence of NaCl (gray line), in the presence of NaCl (black line), and in the presence of NaCl using the NBFIX parameters (dashed line). Also shown are the Na and Cl concentration profiles without (solid red and blue lines) and with (dashed red and blue lines) the NBFIX parameters. There is no noticeable difference in electron density profile or salt distribution using NBFIX.

A.7. References

Bangham AD. 1968. Membrane models with phospholipids. Prog Biophys Mol Biol 18: 29-95.

Berger O, Edholm O, Jahnig F. 1997. Molecular dynamics simulations of a fluid bilayer of dipalmitoylphosphatidylcholine at full hydration, constant pressure, and constant temperature. Biophys J 72: 2002-2013.

Bockmann RA, Grubmuller H. 2004. Multistep binding of divalent cations to phospholipid bilayers: a molecular dynamics study. Angew Chem Int Ed Engl 43: 1021-1024.

Bockmann RA, Hac A, Heimburg T, Grubmuller H. 2003. Effect of sodium chloride on a lipid bilayer. Biophys J 85: 1647-1655.

Brooks BR, et al. 2009. CHARMM: the biomolecular simulation program. J Comput Chem 30: 1545-1614.

Clarke RJ, Lupfert C. 1999. Influence of anions and cations on the dipole potential of phosphatidylcholine vesicles: a basis for the Hofmeister effect. Biophys J 76: 2614-2624.

Cordomi A, Edholm O, Perez JJ. 2008. Effect of ions on a dipalmitoyl phosphatidylcholine bilayer. a molecular dynamics simulation study. J Phys Chem B 112: 1397-1408.

Cunningham BA, Gelerinter E, Lis LJ. 1988. Monovalent ion-phosphatidylcholine interactions: an electron paramagnetic resonance study. Chem Phys Lipids 46: 205-211.

Eisenberg M, Gresalfi T, Riccio T, McLaughlin S. 1979. Adsorption of monovalent cations to bilayer membranes containing negative phospholipids. Biochemistry 18: 5213-5223.

Grossfield A, Zuckerman DM. 2009. Quantifying uncertainty and sampling quality in biomolecular simulations. Annu Rep Comput Chem 5: 23-48.

Gurtovenko AA. 2005. Asymmetry of lipid bilayers induced by monovalent salt: atomistic molecular-dynamics study. J Chem Phys 122: 244902.

Hanai T, Haydon DA, Taylor J. 1965. Polar group orientation and the electrical properties of lecithin bimolecular leaflets. J Theor Biol 9: 278-296.

Khavrutskii IV, Gorfe AA, Lu B, McCammon JA. 2009. Free energy for the permeation of Na(+) and Cl(-) ions and their ion-pair through a zwitterionic dimyristoyl phosphatidylcholine lipid bilayer by umbrella integration with harmonic fourier beads. J Am Chem Soc 131: 1706-1716.

Klauda JB, Venable RM, Freites JA, O'Connor JW, Tobias DJ, Mondragon-Ramirez C, Vorobyov I, MacKerell AD, Jr., Pastor RW. 2010. Update of the CHARMM all-atom additive force field for lipids: validation on six lipid types. J Phys Chem B 114: 7830-7843.

Lee SJ, Song Y, Baker NA. 2008. Molecular dynamics simulations of asymmetric NaCl and KCl solutions separated by phosphatidylcholine bilayers: potential drops and structural changes induced by strong Na+-lipid interactions and finite size effects. Biophys J 94: 3565-3576.

Loosley-Millman ME, Rand RP, Parsegian VA. 1982. Effects of monovalent ion binding and screening on measured electrostatic forces between charged phospholipid bilayers. Biophys J 40: 221-232.

Macdonald PM, Seelig J. 1988. Anion binding to neutral and positively charged lipid membranes. Biochemistry 27: 6769-6775.

McDaniel RV, McLaughlin A, Winiski AP, Eisenberg M, McLaughlin S. 1984. Bilayer membranes containing the ganglioside GM1: models for electrostatic potentials adjacent to biological membranes. Biochemistry 23: 4618-4624.

Pabst G, Hodzic A, Strancar J, Danner S, Rappolt M, Laggner P. 2007. Rigidification of neutral lipid bilayers in the presence of salts. Biophys J 93: 2688-2696.

Pandit SA, Bostick D, Berkowitz ML. 2003. Molecular dynamics simulation of a dipalmitoylphosphatidylcholine bilayer with NaCl. Biophys J 84: 3743-3750.

Parsegian VA, Fuller N, Rand RP. 1979. Measured work of deformation and repulsion of lecithin bilayers. Proc Natl Acad Sci U S A 76: 2750-2754.

Petrache HI, Kimchi I, Harries D, Parsegian VA. 2005. Measured depletion of ions at the biomembrane interface. J Am Chem Soc 127: 11546-11547.

Petrache HI, Zemb T, Belloni L, Parsegian VA. 2006. Salt screening and specific ion adsorption determine neutral-lipid membrane interactions. Proc Natl Acad Sci U S A 103: 7982-7987.

Petrache HI, Tristram-Nagle S, Gawrisch K, Harries D, Parsegian VA, Nagle JF. 2004. Structure and fluctuations of charged phosphatidylserine bilayers in the absence of salt. Biophys J 86: 1574-1586.

Phillips JC, Braun R, Wang W, Gumbart J, Tajkhorshid E, Villa E, Chipot C, Skeel RD, Kale L, Schulten K. 2005. Scalable molecular dynamics with NAMD. J Comput Chem 26: 1781-1802.

Roux B, Luo Y. 2010. Simulation of Osmotic Pressure in Concentrated Aqueous Salt Solutions. Journal of Physical Chemistry Letters 1: 183-189.

Roux M, Bloom M. 1990. Ca2+, Mg2+, Li+, Na+, and K+ distributions in the headgroup region of binary membranes of phosphatidylcholine and phosphatidylserine as seen by deuterium NMR. Biochemistry 29: 7077-7089.

Rydall JR, Macdonald PM. 1992. Investigation of anion binding to neutral lipid membranes using 2H NMR. Biochemistry 31: 1092-1099.

Sachs JN, Woolf TB. 2003. Understanding the Hofmeister effect in interactions between chaotropic anions and lipid bilayers: molecular dynamics simulations. J Am Chem Soc 125: 8742-8743.

Sachs JN, Petrache HI, Woolf TB. 2003. Interpretation of small angle X-ray measurements guided by molecular dynamics simulations of lipid bilayers. Chem Phys Lipids 126: 211-223.

Sachs JN, Nanda H, Petrache HI, Woolf TB. 2004. Changes in phosphatidylcholine headgroup tilt and water order induced by monovalent salts: molecular dynamics simulations. Biophys J 86: 3772-3782.

Szekely O, Steiner A, Szekely P, Amit E, Asor R, Tamburu C, Raviv U. 2011. The structure of ions and zwitterionic lipids regulates the charge of dipolar membranes. Langmuir 27: 7419-7438.

Tatulian SA. 1987. Binding of alkaline-earth metal cations and some anions to phosphatidylcholine liposomes. Eur J Biochem 170: 413-420.

Vacha R, Siu SW, Petrov M, Bockmann RA, Barucha-Kraszewska J, Jurkiewicz P, Hof M, Berkowitz ML, Jungwirth P. 2009. Effects of alkali cations and halide anions on the DOPC lipid membrane. J Phys Chem A 113: 7235-7243.

van Buuren AR, Marrink SJ, Berendsen HJ. 1993. A molecular dynamics study of the decane/water interface. Journal of Physical Chemistry 97: 9206-9212.

Winiski AP, McLaughlin AC, McDaniel RV, Eisenberg M, McLaughlin S. 1986. An experimental test of the discreteness-of-charge effect in positive and negative lipid bilayers. Biochemistry 25: 8206-8214.

Appendix B. Table of ligands and receptors of the human tumor necrosis factor (TNF) superfamily

Table B-1. Ligands and receptors of the human TNF superfamily. Table taken directly from Aggarwal et al. [1]

Symbol	Ligand (alias)	Cellular expression	Symbol	Receptor (alias)	Cellular expression
TNFSF1	TNF-β (LT-α)	NK, T, and B cells	TNFRSF1A	TNFR1 (DR1)	Hematopoietic and immune cells
			TNFRSF1B	TNFR2	Immune and endothelial cells
TNFSF2	TNF-α	Macrophages and NK, T, and B cells	TNFRSF1A/B	TNFR1/2	Immune and endothelial cells
TNFSF3	LT-β	Activated $CD4^+$ T cells and T, DC, and NK cells	TNFRSF3	LT-βR	NK cells, $CD4^+$ and $CD8^+$T cells
TNFSF4	OX40L (CD252, gp34)	B and T cells, DCs, endothelial and smooth muscle cells	TNFRSF4	OX40 (CD134)	Activated $CD4^+$ T cells and neutrophils
TNFSF5	CD40L (CD154, gp39)	Activated $CD4^+$ T lymphocytes, NK cells, mast cells, basophils, and eosinophils	TNFRSF5	CD40 (p50)	B cells, monocytes, DCs, and thymic epithelium, Reed-Sternberg cells
TNFSF6	FasL (CD95L, Apo1L)	Activated splenocytes, thymocytes, nonlymphoid tissues, and NK cells	TNFRSF6	Fas (CD95, Apo1, DR2)	Epithelial cells, hepatocytes, activated mature lymphocytes, and transformed cells
			TNFRSF6B	DcR3	Lung and colon cells

Symbol	Ligand (alias)	Cellular expression	Symbol	Receptor (alias)	Cellular expression

TNFSF7	CD27L (CD70)	NK, T, B, and mast cells, smooth muscle and thymic epithelial cells	TNFRSF7	CD27	Hematopoietic progenitors, and $CD4^+$ and $CD8^+$T cells
TNFSF8	CD30L (CD153)	Activated T cells, B cells, and monocytes, granulocytes, and medullary thymic epithelial cells	TNFRSF8	CD30	Reed-Sternberg cells
TNFSF9	4-1BBL	APCs (B cells, macrophages, and DCs), mast cells	TNFRSF9	4-1BB (CD137, ILA)	T, NK, and mast cells, and neutrophils
TNFSF10	TRAIL (Apo2L)	NK and T cells, DCs	TNFRSF10A	TRAILR1 (DR4, Apo2)	Most normal and transformed cells
			TNFRSF10B	TRAILR2 (DR5)	Most normal and transformed cells
			TNFRSF10C	TRAILR3 (DcR1)	Most normal and transformed cells
			TNFRSF10D	TRAILR4 (DcR2)	Most normal and transformed cells
			TNFRSF11B	OPG (OCIF)	Most normal and transformed cells

Symbol	Ligand (alias)	Cellular expression	Symbol	Receptor (alias)	Cellular expression
TNFSF11	RANKL (TRANCE, OPGL, ODF)	T cells, thymus, and lymph nodes	TNFRSF11A	RANK (TRANCER)	Osteoclasts, osteoblasts, and activated T cells
			TNFRSF11B	OPG (OCIF)	Osteoclast precursors, endothelial cells, and others
TNFSF12	TWEAK (Apo3L)	Monocytes	TNFRSF12A	TWEAKR (FN14)	Endothelial cells and fibroblasts
TNFSF13	APRIL (TALL-2, TRDL-1)	Macrophages, lymphoid cells, and tumor cells	TNFRSF13A/17	BCMA	B cells, PBLs, spleen, thymus, lymph nodes, liver, and adrenals
			TNFRSF13B	TACI	B cells, activated T cells, PBLs, spleen, thymus, and small intestine
TNFSF13B	BAFF (BLYS, THANK)	T cells, monocytes, macrophages, and DCs	TNFRSF13B	TACI	B cells, activated T cells, PBLs, spleen, thymus, and small intestine
			TNFRSF13C	BAFFR	B cells, resting T cells, PBLs, spleen, lymph nodes
			TNFRSF17	BCMA	B cells, resting T cells, PBLs, spleen, lymph nodes
TNFSF14	LIGHT (HVEML, LT-γ)	T cells, granulocytes, monocytes, and DCs	TNFRSF14	LIGHTR (HVEM)	T and B cells, monocytes, and lymphoid cells
			TNFRSF3	LT-βR	Nonlymphoid hematopoietic and stromal cells

Symbol	Ligand (alias)	Cellular expression	Symbol	Receptor (alias)	Cellular expression
TNFSF15	VEGI (TL1A)	Endothelial cells	TNFRSF25	DR3	NK cells, $CD4^+$ and $CD8^+$T cells
		APCs (B cells, macrophages, and DCs)	TNFRSF6B	DcR3	Activated T cells
TNFSF18	GITRL	HUVECs	TNFRSF18	GITR (AITR)	$CD4^+CD25^+$ T cells
	EDA-A1	Skin		EDAR	Ectodermal derivative
	EDA-A2	Skin		XEDAR	Ectodermal derivative, embryonic hair follicles
NI			TNFRSF19	TROY (TAJ)	Embryo skin, epithelium, hair follicles, and brain
NI			TNFRSF19L	RELT	Lymphoid tissues, hematopoietic tissues
NI			TNFRSF21	DR6	Resting T cells
NI			TNFRSF16	NGFR (CD271)	Neuronal axons, Schwann cells, perineural cells

NI indicates not identified; OX40L, OX40 ligand; Fas, fibroblast-associated; TRANCE, TNF-related activation-induced cytokines; OPGL, OPG ligand; ODF, osteoclast differentiation factor; TALL, TNF- and APOL-related leukocyte expressed ligand; TRDL, TNF-related death ligand; HVEM, herpesvirus entry mediator; GITR, glucocorticoid-induced TND receptor; APCs, antigen-presenting cells; HUVECs, human umbilical vein endothelial cells; ILA, induced by lymphocyte activation; OCIF, osteoclastogenesis inhibitory factor; FN14, fibroblast growth factor-inducible immediate-early response gene 14; PBLs, peripheral blood lymphocytes; AITR, activation-inducible TNF receptor superfamily member; XEDAR, X-linked ectodysplasin receptor; TROY, TNFRSF expressed on the mouse embryo; TAJ, toxicity and JNK inducer; RELT, receptor expressed in lymphoid tissues; and NGFR, nerve growth factor receptor.

Reference:

[1] Aggarwal, B. B., Gupta, S. C., and Kim, J. H. (2012) *Blood* **119**, 651-65.

Appendix C. List of Abbreviations

Throughout this manuscript, care was taken to clarify non-standard abbreviations and to avoid jargon.

Table C-1. List of abbreviations

A_L	Area per lipid
BS3	Bis[sulfosuccinimidyl] suberate
cDNA	Complementary DNA
CFP	Cyan fluorescent protein
CHARMM	Chemistry at HARvard Molecular Mechanics
co-IP	co-immunoprecipitation
CRD	Cysteine rich domain
DcR1	Decoy receptor 1
DcR2	Decoy receptor 2
DD	Death domain
DED	Death effector domain
D_{HH}	Lipid headgroup to headgroup distance, a measure of bilayer thickness
DISC	Death-inducing signaling complex
DME	Dimethyl ether
DMS	Dimethyl sulfide
DR4	Death receptor 4 (also TRAIL-R1)
DR5	Death receptor 5 (also TRAIL-R2)
DR5-L	Death receptor 5, long isoform
DR5-S	Death receptor 5, short isoform
DTT	Dithiothreitol, a reducing agent
ECD	Extracellular domain
FADD	Fas-associated death domain
FasL	Fas ligand
FBS	Fetal bovine serum
FRET	Fluorescence (or Föster) resonance energy transfer
GBSW	Generalized born model with simple, smoothed switching

GFP	Green fluorescent protein
GG4	Glycine-X-X-X-Glycine, a helix dimerization motif (X represents any amino acid)
GROMOS	A molecular dynamics force field simulation, developed at Univ. of Groningen
GxxxG	see GG4
HEK293	Human embryonic kidney 293 cells (also 293 cells)
IRES	Internal ribosomal entry site
IκBα	nuclear factor of kappa light polypeptide gene enhancer in B-cells inhibitor, alpha
kD	kilodaltons, a measure of molecular mass
LTα	Lymphotoxin-alpha
MD	Molecular dynamics
Met	Methionine residue
MIP	Maximum intensity projection
MMTSB	Multiscale modeling tools for structural biology
mRNA	messenger RNA
mTNF	membrane-bound TNF
NAMD	Not (just) another molecular dynamics program, MD simulation package
NFκB	Nuclear factor kappa B
NPT	Isothermal, isobaric ensemble with constant number of atoms
ns	nanoseconds
p53	protein 53 (or tumor protein 53), tumor suppressor involved in cancer prevention
PAGE	Polyacrylamide gel electrophoresis
PBS	Phosphate buffered saline
PC	Phosphatidylcholine
PCR	Polymerase chain reaction
PDB	Protein Data Bank (www.pdb.org)
Phe	Phenylalanine residue (single letter symbol - F)
PLAD	Pre-ligand assembly domain
PME	Particle mesh Ewald
POPC	1-palmitoyl-2-oleoyl-sn-glycero-3-phosphocholine
ps	picoseconds
QM	Quantum mechanical
RDF	Radial distribution function
REMD	Replica exchange molecular dynamics
RMSD	Root mean squared deviation
RNAi	RNA interference

RT	Room temperature, or reverse transcription
SDS	Sodium dodecyl sulfate
shRNA	small hairpin RNA
siRNA	small interfering RNA
SPC	Single point charge, explicit water molecule for MD simulation
sPLAD	soluble pre-ligand assembly domain
SPOTS	Signaling protein oligomeric transduction structures
βME	Beta-mercaptoethanol
sTNF	soluble tumor necrosis factor ligand
TCA	Trichloroacetic acid
TIP3P	Transferable intermolecular potential, three-position model, explicit water molecule for MD simulation
TM	Transmembrane
TNF	Tumor necrosis factor
TNFR	Tumor necrosis factor receptor
TNF-β	Tumor necrosis factor-beta (also called LTα)
TNF-α	Tumor necrosis factor-alpha
TRAIL	TNF-related apoptosis-inducing ligand
TRAIL-R	TRAIL receptor
TRAIL-R1	TRAIL receptor 1 (also DR4)
TRAIL-R2	TRAIL receptor 2 (also DR5)
TRAIL-R3	TRAIL receptor 3 (also DcR1)
TRAIL-R4	TRAIL receptor 4 (also DcR2)
Trp	Tryptophan residue (single letter symbol - W)
Tyr	Tyrosine residue (single letter symbol - Y)
VMD	Visual Molecular Dynamics
XFP	Any fluorescent protein (i.e. GFP, CFP, YFP, RFP, etc.)
YFP	Yellow fluorescent protein